United States
Environmental Protection
Agency

National Risk Management
Research Laboratory
Ada, OK 74820

EPA/600/R-97/102
October 1997

EPA

# NAPL: Simulator Documentation

# NAPL: Simulator Documentation

by

Joseph Guarnaccia and George Pinder
Research Center for Groundwater Remediation Design
The University of Vermont
Burlington, VT 05401

and

Mikhail Fishman
U. S. Environmental Protection Agency
Robert S. Kerr Environmental Research Center
Ada, Oklahoma 74820

Cooperative Agreement CR-820499

Project Officer
Thomas E. Short
U. S. Environmental Protection Agency
Robert S. Kerr Environmental Research Center
Subsurface Protection and Remediation Division
Ada, Oklahoma 74820

National Risk Management Research Laboratory
Office of Research and Development
U.S. Environmental Protection Agency
Cincinnati, OH 45268

## DISCLAIMER

The U. S. Environmental Protection Agency through its Office of Research and Development partially funded and collaborated in the research described here under assistance agreement number CR-820499 to The University of Vermont. It has been subjected to the Agency's peer and administrative review and has been approved for publication as an EPA document. Mention of trade names or commercial products does not constitute endorsement or recommendation for use.

## FOREWORD

The U.S. Environmental Protection Agency is charged by Congress with protecting the Nation's land, air, and water resources. Under a mandate of national environmental laws, the Agency strives to formulate and implement actions leading to a compatible balance between human activities and the ability of natural systems to support and nurture life. To meet these mandates, EPA's research program is providing data and technical support for solving environmental problems today and building a science knowledge base necessary to manage our ecological resources wisely, understand how pollutants affect our health, and prevent or reduce environmental risks in the future.

The National Risk Management Research Laboratory is the Agency's center for investigation of technological and management approaches for reducing risks from threats to human health and the environment. The focus of the Laboratory's research program is on methods for the prevention and control of pollution to air, land, water, and subsurface resources; protection of water quality in public water systems; remediation of contaminated sites and ground water, and prevention and control of indoor air pollution. The goal of this research effort is to catalyze development and implementation of innovative, cost-effective environmental technologies; develop scientific and engineering information needed by EPA to support regulatory and policy decisions; and provide technical support and information transfer to ensure effective implementation of environmental regulations and strategies.

This report focuses on the simulation of the contamination of soils and aquifers which results from the release of organic liquids commonly referred to as Non-Aqueous Phase Liquids (NAPLs). The approach used in this simulation is applicable to three interrelated zones: a vadose zone which is in contact with the atmosphere, a capillary zone, and a water-table aquifer zone. The simulator accommodates three mobile phases: water, NAPL, and gas. The numerical solution algorithm is based on a Hermite collocation finite element discretization. The simulator provides an accurate solution of a coupled set of non-linear partial differential equations that are generated by combining fundamental balance equations with constitutive and thermodynamic relationships.

Clinton W. Hall, Director
Subsurface Protection and Remediation Division
National Risk Management Research Laboratory

**Abstract**

A mathematical and numerical model is developed to simulate the transport and fate of NAPLs in near-surface granular soils. The resulting three-dimensional, three phase simulator is called NAPL. The simulator accommodates three mobile phases: water, NAPL and gas, as well as water- and gas-phase transport of NAPL contaminants. The numerical solution algorithm is based on a Hermite collocation finite element discretization. Particular attention has been paid to the development of a sub-model that describes three-phase hysteretic permeability-saturation-pressure (k-S-P) relationships, and that considers the potential entrapment of any fluid when it is displaced. In addition rate-limited dissolution and volatilization mass transfer models have been included. The overall model has been tested for self-consistency using mass balance and temporal and spatial convergence analysis. The hysteretic k-S-P and mass exchange models have been tested against experimental results. Several example data sets are provided, including a setup of the artificial aquifer experiments being conducted at the EPA's Subsurface Protection and Remediation Division of the National Risk Management Research Laboratory in Ada, OK (formerly RSKERL) at this writing.

# Contents

# List of Figures

# List of Tables

# 1. INTRODUCTION

## 1.1. PROBLEM

The physical problem which is addressed herein is the contamination of a pristine porous medium as the result of releases of organic liquids, commonly referred to as Non-Aqueous Phase Liquids (NAPLs), in near-surface heterogeneous granular soils. The organic liquids can be either lighter than water (identified as LNAPLs, i. e., petroleum hydrocarbon-based) or heavier than water (identified as DNAPLs, i. e., chlorinated hydrocarbon-based). By near-surface we mean that the scale which characterizes fluid pressure is on the order of atmospheric pressure. In addition the soil domain can be idealized as consisting of three interrelated zones: a vadose zone which is in contact with the atmosphere, a capillary fringe zone, and a water-table aquifer zone. A particular problem of interest may include all three zones or a subset thereof. By granular soils we mean those soils which are stable (non-deforming) and relatively chemically inert (the soil particles do not interact with the soil fluids). Therefore, the soil is idealized as containing a high percentage of quartz particles and only a minor percentage of clay particles and organic matter.

A conceptual illustration of surface-release-generated NAPL migration in the vadose, capillary fringe and aquifer zones is provided in Figure 1.1. There are three fundamental mechanisms for NAPL migration. First, the NAPL infiltrates into the soil and migrates both vertically and laterally under the influence of gravitational and capillary forces. The distribution of the NAPL liquid is a function of fluid properties (density, viscosity, interfacial tension, wetting potential and variable chemical composition), soil properties (grain size distribution, mineral content, moisture content, porosity, hydraulic conductivity and spatial heterogeneity), and system forcing history. If the source is periodic in nature, then during drying periods, not all the NAPL will drain from the pore space, leaving behind an immobile residual, held in place by capillary forces. If the NAPL is more dense than water, it will migrate through the capillary fringe and continue

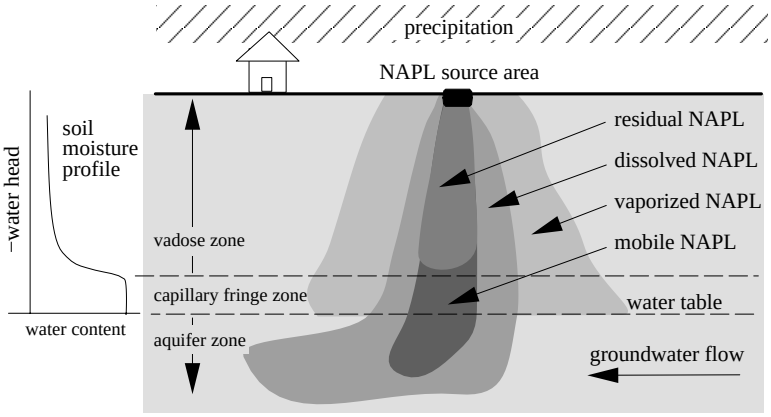


Figure 1.1: Definition illustration of NAPL contamination in near-surface soils due to an intermittant surface release.

its vertical migration until either the mobility becomes zero (all the NAPL liquid is at the immobile residual state) or the NAPL front encounters an impenetrable geologic horizon

The second contaminant transport mechanism is dissolution and consequent advection in the downward-flowing water-phase, with precipitation providing the water source in the vadose zone. In the case of a DNAPL, flowing groundwater picks up dissolved NAPL constituents.

The third transport mechanism is transport as a vapor NAPL constituent in the soil gas, where the increased gas-phase density induces downward movement. Partitioning between the gas- and water-phase contaminants further enhances the migratory potential of the NAPL constituents.

## 1.2. FOCUS

The focus of this investigation is to develop a physically complete subsurface flow and transport mathematical model (also referred to herein as the simulator) to study the movement and fate of NAPL contaminants in near-surface granular soils. Specifically, three fundamental, interrelated, physical processes have been identified: multiphase flow, interphase mass transfer, and constituent mass transport. The multiphase flow process defines the time-dependent volumetric extent of the mobile and immobile components of the water, NAPL and gas phases. The

interphase mass-transfer process defines how the NAPL contaminants partition between phases. The constituent mass transport defines the temporal and spatial distribution of the NAPL contaminants within a given phase. The three processes are related in a nonlinear way since the phase velocity and mass exchange terms are both functions of, among other things, phase volumetric content, and the phase fluid properties (density, viscosity, and interfacial tension) are in general a function of the chemical composition of the phase.

The model presented herein is developed with a focus on better quantifying these three fundamental physical processes as they exist in the natural environment. Particular attention has been paid to quantifying the following processes:

1. fluid entrapment and release;
2. hysteresis in the relative permeability-saturation-capillary pressure model;
3. rate-limited mass transfer to describe NAPL dissolution and volatilization;
4. advective-dispersive transport in both the water and gas phases.

The major purpose of developing such a simulator is that, once compiled, it can be used to verify the theory describing the physics of the problem and to quantify parameter sensitivity. In addition, the information derived from verification and sensitivity analysis can be used to simplify the system (for example, derive and evaluate simpler constitutive models) which is an important consideration given the computationally demanding nature of the problem (the solution of coupled nonlinear equations with sharp-front transport characteristics). Through this type of development, the resulting simulator, coupled with dedicated pre- and post-processing software for data input and output visualization, respectively, will be an efficient and effective engineering tool to be used for field-scale analysis.

## 1.3. APPROACH

To describe the physical problem mathematically, a set of coupled nonlinear partial differential balance equations (PDE's) which govern the temporal and spatial variability of the system, and a set of constitutive and thermodynamic equations which relate physically-based parameters occurring in the PDE's (for example relative permeability) to the dependent variables (for example fluid pressure and saturation) must be defined. There are two constitutive models which are of particular importance with regard to this simulator:

1. a model of three-phase relative permeability-saturation-capillary pressure relationships which includes flow- path-history-dependent functionals (hysteresis), fluid entrapment considerations, and functional dependence on fluid and soil properties;

2. a model of rate-limited interphase mass transfer processes, including NAPL dissolution and volatilization.

The resulting mathematical interpretation of the physical system is solved using a numerical solution algorithm which employs the following conceptual tools:

- An implicit-in-time collocation finite element method with Hermite cubic basis functions is used to generate the systems of algebraic equations.
- A successive substitution iteration scheme is used for nonlinear terms.
- A sequential solution procedure is used to solve the coupled balance equations to minimize the system matrix order and bandwidth, where the phase flow equations are solved sequentially using a total velocity formulation, and given the flow solution, the transport equations are then solved.

## 1.4. MODEL CAPABILITIES

The mathematical model which is presented in this documentation can be characterized by a list of attributes. This list is intended to provide the reader with a summary of the capabilities and limitations of the simulator.

1. Problems in one, two and three spatial dimensions (Cartesian coordinate system) are applicable.

2. The finite element mesh utilizes rectangular elements.

3. The simulator can accommodate as many as three-fluid phases, identified as a water-phase, a NAPL-phase and a gas-phase, and can model flow of either one, two or three phases in any combination.

4. Darcy's law is a valid model for quantifying water-, NAPL-, and gas-phase advection;

5. Fick's law is a valid model for quantifying water- and gas-phase diffusion processes.

6. The water phase is characterized as follows:

   - it is incompressible;
   - it is made up of two species: water and dissolved NAPL;
   - its properties are a function of contaminant concentration only;
   - the dissolved NAPL can vaporize into the gas phase and adsorb onto the solid phase.

7. The NAPL-phase is characterized as follows:

   - it is incompressible;
   - it is made up of a single chemical species;
   - it is able to dissolve into the water phase;
   - it is able to volatilize into the gas phase.

8. The gas phase is characterized as follows:

   - it is incompressible[1];
   - it is made up of two species: gas and volatilized NAPL;
   - its properties are a function of contaminant concentration only;

9. The porous medium is characterized as follows:

   - it is non-deforming;
   - it is generally heterogeneous and isotropic;
   - it is made up of two species: soil and adsorbed NAPL.

10. Isothermal conditions prevail.

[1]The model is intended to be applied to physical problems where pressure gradients are small, and where the time-scale defining gas-phase pressure response to forcing is much shorter than that which defines gas-phase saturation response. Therefore the gas-phase is considered effectively incompressible and Darcy's law is assumed to apply.

11. Mass transfer relationships are defined by:

    - NAPL phase dissolution is governed by a rate-limited, first-order, kinetic rule;
    - NAPL phase vaporization is governed by a rate-limited, first-order, kinetic rule;
    - dissolved NAPL species vaporization is governed by a rate limited, first-order, kinetic rule;
    - dissolved NAPL species adsorbtion is governed by a linear equilibrium partitioning rule.

12. The rules and relationships which define the multiphase flow parameters are as follows:

    - the porous medium is isotropic, and it may be saturated with one, two or three phases;
    - when more than one phase is present the relationship between relative permeability, saturation and capillary pressure (called the k-S-P model) is based on wettability considerations and two-phase data, where phase wettability is constrained to follow from most to least: water-NAPL-gas.
    - the k-S-P model is subject to hysteresis due to capillary and fluid entrapment effects;
    - the van Genuchten (1980) saturation-pressure model is modified to accommodate hysteresis;
    - the Mualem (1976) relative permeability-saturation model is modified to accommodate hysteresis;
    - the capillary pressure between phases can be scaled to accommodate variable fluid and soil properties.

13. Boundary and external forcing conditions are summarized as follows:

    - Dirichlet data for the multiphase flow problem is specified as either one of the three phase pressures known or all of the primary flow variables known (i. e., both pressure and saturation). Dirichlet data for contaminant transport is specified as a known value for the species of interest.

- Non-zero flux conditions for a phase or species within a phase are accommodated by specifying an appropriate point source or sink term (i. e., a well).
- Diffusive mass flux of the NAPL species in the gas-phase through a boundary layer at the interface between the ground surface and the atmosphere is accounted for by the use of a mixed boundary condition.[2]

14. The numerical model includes the following features:

    - The code is written in standard FORTRAN77 with the intent of making it portable.
    - The routines which can run in parallel mode have been coded to do so using the Silicon Graphics f77 compiler.
    - The code has a re-start facility.
    - The code is memory intensive, especially in 3-D mode where its utility for solving 3-D problems is limited. Therefore, a 2-D version is also included as part of this simulation package.
    - Standard upstream weighting as a means of adding artificial diffusion to the solution of parabolic equations is *not* utilized in this simulator. Instead, a physically-based diffusion term is added to the solution in a point-wise fashion when necessary, the magnitude of which is based on a user-defined critical Peclet number.
    - Time-step control is provided by two algorithms. One is based on the number of iterations required for convergence on the nonlinearity, and one is based on a user-defined maximum local Courant number.
    - The simulator has been integrated with a commercially available graphical user interface (GUI), and any interested users can contact the authors for more information.

## 1.5. ORGANIZATION

This report is organized as follows. The conclusions and recommendations are provided in Sections 2 and 3, respectively. Section 4 describes the mathematical

[2] The two-dimensional version of the simulator includes the mixed-type boundary condition for gas-phase transport, but the three-dimensional version does not.

model which includes development of the governing and constitutive equations. Section 5 provides a detailed description of the hysteretic $k - S - P$ model used in the simulator. Section 6 presents the numerical approach used to make the mathematical model amenable to computational solution. The development in this Section includes equation discretization, linearization and iterative solution.

Section 7 details the data input and output structure of the simulator called NAPL. Section 8 details the analysis used to verify the mathematical and numerical models, including convergence and comparison to experimental results. This Section also details a set of example problems which are tutorial in nature.

# 2. CONCLUSIONS

The movement of NAPL in a porous medium environment can be described by a coupled set of non-linear partial differential equations that are generated by combining fundamental balance equations with constitutive and thermodynamic relationships. Three-phase coupled flow, including hysteresis and mass transfer effects, is considered. Examination of the literature suggests that the model provided above is the most physically comprehensive mathematical representation for the problem of defining the emplacement of NAPL residual. The ability to reproduce a physically complex NAPL experiment without calibration demonstrates that this model is a suitable real-world surrogate.

The nature of the model equations requires the use of a numerical technique to obtain a solution to physically meaningful problems. The method selected in this work, collocation finite elements, provides a very accurate solution for the examples tested, including one field application. The iterative procedure employed allows for the solution of three-dimensional problems on conventional computer systems.

# 3. RECOMMENDATIONS

While the work described herein provides an accurate, physically sophisticated simulator for NAPL , additional work on this software is recommended:

1. The solution algorithm, while adequate for small problems, is inappropriate for large, three-dimensional field applications. A faster, less computer - memory intensive solution technique is needed.

2. The new permeability-saturation-pressure relationship should be examined experimentally.

3. The current model allows for a single species NAPL. A multi-component NAPL capability would be an important extension.

4. More model verifications using carefully conducted experiments would be helpful. Comparisons between various currently existing models would be enlightening.

5. The model should be extended to accommodate various remediation strategies. Consider for example:

   **(a)** the use of surfactants and co-solvents for NAPL mobilization and removal;

   **(b)** the accommodation in the model of biochemical transformations;

   **(c)** the inclusion of the NAPL model into optimal design software;

   **(d)** the effect of thermal forcing (i. e., steam stripping).

# 4. THEORETICAL DEVELOPMENT

## 4.1. OVERVIEW

In this section a mathematical model based upon the attributes presented in the previous section will be developed. The mathematical model is made up of two major components: the mass balance equations which define the distribution in time and space of the primary variables, and the constitutive equations which define the inter-relationship between primary and secondary variables[1].

The balance equations describe the conservation of mass of each phase (fluid and solid) and each constituent within a particular phase (species) as they move and intermingle within a porous medium. One mass balance equation can be generated for each phase and constituent of interest. Each equation is composed of terms which define the various components of mass transport at the macroscopic scale: accumulation, advection, dispersion, external sources and sinks, and mass transfer between phases. Each term in turn is defined by a set of parameters which quantifies the physics of the transport process for a particular physical system.

In order to solve the resulting balance equations they must be augmented by a set of *constitutive relationships* which relate the primary and secondary variables. In the discussion which follows, the constitutive relationships are separated into four categories:

1. those which define the fluid properties *density*, *compressibility* and *viscosity*;
2. those which define fluid flow or *advection*;
3. those which define non-advective species transport, namely *dispersion*, and *diffusion;*
4. those which define *interphase mass exchange*.

[1]The primary variables are those which are advanced in time and space by solving the mass balance equations. The secondary variables are those variables which are functions of the primary variables.

As will be seen, while the constitutive relationships can be categorized as indicated, they exhibit inter-functional dependence through phase pressure, saturation and compositional dependence. Therefore, the equation set that is generated by combining the balance equations and the constitutive relationships is coupled and nonlinear.

Another outcome of this development is a list of primary variables which are used to solve the balance equations, and an outline of the simplifying assumptions employed thereby providing a basis for model applicability. Given proper initial and boundary conditions, the solution of the equation set will yield the phase volume and pressure distributions and the constituent concentrations in time and in space.

In the following discussion, the measurement unit scale representing a particular measurable quantity is written in brackets. For example, the units for fluid viscosity are $[M/(TL)]$, where $M$ represents *mass*, $T$ represents *time* and $L$ represents *length*.

## 4.2. MASS BALANCE EQUATIONS

As a point of departure, let us employ the equation development of Pinder and Abriola (1986). First, consider *the mass balance law for each fluid constituent*, an ordered pair $(\iota, \alpha)$ representing a species $\iota$ in a fluid phase $\alpha$:

$$\frac{\partial\left(\varepsilon S_\alpha \rho_\iota^\alpha\right)}{\partial t}+\boldsymbol{\nabla}\bullet[\varepsilon S_\alpha \rho_\iota^\alpha \mathbf{v}^\alpha]-\boldsymbol{\nabla}\bullet\left[\varepsilon S_\alpha \rho^\alpha \mathbf{D}^\alpha \bullet \boldsymbol{\nabla}(\frac{\rho_\iota^\alpha}{\rho^\alpha})\right]+\varepsilon S_\alpha \kappa_\iota^\alpha \rho_\iota^\alpha = \rho_\iota^\alpha Q^\alpha+\widehat{\rho}_\iota^\alpha \quad (4.1)$$

where the *five* constituents $(\iota, \alpha)$ relevant to this simulator are identified as: $(w, W)$,a water species in the water phase; $(n, W)$, a NAPL species in the water phase; $(n, N)$, a NAPL species in the NAPL phase; $(n, G)$, a NAPL species in the gas phase; and $(g, G)$, a gas species in the gas phase[2]. Other symbols occurring in equation 4.1 are used to represent the following:

$\varepsilon$ is the *porosity* of the porous medium.

$S_\alpha$ is the *saturation* of the $\alpha$-phase.

[2]The convention used to identify phase and species is that the phase is represented by upper-case letters [i. e., W (water), N (NAPL), G (gas), and S (solid)], and the components of the phase (species) are represented by lower-case letters [i. e., w (water), n (NAPL), g (gas)].

$\rho_\iota^\alpha$ is the *mass concentration* of species $\iota$ in the $\alpha$-phase $[M/L^3]$.

$\mathbf{v}^\alpha$ is the mass average *velocity* of phase $\alpha$, a vector $[L/T]$.

$\mathbf{D}^\alpha$ is the *dispersion coefficient* for the $\alpha$-phase, a symmetric second-order tensor $[L^2/T]$.

$Q^\alpha$ is the *point source* (+) or sink (-) $\alpha$-phase mass $[1/T]$.

$\kappa_\iota^\alpha$ is the *decay coefficient* for species $\iota$ in the $\alpha$-phase $[1/T]$.

$\widehat{\rho}_\iota^\alpha$ is the source or sink of mass for a species $\iota$ in the $\alpha$-phase $[M/L^3T]$ due to *interphase mass exchange* (i. e., dissolution, volatilization and adsorption).

The exchange of mass for each constituent in equation 4.1 is defined by:

$$\begin{aligned} \widehat{\rho}_w^W &= 0 \\ \widehat{\rho}_n^W &= E_n^W - E_{n/W}^G - E_{n/W}^S \\ \widehat{\rho}_n^N &= -\left(E_n^W + E_n^G\right) \\ \widehat{\rho}_n^G &= E_n^G + E_{n/W}^G \\ \widehat{\rho}_g^G &= 0 \end{aligned} \tag{4.2}$$

where

$E_n^W$ represents *dissolution mass transfer* of the NAPL species from the NAPL phase to the water phase;

$E_{n/W}^G$ represents *volatilization mass transfer* of the NAPL species from the water phase to the gas phase;

$E_n^G$ represents *volatilization mass transfer* of the NAPL species from the NAPL phase to the gas phase;

$E_{n/W}^S$ represents *adsorption mass transfer* of the NAPL species from the water phase to the soil.

A sixth mass balance equation is required to describe the NAPL species mass which is adsorbed onto the soil. This equation is written as:

$$\frac{\partial\left([1-\varepsilon]\rho^S\omega_n^S\right)}{\partial t} + [1-\varepsilon]\rho^S\kappa_n^S\omega_n^S = E_{n/W}^S \tag{4.3}$$

where $\rho^S$ is the density of the soil $[M/L^3]$ and $\omega_n^S$ is the *mass fraction* of the adsorbed NAPL on the solid [dimensionless]. As described in Section 4.8.2, the balance equation 4.3 is replaced by the following linear equilibrium relationship:

$$\omega_n^S = K_d \rho_n^W \tag{4.4}$$

where $K_d$ is a distribution coefficient $[L^3/M]$.

To ensure global mass conservation, the following definitions and constraints on fluid volume, density and mass exchange are employed:

1. The $\alpha$-phase saturations must sum to one:

$$S_W + S_N + S_G = 1 \tag{4.5}$$

2. The $\alpha$-phase mass density, $\rho^\alpha$ $[M/L^3]$, is the sum of the species mass concentrations in the $\alpha$-phase:

$$\rho^\alpha = \sum_{\iota=w,n,g} \rho_\iota^\alpha \ , \ \alpha = W, N, G \tag{4.6}$$

3. The sum of mass fluxes of all species $\iota$ into the $\alpha$-phase, must equal the total mass change in the $\alpha$-phase:

$$\widehat{\rho}^\alpha = \sum_{\iota=w,n,g} \widehat{\rho}_\iota^\alpha \ , \ \alpha = W, N, G \tag{4.7}$$

4. The total mass change over all phases must be zero:

$$\sum_{\alpha=W,N,G} \widehat{\rho}^\alpha = 0$$

5. The sum of the reacting mass must be equal to the sum of the produced mass:

$$\sum_{\iota=w,n,g} \kappa_\iota^\alpha \rho_\iota^\alpha = 0 \ , \ \alpha = W, N, G$$

A set of *fluid phase mass balance equations* can be generated by summing the balance equations 4.1 for each species within the phase, and by incorporating equations 4.2, 4.6 and 4.7. The three resulting fluid-phase mass balance equations are:

Water-phase:

$$\frac{\partial\left(\varepsilon S_W \rho^W\right)}{\partial t} + \boldsymbol{\nabla} \bullet \left[\varepsilon S_W \rho^W \mathbf{v}^W\right] = \rho^W Q^W + E_n^W - E_{n/W}^G - E_{n/W}^S \quad (4.8)$$

NAPL-phase:

$$\frac{\partial\left(\varepsilon S_N \rho^N\right)}{\partial t} + \boldsymbol{\nabla} \bullet \left[\varepsilon S_N \rho^N \mathbf{v}^N\right] = \rho^N Q^N - E_n^W - E_n^G \quad (4.9)$$

Gas-phase:

$$\frac{\partial\left(\varepsilon S_G \rho^G\right)}{\partial t} + \boldsymbol{\nabla} \bullet \left[\varepsilon S_G \rho^G \mathbf{v}^G\right] = \rho^G Q^G + E_n^G + E_{n/W}^G \quad (4.10)$$

With this development, the physical problem can be cast into a mathematical representation consisting of *five mass balance equations*. Of the balance equations written, the following five are used in the simulator:

**1 to 3)** The three fluid-phase balance equations, equations 4.8, 4.9 and 4.10. These equations define the temporal and spatial distribution and the flow properties of the water-, NAPL- and gas-phases throughout the domain.

**4 and 5)** The two NAPL species balance equations, equations 4.1 with $(\iota, \alpha) = (n, W)$ and $(n, G)$. These equations define the temporal and spatial distribution of the NAPL species as they are transported within and between their respective phases.

## 4.3. PRIMARY VARIABLES

Five primary (or dependent) variables are required to solve the balance equations listed in the previous Section. The five primary variables used in the simulator are:

$$\left\{P^W, S_W, S_{Tw}, \rho_n^W, \rho_n^G\right\} \quad (4.11)$$

where $P^W$ is the pressure in the water phase $[M/(LT^2)]$, and from equation 4.5 we have defined a new saturation measure,

$$S_{Tw} = S_W + S_N = 1 - S_G$$

called the *total liquid phase saturation*. These variables in 4.11 are defined such that they are continuous in time and space. In addition, they are intended to apply regardless of which phase configuration exists (i. e. one-, two-, or three-phase flow). The following constraints on the relationship between the pressure and saturation variables allow for this attribute to be implemented:

1. The *property of fluid wettability* is defined as, from most to least, water-NAPL-gas.

2. The *property of capillary pressure* between immiscible phases is defined as a function of phase saturation, called herein a saturation-pressure model ($S-P$ model), where $P_{c\alpha\beta} = P^{\alpha} - P^{\beta}$ is the capillary pressure between the nonwetting $\alpha$-phase and the wetting $\beta$-phase[3]. In addition when all three phases are present, the NAPL-phase renders the water-gas interactions negligible, and three-phase behavior can be gleaned from two, two-phase $S-P$ models[4]:

$$\begin{aligned} P_{cNW} &= P_{cNW}(S_W) = P^N - P^W \\ P_{cGN} &= P_{cGN}(S_{Tw}) = P^G - P^N \end{aligned} \tag{4.12}$$

3. The functions $P_{cNW}(S_W)$ and $P_{cGN}(S_{Tw})$ are defined such that:

   **(a)** they are continuous in time and space regardless of phase configuration;

   **(b)** for the two-phase water-gas case, $P_{cGW}$ is determined from:

$$P_{cGW} = P_{cNW} + P_{cGN} \tag{4.13}$$

   **(c)** $P_{cGW}$, $P_{cNW}$ and $P_{cGN}$ are related through the following scaling rule:

$$\frac{P_{cNW}}{\sigma_{NW}} = \frac{P_{cGN}}{\sigma_{GN}} = \frac{P_{cGW}}{\sigma_{GW}} \tag{4.14}$$

   where $\sigma_{GW}$, $\sigma_{NW}$ and $\sigma_{GN}$ are the interfacial tensions along the interfaces between the gas and water phases, the NAPL and water phases,

[3]Because the definition of the S-P model is an important component of this simulator, its development is detailed in Chapter 5.

[4]For the case when NAPL is the intermediate wetting fluid, $S_{Tw}$ is called the total wetting phase saturation. By convention the $S-P$ relationship is written in terms of the wetting phase saturation.

and the gas and NAPL phases, respectively. In order for equations 4.13 and 4.14 to be compatible, the interfacial tensions are constrained to be related by:

$$\sigma_{GW} - \sigma_{NW} - \sigma_{GN} = 0 \tag{4.15}$$

An important outcome of applying the capillary pressure scaling rule (equation 4.14) and the constraint of a neutral spreading coefficient (equation 4.15) is that, of the three capillary pressure relationships required to model two- and three-phase flow, *only one of the three relationships needs to be measured, with the other two gleaned from the use of equation 4.14.*

4. The NAPL and gas-phase pressures are nonlinear functions of $P^W$, $S_W$ and $S_{Tw}$ as indicated from the following definitions:

$$\begin{aligned} P^N &= P^W + P_{cNW}(S_W) \\ P^G &= P^W + P_{cNW}(S_W) + P_{cGN}(S_{Tw}) \end{aligned} \tag{4.16}$$

The constitutive models which define the relationships between the primary and secondary variables are derived with reference to the primary variables in 4.11 and the constraints imposed on the relation between fluid-phase pressure and saturation.

## 4.4. FLUID PROPERTIES

The $\alpha$-phase fluid properties of interest are the density, $\rho^\alpha[M/L^3]$, viscosity, $\mu^\alpha[M/(TL)]$, and the interfacial tension between immiscible phases $\alpha$ and $\beta$, $\sigma_{\alpha\beta}$ $[M/T^2]$. Under the assumption of isothermal conditions, these parameters are, in general, a function of the chemical makeup of the phase (i.e. phase composition) and the applied pressure (to the degree that it effects the phase properties via phase compressibility). Assuming that natural or induced pressure variations characteristic of applications involving near-surface soils in contact with the atmosphere are small (Sleep and Sykes, 1989, Mendoza and Frind, 1990, and Brusseau, 1991), *the dependance of fluid properties on pressure is neglected in this simulator.*

### 4.4.1. Density

The dependance of fluid density on composition is modeled as follows:

$$
\begin{aligned}
\rho^N &= \rho^{Nr} = \text{constant} \\
\rho^W &= \rho^{Wr} + \rho_n^W \left[1 - \frac{\rho^{Wr}}{\rho^{Nr}}\right] \qquad (4.17) \\
\rho^G &= \rho^{Gr} + \rho_n^G \left[1 - \frac{\rho^{Gr}}{\rho^{Nr}}\right] \qquad (4.18)
\end{aligned}
$$

where $\rho^{Wr}$, $\rho^{Nr}$ and $\rho^{Gr}$ are the mass densities of pure-phase water, NAPL and gas, respectively.

### 4.4.2. Viscosity

Fluid viscosities are modeled as a function of composition as follows:

$$
\begin{aligned}
\mu^N &= \text{constant} \\
\log \mu^W &= \left(\frac{\rho_n^W}{\rho^{Nr}}\right) \log \mu^{Nr} + \left(1 - \frac{\rho_n^W}{\rho^{Nr}}\right) \log \mu^{Wr} \qquad (4.19) \\
\log \mu^G &= \left(\frac{\rho_n^G}{\rho^{Nr}}\right) \log \mu^{Nr} + \left(1 - \frac{\rho_n^G}{\rho^{Nr}}\right) \log \mu^{Gr} \qquad (4.20)
\end{aligned}
$$

where $\mu^{Wr}$, $\mu^{Nr}$and $\mu^{Gr}$ are the pure liquid phase viscosities of the water, NAPL and gas, respectively.

### 4.4.3. Interfacial Tension

The interfacial tensions between fluid phases are assumed to be known constants. The combination of interfacial tension and contact angle defines fluid wettability. Regardless of the values of the interfacial tensions, the contact angle is assumed to be such that the fluid wetting order is constant, and follows, from most to least, water-NAPL-gas.

The interfacial tensions are used to scale the capillary pressures as indicated in equation 4.14. In addition, in order to model the general case where the number of phases saturating the pore space can vary over time between one, two and three, the simulator employes the algebraic constraints 4.13 and 4.15. Therefore, *only two of the interfacial tensions are independent with the third defined by equation 4.15. The two independent values can be considered fitting parameters.*

## 4.5. PHASE ADVECTION

Fluid flow is defined by the parameter $\mathbf{v}^\alpha$ in equations 4.1 and 4.8 through 4.10. The phase velocity is written in terms of the multiphase extension of Darcy's law:

$$\mathbf{v}^\alpha = -\frac{\mathbf{k}k_{r\alpha}}{\varepsilon S_\alpha \mu^\alpha} \bullet (\boldsymbol{\nabla} P^\alpha - \gamma^\alpha \boldsymbol{\nabla} z) \ , \alpha = W, N, G \tag{4.21}$$

where $P^\alpha$ is the $\alpha-$phase pressure $[M/(LT^2)]$, $\gamma^\alpha = \rho^\alpha g$ is the specific weight of the phase $[M/T^2]$, $g$ is the acceleration due to gravity $[L/T^2]$, $\mathbf{k}$ is the intrinsic permeability $[L^2]$, *considered a scalar herein*, and $k_{r\alpha}$ is the relative permeability.

The $\alpha-$phase relative permeability is a scaling factor, $0 \leq k_{r\alpha} \leq 1$, which accounts for the case where the porous medium is not fully saturated with the $\alpha-$phase. This parameter is in general a function of the $\alpha-$phase saturation. Given the assumption that the phase wetting-order is constant, and follows, from most to least, water-NAPL-gas, the following functional dependance is assumed:

$$\begin{aligned} k_{rW} &= k_{rW}(S_W) \\ k_{rN} &= k_{rN}(S_W, S_{Tw}) \\ k_{rG} &= k_{rG}(S_{Tw}) \end{aligned} \tag{4.22}$$

where the relationships listed reduce to their proper two-phase forms when appropriate. Since the definition of the relationship between the relative permeability and saturation (called herein the $k-S$ model) is a major component of this simulator, it is developed from both a conceptual and empirical viewpoint in Chapter 5.

Given that $P^W$, $S_W$ and $S_{Tw}$ are the primary flow variables, and that the phase pressures are related to one another through capillary pressure relationships, 4.12 and 4.13, the form of equation 4.21 for each fluid phase of interest is detailed here as:

$$\begin{aligned} \mathbf{v}^W &= -\frac{\mathbf{k}k_{rW}}{\varepsilon S_W \mu^W} \bullet \left(\boldsymbol{\nabla} P^W - \gamma^W \boldsymbol{\nabla} z\right) \\ \mathbf{v}^N &= -\frac{\mathbf{k}k_{rN}}{\varepsilon S_N \mu^N} \bullet \left(\boldsymbol{\nabla} \left(P^W + P_{cNW}\right) - \gamma^N \boldsymbol{\nabla} z\right) \\ \mathbf{v}^G &= -\frac{\mathbf{k}k_{rG}}{\varepsilon S_G \mu^G} \bullet \left(\boldsymbol{\nabla} \left(P^W + P_{cNW} + P_{cGN}\right) - \gamma^G \boldsymbol{\nabla} z\right) \end{aligned} \tag{4.23}$$

## 4.6. DISPERSION COEFFICIENT

The dispersive flux of the NAPL species in both the water and gas phases is defined by the third term in equation 4.1. For the case where phase density is related to phase composition as defined in equations 4.17 and 4.18 the dispersion term in equation 4.1 is simplified as:

$$\rho^{\alpha}\mathbf{D}^{\alpha} \bullet \boldsymbol{\nabla}(\frac{\rho_{\iota}^{\alpha}}{\rho^{\alpha}}) \approx \left(\frac{\rho^{\alpha r}}{\rho^{\alpha}}\right)\mathbf{D}^{\alpha} \bullet \boldsymbol{\nabla}\rho_{\iota}^{\alpha} \tag{4.24}$$

This relationship shows that if $\rho^{\alpha}$ is a constant equal to $\rho^{\alpha r}$, then the standard definition for dispersive flux applies, but if $\rho^{\alpha}$ is a function of phase composition, then dispersive flux becomes a nonlinear function of concentration.

The dispersion coefficient, $\mathbf{D}^{\alpha}$, is a second-rank tensor, and its components in ($x$, $y$, $z$) Cartesian coordinates are represented as (Scheidegger, 1961):

$$\begin{aligned}
D_{xx}^{\alpha} &= a_T^{\alpha}\left|v^{\alpha}\right| + \left(a_L^{\alpha} - a_T^{\alpha}\right)\left(v_x^{\alpha}\right)^2 / \left|v^{\alpha}\right| + \tau^{\alpha} D_m^{\alpha} \\
D_{yy}^{\alpha} &= a_T^{\alpha}\left|v^{\alpha}\right| + \left(a_L^{\alpha} - a_T^{\alpha}\right)\left(v_y^{\alpha}\right)^2 / \left|v^{\alpha}\right| + \tau^{\alpha} D_m^{\alpha} \\
D_{zz}^{\alpha} &= a_T^{\alpha}\left|v^{\alpha}\right| + \left(a_L^{\alpha} - a_T^{\alpha}\right)\left(v_z^{\alpha}\right)^2 / \left|v^{\alpha}\right| + \tau^{\alpha} D_m^{\alpha} \\
D_{xy}^{\alpha} &= D_{yx}^{\alpha} = \left(a_L^{\alpha} - a_T^{\alpha}\right) v_x^{\alpha} v_y^{\alpha} / \left|v^{\alpha}\right| \\
D_{yz}^{\alpha} &= D_{zy}^{\alpha} = \left(a_L^{\alpha} - a_T^{\alpha}\right) v_y^{\alpha} v_z^{\alpha} / \left|v^{\alpha}\right| \\
D_{xz}^{\alpha} &= D_{zx}^{\alpha} = \left(a_L^{\alpha} - a_T^{\alpha}\right) v_x^{\alpha} v_z^{\alpha} / \left|v^{\alpha}\right|
\end{aligned} \tag{4.25}$$

where $\alpha$ = W and G, $a_L^{\alpha}$ is the longitudinal dispersivity [L], $a_T^{\alpha}$ is the transverse dispersivity [L], $v_x^{\alpha}$, $v_y^{\alpha}$ and $v_z^{\alpha}$ are the components of the interstitial pore water velocity vector (equation 4.21), $|v^{\alpha}|$ is the mean phase velocity magnitude, $D_m^{\alpha}$ is the $\alpha$-phase coefficient of molecular diffusion [$L^2$/T], and $\tau^{\alpha}$ accounts for diffusion porosity and tortuosity effects [dimensionless]. The approximation for $\tau^{\alpha}$ used in the simulator is provided by the Millington and Quirk (1961) model:

$$\tau^{\alpha} = \varepsilon^{1/3}\left(S_{\alpha}\right)^{7/3}$$

## 4.7. NATURAL DEGRADATION

Many NAPL's are subject to biological and chemical degradation in the soil, and therefore they are not stable in the natural environment. To account for this natural attenuation phenomenon a constant first-order degradation rate is

assumed for account for all degradation processes. With this, the decay coefficients in equation 4.1, $\kappa_n^W$ and $\kappa_n^G$ $[1/T]$, are defined in terms of the half-life, $t_{1/2}$ $[T]$, of the NAPL species as:

$$\kappa_n^W = \kappa_n^G = \ln(2)/t_{1/2} \tag{4.26}$$

where the assumption is made that $t_{1/2}$ is the same for the NAPL species in the gas and water phases.

## 4.8. MASS TRANSFER

To obtain a perspective on current research applications in mass transfer processes affecting the fate of NAPLs in near surface granular soils, consider Figures 4.1, 4.2 and 4.3 which summarize relevant publications. Upon review of these figures the following conclusions can be drawn:

1. Four types of mass transfer processes are important in defining the physics of the fate of NAPLs in near surface granular soils:

   **(a)** dissolution mass transfer of pure phase NAPL to the water phase;

   **(b)** evaporation mass transfer of pure phase NAPL to the gas phase;

   **(c)** evaporation mass transfer of NAPL species in the water phase to the gas phase;

   **(d)** adsorption mass transfer of NAPL species in the water phase to the soil phase.

   Adsorption of NAPL species in the gas phase directly to the soil phase is neglected.

2. Three basic mass transfer models are typically utilized :

   **(a)** *Local equilibrium model:* (indicated by 'E' in the review figures) Based on the assumption that equilibrium partitioning dictates NAPL phase concentrations. This model-type has been shown to have utility in problems involving low Darcy velocities and homogeneous soil properties.

| reference | phases and components considered | exchange processes modeled | kinetic process | parameter variability | investigation type | comment |
|---|---|---|---|---|---|---|
| Armstrong et al. (1994) | $S_W>0$, $k_{rW}=0$<br>$S_G>0$, $k_{rG}>0$<br>$S_N=0$<br>$\rho_n^G$, $\rho_n^W$, $\omega_n^S$ | $\hat{\rho}_{n/W}^G$ Henry's law − E and K<br>$\hat{\rho}_n^W$ E and K<br>$\hat{\rho}_{n/W}^S$ organic carbon partitioning − E and K | diffusive boundary layer | constant rate coefficients<br>variable temperature and soil properties<br>$P^G$ = constant<br>$S_W$ = constant<br>$\rho^G$ = f(composition) | numerical model: advective/ dispersive gas−phase transport | • focus on soil gas venting application<br>• rate−limited gas−water mass transfer is the controlling process for the time−scale chosen<br>• first−order kinetic is adequate<br>• cannot calibrate the model with effluent concentrations |
| Mendoza and Frind (1990) | $S_W>0$, $k_{rW}=0$<br>$S_G>0$, $k_{rG}>0$<br>$S_N=0$<br>$\rho_n^G$, $\omega_n^S$ | $\hat{\rho}_{n/W}^G$ Henry's law − E<br>$\hat{\rho}_{n/W}^S$ organic carbon partitioning − E | N/A | isothermal<br>$P^G$ = constant<br>$S_W$ = constant<br>$\rho^G$ = f(composition)<br>$\mu^G$ = f(composition)<br>looked at layered soils | numerical model: advective/ dispersive gas−phase transport | • density−driven gas−phase transport is important when NAPL source is present and in high−K soils<br>• three important transport processes: diffusion, density−driven advection, vapor source mass flux |
| Sleep and Sykes (1989) | $S_W>0$, $k_{rW}>0$<br>$S_G>0$, $k_{rG}>0$<br>$S_N>0$, $k_{rN}=0$<br>$\rho_n^G$, $\rho_n^W$ | $\hat{\rho}_{n/W}^G$ Henry's law − K<br>$\hat{\rho}_n^W$ K | diffusive boundary layer | constant rate coefficients<br>uncoupled water−gas flow<br>$P^G$ = constant<br>$S_N$ = constant<br>$\rho^W$ = constant<br>$\rho^G$ = f(composition) | numerical model: advective/ dispersive gas− and water−phase transport | • density−driven gas−phase transport is important<br>• neglected the effects of capillarity |
| Falta et al. (1989) | $S_W>0$, $k_{rW}=0$<br>$S_G>0$, $k_{rG}>0$<br>$S_N>0$, $k_{rN}=0$<br>$\rho_n^G$, $\omega_n^S$ | $\hat{\rho}_{n/W}^G$ Henry's law − E<br>$\hat{\rho}_{n/W}^S$ organic carbon partitioning − E | N/A | get saturated vapor conc− entration from ideal gas law<br>homogeneous soil<br>$S_W$= constant<br>$S_N$ = constant<br>$\mu^G$ = constant<br>$\rho^G$ = f(composition) | numerical model: advective/ dispersive gas−phase transport | • the magnitude of density−driven gas−phase flow velocity varies linearly with K and density contrast between pure and contaminated gas<br>• need to look at: soil heterogeneity, multi−component organic liquids, the effect of gas−phase pressure forcing |

Figure 4.1: Summary of recent studies of mass exchange processes in NAPL contaminated soils.

| reference | phases and components considered | exchange processes modeled | kinetic process | parameter variability | investigation type | comment |
|---|---|---|---|---|---|---|
| Brusseau (1991) | $S_W>0$, $k_{rW}=0$<br>$S_G>0$, $k_{rG}>0$<br>$S_N=0$<br>$\rho_n^G$ , $\rho_n^W$ , $\omega_n^S$ | $\hat{\rho}_{n/W}^G$ Henry's law − E<br>$\hat{\rho}_{n/W}^S$ organic carbon partitioning − E and K | diffusive boundary layer | constant rate coefficients<br>variable soil properties<br>isothermal<br>$P^G$ = constant<br>$S_W$ = constant<br>$\rho^G$ = constant | numerical model: advective gas−phase transport | • focus on rate−limited sorption<br>• differentiate between advective and non−advective domains<br>• for gas−phase transport: Darcy's and Fick's laws apply<br>• the limiting mass transfer step is solid to water for water at residual |
| Brusseau (1992) | $S_W>0$, $k_{rW}>0$<br>$S_G=0$<br>$S_N>0$, $k_{rN}=0$<br>$\rho_n^W$ , $\omega_n^S$ | $\hat{\rho}_n^W$ E and K<br>$\hat{\rho}_{n/W}^S$ E and K | diffusive boundary layer | constant rate coefficients<br>multi−component NAPL<br>heterogeneous soil due to residual NAPL<br>isothermal<br>$S_N$ = constant | numerical model: advective/ dispersive water−phase transport | • focus on rate−limited mass transfer<br>• heterogeneity due to NAPL residual greatly affects mass transfer<br>• rate−limited mass transfer is an important consideration under reduced−gradient conditions |
| Rabideau and Miller (1994) | $S_W=1$<br>$\rho_n^W$ , $\omega_n^S$ | $\hat{\rho}_{n/W}^S$ E and K | diffusive boundary layer | constant rate coefficients<br>layered soils | numerical model: pump−and−treat application | • when $S_N = 0$, mass transfer is most sensitive to spatially variable K and sorption capacity, and/or sorption non−equilibrium with heterogeneity dominating |
| Powers et al. (1991 and 1992) | $S_W>0$, $k_{rW}>0$<br>$S_G=0$<br>$S_N>0$, $k_{rN}=0$<br>$\rho_n^W$ | $\hat{\rho}_n^W$ E and K | first−order mass transfer | variable rate coefficients<br>homogeneous soils<br>consider variable NAPL saturation and residual blob shape | numerical model: pump−and−treat application | • rate−limited mass transfer is important for spills of small areal extent, high Darcy velocities, large blob sizes, and low residual $S_N$ |
| Miller et al. (1990)<br>Imhoff et al. (1992) | $S_W>0$, $k_{rW}>0$<br>$S_G=0$<br>$S_N>0$, $k_{rN}=0$<br>$\rho_n^W$ | $\hat{\rho}_n^W$ K | first−order mass transfer | variable rate coefficients<br>homogeneous soils<br>consider variable NAPL saturation and residual blob shape | experimental: determine rate−coefficient parameters | • diffusive boundary layer is an inadequate exchange model<br>• exchange rate is a strong function of water velocity and NAPL saturation |

Figure 4.2: Continued: Summary of recent studies of mass exchange processes in NAPL contaminated soils.

| reference | phases and components considered | exchange processes modeled | kinetic process | parameter variability | investigation type | comment |
|---|---|---|---|---|---|---|
| Sleep and Sykes (1993a, b) | $S_W>0$, $k_{rW}>0$<br>$S_G>0$, $k_{rG}>0$<br>$S_N>0$, $k_{rN}>0$<br>$\rho_n^G$, $\rho_n^W$, $\omega_n^S$ | $\hat{\rho}_{n/W}^G$ Henry's law − E<br>$\hat{\rho}_n^W$ E<br>$\hat{\rho}_n^G$ E<br>$\hat{\rho}_{n/w}^s$ organic carbon partitioning −E | N/A | phase densities are a function of pressure and composition<br>phase viscosities are a function of composition<br>heterogeneous soil<br>multi−component NAPL<br>isothermal | numerical model: 3−phase, 3D compositional simulator | • multi−component DNAPL rem−ediation in heterogeneous soil at the field−scale<br>• investigate the effect that infiltrating water fronts have on DNAPL vapor transport |
| Falta et al. (1992a, b) | $S_W>0$, $k_{rW}>0$<br>$S_G>0$, $k_{rG}>0$<br>$S_N>0$, $k_{rN}>0$<br>$\rho_n^G$, $\rho_n^W$, $\omega_n^S$ | $\hat{\rho}_{n/W}^G$ Henry's law − E<br>$\hat{\rho}_n^W$ E<br>$\hat{\rho}_n^G$ E<br>$\hat{\rho}_{n/w}^s$ organic carbon partitioning −E | N/A | use ideal gas law for gas−phase properties<br>gas not a function of P<br>fluid properties are a function of composition and temperature<br>homogeneous soils<br>single−component NAPL | numerical model: 3−phase steam injection simulations | • local chemical and thermal equilibrium<br>• NAPL saturation allowed to go to 0, but water and gas saturations forced to be >0 |
| Delshad et al. (1995) | $S_W>0$, $k_{rW}>0$<br>$S_G>0$, $k_{rG}>0$<br>$S_N>0$, $k_{rN}>0$<br>$\rho_n^W$ | $\hat{\rho}_n^W$ K | first−order kinetic | use ideal gas law for gas−phase properties<br>water properties are a function of composition<br>NAPL properties are constant<br>heterogeneous soils<br>single−component NAPL<br>non−isothermal | numerical model: 3−phase NAPL remediation using surfactants | • model emplacement of residual NAPL and rate−limited NAPL dissolution<br>• fluid properties a function of surfactant concentration<br>• residual NAPL a function of capillary and Bond numbers<br>• compare results with field data |
| Guarnaccia et al. (1997) | $S_W>0$, $k_{rW}>0$<br>$S_G>0$, $k_{rG}>0$<br>$S_N>0$, $k_{rN}>0$<br>$\rho_n^G$, $\rho_n^W$, $\omega_n^S$ | $\hat{\rho}_{n/W}^G$ Henry's law − K<br>$\hat{\rho}_n^W$ K<br>$\hat{\rho}_n^G$ K<br>$\hat{\rho}_{n/w}^s$ organic carbon partitioning −E | first−order kinetic | water and gas density and viscosity are a function of NAPL concentration<br>fluid properties not a function of P or T<br>heterogeneous soils<br>single−component NAPL with constant properties | numerical model: 3−phase NAPL remediation | • model emplacement of residual NAPL and volatilization, dissolution and adsorption mass transfer |

Figure 4.3: Continued: Summary of recent studies of mass exchange processes in NAPL contaminated soils.

**(b)** *Rate-limited mass exchange model*: (indicated by 'K' in the review figures) Based on the assumption that mass transfer between phases is limited by diffusive transport across a stagnant boundary layer according to Fick's law (diffusive boundary layer). The model has limited utility because the thickness of the boundary layer cannot be estimated, and it neglects advective, viscosity- and density-driven processes.

**(c)** *First-order kinetic mass transfer model*: (indicated by 'K' in the review figures) More general than the rate-limited mass exchange model in that it considers advective- diffusive processes and changing interfacial contact area. Theoretical considerations and experimental data are used to define the functional form of the coefficients.

3. The use of rate-limited mass transfer provides predictive flexibility, as local equilibrium conditions can be simulated by increasing the rate coefficient.

4. Factors which favor rate-limited mass transfer include: heterogeneous soils, inhomogeneous residual distribution, inhomogeneous blob size distribution, and high fluid flow rates.

5. Modeling pump-and-treat remediation of NAPL-contaminated soils must include rate-limited mass transfer to mimic both experimental- and field-scale data, specifically effluent concentration tailing.

6. With respect to modelling desorption of NAPL from liquid unsaturated soils, where the transport path of an adsorbed NAPL species is soil-to-water, water-to-gas, data suggests that one need consider only one of the mass transfer processes as rate limited since the rate-limited process will dictate the overall mass entering the gas phase.

7. Henry's law is usually used to define vapor concentrations of a NAPL species dissolved in the water phase.

8. The amount of NAPL mass which can be adsorbed onto the soil is usually defined using an organic carbon-based model.

### 4.8.1. Liquid-Liquid Mass Transfer

When the organic phase is at an immobile residual state, saturation is no longer considered a function of capillary pressure since capillary pressure becomes undefined. Consider the NAPL phase balance equation 4.9 for the case of an immobile

residual with constant phase density, constant porosity, and no external sources or sinks. For these conditions equation 4.9 reduces to:

$$\varepsilon \rho^N \frac{\partial S_N}{\partial t} = -E_n^W - E_n^G \tag{4.27}$$

This equation states that change in NAPL saturation is due to mass transfer processes.

The dissolution model defining the mass exchange term, $E_n^W$, is assumed to be a first-order kinetic-type reaction of the form:

$$E_n^W = C_n^W \left( \overline{\rho}_n^W - \rho_n^W \right) \tag{4.28}$$

where $C_n^W$ $[1/T]$ is the rate coefficient which regulates the rate at which equilibrium is reached, and $\overline{\rho}_n^W$ $[M/L^3]$ is the equilibrium concentration of the NAPL species in the water phase (solubility limit). In the simulator, $\overline{\rho}_n^W$ is assumed to be a measurable constant value.

To determine the parametric from of $C_n^W$, the work of Imhoff et al. (1992) is employed. They conducted column experiments designed to study dissolution kinetics of residual trichloroethylene (TCE) in a uniform sand by flushing the system with clean water and tracking the dissolution front as a function of time. Using a lumped parameter model, they derived the following power-law relationship for $C_n^W$:

$$C_n^W = \beta_1^{WN} (\varepsilon S_N)^{\beta_2} \left| v^W \right|^{\beta_3} \tag{4.29}$$

where$\beta_2 \approx 0.5$ and $\beta_3 \approx 1.0$ are dimensionless fitting parameters. The parameter $\beta_1^{WN}$ $[1/T]$ is the rate coefficient, and it is fit to available experimental- or field-scale data.

The volatilization model defining the mass exchange term, $E_n^G$, is assumed to follow a similar model as for dissolution, i. e.:

$$E_n^G = C_n^G \left( \overline{\rho}_n^G - \rho_n^G \right) \tag{4.30}$$

where $C_n^G$ $[1/T]$ is the *rate coefficient* which regulates the rate at which equilibrium is reached, and $\overline{\rho}_n^G$ $[M/L^3]$ is the constant equilibrium vapor concentration of the NAPL species in the gas phase (vapor solubility limit). The rate coefficient, $C_n^G$ is assumed to have the form:

$$C_n^G = \beta_1^{GN} (\varepsilon S_N)^{\beta_2} \tag{4.31}$$

where$\beta_2$ is the same as for the dissolution model, and $\beta_1^{GN}$ [1/T] is fit to available data.

Consider now the volatilization of a dissolved NAPL species in the water phase to the gas phase. Assuming that the water phase is at residual saturation in the vadose zone, and that there are no external sources or sinks of mass, then equation 4.8 can be written as:

$$\varepsilon S_W \frac{\partial \rho^W}{\partial t} = E_n^W - E_{n/W}^G - E_{n/W}^S \tag{4.32}$$

where the exchange term $E_n^W$ is defined in equation 4.28, and $E_{n/W}^G$ governs the volatilization mass transfer of a dissolved NAPL species in the water phase to the gas phase:

$$E_{n/W}^G = C_{n/W}^G \left( H\rho_n^W - \rho_n^G \right) \tag{4.33}$$

where $H$ is the dimensionless Henry's law coefficient which is defined at equilibrium conditions as follows:

$$H = \rho_n^G / \rho_n^W$$

and $C_{n/W}^G$ $[1/T]$ is the mass transfer rate coefficient which is assumed to be defined by the power law:

$$C_{n/W}^G = \beta_1^{GW} (\varepsilon S_W)^{\beta_2} \tag{4.34}$$

where the fitting parameter $\beta_2$ is assumed to be the same as for the liquid-liquid mass transfer models, and $\beta_1^{GW}$ $[1/T]$ is fit to the available data.

### 4.8.2. Liquid-Solid Mass Transfer

Finally, mass exchange due to adsorption, $E_{n/W}^S$, is assumed to be defined by a linear equilibrium model:

$$\omega_n^S = K_d \rho_n^W \tag{4.35}$$

where $K_d$ is the distribution coefficient $[L^3/M]$ defined as a function of the organic carbon content of the soil and the relative hydrophobicity of the dissolved NAPL species:

$$K_d = f_{oc} K_{oc} \tag{4.36}$$

where $f_{oc}$ is the mass fraction of organic carbon and $K_{oc}$ is the organic carbon partition coefficient. Combination of equations 4.3 and 4.35 yields the following definition for $E_{n/W}^S$:

$$E_{n/W}^S = \rho^b K_d \left( \frac{\partial \rho_n^W}{\partial t} + \kappa_n^S \rho_n^W \right) \tag{4.37}$$

where $\rho^b = [1 - \varepsilon]\rho^S$ is the bulk density of the soil.

## 4.9. SUMMARY

The physical problem can be cast into a mathematical representation consisting of five mass balance equations: *three fluid-phase balance equations* [equations 4.8, 4.9 and 4.10], and *two NAPL species balance equations* [equations 4.1 with $(\iota, \alpha) = (n, W)$ and $(n, G)$].

The five primary variables used in the simulator to solve the balance equations are $P^W, S_W, S_{Tw}, \rho_n^W$ and $\rho_n^G$. All other parameters which constitute the balance equations are assumed to be known physical constants or functions of the primary variables.

The required physical constants are:

1. The reference fluid properties density and viscosity: $\rho^{Wr}$, $\rho^{Nr}$, $\rho^{Gr}$, $\mu^{Wr}$, $\mu^{Nr}$, $\mu^{Gr}$.

2. The interfacial tensions, $\sigma_{GW}$, $\sigma_{NW}$ and $\sigma_{GN}$. These parameters are used to scale the capillary pressures as per equation 4.14. Their magnitudes are constrained to be related by equation 4.15. This constraint is required to model the general case of two- and three-phase flow. The two independent values can be considered fitting parameters.

3. The parameters which define water- and gas-phase dispersion: $a_L^W$, $a_T^W$, $D_m^W$, $a_L^G$, $a_T^G$, $D_m^G$.

4. The parameters which define the mass transfer include: the rate coefficients: $\beta_1^{NW}$, $\beta_1^{GN}$, $\beta_1^{GW}$ and the fitting parameters: $\beta_2$, $\beta_3$, the solubility limits: $\overline{\rho}_n^W$, $\overline{\rho}_n^G$, the Henry's law coefficient: $H$, and the organic carbon-based partitioning parameters: $f_{oc}$, $K_{oc}$,

5. Soil properties porosity and permeability, where permeability is assumed to be a scalar.

The constitutive relationships which relate the primary and secondary variables are:

1. The saturation-pressure model ($S - P$ model) is predicated on the assumption that phase wetting follows, from most to least, water-NAPL-gas, and

when all three phases are present, only two saturation-capillary pressure functions exist, $P_{cNW}(S_W)$ and $P_{cGN}(S_{Tw})$. Requiring that

- $P_{cNW}(S_W)$ and $P_{cGN}(S_{Tw})$ are continuous in time and space regardless of phase configuration,
- $P_{cGW} = P_{cNW} + P_{cGN}$, and
- the capillary pressures are related through interfacial tension scaling, equation 4.14,

allows the simulator to model the general case of two- and three-phase flow without changing primary variables. An in depth presentation of the $S - P$ model is provided in Chapter 5.

2. The saturation-pressure model ($k - P$ model) is given by equation 4.22. A detailed discussion of these functional dependencies is provided in Chapter 5.

3. The density and viscosity of the water and gas phases are functions of NAPL species mass concentrations only, equations 4.17, 4.18, 4.19 and 4.20;

4. The phase velocity is defined using Darcy's law, equation 4.21, and it is considered for the three phases and two species of interest.

5. The phase dispersion coefficient is defined by equation 4.25, and it is used to define the dispersive mass flux of the NAPL species in the water- and gas-phases.

6. The following predictive mass transfer models are employed:

- a first order kinetic model for dissolution and volatilization mass transfer, equations 4.28, 4.30 and 4.33; and
- an equilibrium adsorption/desorption model, equation 4.35.

# 5. HYSTERETIC κ-S-P MODEL

With respect to modeling three-phase flow in porous media, a substantial amount of research defining appropriate constitutive relationships exists in both the petroleum reservoir and the water resources literature. From an historical perspective, the development and application of many of the basic physical models quantifying the physics of three-phase flow in porous media appeared first in the petroleum reservoir literature. These models are applied to predictive modeling of oil and natural gas recovery from petroleum reservoirs. This early work is summarized in the books of Collins (1961), Aziz and Settari (1979), and Marle (1981).

Relatively recently, the problem of quantifying the spatial and temporal distribution of NAPL's in the mobile or immobile residual state, due to surface or near-surface release(s), has become a major concern in the water resources area. All of the predictive models derived for this application are built upon the applicable theoretical underpinnings previously derived in the petroleum reservoir literature. However, because of the substantially different physical problem (geologic environment, fluid properties and driving forces), and engineering goals (NAPL recovery techniques) encountered within the two disciplines, there is a need to augment existing theory for petroleum reservoir applications, and to develop new sub-models to describe physical processes unique to water resources applications.

Considering this perspective, a review of the state-of-the-art modeling tools available to describe three-phase flow in near-surface granular soils is provided in Figures 5.1 and 5.2. These summary figures highlight the major physical model components, where the $S-P$ model describes the functional relationship between saturation and capillary pressure, and the $k-S$ model describes the functional relationship between the relative permeability and saturation. In addition the following parameters are defined: $S_\alpha$, $\alpha$ = W (water), N (NAPL), and G (gas), is the $\alpha$-phase saturation (the percent of the pore space occupied by the $\alpha$-phase), $S_{Tw} = S_W + S_N$ is the total liquid saturation, $P_{c\alpha\beta} = P^\alpha - P^\beta$, is the capillary pressure between nonwetting and wetting immiscible fluids $\alpha$ and $\beta$, respectively,

and $k_{r\alpha}$, $\alpha$ = W, N, G, is the $\alpha$-phase relative permeability (scales the intrinsic permeability to account for variable $\alpha$-phase saturation).

Based on conclusions able to be drawn from review of the models summarized in Figures 5.1 and 5.2, a relative permeability-saturation-capillary pressure model ($k - S - P$ model) is derived which:

1. is capable of modeling the simultaneous flow of a water phase (W), NAPL phase (N), and gas phase (G);
2. is based on wettability considerations and two-phase data;
3. reduces to the appropriate two-phase and single-phase cases;
4. employs capillary pressure scaling to accommodate variable soil and fluid properties;
5. includes flow-path, history-dependent functionals (hysteresis);
6. includes a mechanism for fluid entrapment as it is displaced from the pore space.

For completeness and clarity in presentation the concepts which characterize the $k - S - P$ model that were introduced in Chapter 4 will be reiterated herein. The presentation of the three-phase hysteretic $k - S - P$ model is organized as follows. First, a set of physical and model constraints which will allow for the accommodation of attributes 1 through 4 above will be presented. This will provide a basis for the definition of functional dependency. Second, with this conceptual model as a foundation, a closed-form empirical $k - S - P$ model which incorporates attributes 5 and 6 above will be developed as a series of three interrelated sub-models: entrapment/release, saturation-pressure, and relative permeability-saturation. In addition, for clarity, the $k - S - P$ model will be developed first for the two-phase case. The two-phase model will then be augmented to accommodate three-phase flow. Third, a section is included which addresses $k - S - P$ model implementation issues. These issues include details on how certain model parameters affect the shape of the $k - S - P$ functionals, and details on the definition of a set of computations which will ensure that the functionals generated are well behaved and amenable to inclusion into a numerical model. Finally, the use of capillary pressure scaling in the simulator to account for variable fluid and soil properties is discussed.

| reference | S−P model | k−S model | hyster−esis | entrap−ment | numerical model | air phase pressure | $P_C$ scaling | verification | comment |
|---|---|---|---|---|---|---|---|---|---|
| Eckberg and Sunada (1984) | $S_W(P_{cNW})$ $S_{Tw}(P_{cGN})$ | N/A | no | no | yes | constant | none | laboratory experiment | Drainage only; $S_W(P_{cNW})$ was a good predictor, $S_{Tw}(P_{cGN})$ was not. |
| Abriola (1984) Pinder and Abriola (1986) | $S_W(P_{cNW})$ $S_{Tw}(P_{cGW})$ | $k_{rW}(S_W)$ $k_{rN}(S_W,S_G)$ | no | no | yes | constant | none | 2−phase data only | Assume this model is applicable when water is mobile. |
| Faust (1985) Faust et al. (1989) | $S_W(P_{cNW})$ $S_{Tw}(P_{cGN})$ | $k_{rW}(S_W)$ $k_{rN}(S_W,S_G)$ | no | no | yes | constant | none | field data | Field−scale simulations |
| Parker et al. (1987), Kuppusamy et al. (1989), Lenhard and Parker (1988), Lenhard et al. (1988), Kaluar−achchi and Parker (1989) | $S_W(P_{cNW})$ $S_{Tw}(P_{cGN})$ | $k_{rW}(S_W)$ $k_{rN}(S_W,S_G)$ $k_{rG}(S_G)$ | no | no | yes | constant | surface tension | laboratory experiment | • analysis of monotonic drainage<br>• discrepancies in $S_{Tw}(P_{cGN})$ funct−ional due to constant gas presure assumption<br>• surface tension scaling is a valuable tool if real data is not available<br>• 1−way transition from W−G to W−N−G system<br>• poor mass balance reported |
| Parker and Lenhard (1987) Lenhard and Parker (1987), Lenhard et al. (1989), Lenhard(1992) | $S_W(P_{cNW})$ $S_{Tw}(P_{cGN})$ | $k_{rW}(S_W)$ $k_{rN}(S_W,S_G)$ $k_{rG}(S_G)$ | both S−P and k−S | NAPL by water, gas by water and NAPL | yes | constant | surface tension | 2−phase S−P model by lab−oratory experiment | • surface tension scaling provided qualitatively good results<br>• need to better determine nonwetting phase residual saturations<br>• a wetting phase cannot be trapped by a nonwetting phase<br>• numerical experiments indicate that entrapment processes dominate the solution |
| Ferrand et al. (1990) | $S_W(P_{cNW})$ $S_{Tw}(P_{cGN})$ | N/A | no | no | no | constant | surface tension | laboratory experiment | Drainage only; S−P model was adequate except near residual |

Figure 5.1: Summary of conceptual and numerical models describing three-phase flow in granular soils.

| reference | S–P model | k–S model | hyster–esis | entrap–ment | numerical model | air phase pressure | $P_C$ scaling | verification | comment |
|---|---|---|---|---|---|---|---|---|---|
| Forsyth and Shao (1991) Huyakorn et al. (1994) | $S_W(P_{cNW})$ $S_{Tw}(P_{cGN})$ | $k_{rW}(S_W)$ $k_{rN}(S_W,S_G)$ $k_{rG}(S_G)$ | no | force constant NAPL residual | yes | variable | none | none | • use a blending parameter to force a smooth transition between 2– and 3–phase functionals<br>• force a constant residual NAPL by modifying $k_{rN}$ functional |
| Falta et al. (1992a,b) | $S_W(P_{cNW})$ $S_{Tw}(P_{cGW})$ | $k_{rW}(S_W)$ $k_{rN}(S_W,S_G)$ $k_{rG}(S_G)$ | no | force constant NAPL residual | yes | variable | surface tension | laboratory experiment | • put constraint on interfacial tensions to ensure proper S–P functionals for 2– and 3–phase flow<br>• force a constant residual NAPL by modifying $k_{rN}$ functional |
| Essaid et al. (1993) | $S_W(P_{cNW})$ $S_{Tw}(P_{cGN})$ | $k_{rW}(S_W)$ $k_{rN}(S_W,S_G)$ | S–P model only | NAPL by water, gas by NAPL | yes | constant | surface tension and per–meability | field data | Hysteresis, entrapment and variation in hydraulic properties are the most important modeling features |
| Sleep and Sykes (1993a, b) Sleep (1995) | $S_W(P_{cNW})$ $S_{Tw}(P_{cGN})$ | $k_{rW}(S_W)$ $k_{rN}(S_W,S_G)$ $k_{rG}(S_G)$ | no | force constant NAPL residual | yes | variable | surface tension | compare with analytical | • put constraint on interfacial tensions to ensure proper S–P functionals for 2– and 3–phase flow<br>• force a constant residual NAPL by modifying $k_{rN}$ functional |
| Van Geel and Sykes (1995a, b) | $S_W(P_{cNW})$ $S_{Tw}(P_{cGN})$ | $k_{rW}(S_W)$ $k_{rN}(S_W,S_G)$ $k_{rG}(S_G)$ | no | NAPL by water, gas by water and NAPL | yes | variable | surface tension | laboratory experiment | • surface tension scaling provided qualitatively good results<br>• does not account for NAPL trapped by gas<br>• numerical experiments indicate that entrapment processes dominate the solution<br>• solution sensitive to soil hydraulic properties |
| Guarnaccia et al. (1997) | $S_W(P_{cNW})$ $S_{Tw}(P_{cGN})$ | $k_{rW}(S_W)$ $k_{rN}(S_W,S_G)$ $k_{rG}(S_G)$ | both S–P and k–S | any phase displaced can be entrapped | yes | variable | surface tension and per–meability | compare to analytical models and published laboratory data | • agrees well with published adta accounta for NAPL trapped by gas<br>• numerical experiments indicate that entrapment processes dominate the solution<br>• solution sensitive to soil hydraulic properties |

Figure 5.2: Continued: Summary of conceptual and numerical models describing three-phase flow in granular soils.

## 5.1. CONCEPTUAL MODEL OVERVIEW

If fluid wettability is constrained to follow, from most to least, water-NAPL-gas, and the intermediate wettability of the NAPL phase is assumed to render the water-gas phase interactions negligible, then three-phase flow behavior can be gleaned from readily available two-phase data as follows:

| | water | NAPL | gas |
|---|---|---|---|
| $S-P$ | $S_W = S_W\left(P_{cNW}\right)$ | $S_N = 1 - S_W - S_G$ | $S_G = S_G\left(P_{cGN}\right)$ |
| $k-S$ | $k_{rW} = k_{rW}\left(S_W\right)$ | $k_{rN} = k_{rN}\left(S_W, S_G\right)$ | $k_{rG} = k_{rG}\left(S_G\right)$ |

(5.1)

This representation allows us to combine saturations based on wettability considerations, where the total wetting phase saturation relative to the gas phase is $S_{Tw} = S_W + S_N$, implying $S_{Tw}(P_{cGN}) = 1 - S_G$, and the total nonwetting phase saturation relative to the water phase is $S_{Tn} = S_N + S_G$, implying $S_W(P_{cNW}) = 1 - S_{Tn}$. The motivation for using equation 5.1 as a representation for three-phase flow is two fold. First, three-phase $k-S-P$ data is generally not available. Second, many natural subsurface systems conform to the wettability and spreading assumption, most notably the cases where the NAPL is a hydrocarbon derivative and the soil contains a high percentage of quartz and a low percentage of organic matter. However, as noted in several recent publications [most notably, Bradford and Leij (1995 and 1996)], there are many natural systems which do not conform to this assumption, namely those systems where the NAPL is a mixture of many different chemicals, and where the soil is mineralogically heterogeneous and contains significant amounts of organic matter. Therefore, *the wettability assumption utilized herein must be recognized as a limiting attribute for model applicability.*

In order to model the general conditions of two- and three-phase flow, a second set of constraints is imposed. First, for the two-phase water-gas case, $P_{cGW}$ is determined from the algebraic constraint:

$$P_{cGW} = P_{cNW} + P_{cGN} \tag{5.2}$$

Second that the magnitude of the capillary pressure between any two immiscible fluid phases is proportional to the interfacial tension between those phases (after Leverett, 1941):

$$\frac{P_{cNW}}{\sigma_{NW}} = \frac{P_{cGN}}{\sigma_{GN}} = \frac{P_{cGW}}{\sigma_{GW}} \tag{5.3}$$

where $\sigma_{GW}$, $\sigma_{NW}$ and $\sigma_{GN}$ are the interfacial tensions along the interfaces between the gas and water phases, the NAPL and water phases, and the gas and NAPL phases, respectively. Finally, note that for equations 5.2 and 5.3 to be compatible the value of the parameters $\sigma_{GW}$, $\sigma_{NW}$ and $\sigma_{GN}$ must be constrained to be related as:

$$\sigma_{GW} = \sigma_{NW} + \sigma_{GN} \tag{5.4}$$

Equation 5.4 defines a neutral spreading coefficient. Therefore, only two of the interfacial tensions are independent with the third defined by equation 5.4. The two independent values can be considered fitting parameters. Several recent papers have questioned the use of constraints 5.3 and 5.4 (Wilson et al, 1990 and McBride et al., 1992, among others). To date, the sensitivity of the solution to this type of model constraint has not been formally addressed.

Section 5.5 continues the discussion of the use of capillary pressure scaling in the simulator.

## 5.2. TWO-PHASE MODEL

Hysteresis in the $k - S - P$ relationship is assumed to be caused by two main processes, *fluid entrapment effects* and *capillary and contact angle effects*. These effects are summarized as follows:

1. *Fluid entrapment effects* - When a fluid is drained from the pore space, a volumetric fraction is rendered effectively immobile[1] either by capillary isolation in the case of a nonwetting phase, or by capillary and adhesive forces in the case of a wetting phase. Trapped volumes can be re-mobilized either by physio-chemical processes (for example, by changing the capillary or Bond numbers) or by imbibition of the displaced phase. In addition, if the fluids are slightly miscible, mass-transfer processes can result in a total reduction of entrapped phase.

2. *Capillary and contact angle effects* - Assuming that the pore throats control the wetting-phase drainage process and the pore bodies control the wetting-phase imbibition process, and that the curvature of the menisci are enhanced during wetting-phase drainage, *the characteristic capillary pressure defining displacement will be higher for drainage than for imbibition.*

[1] That is, the volume of fluid will no longer respond to a gradient in potential.

Figure 5.3 presents a qualitative look at the two-phase hysteretic $S-P$ curve-type summary for the case when both capillary and entrapment effects are included. The nomenclature for curve-type name describes whether the flow-path is draining (D) or imbibing (I) with respect to the wetting phase, and how the curve was spawned, primary (P), main (M), or scanning (S). Table 5.1 provides a descriptive summary of the curve-types considered in this development, where the curve-type numbering scheme aligns odd numbers with drainage curves and even numbers with imbibition curves. Note that while the subscripts W and G indicate water and gas phases, respectively, they can be considered to represent a generic wetting-nonwetting phase pair. In addition, the parameters $S_{\alpha r}$ are the residual $\alpha$-phase saturations, where the residual saturation is defined herein as the saturation at which the phase effectively no longer responds to a gradient in potential over the time-scale of interest.

Finally with respect to Figure 5.3, note that the different pressure scales characterizing drainage and imbibition curves are a result of capillary effects, and the end-points defining curves 1 through 4 are determined by fluid entrapment effects.

Figures 5.4 and 5.5 present a qualitative look at the two-phase hysteretic $k-S$ curve-type summary for the data presented in Figure 5.3. Hysteresis in $k_{rW}(S_W)$ and $k_{rG}(S_G)$ is assumed to be caused by fluid entrapment effects only. To see the connection between hysteresis in the $k-S$ relationships and phase entrapment, let us define the *entrapped phase volume* as that volume which will no longer respond to a gradient in potential. Since the two-phase extension of Darcy's law applies only to that quantity which is hydraulically connected, the trapped volume must be regarded as part of the porous matrix. Therefore, $k_{r\alpha}$ is not only a function of $S_\alpha$ but specifically a function of that percentage of $S_\alpha$ which is hydraulically connected. Figures 5.4 and 5.5 show that the magnitude of the relative permeability at a particular saturation is a function of entrapment considerations. Note that another definition of residual saturation is the saturation at which the relative permeability is zero.

### 5.2.1. Entrapment and Release Sub-Model

Consider the following example of a water-gas displacement process intended to qualify the salient features of the conceptual model for phase entrapment and release, where water represents a general wetting phase and gas represents a general nonwetting phase. A porous medium is initially saturated with water which

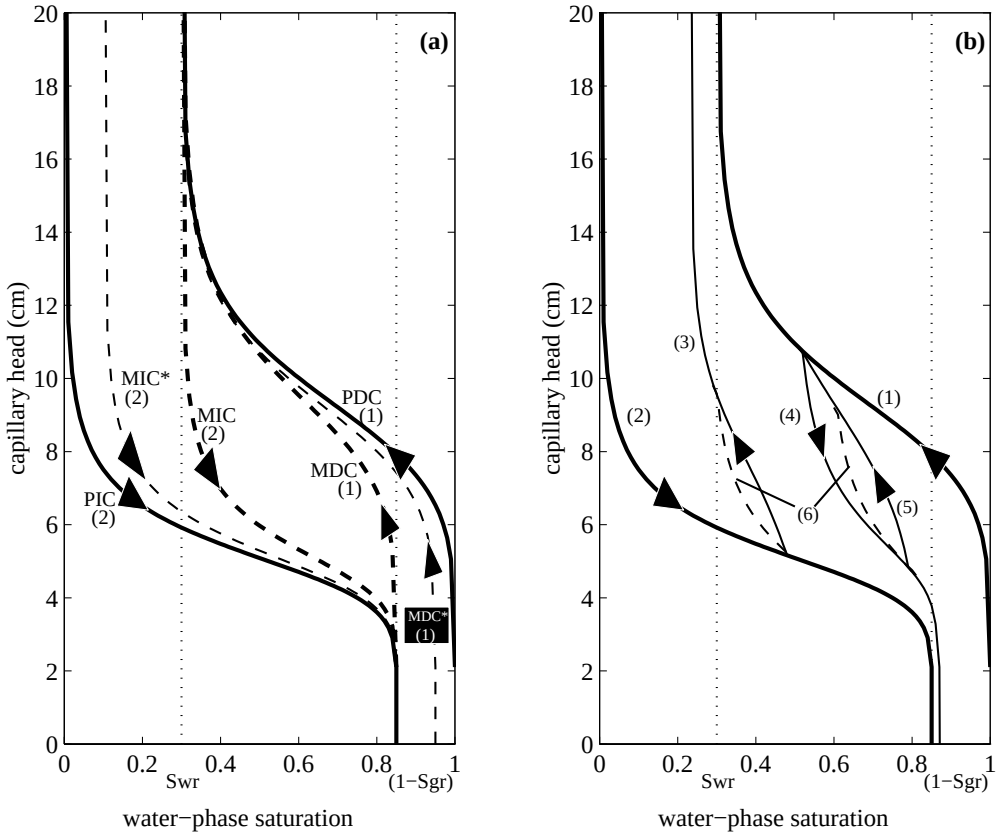


Figure 5.3: Definition plot of the hysteretic relationship between saturation and capillary pressure employing the empirical model used in the simulator. Curve position and shape is governed by the mobility status and the magnitude of the phase saturations when the curve is spawned and whether the displacement process is drainage ($D$) or imbibition ($I$) with respect to the wetting phase. Primary ($P$) and Main ($M$) curves are spawned when only one phase is mobile [curve numbers 1 and 2]. Scanning ($S$) curves are spawned when both phases are mobile [curve numbers 3 to 6]. The curve-type numbering scheme is set such that odd numbers are aligned with drainage curves [1 = $PDC$ or $MDC$, 3 and 5 = $SDC$] and even numbers are aligned with imbibition curves [2 = PIC or MIC, 4 and 6 = $SIC$].

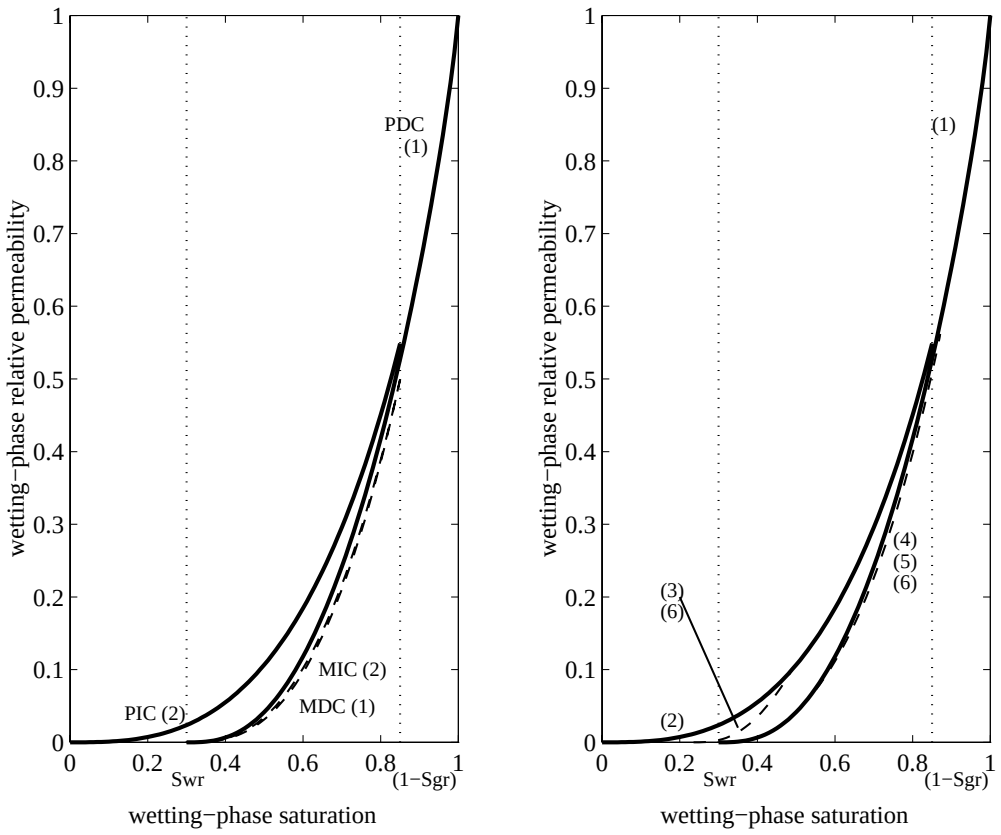


Figure 5.4: The resulting hysteretic $k - S$ functionals for the wetting phase generated from the empirical model used in the simulator and the data defining the $S - P$ relationship. Note that the $MDC$ and $MIC$, shown as dashed lines, are practically coincident, and that the scanning curves, shown as dashed lines, are group-labled because by model definition they are coincident.

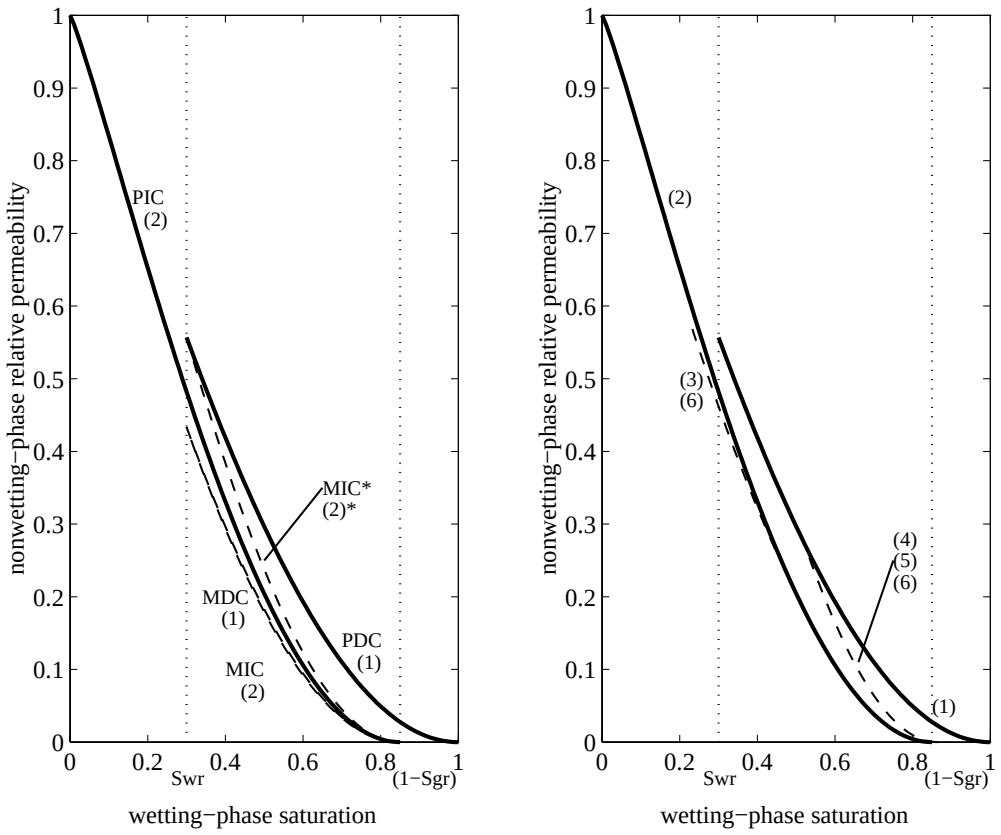


Figure 5.5: The resulting hysteretic $k - S$ functionals for the nonwetting phase using the data defining the $S - P$ relationship and the empirical model used in the simulator. Note that the curve labeled $MIC^*$ is obtained upon reversal from a $PDC$ where no nonwetting phase was previously trapped. Subsequent reversals follow the $MDC$ and $MIC$ which are practically coincident. Also note that the scanning curves are group-labled because by model definition they are coincident.

| number | name | qualitative notes |
|---|---|---|
| 1 | PDC-Primary Drainage Curve<br>MDC- Main Drainage Curve<br><br>MDC* | - origin at $S_W$=1<br>- origin at $S_W$=1-$S_{Gr}$ and only the wetting phase is mobile<br>- origin at 1>$S_W$>1-$S_{Gr}$ and only the wetting phase is mobile |
| 2 | PIC-Primary Imbibition Curve<br>MIC- Main Imbibition Curve<br><br>MIC* | - origin at $S_W$=0<br>- origin at $S_W$=$S_{Wr}$ and only the nonwetting phase is mobile<br>- origin at 0<$S_W$<$S_{Wr}$ and only the nonwetting phase is mobile |
| 3 | $SDC_1$- First-order Scanning Drainage Curve | originates at a flow reversal point from a PIC or MIC while both phases are mobile |
| 4 | $SIC_1$- First-order Scanning Imbibition Curve | originates at a flow reversal point from a PDC or MDC while both phases are mobile |
| 5 | $SDC_2$- Second-order Scanning Drainage Curve | originates at a flow reversal point from an $SIC_1$ while both phases are mobile |
| 6 | $SIC_2$- Second-order Scanning Imbibition Curve | originates at a flow reversal point from an $SDC_1$ while both phases are mobile |

Table 5.1: TWO-PHASE k-S-P CURVE-TYPE DEFINITION

is considered a continuum, and therefore, the initial trapped quantity is defined as zero. Water is then displaced by the gas until the water effectively ceases to flow as water films surrounding the soil grains thin to the point that adhesive and capillary forces dominate pressure gradients. Over the displacement process the trapped quantity of water rises from zero to a maximum, called the irreducible or residual. The *residual wetting phase saturation*, $S_{Wr}$, is a function of the porous medium properties and the chemistry of both the wetting and nonwetting phases. The concept of a saturation-dependent entrapment mechanism is based on the interpretation that as the different pore classes are drained (the larger ones first), some water is rendered effectively immobile as it adheres to the empty pore walls. This displacement process is called *primary drainage* (the PDC in Figure 5.3). With respect to the gas phase, it is assumed that no trapped saturation results as it displaces the water.

If at this point (that is, at $S_W = S_{Wr}$) the water phase is imbibed, thereby displacing the gas-phase, two phenomenon occur. First, some of the trapped water phase is remobilized as the in-flowing water thickens the water film associated with the smaller pores thus reducing the trapped quantity. Second, as the gas phase is displaced, a volumetric fraction becomes disconnected from the flowing volume and isolated in a pore or series of pores by the mechanisms of snap-off and bypassing [see Wilson et al., 1990, pages 110 to 123]). The resulting trapped gas saturation rises from zero to a maximum residual value where the gas phase ceases to flow. The *residual nonwetting phase saturation*, $S_{Gr}$, is a function of the porous medium properties and the chemistry of both the wetting and non-wetting phases. This process is called *main imbibition* (the MIC in Figure 5.3). At this point (that is, $S_W = 1 - S_{Gr}$) the water-phase is the only mobile phase, however, since the water saturation did not return to unity, some trapped water phase can still exist (for example, in some of the larger pores predominately filled with gas). In addition, as the gas dissolves in the water phase over time, the water saturation approaches unity and, as it does, the trapped quantity approaches zero.

The above displacement experiment involves the situation incurred when full drainage and imbibition cycles are realized (primary and main curve-types). That is, displace one fluid until it ceases to flow. Three conceptual attributes are highlighted in this description. The first two involve flow-path dependent entrapment and release mechanisms, where trapped quantities increase as a phase drains from the pore space and decrease as the phase fills the pore space. The third is that if the fluids are slightly miscible, mass transfer processes can result in a total reduction of entrapped phase.

The final conceptual attribute has to do with the case of an incomplete displacement process and the *spawning of a scanning curve*. That is, what happens when a flow reversal occurs before one of the phases is rendered immobile. For example, consider the $SIC_1$ (curve 4) in Figure 5.3. First, at the point of premature reversal along the PDC, according to the previous argument the trapped water phase will have a value somewhere between the extremes, zero and full residual ($S_{Wr}$), and the gas phase will have zero trapped volume. In general, an imbibing nonwetting phase tends to fill the larger pore classes first, so from a physical point of view, it seems reasonable to assume that if incomplete drainage occurred before reversal, then not all the different pore classes would be filled by the gas-phase, and upon water imbibition, the full gas-phase residual would not be realized. Instead, a value between the extremes would be appropriate, as shown by curve 4 in Figure 5.3.

This concept was first quantified by Land (1968), who developed an empirical model, based on experimental observation, to estimate the residual nonwetting phase saturation magnitude. The model utilizes the assumption that the difference in the reciprocals of the initial and residual nonwetting phase saturations is a constant for a given sand. That is, for the gas-water system described above, if one assumes that the maximum possible gas-phase residual, $S_{Gr}$, is obtained for the case of gas-phase drainage from $S_G = 1$ (i. e., for the PIC, all the pore classes are initially filled with the gas-phase), then a reduced residual, $S^*_{Gr} < S_{Gr}$, will be obtained for the case of gas-phase drainage from $S_G = S_G^{\max} < 1$ (i. e., for an MIC or $SIC_1$, not all the pore classes are initially filled with gas-phase) according to the rule (after Land [1968]):

$$\frac{1}{S^*_{Gr}} - \frac{1}{S_G^{\max}} = \frac{1}{S_{Gr}} - 1 \tag{5.5}$$

Given this *qualitative* interpretation of the physics of phase entrapment and release, let us now derive an analogous *quantitative empirical* representation. To facilitate our discussion on fluid entrapment, let us differentiate between the fluid volume which is 'free' to respond to a gradient in potential (i. e. hydraulically connected) and the volume which is 'trapped' and cannot respond to a gradient in potential (i. e. hydraulically disconnected). In terms of $\alpha$-phase saturation this differentiation is written as:

$$S_\alpha = S_{\alpha f} + S_{\alpha t} \tag{5.6}$$

where the subscripts $f$ and $t$ indicate free and trapped, respectively. It is clear that free and trapped saturations can not be measured per se. Therefore, equation

5.6 must be considered an empirical vehicle upon which to derive a model which will approximate the qualitative aspects introduced above.

To this end, let us assume that the trapped quantity, $S_{\alpha t}$, can be described by a saturation-dependent blending rule of the form:

$$S_{\alpha t} = S_{\alpha t}^{\min} + \left(S_{\alpha r}^{*} - S_{\alpha t}^{\min}\right) \left[\frac{S_{\alpha}^{\max} - S_{\alpha}}{S_{\alpha}^{\max} - S_{\alpha r}^{*}}\right]^{e} , \qquad e > 0 \tag{5.7}$$

where $S_{\alpha t}$ is constrained to lie within predefined, flow-path, history-dependent, limits, $S_{\alpha t}^{\min} \leq S_{\alpha t} \leq S_{\alpha r}^{*}$. The parameters in equation 5.7 will be described in turn. $S_{\alpha t}^{\min}$ is the lower limit of entrapped $\alpha$-phase. It is intended to quantify the condition which exists for MDCs and MICs where there is some non-zero residual $\alpha$-phase saturation at the time when the $\alpha$-phase was re-imbibed. Given the magnitude of the residual at the origin of a *main curve*, $S_{\alpha r(j)}$, $\alpha$ = G and j = 1 for an MDC, and $\alpha$ = W and j = 2 for an MIC, $S_{\alpha t}^{\min}$ is computed as:

$$S_{\alpha t}^{\min} = S_{\alpha r(j)} \left[\frac{1 - S_{\alpha}}{1 - S_{\alpha r(j)}}\right] , \qquad 0 \leq S_{\alpha t}^{\min} \leq S_{\alpha r(j)} \tag{5.8}$$

where it is assumed that a linear relationship exists between $S_{\alpha t}^{\min}$ and $S_{\alpha}$.

The parameter $S_{\alpha}^{\max}$ is the highest $\alpha$-phase saturation that has occurred since it was last at immobile residual conditions, i. e., the maximum imbibed $\alpha$-phase saturation which is available for displacement. Specifically, $S_{G}^{\max}$ is the furthest progression along a PDC or MDC, and $S_{W}^{\max}$ is the furthest progression along a PIC or MIC.

The parameter $S_{\alpha r}^{*}$ is the magnitude of the residual $\alpha$-phase, $0 \leq S_{\alpha r}^{*} \leq S_{\alpha r}$, at the terminus of an $\alpha$-phase drainage process. Its value is computed using the model of Land (1968), modified from equation 5.5 to include the following additional processes:

- a wetting phase trapped by a nonwetting phase;
- the existence of previously entrapped phase, which acts as a lower limit for further entrapment.

The resulting empirical relationship defining $S_{\alpha r}^{*}$ is written as:

$$\begin{aligned} S_{\alpha r}^{*} &= S_{\alpha t}^{\min} + \frac{S_{\alpha}^{\max} - S_{\alpha t}^{\min}}{1 + R_{\alpha}\left(S_{\alpha}^{\max} - S_{\alpha t}^{\min}\right)} \\ R_{\alpha} &= \left(S_{\alpha r} - S_{\alpha t}^{\min}\right)^{-1} - \left(1 - S_{\alpha t}^{\min}\right)^{-1} \end{aligned} \tag{5.9}$$

Finally with respect to equation 5.7, $e$ represents a blending parameter which governs how fast the phase becomes entrapped during drainage flow conditions or released from entrapment during imbibition flow conditions ($e > 0$, and for example, $e = 1$ yields a linear relationship between $S_{\alpha t}$ and $S_\alpha$).

In summary, the trapping model, equations 5.7, 5.8 and 5.9, is designed to represent any wetting-nonwetting, two-phase system, and it utilizes *three fitting parameters*: $S_{Wr}$, $S_{Gr}$ and $e$. The remaining parameters, $S^*_{\alpha r}$, $S^{\max}_\alpha$ and $S^{\min}_{\alpha t}$, are functions of flow-path history as discussed above.

### 5.2.2. Saturation-Pressure Sub-Model

The two-phase hysteretic saturation-capillary pressure sub-model which is described below is based on that derived in Luckner et al. (1989). As a point of departure for this presentation, consider the van Genuchten (1980) saturation-pressure function for monotonic, non-hysteretic, displacement written here as:

$$h_c(S_e) = \left[(S_e)^{-1/m} - 1\right]^{1/\eta} (a)^{-1} \tag{5.10}$$

$$S_e = \frac{S_W - S_r}{S_s - S_r}\,, \qquad 0 \le S_e \le 1 \tag{5.11}$$

where, $h_c$ is the capillary pressure head:

$$h_c = P_c/(\rho^W g) \tag{5.12}$$

and $S_e$ is the *effective water saturation* which is the $S_W$ normalized by the extremes in saturation attainable along a given flow path, where $S_r$ is the minimum and $S_s$ is the maximum. For example, referring to Figure 5.3, note that for the PDC, $S_r = S_{Wr}$ and $S_s = 1$, and for the PIC, $S_r = 0$ and $S_s = 1 - S_{Gr}$. In addition, with respect to equation 5.10, the parameter $a$ $[1/L]$ is a scaling parameter which is related to the displacement pressure head. Note that due to capillary and contact angle effects the pressure scale characterizing wetting phase drainage is greater than that for imbibition (depicted graphically in Figure 5.3). This fact requires the specification of two limiting values for $a$, one applied to wetting phase drainage curves ($a_d$) and one applied to wetting phase imbibition curves ($a_i$), where it is clear that, $a_i > a_d$. Finally, the parameter $\eta$ is a curve fitting parameter which reflects the pore-size distribution of the porous medium, and $m = 1 - 1/\eta$.

The $S - P$ model defined by equations 5.10 and 5.11, valid for monotonic (M) displacement only, can be used to obtain a closed-form empirical relationship

between saturation and capillary pressure for any one of the primary and main drainage and imbibition curves, $f = 1$ and 2 (Table 5.1 and Figure 5.3), provided the following parameter set is known:

$$S - P|_M \Longrightarrow \{S_{Wr}, S_{Gr}, a_d, a_i, \eta\}$$

where the notation $S - P|_M$ indicates that the $S-P$ model is defined for monotonic displacement. These parameters are determined either by fitting them to experimental data, approximating them based on soil properties, or a combination of the two (see for example Nielsen and Luckner, 1992).

Let us now modify the non-hysteretic $S - P$ model defined by equations 5.10 and 5.11 to account for hysteresis caused by the two main processes identified above: fluid entrapment and capillary and contact angle effects. Fluid entrapment effects are accounted for by making the parameters $S_r$ and $S_s$ functions of saturation, flow-path history, and the trapping parameters computed in equation 5.7. Hysteresis due to capillary and contact angle effects is accounted for by making the scaling parameter, $a$, a function of saturation and flow-path history. The parameter $\eta$ is assumed independent of flow-path.

The resulting closed-form empirical relationship between saturation and capillary pressure, assumed to be valid for primary, main and scanning curve-types, is written as:

$$h_{c(f)} = \left[(S_{e(f)})^{-1/m} - 1\right]^{1/\eta} (a_{(f)})^{-1} \tag{5.13}$$

$$S_{e(f)} = \frac{S_W - S_{r(f)}}{S_{s(f)} - S_{r(f)}}, \qquad 0 \leq S_{e(f)} \leq 1 \tag{5.14}$$

where the subscript $(f)$ indicates that the parameter is valid for a specific curve-type, i. e., $f = 1$, 2, 3, 4, 5, or 6, as referenced in Table 5.1[2]. This hysteretic (H) version of equations 5.10 and 5.11 can be computed provided the following parameter set is known:

$$S - P|_H \Longrightarrow \left\{S_{Wr}, S_{Gr}, a_d, a_i, \eta, S_{r(f)}, S_{s(f)}, a_{(f)}\right\}$$

where the notation $S - P|_H$ indicates that the $S - P$ model is defined such that hysteresis is accommodated, and it is assumed that the parameters $S_{Wr}$, $S_{Gr}$, $a_d$, $a_i$ and $\eta$ are provided as described above. This leaves the flow-path, history-dependent parameters $a_{(f)}$, $S_{r(f)}$ and $S_{s(f)}$ to be computed.

[2] The simulator is limited to these six flow path types.

Table 5.2 provides the details for evaluating the scaling parameter $a_{(f)}$, where $S_{0(\bullet)}$ is the reversal point saturation at which curve $(\bullet)$ was spawned, and $\beta$ is a blending parameter. First note that $a_d \leq a_{(f)} \leq a_i$, and for primary and main curve-types ($f = 1, 2$) the limiting values are utilized. Second, note the use of a blending function to define $a_{(f)}$ for scanning curve-types ($f = 3, 4, 5, 6$). The purpose of the blending function is for numerical model implementation purposes. When a flow reversal results in the generation of a scanning curve, there is a commensurate jump in the slope of the $S - P$ functional. That is, while the functional itself is continuous, its slope is discontinuous (for example, see Figure 5.3 curve 4). Since the slope of the curve affects the magnitude of the phase mass flux, a strong discontinuity can lead to convergence problems in a numerical scheme as the relationship between the flow parameters and the discrete time- and space-scales is dramatically altered. For example, a large increase in mass flux may require a much smaller time step (related to the Courant number) not only to limit temporal discretization errors, but also to allow for convergence of the linearized system of equations. Therefore, in order to limit numerical difficulties associated with functional discontinuities, the blending function has been incorporated to allow for a smooth transition in slope when a flow reversal occurs.

A blending parameter, $\beta$, has been included to provide modeling flexibility, where in general $\beta \geq 0$. For example, an instantaneous change in $a_{(f)}$ occurs when $\beta = 0$, and as $\beta$ gets larger the transition from the reversal point value is delayed. As an implementation illustration, consider a reversal from a PDC to an $\text{SIC}_1$. As shown in Table 5.2, for the new curve 4, $a_{(4)}(S_W)$ varies from $a_d$ at the reversal point, $S_{0(4)}$, to $a_i$ at the terminal saturation, $S_W = 1 - S_{Gt}$, according to the power law defined by the parameter $\beta$.

Given the data quantifying phase entrapment, equations 5.7 and 5.9, and the value of $a_{(f)}$, the parameters $S_{r(f)}$ and $S_{s(f)}$ are determined by following the scaling procedure of Scott et al. (1983) (see also Kool and Parker, 1987, Parker and Lenhard, 1987, Lenhard and Parker, 1987, Luckner et al., 1989, and Lenhard et al., 1991). Effectively the model requires that any $S - P$ functional defined by equation 5.13 pass through two predetermined constraint points chosen to ensure the following:

**constraint (1)** That the functional either terminate at the proper residual saturation as defined in equation 5.7 or terminate such that a closed scanning loop results, whichever is appropriate.

**constraint (2)** That the functional remain continuous as definitive parameters

| f | name | definition of $a$ | computational details |
|---|---|---|---|
| 1 | PDC<br>MDC<br>MDC* | $\left\{ \quad a_1 = a_d \right.$ | |
| 2 | PIC<br>MIC<br>MIC* | $\left\{ \quad a_2 = a_i \right.$ | |
| 3 | $SDC_1$ | $a_3 = a_i - (a_i - a_d)\left[\frac{S_{0(3)} - S_W}{S_{0(3)} - S_{Wt}}\right]^{\beta}$ | grade change between $a_{\mathrm{i}}$ and $a_{\mathrm{d}}$ over the span of curve 3 |
| 4 | $SIC_1$ | $a_4 = a_d + (a_i - a_d)\left[\frac{S_W - S_{0(4)}}{1 - S_{Gt} - S_{0(4)}}\right]^{\beta}$ | grade change between $a_{\mathrm{d}}$ and $a_{\mathrm{i}}$ over the span of curve 4 |
| 5 | $SDC_2$ | $a_5 = a_4 - (a_4 - a_d)\left[\frac{S_{0(5)} - S_W}{S_{0(5)} - S_{0(4)}}\right]^{\beta}$ | grade change between $a_{(4)}$, the value of $a$ when the reversal occured, and $a_{\mathrm{d}}$ over the span of curve 5 |
| 6 | $SIC_2$ | $a_6 = a_5 + (a_4 - a_5)\left[\frac{S_W - S_{0(6)}}{S_{0(5)} - S_{0(6)}}\right]^{\beta}$ | grade change between $a_{(5)}$, the value of $a$ when the reversal occured, and $a_{(4)}$ over the span of curve 6 |

Table 5.2: DEFINITION OF THE SCALING PARAMETER 'a' FOR THE TWO-PHASE HYSTERETIC S-P MODEL

are altered to reflect changing entrapment and capillary effects.

Constraint 1 is required first to ensure that residual saturation data is honored. For example, in Figure 5.3, curve (4) terminates at $S_s = (1 - S^*_{Gr})$, the point where the gas-phase ceases to flow, and curve (3) terminates at $S_r = S^*_{Wr}$, the point where the water-phase ceases to flow, where $S^*_{Gr}$ and $S^*_{Wr}$ are computed from equation 5.9. The second part of this constraint, that there be closed scanning loops, is required so that erroneous pumping effects do not occur during cyclic flow reversals (Janes, 1984). For example, curve (5), a second order scanning drainage curve, ties back in with the PDC at the point where the scanning loop originated.

Constraint 2 is required because a continuous capillary pressure field is required for mass conservation. It becomes an important consideration when viewed from the standpoint that the $S - P$ model is to be implemented in a time-discrete numerical model where saturation is the dependent variable and where parameter update is lagged in time with respect to saturation. That is, given the saturation solution at the advanced time step (superscript $n + 1$), $S_W^{n+1}$, the corresponding capillary head, $h_c^{n+1}$ is determined from equation 5.13 with the parameter set: $\left\{S_W^{n+1}, S^n_{r(f)}, S^n_{s(f)}, a^n_{(f)}, \eta\right\}$, where the superscript $n$ indicates that the saturation-dependent parameters are dated at the previous time step. To prepare for the next time step, $a_{(f)}$ is updated as discussed above, and $S_{r(f)}$ and $S_{s(f)}$ are updated such that not only is constraint 1 satisfied, but that $h_c$ does not change value.

Tables 5.3 and 5.4 provide the quantitative details, consistent with the constraints listed above, for evaluating the curve-type-specific parameters $S_{r(f)}$ and $S_{s(f)}$. From a qualitative perspective the following descriptive statements regarding $S_{r(f)}$ and $S_{s(f)}$ apply:

- For curves PDC, MDC, MDC*, $\text{SDC}_1$ ($f = 1$ and 3): $S_r = S_{Wt}$ [from equation 5.7] so that constraint 1 is satisfied, and $S_s$ becomes a scaling parameter so that constraint 2 is satisfied, and as such, it has no physical meaning.

- For curves PIC, MIC, MIC*, $\text{SDC}_1$ ($f = 2$ and 4): $S_s = (1 - S_{Gt})$ [from equation 5.7] so that constraint 1 is satisfied, and $S_r$ becomes a scaling parameter so that constraint 2 is satisfied, and as such, it has no physical meaning.

| f | name | definition of $S_r$ | computational details |
|---|---|---|---|
| 1 | PDC<br>MDC<br>MDC* | $S_{r(1)} = S_{Wt}$ | $S_{Wt}$ from equation 5.7 |
| 2 | PIC<br>MIC<br>MIC* | $S_{r(2)} = \frac{S_W - \overline{S}_e S_{s(2)}}{1 - \overline{S}_e}$ | computed after $S_{s(2)}$ has been updated |
| 3 | $SDC_1$ | $S_{r(3)} = S_{Wt}$ | $S_{Wt}$ from equation 5.7 |
| 4 | $SIC_1$ | $S_{r(4)} = \frac{S_W - \overline{S}_e S_{s(4)}}{1 - \overline{S}_e}$ | computed after $S_{s(4)}$ has been updated |
| 5 | $SDC_2$ | $S_{r(5)} = \frac{\overline{S}_{e(4)} S_W - \overline{S}_e S_{s(4)}}{\overline{S}_{e(4)} - \overline{S}_e}$ | force closure at the point where the scanning loop originated |
| 6 | $SIC_2$ | $S_{r(6)} = \frac{\overline{S}_{e(j)} S_W - \overline{S}_e S_{s(j)}}{\overline{S}_{e(j)} - \overline{S}_e}$ | j = 3 if imbibition and spawned from an $SDC_1$<br>5 if imbibition and spawned from an $SDC_2$<br>6 if drainage |

Table 5.3: DEFINITION OF THE SCALING PARAMETER 'Sr' FOR THE TWO-PHASE HYSTERETIC S-P MODEL

- For curves $SDC_2$ and $SIC_2$ ($f = 5$ and 6): both $S_s$ and $S_r$ become scaling parameters so that the closed scanning loop part of constraint 1 and constraint 2 are both satisfied.
- For application in a time-discrete numerical model, the $S - P$ model enforces residual saturations, conserves mass, and converges as the increment in saturation change approaches zero.

**Summary and Evaluation Procedure**

The empirical hysteretic $S - P$ model is defined by equations 5.7, 5.13 and 5.14. It requires the input of the following parameter set:

$$e, S_{Wr}, S_{Gr}, a_d, a_i, \eta$$

| f | name | definition of $S_s$ | computational details |
|---|---|---|---|
| 1 | PDC<br>MDC<br>MDC* | $S_{s(1)} = \frac{S_W - S_{r(1)}}{\overline{S}_e} + S_{r(1)}$ | computed after $S_{r(1)}$ has been updated |
| 2 | PIC<br>MIC<br>MIC* | $S_{s(2)} = 1 - S_{Gt}$ | $S_{Gt}$ from equation 5.7 |
| 3 | $SDC_1$ | $S_{s(3)} = \frac{S_W - S_{r(3)}}{\overline{S}_e} + S_{r(3)}$ | computed after $S_{r(3)}$ has been updated |
| 4 | $SIC_1$ | $S_{s(4)} = 1 - S_{Gt}$ | $S_{Gt}$ from equation 5.7 |
| 5 | $SDC_2$ | $S_{s(5)} = \frac{S_W - S_{r(5)}}{\overline{S}_e} + S_{r(5)}$ | computed after $S_{r(5)}$ has been updated |
| 6 | $SIC_2$ | $S_{s(6)} = \frac{S_W - S_{r(6)}}{\overline{S}_e} + S_{r(6)}$ | computed after $S_{r(6)}$ has been updated |

Table 5.4: DEFINITION OF THE SCALING PARAMETER 'Ss' FOR THE TWO-PHASE HYSTERETIC S-P MODEL

Given these values a sequential, step-wise, procedure is used to compute the $S-P$ functionals. The computational steps are listed as follows:

1. Given initial data for the parameter set: $\left\{S_W^n, S_{r(f)}^n, S_{s(f)}^n, a_{(f)}^n\right\}$, compute the solution for the next time step: $S_W^{n+1}$. Given $\left\{S_W^{n+1}, S_{r(f)}^n, S_{s(f)}^n, a_{(f)}^n\right\}$, compute $h_c^{n+1}$ from equation 5.13.

2. Compute $S_{Wt}$ and $S_{Gt}$ from equation 5.7 with $S_W = S_W^{n+1}$.

3. Determine which curve-type is appropriate given the change in saturation:

$$\delta S_W = S_W^{n+1} - S_W^n$$

and the current value of $f$.

**$f$ is currently 1 or 3**: If $\delta S_W > \epsilon$, where $\epsilon$ is a small positive number, then a reversal is indicated and $f$ is incremented by one, otherwise a reversal is not indicated and $f$ is not altered.

- $f$ **is currently 5**: A reversal is indicated if $\delta S_W > \epsilon$ and $f$ is incremented by one. A closed scanning loop is indicated if $S_W \leq S_{0(4)}$, where $S_{0(4)}$ is the reversal point saturation at which curve 4 was spawned, and $f$ is reset to equal one. If neither of these things happen then $f$ is not altered.
- $f$ **is currently 2 or 4**: If $\delta S_W < -\epsilon$, then a reversal is indicated and $f$ is incremented by one, otherwise a reversal is not indicated and $f$ is not altered.
- $f$ **is currently 6**: Since this is the highest-order curve considered in this simulator, a flow reversal will not produce a new drainage curve. A closed scanning loop is indicated if either $S_W^{n+1} \geq S_{0(5)}$, or $S_W^{n+1} \leq S_{0(6)}$, where $S_{0(\bullet)}$ is the reversal point saturation at which curve $(\bullet)$ was spawned. For the former, $f$ is reset to equal four, and for the latter, $f$ is reset to five. If neither of these things happen then $f$ is not altered.

4. Given the updated value of $f$ from part 3, compute the value of $a_{(f)}$ from Table 5.2 with $S_W = S_W^{n+1}$.

5. Given $h_c^{n+1}$ from part 1 and $a_{(f)}$ from part 4, compute $\overline{S}_e$ using equation 5.13. This step is included for the continuity requirement.

6. Given $\overline{S}_e$ from part 5, compute $S_{s(f)}$ and $S_{r(f)}$ as described in Tables 5.4 and 5.3 with $S_W = S_W^{n+1}$.

### 5.2.3. Relative Permeability-Saturation Sub-Model

A closed-form empirical model used to predict relative permeability for a two-phase system is derived by employing the Mualem (1976) statistical model. The Mualem model relates the water relative permeability to saturation by a series of theoretical steps. First, the capillary pressure-saturation functional is assumed to be analogous to the pore-size distribution function. Second, using the capillary law, the capillary pressure at which a pore will drain or fill is uniquely related to the pore radii. Third, the water relative permeability is obtained by integrating over the contributions of water-filled pores:

$$k_{rW}(S_W) = (S_{eW})^{\zeta} \left[ \frac{g(0, S_{eW})}{g(0,1)} \right]^2 \tag{5.15}$$

where

$$g(A,B) = \int_A^B h_c^{-1} dS_{eW}$$

and $S_{eW}$ is an *effective water saturation*. It is a normalized saturation, analogous to that defined by equation 5.11, which is a measure of the saturation range over which water will flow. We identify herein two unique definitions of $S_{eW}$ which apply to the $k_{rW}(S_W)$ functional:

**Definition 1.** $S_{eW}$ = *[reduced saturation]/[total % pore volume available for flow]*

$$S_{eW} = (S_W - S_{Wt}) \,/\, (1 - S_{Wt} - S_{Gt}) \tag{5.16}$$

**Definition 2.** $S_{eW}$ = *[reduced saturation]/[total % pore volume available for water flow]*

$$S_{eW} = (S_W - S_{Wt}) \,/\, (1 - S_{Wt}) \tag{5.17}$$

Note, that the terms $S_{Wt}$ and $S_{Gt}$ are those which are computed from equation 5.7.

The term in brackets in equation 5.15 represents the ratio of the pores that are contributing to water flow at a particular effective saturation, $g(0, S_{eW})$, to all pores contributing to water flow, $g(0,1)$. The term pre-multiplying the integrals accounts for tortuosity effects and incomplete correlation between pores, and $\zeta$ is a pore connectivity parameter.

Substitution of the van Genuchten saturation-pressure relationship (equation 5.10) into equation 5.15 gives (Parker et al., 1987):

$$g(A,B) = a\left[\left(1 - A^{1/m}\right)^m - \left(1 - B^{1/m}\right)^m\right] \tag{5.18}$$

and equation 5.15 becomes:

$$k_{rW}(S_W) = ({}^aS_{eW})^\zeta \left\{1 - \left[1 - \left({}^bS_{eW}\right)^{1/m}\right]^m\right\}^2 \tag{5.19}$$

where the prescripts on the effective saturations indicate that, *for model flexibility*, the user can choose not only which definition of $S_{eW}$ is to be used (i.e., equations 5.16 or 5.17), but can choose a different definition of $S_{eW}$ for each of the two terms in equation 5.19. Note that this relationship indicates that $k_{rW}(S_W = 1) = 1$, and $k_{rW}(S_W = S_{Wt}) = 0$ (where $S_{Wt}$ is the residual water saturation in the limit as $S_W$ approaches $S^*_{Wr}$, as per equation 5.7).

An analogous derivation for the gas phase takes into account that the pores will fill with the nonwetting phase from the largest to the smallest. As in Luckner et al. (1989) and Parker et al. (1987), the relationship can be written as:

$$k_{rG}(S_G) = (S_{eG})^{\varphi} \left[ \frac{g(S_{eW}, 1)}{g(0, 1)} \right]^2 \tag{5.20}$$

where $\varphi$ is a pore connectivity parameter for the gas-phase, and $S_{eG}$ is the normalized or *effective gas saturation* which, when applied to the $k_{rG}(S_G)$ functional, is assumed to have two admissible definitions:

**Definition 3.** $S_{eG}$ = *[reduced saturation]/[total % pore volume available for flow]*

$$S_{eG} = (S_G - S_{Gt}) \,/\, (1 - S_{Wt} - S_{Gt}) \tag{5.21}$$

**Definition 4.** $S_{eG}$ = *[reduced saturation]/[total % pore volume available for gas flow]*

$$S_{eG} = (S_G - S_{Gt}) \,/\, (1 - S_{Gt}) \tag{5.22}$$

where the terms $S_{Wt}$ and $S_{Gt}$ are those which are computed from equation 5.7.

Substituting the van Genuchten saturation-pressure relationship (equation 5.10) into equation 5.20 gives:

$$k_{rG}(S_G) = ({}^{a}S_{eG})^{\varphi} \left[ 1 - \left[ 1 - \left( {}^{b}S_{eG} \right) \right]^{1/m} \right]^{2m} \tag{5.23}$$

where the substitution, $1 - S_{eG} = S_{eW}$, has been made, and the prescripts on the effective saturations indicate the user can choose different definitions of $S_{eG}$ (i.e., equations 5.21 or 5.22) for each of the two terms in equation 5.23. This relationship indicates that $k_{rG}(S_G = 1) = 1$, and $k_{rG}(S_G = S_{Gt}) = 0$ (where $S_{Gt}$ is the residual gas saturation in the limit as $S_G$ goes to $S^*_{Gr}$, as per equation 5.7).

In summary, the two-phase relative permeability-saturation sub-model, equations 5.19 and 5.23, written for a water-gas system, is assumed valid for any wetting-nonwetting phase system. It includes hysteresis as the result of fluid entrapment effects through the definition of the effective saturations. In addition, it utilizes data from the saturation-pressure sub-model, the parameter $m$, and data from the entrapment/release sub-model, the parameters $S_{Wt}$ and $S_{Gt}$. The $k - S$ sub-model includes two fitting parameters, $\zeta$ and $\varphi$, and an additional model fitting feature is included by allowing the user to choose the definition for effective saturation (equations 5.16 or 5.17 and 5.21 or 5.22).

## 5.3. THREE-PHASE MODEL

The two-phase $k - S - P$ model derived in Section 5.2 is now adapted for the three-phase case. To reiterate, the fundamental assumptions which are used to construct the three-phase model are:

1. Water is the most wetting phase, and it spreads as a film over the soil grains. NAPL has intermediate wettability, and it spreads as a film over the water. Gas is the least wetting phase, and it is surrounded by the total wetting phase, i. e., the water and NAPL. This idealization allows a three-phase $k - S - P$ model to be generated using two-phase data as shown by the functional dependencies in equation 5.1.

2. The functionals $P_{cNW}(S_W)$ and $P_{cGN}(S_{Tw})$ are defined such that $P_{cGW} = P_{cNW} + P_{cGN}$ regardless of which phases are present in the domain. For this to be the case then $P_{cNW}(S_W)$ and $P_{cGN}(S_{Tw})$ must be continuous in time and space for any phase configuration, and the three fluid pair capillary pressures must be related through the interfacial tension scaling relationship 5.3, with the interfacial tension values constrained to yield a neutral spreading coefficient (equation 5.4).

3. The three-phase $k - S$ functionals are defined such that they reduce to the appropriate two-phase functionals when appropriate.

As with the two-phase model, the three-phase model can be idealized as three inter-related sub-models: entrapment-release, saturation-capillary pressure, and relative permeability-saturation. These sub-models are presented in turn.

### 5.3.1. Entrapment and Release Sub-Model

The addition of a third phase complicates the entrapment description, but the following qualitative statements are assumed to hold:

- $\alpha$-phase drainage results in an increase in trapped $\alpha$-phase volume;
- $\alpha$-phase imbibition results in a decrease in trapped $\alpha$-phase volume;
- an incomplete displacement process will admit residual saturations less than the maximum measured value.

It is this conceptual model we wish to adapt into an empirical model to quantify phase entrapment and release for three-phase immiscible flow.

Since the water phase is most wetting, we idealize the entrapment mechanism as reducing to a wetting phase, $S_W$, being displaced by a nonwetting phase, $S_{Tn}$, where $S_{Tn} = S_N + S_G$. Therefore, we assume that the magnitude of $S_{Wt}$ will be the same regardless of which phase(s) displaced it. The same argument holds for the gas phase: since it is most nonwetting, we idealize the entrapment mechanism as reducing to a nonwetting phase, $S_G$, being displaced by a wetting phase, $S_{Tw}$, where $S_{Tw} = S_W + S_N$. Therefore, the trapping model, equations 5.7, 5.8 and 5.9, is assumed to describe water and gas phase entrapment ($\alpha$ = W and G) for both the two-phase water-gas system and the three-phase water-NAPL-gas system where the NAPL has intermediate wettability..

With respect to the NAPL phase, since the trapping mechanisms are different for wetting and nonwetting phases, the magnitude of trapped NAPL-phase should be a function of which phase displaced it. From two-phase displacement experiments, one can measure the maximum NAPL residual in a water-NAPL system, $S_{Nnr}$, and in a NAPL-gas system, $S_{Nwr}$, where the subscript $Nnr$ indicates NAPL residual as a nonwetting phase, and $Nwr$ indicates NAPL residual as a wetting phase. In general, $S_{Nnr} \neq S_{Nwr}$. Since we are using the same phase entrapment model for both the water and gas phases, with the fundamental difference being that the measured residual values are different, consider the following entrapment model for NAPL. Like the water and gas phases, the NAPL entrapment is defined using equations 5.7, 5.8 and 5.9, for $\alpha$ = N, and $S_{Nr}$ is defined as a linear function of water and gas saturations (after Fayers and Matthews, 1984), i. e.:

$$S_{Nr} = S_{Nwr}\left(\frac{S_G}{S_W + S_G}\right) + S_{Nnr}\left(\frac{S_W}{S_W + S_G}\right) \tag{5.24}$$

In summary, the trapping model, equations 5.7, 5.8, 5.9 and 5.24, valid for $\alpha$ = W, G and N, is designed to represent a three-phase system where the NAPL has intermediate wettability between water and gas. In addition, it reduces to the appropriate two-phase model when appropriate. It utilizes five fitting parameters: $S_{Wr}$, $S_{Gr}$ , $S_{Nwr}$, $S_{Nnr}$ and $e$. The remaining nine parameters, $S^*_{\alpha r}$, $S^{\max}_{\alpha}$ and $S^{\min}_{\alpha t}$, $\alpha$ = W, G, N, are functions of flow-path history.

### 5.3.2. Saturation-Pressure Sub-Model

In Section 5.1 we introduced the fundamental assumption that the three-phase $S - P$ model can be decomposed into two, two-phase $S - P$ models by virtue of

the fact that the NAPL phase is constrained to be the intermediate wetting fluid. Based on the material presented in Section 5.1, the two relevant $S-P$ relationships are: $P_{cNW}(S_W)$ and $P_{cGN}(S_{Tw})$. As will be seen shortly, these relationships are interrelated through fluid entrapment considerations.

First let us view each $S-P$ relationship as a unique two-phase system, where the two-phases are idealized as follows:

| functional | wetting phase saturation | nonwetting phase saturation |
|---|---|---|
| $P_{cNW}(S_W)$ | $S_W$ | $S_{Tn} = S_N + S_G$ |
| $P_{cGN}(S_{Tw})$ | $S_{Tw} = S_W + S_N$ | $S_G$ |

It can be seen from this table that in the limit as $S_W \rightarrow 0$, $P_{cGN}(S_N)$ represents the two-phase NAPL-gas system where NAPL is the wetting phase, and that in the limit as $S_G \rightarrow 0$, $P_{cNW}(S_W)$ represents the two-phase water-NAPL system where NAPL is the nonwetting phase. In addition, in the limit as $S_N \rightarrow 0$, $S_{Tw} = S_W$ and $S_{Tn} = S_G$, and $P_{cGW} = P_{cNW}(S_W) + P_{cGN}(S_W)$ represents the two-phase water-gas system.

Second, from equation 5.3 we know that the magnitude of the capillary pressure between any two phases is related through interfacial tension scaling. Therefore, assuming that one of the phase pairs is used to fit the empirical model parameters $a_d$, $a_i$and $\eta$, then equation 5.13 can be used to represent $P_{cNW}(S_W)$ and $P_{cGN}(S_{Tw})$, in terms of equivalent water head, by scaling $h_c$ in the appropriate way. Specifically:

| phase pair measured | $h_{cNW}$ | $h_{cGN}$ |
|---|---|---|
| $W-G$ | $h_c\left(\frac{\sigma_{NW}}{\sigma_{GW}}\right)$ | $h_c\left(\frac{\sigma_{GN}}{\sigma_{GW}}\right)$ |
| $W-N$ | $h_c$ | $h_c\left(\frac{\sigma_{GN}}{\sigma_{NW}}\right)$ |
| $N-G$ | $h_c\left(\frac{\sigma_{NW}}{\sigma_{GN}}\right)$ | $h_c$ |

where $h_{cNW} = P_{cNW}/(\rho^W g)$ and $h_{cGN} = P_{cGN}/(\rho^W g)$, and the values of the $\sigma$'s are constrained to be related by equation 5.3.

Third, equation 5.13 is used to evaluate $h_{cNW}$ and $h_{cGN}$ by following the procedure detailed in Section 5.2.2 for each functional separately, using Table 5.5 to make the appropriate variable substitution. Specifically, consider that the evaluation procedure outlined in Section 5.2.2 is for a generic two-phase system, defined by the parameter set: $\{h_c, S_W, S_{Wt}, S_{Gt}\}$, where $S_W$ and $S_G$ are generic wetting and nonwetting phases, respectively. Then the $P_{cNW}(S_W)$ functional

| functional | two-phase model variables used in equations 5.13 and 5.14 and in Tables 5.2, 5.3 and 5.4 | analogous variable in the three-phase model |
|---|---|---|
| $P_{cNW}(S_W)$ | $h_c$ | $h_{cNW}$ |
| | $S_W$ | $S_W$ |
| | $S_{Wt}$ | $S_{Wt}$ |
| | $S_{Gt}$ | $S_{Nt} + S_{Gt}$ |
| $P_{cGN}(S_{Tw})$ | $h_c$ | $h_{cGN}$ |
| | $S_W$ | $S_{Tw}$ |
| | $S_{Wt}$ | $S_{Wt} + S_{Nt}$ |
| | $S_{Gt}$ | $S_{Gt}$ |

Table 5.5: THE RELATION BETWEEN TWO- AND THREE-PHASE S-P MODEL PARAMETERS

is computed by substituting the parameter set: $\{h_{cNW}, S_W, S_{Wt}, (S_{Nt} + S_{Gt})\}$, and the $P_{cGN}(S_{Tw})$ functional is computed by substituting the parameter set: $\{h_{cGN}, S_{Tw}, (S_{Wt} + S_{Nt}), S_{Gt}\}$.

In summary, the three-phase hysteretic $S - P$ model requires the following input data set:

1. the curve-fit parameters: $a_d, a_i, \eta$, as defined by one of the three fluid pairs
2. the four residual saturations: $S_{Wr}, S_{Nwr}, S_{Nnr}, S_{Gr}$;
3. the blending parameter for entrapment, $e$;
4. two of the three interfacial tension parameters: $\sigma_{GW}, \sigma_{NW}, \sigma_{GN}$, with the third defined such that $\sigma_{GW} - \sigma_{NW} - \sigma_{GN} = 0$.

### 5.3.3. Relative Permeability-Saturation Sub-Model

The three-phase $k - S$ model is built upon the following fundamental assumption: the most wetting phase fills the smallest pores, the least wetting fills the largest pores, and the intermediate wetting phase fills the intermediate size pores. The main outcome of this assumption is that the wetting and nonwetting phases become spatially segregated to the extent that their relative permeability functions become dependent only upon their respective saturations. In addition it is assumed that the relative permeability functions apply for two- or three-phase

systems. Therefore, for the three-phase system, as long as the wettability assumption holds, the water-phase relative permeability is given by equation 5.19 and the gas-phase relative permeability is given by equation 5.23 with the definitions for effective saturations (i.e., equations 5.16, 5.17, 5.21, and 5.22) altered to account for the presence of trapped NAPL, i. e.,

**Definition 5.** *$S_e$ =[reduced saturation]/[total % pore volume available for flow]*

$$S_{eW} = (S_W - S_{Wt}) / (1 - S_{Wt} - S_{Nt} - S_{Gt}) \quad (5.25)$$
$$S_{eG} = (S_G - S_{Gt}) / (1 - S_{Wt} - S_{Nt} - S_{Gt}) \quad (5.26)$$

**Definition 6.** *$S_e$ = [reduced saturation]/[total % pore volume available for phase flow]*

$$S_{eW} = (S_W - S_{Wt}) / (1 - S_{Wt}) \quad (5.27)$$
$$S_{eG} = (S_G - S_{Gt}) / (1 - S_{Gt}) \quad (5.28)$$

where again the trapped quantities are computed from equation 5.7.

With respect to quantifying the intermediate-wetting NAPL-phase, the appropriate Mualem model is given by Parker et al. (1987):

$$k_{rN}(S_W, S_G) = (S_{eN})^{\xi} \left[ \frac{g(S_{eW}, S_{eTw})}{g(0,1)} \right]^2 \quad (5.29)$$

where $\xi$ is a pore connectivity parameter for the NAPL-phase, and $S_{eN}$ is the normalized or *effective NAPL saturation* which, when applied to the $k_{rN}(S_W, S_G)$ functional, is assumed to have two admissible definitions:

**Definition 7.** *$S_{eN}$ = [reduced saturation]/[total % pore volume available for flow]*

$$S_{eN} = (S_N - S_{Nt}) / (1 - S_{Wt} - S_{Nt} - S_{Gt}) \quad (5.30)$$

**Definition 8.** *$S_{eN}$ = [reduced saturation]/[total % pore volume available for NAPL flow]*

$$S_{eN} = (S_N - S_{Nt}) / (1 - S_{Nt}) \quad (5.31)$$

The term in brackets in equation 5.29 represents the ratio of the pores that are contributing to NAPL flow at a particular combination of effective saturations, $g(S_{eW}, S_{eTw})$, to all pores contributing to water flow, $g(0,1)$. The parameter $S_{eTw}$ is the normalized or *effective total wetting phase saturation* which, when applied to the $k_{rN}(S_W, S_G)$ functional, is assumed to have three admissible definitions:

**Definition 9.** $S_{eTw}$ = *[reduced saturation]/[total % pore volume available for flow]*

$$S_{eTw} = \frac{S_W + S_N - S_{Wt} - S_{Nt}}{(1 - S_{Wt} - S_{Nt} - S_{Gt})} \tag{5.32}$$

**Definition 10.** $S_{eTw}$ = *[reduced saturation]/[total % pore volume available for NAPL and water flow]*

$$S_{eTw} = \frac{S_W + S_N - S_{Wt} - S_{Nt}}{(1 - S_{Wt} - S_{Nt})} \tag{5.33}$$

**Definition 11.** $S_{eTw}$ = *[reduced saturation]/[total % pore volume available for NAPL flow]*

$$S_{eTw} = \frac{S_W + S_N - S_{Nt}}{(1 - S_{Nt})} \tag{5.34}$$

where the trapped quantities are computed from equation 5.7.

Finally, let us substitute $(1 - S_{eTn})$ for $S_{eW}$ in equation 5.29, where $S_{eTn}$ is the normalized or *effective total nonwetting phase saturation*. The parameter $S_{eTn}$ is assumed to have three admissible definitions:

**Definition 12.** $S_{eTn}$ = *[reduced saturation]/[total % pore volume available for flow]*

$$S_{eTn} = \frac{S_N + S_G - S_{Nt} - S_{Gt}}{(1 - S_{Wt} - S_{Nt} - S_{Gt})} \tag{5.35}$$

**Definition 13.** $S_{eTn}$ = *[reduced saturation]/[total % pore volume available for NAPL and gas flow]*

$$S_{eTn} = \frac{S_N + S_G - S_{Nt} - S_{Gt}}{(1 - S_{Gt} - S_{Nt})} \tag{5.36}$$

**Definition 14.** $S_{eTn}$ = *[reduced saturation]/[total % pore volume available for NAPL flow]*

$$S_{eTn} = \frac{S_N + S_G - S_{Nt}}{(1 - S_{Nt})} \tag{5.37}$$

Substitution of equation 5.18 into equation 5.29 leads to:

$$k_{rN}(S_W, S_G) = (S_{eN})^{\xi} \left\{ \left[ 1 - (1 - S_{eTn})^{1/m} \right]^m - \left[ 1 - (S_{eTw})^{1/m} \right]^m \right\}^2 \tag{5.38}$$

where the effective saturations are as defined above.

In summary the three-phase $k - S$ model is described by the following phase relative permeability functionals:

Water-phase - equation 5.19, with ${}^{a}S_{eW}$ and ${}^{b}S_{eW}$ defined either by equation 5.25 or 5.27;

Gas-phase - equation 5.23 with ${}^{a}S_{eG}$ and ${}^{b}S_{eG}$ defined either by equation 5.26 or 5.28;

NAPL-phase - equation 5.38 with $S_{eN}$ defined either by equation 5.30 or 5.31, $S_{eTw}$ defined either by equation 5.32, 5.33 or 5.34, and $S_{eTn}$ defined either by equation 5.35, 5.36 or 5.37.

The model includes hysteresis as the result of fluid entrapment effects through the definition of the effective saturations. In addition, it utilizes data from the saturation-pressure sub-model, the parameter $m$, and includes three fitting parameters, $\zeta$, $\xi$ and $\varphi$. The choice of effective saturation definition provides additional flexibility. Finally, it reduces to the appropriate two-phase model when appropriate.

## 5.4. MODEL IMPLEMENTATION

The hysteretic $k-S-P$ model described in this Section is effectively an alteration of the van Genuchten (1980) and Luckner et al. (1989) empirical models (subsequently referred to as the VG model). The alterations include a set of predefined empirical relationships which describe hysteresis due to capillary and fluid entrapment effects. The validity of the resulting model with respect to representing the hydraulic properties of granular soils must be a consideration. In addition, in order to be amenable for implementation in a numerical simulator, the resulting model must generate $k-S-P$ functionals which are well behaved over the full range of saturations. For example, recall that the formulation requires the $S-P$ functionals to be continuous in time and space, but that if the model defined by equation 5.13 were to be used directly, at $S_e = 0$, $h_c = \infty$ and $dh_c/dS_e = \infty$, and at $S_e = 1$, $h_c = 0$ and $dh_c/dS_e = \infty$. Therefore, additional computational steps must be taken to ensure that the functionals have finite slope, and that numerically pathologic scanning curves are not generated. Finally, a necessary attribute of the time-discrete $S-P$ model is that it generate a unique set of curves as the time step becomes small, and for mass balance considerations, that the functionals be continuous. These issues are addressed in the subsections below.

### 5.4.1. Phase Entrapment and Release

One important difference between the VG model and the current model has to do with the definition of effective saturation. Consider the case of describing the primary drainage curve (PDC). The PDC is defined by both models using equations 5.10 and 5.11. The difference between the VG model and the current model is in the definition of $S_r$, where, according to the VG model, $S_r = S_{Wr}$ is a constant, and according to the current model, $S_r = S_{Wt}(S_w)$ is a variable function of $S_W$ as defined by equation 5.7. The functional form of $S_{Wt}(S_w)$ is dependent on the blending parameter, $e$, which governs how fast a phase becomes entrapped during drainage flow conditions or released from entrapment during imbibition flow conditions. Note that with respect to the PDC, for $e = 0$, the current model reduces to the VG model, and for $e > 0$, the current model becomes a modified form of the VG model, where as $e$ gets larger, water entrapment is delayed with respect to the change in $S_W$. In Figure 5.6 we consider the effect that this modification has on the $k - S - P$ functionals. Let us assume that some soil moisture retention data was fit to the VG model, where the best-fit is given by the following parameter set: $a_d = 0.02$, $a_i = 0.04$, $\eta = 6.5$, $S_{Wr} = 0.17$, and $S_{Gr} = 0.20$. The plots show primary drainage (PDC) and main imbibition (MIC) for $S - P$ and $k - S$. The dashed lines represent the VG model (note, also the current model with $e = 0$). The solid lines represent the current model with $e = 1$ (a linear entrapment model). The general effect in employing the entrapment model is that, relative to the VG model, the capillary pressure is under-predicted during drainage events and over-predicted during imbibition events. In addition, phase relative permeability is over-predicted during phase drainage. One can avoid these discrepancies by fitting the parameters defining the present model to experimental data directly.

### 5.4.2. S-P Curve Pressure Scale Transition

As discussed in Section 5.2.2, a reversal in flow direction can result in a dramatic change in slope of the $S - P$ functional as the pressure scale changes due to capillary and contact angle effects. The change in pressure scale is accounted for by the curve-type-dependent parameter $a_{(f)}$. Because a discontinuity in slope can lead to convergence and stability problems in the numerical model, a blending rule (defined in Table 5.2) is included in the $S - P$ model. This rule governs how fast $a_{(f)}$ changes as a function of saturation after a reversal occurs. The slower $a_{(f)}$ changes over the span of the new curve, the smaller the discontinuity in slope

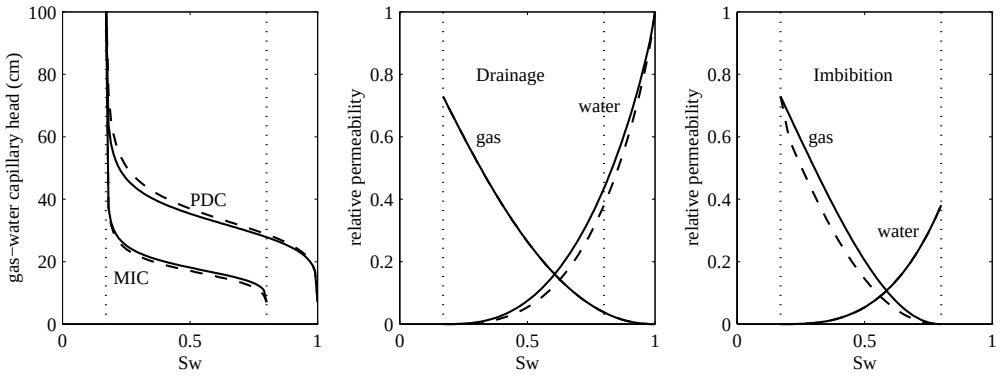


Figure 5.6: An illustration of the effect that the entrapment model blending parameter e has on the shape of the $k - S - P$ functionals. For the solid curves, $e = 1$, and for the dashed curves $e = 0$.

will be at the flow reversal point.

For example, consider the displacement process depicted in Figure 5.7 where a flow reversal along a PDC occurs at $S_W = 0.40$ and an SIC is spawned. The $S-P$ model is defined by the following parameter set: $e = 1$, $a_d = 0.02$, $a_i = 0.04$, $\eta = 6.5$, $S_{Wr} = 0.17$, and $S_{Gr} = 0.20$. The SIC described by the dashed curve was generated with $\beta = 0$, where the transition is instantaneous and the discontinuity is a maximum. The SIC described by the solid curve was generated with $\beta = 0.2$, where the transition is delayed thereby reducing the discontinuity. Numerical experiments indicate that $\beta = 0.2$ yields a sufficiently smooth transition function.

### 5.4.3. S-P Curve Restriction Parameters

Four auxiliary computational procedures are included in the $S-P$ model to ensure that the functionals are well behaved over the full range of saturations for which they are defined.

1. The $S - P$ functionals are approximated by linear extrapolation near their endpoints to ensure finite values of capillary pressure and slope. Using equation 5.10 as the base-model, the $h_c(S_e)$ functional which includes the extrapolation computation becomes:

   $h_c(S_e) \quad =$

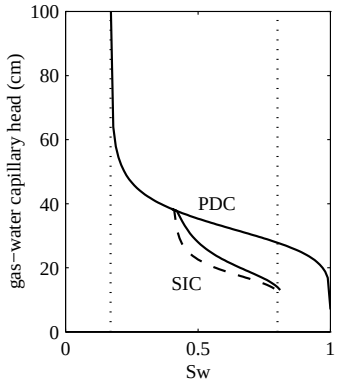


Figure 5.7: The effect of using the blending rule described in Table 5.2 to define $a_{(f)}$ as it changes from $a_d$ to $a_i$ at a flow reversal from a $PDC$ to an $SIC$. The dashed $SIC$ uses the blending rule with $beta = 0$ (i. e., an instantaneous transition), and the solid $SIC$ uses the blending rule with $beta = 0.2$.

$$\begin{cases} [(S_e)^{-1/m} - 1]^{1/\eta}(a)^{-1} & S_{er}^c < S_e < (1 - S_{es}^c) \\ h_c(S_{er}^c) + \\ \quad [S_W - S_r - S_{er}^c(S_s - S_r)]\frac{dh_c}{dS_W}(S_{er}^c) & S_e \leq S_{er}^c \\ h_c(1 - S_{es}^c) + \\ \quad [S_W - S_s - S_{es}^c(S_s - S_r)]\frac{dh_c}{dS_W}(1 - S_{es}^c) & S_e \geq (1 - S_{es}^c) \end{cases} \tag{5.39}$$

where $S_{er}^c$ and $S_{es}^c$ are critical effective saturations at the residual end and at the saturated end, respectively, at which point the linearization takes place. Values for $S_{er}^c$ and $S_{es}^c$ are of order 0.001.

2. A pathologic $S - P$ functional will be generated if the denominator defining effective saturation in equation 5.14 is too small. Therefore, a constraint is included which limits how small the denominator can be, i. e.:

$$S_{s(f)} - S_{r(f)} \geq span$$

where *span* is the specified tolerance. Numerical experiments indicate $span \geq 0.01$ is appropriate. For those $S - P$ functionals where parameter update would produce a 'span' in violation of this constraint, the current functional is retained.

3. A pathologic scanning curve will be generated if it is spawned too close to the parent-curve endpoints. Therefore, a constraint is imposed which denies scanning-curve generation unless the effective saturation of the parent-curve is between the limits:

$$\epsilon < S_{e(f)} < (1 - \epsilon)$$

where $\epsilon$ is the specified tolerance. Numerical experiments indicate $\epsilon > 0.01$ and $\epsilon > span$ is appropriate.

4. To eliminate premature reversals due to numerical irregularities, a tolerance in saturation change is defined:

$$\begin{aligned} S_W^{n+1} - S_W^{\min} &> r_d \\ S_W^{\max} - S_W^{n+1} &< r_i \end{aligned}$$

where $S_W^{\min}$ is the minimum wetting phase saturation recorded for the current drainage curve, $S_W^{\max}$ is the maximum wetting phase saturation recorded for the current imbibition curve, $r_d$ is the tolerance to indicate a reversal from drainage to imbibition, and $r_i$ is the tolerance to indicate a reversal from imbibition to drainage. Numerical experiments indicate $r$ values of order 0.001 is appropriate.

### 5.4.4. Mass Balance and Consistency

By choosing the primary flow variables to be saturation and pressure, the mathematical formulation requires that the relationship between saturation and capillary pressure is both continuous and approaches a unique path as the time step is reduced. To show how the model addresses these issues consider the following example flow scenario presented in Figure 5.8. A water drainage process has taken the $S - P$ relationship along the $PDC$ to point 1, at which time a reversal to imbibition is indicated. An $SIC$ curve is generated (the dashed curve) by forcing it to pass through the current point 1 and $1 - S_{Gt}$ (the point 1') where $S_{Gt}$ is the entrapped nonwetting phase saturation, currently zero. Over the time step the $S - P$ model parameters are held fixed and imbibition has progressed to point 2 on the dashed curve. To prepare for the next time step, $S - P$ model parameter update begins with the definition of phase entrapment, which is computed from equation 5.7 to be at point 2'. If the remaining parameters were updated by fitting the curve between points 1 and 2', the dotted line would result, thereby creating a jump in capillary pressure (a drop in $P_c$ from point 2 to 2*. To avoid

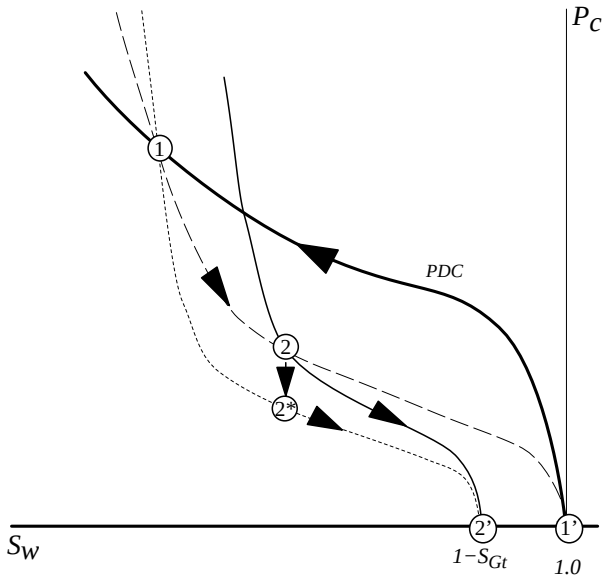


Figure 5.8: Graphical representation of how the $S-P$ functional retains continuity over a time step. Initial drainage is from point 1' to 1. Then a reversal is indicated, and the $\text{SIC}_1$ is generated (the dashed curve between points 1 and 1'). Over the time step $S_W$ increases to the point 2 along the dashed curve. Model parameters are updated to fit the $\text{SIC}_1$ between points 2 (the current point) and 2' (the updated trapped phase condition, $1 - S_{Gt}$), thereby generating the thin solid curve.

this, the parameters are computed such that the new $S - P$ curve (the thin solid curve) passes through points 2 and 2', therefore preserving continuity.

Finally, one can see that as the change in saturation over a time step becomes small, the discontinuity becomes small and the scanning curve approaches a unique path.

## 5.5. CAPILLARY PRESSURE SCALING

Leverett (1941) reasoned that the capillary pressure between two immiscible fluids should depend on the porosity, the interfacial tension between the immiscible phases, and some sort of mean pore radius. Assuming that the ratio of the permeability to porosity is proportional to the square of the mean pore radius, Leverett

defined the dimensionless function of saturation called the $J-function$. For the three-phase system considered herein, a $J-function$ can be written for each capillary pressure:

$$\begin{aligned} J(S) &= \frac{P_{cGW}(S)}{\sigma_{GW}}\left(\frac{k}{\varepsilon}\right)^{1/2} \\ J(S) &= \frac{P_{cNW}(S)}{\sigma_{NW}}\left(\frac{k}{\varepsilon}\right)^{1/2} \\ J(S) &= \frac{P_{cGN}(S)}{\sigma_{GN}}\left(\frac{k}{\varepsilon}\right)^{1/2} \end{aligned} \tag{5.40}$$

where $S$ is the wetting phase saturation. Note that the interfacial tension scaling equation 5.3 employs the concept of the $J-function$.

Leverett scaling of the capillary pressure has been used extensively in the water resources literature, for surface tension scaling (see for example Demond and Roberts, 1991, and for the modelling of three-phase systems, see Figures 5.1 and 5.2), and for soil property scaling to accommodate heterogeneity (see for example, Kueper and Frind,1991).

In concept, using the $J$-function to scale capillary pressure allows one to take the $S-P$ results for a particular soil-type with parameters $k^*$ and $\varepsilon^*$ and fluid-pair with interfacial tension $\sigma^*$, and generalize them to include other similar soil-types with parameters $k$ and $\varepsilon$ and fluid-pairs with interfacial tension $\sigma_{\alpha\beta}$.

This concept is intimately incorporated into the simulator. As discussed in Section 5.1, interfacial tension scaling is used to enable the simulator to model the general case of one-, two- and three-phase flow, while employing the primary flow variables: $P^W, S_W, S_{Tw}$. This is accomplished by defining the functions $P_{cNW}(S_W)$ and $P_{cGN}(S_{Tw})$, and by employing equations 5.3, 5.2, and 5.4. An important outcome of applying these constraints is that of the three capillary pressure relationships required to model two- and three-phase flow, *only one of the three relationships needs to be measured, with the other two gleaned from the use of equation 5.3.*

Let $P_c(S)$ be the two-phase system measured, with the parameters $\sigma^*$, $k^*$ and $\varepsilon^*$ defining fluid-pair and soil-type used. $P_c$ and $\sigma^*$ are related to which fluid pair

was measured, i. e.:

| 2-phase system measured | $P_c =$ | $\sigma^* =$ |
|---|---|---|
| $G-W$ | $P_{cGW}$ | $\sigma_{GW} = \sigma_{NW} + \sigma_{GN}$ |
| $N-W$ | $P_{cNW}$ | $\sigma_{NW} = \sigma_{GW} - \sigma_{GN}$ |
| $G-N$ | $P_{cGN}$ | $\sigma_{GN} = \sigma_{GW} - \sigma_{NW}$ |

Therefore, at any point in the domain, given $S_W$ and $S_{Tw}$ and the properties of the soil, $k$ and $\varepsilon$, the required capillary pressures can be computed by rewriting equations 5.40 as:

$$\begin{aligned} P_{cNW}(S_W) &= P_c(S_W)\frac{\sigma_{NW}}{\sigma^*}\left(\frac{k^*}{k}\right)^{1/2}\left(\frac{\varepsilon}{\varepsilon^*}\right)^{1/2} \\ P_{cGN}(S_{Tw}) &= P_c(S_{Tw})\frac{\sigma_{GN}}{\sigma^*}\left(\frac{k^*}{k}\right)^{1/2}\left(\frac{\varepsilon}{\varepsilon^*}\right)^{1/2} \end{aligned} \tag{5.41}$$

# 6. NUMERICAL MODEL DEVELOPMENT

The five mass balance equations (4.1 $[(\iota, \alpha) = (n, W)$ and $(n, G)]$, 4.8, 4.9 and 4.10) coupled with the constitutive and thermodynamic conditions presented in Chapters 4 and 5 provide a complete description of the mathematical system when proper initial and boundary conditions are imposed. The system of equations is represented by the following set of primary variables:

$$\left\{P^W(\mathbf{x}, t), S_W(\mathbf{x}, t), S_{Tw}(\mathbf{x}, t), \rho_n^W(\mathbf{x}, t), \rho_n^G(\mathbf{x}, t)\right\}$$

where $(\mathbf{x}, t) \in \Omega \times (0, T)$, represents the three-dimensional Cartesian spatial coordinates of the domain and temporal scale, respectively.

This section describes the salient features of the numerical model, and it is organized as follows. First, the governing equations are rewritten in the form which is used in the numerical model. Then the numerical discretization and solution strategy used for the set of nonlinear coupled equations is discussed. The numerical model features a sequential solution of the governing equations and an implicit-in-time collocation finite-element discretization. Next, in order to close the system mathematically, the scope of applicable initial and boundary conditions is presented. In addition, in order to improve the robustness of the algorithm, a set of numerical tools, which are designed to ensure that the physical problem and the discrete problem are compatible, is discussed. Finally, the computational steps associated with the numerical model are summarized.

## 6.1. FINAL FORM OF THE BALANCE EQUATIONS

By substituting the relevant functional definitions and simplifying assumptions and using the chain rule of differentiation, the balance equations are rewritten in the form which will be discretized and solved numerically.

### 6.1.1. Water-Phase Flow and Contaminant Transport

The water-phase flow and transport equations (4.8 and 4.1 $[(\iota,\alpha) = (n,W)]$) are coupled through phase pressure and saturation variables, the composition-dependence of phase density and viscosity, and the mass exchange terms. Employing the chain rule of differentiation and rearranging, equation 4.8 is rewritten as:

$$\begin{aligned} & \varepsilon\frac{\partial S_W}{\partial t} + \boldsymbol{\nabla} \bullet \mathbf{q}^W \\ = \; & \frac{1}{\rho^W}\left[\widetilde{\rho}^W Q^W + E_n^W - E_{n/W}^G - E_{n/W}^S - \left(\varepsilon S_W \frac{\partial \rho^W}{\partial t} + \mathbf{q}^W \bullet \boldsymbol{\nabla}\rho^W\right)\right] \end{aligned} \tag{6.1}$$

where $\mathbf{q}^W = \varepsilon S_W \mathbf{v}^W$ is the water flux vector, and $\widetilde{\rho}^W$ is the water density associated with $Q^W$. Substituting equation 4.17 into 6.1 for $\rho^W$ and rearranging yields:

$$\begin{aligned} \varepsilon\frac{\partial S_W}{\partial t} + \boldsymbol{\nabla} \bullet \mathbf{q}^W = Q^W + \frac{E_n^W - E_{n/W}^G - E_{n/W}^S}{\rho^{Wr}} \\ -\frac{r^W}{\rho^{Wr}}\left[\varepsilon S_W \frac{\partial \rho_n^W}{\partial t} + \mathbf{q}^W \bullet \boldsymbol{\nabla}\rho_n^W + \rho_n^W\left(\varepsilon\frac{\partial S_W}{\partial t} + \boldsymbol{\nabla} \bullet \mathbf{q}^W\right) - \widetilde{\rho}_n^W Q^W\right] \end{aligned} \tag{6.2}$$

where $r^W = \left(1 - \rho^{Wr}/\rho^{Nr}\right)$ and $\widetilde{\rho}_n^W$ is the mass concentration associated with $Q^W$.

The dissolved NAPL transport equation (4.1 $[(\iota,\alpha) = (n,W)]$) is rewritten in an analogous way. Using the approximation of the dispersion term defined in equation 4.24, and making the simplifying assumption that that $(\rho^{Wr}/\rho^W)$ is approximately a constant, the dissolved NAPL transport equation becomes:

$$\begin{aligned} & \varepsilon S_W \frac{\partial \rho_n^W}{\partial t} + \mathbf{q}^W \bullet \boldsymbol{\nabla}\rho_n^W + \rho_n^W\left(\varepsilon\frac{\partial S_W}{\partial t} + \boldsymbol{\nabla} \bullet \mathbf{q}^W\right) - \widetilde{\rho}_n^W Q^W \\ & = -\varepsilon S_W \kappa_n^W \rho_n^W + \left(\tfrac{\rho^{Wr}}{\rho^W}\right)\boldsymbol{\nabla} \bullet \left[\varepsilon S_W \mathbf{D}^W \bullet \boldsymbol{\nabla}\rho_n^W\right] \\ & \quad + \left(E_n^W - E_{n/W}^G - E_{n/W}^S\right) \end{aligned} \tag{6.3}$$

Given equation 6.3, the water flow equation 6.2 can be simplified algebraically by substituting the right hand side of equation 6.3 for the last term in brackets

on the right hand side of equation 6.2 to yield upon rearranging:

$$\varepsilon\frac{\partial S_W}{\partial t}+\boldsymbol{\nabla}\bullet\mathbf{q}^W=Q^W+\frac{E_n^W-E_{n/W}^G-E_{n/W}^S}{\rho^{Nr}}$$
$$+r^W\left\{\frac{\varepsilon S_W\kappa_n^W\rho_n^W}{\rho^{Wr}}-\frac{\boldsymbol{\nabla}\bullet\left[\varepsilon S_W\mathbf{D}^W\bullet\boldsymbol{\nabla}\rho_n^W\right]}{\rho^W}\right\} \tag{6.4}$$

This form of the water-phase flow equation highlights the fact that volumetric changes in the water-phase will occur as the result of mass exchange processes, and, when $\rho^W$ is a function of $\rho_n^W$ (i. e., $r^W\neq 0$), as the result of NAPL decay processes and dispersive fluxes.

Algebraic manipulation can also be used to simplify the dissolved NAPL transport equation (6.3) by substituting the right hand side of equation 6.1 for the term in parenthesis on the left hand side of equation 6.3. This operation yields upon rearranging:

$$\varepsilon S_W\frac{\partial\rho_n^W}{\partial t}+\mathbf{q}^W\bullet\boldsymbol{\nabla}\rho_n^W$$
$$+\left(\tfrac{\rho^W}{\rho^{Wr}}\right)\varepsilon S_W\kappa_n^W\rho_n^W-\boldsymbol{\nabla}\bullet\left[\varepsilon S_W\mathbf{D}^W\bullet\boldsymbol{\nabla}\rho_n^W\right]$$
$$=\left(\widetilde{\rho}_n^W-\rho_n^W\right)Q^W+\frac{\left(\rho^W-\rho_n^W\right)}{\rho^{Wr}}\left(E_n^W-E_{n/W}^G-E_{n/W}^S\right) \tag{6.5}$$

where $\widetilde{\rho}_n^W$ is a known concentration when $Q^W$ represents a source ($Q^W$ positive), and $\widetilde{\rho}_n^W=\rho_n^W$ when $Q^W$ represents a sink ($Q^W$ negative). This equation is further manipulated by substituting equations 4.28, 4.33 and 4.37 for the mass exchange terms, and rearranging i. e.,

$$\left[\varepsilon S_W+\left(1-\frac{\rho_n^W}{\rho^{Nr}}\right)\rho^bK_d\right]\frac{\partial\rho_n^W}{\partial t}$$
$$+\left[\frac{\varepsilon S_W\rho^W}{\rho^{Wr}}+\left(1-\frac{\rho_n^W}{\rho^{Nr}}\right)\rho^bK_d\right]\kappa_n^W\rho_n^W$$
$$+\mathbf{q}^W\bullet\boldsymbol{\nabla}\rho_n^W-\boldsymbol{\nabla}\bullet\left[\varepsilon S_W\mathbf{D}^W\bullet\boldsymbol{\nabla}\rho_n^W\right]$$
$$=\left(\widetilde{\rho}_n^W-\rho_n^W\right)Q^W$$
$$+\left(1-\frac{\rho_n^W}{\rho^{Nr}}\right)\left[C_n^W\left(\overline{\rho}_n^W-\rho_n^W\right)-C_{n/W}^G\left(H\rho_n^W-\rho_n^G\right)\right] \tag{6.6}$$

This form of the contaminant transport equation highlights the fact that the relationship between the divergence of the water flux and the mass exchange processes is nonlinear, and that NAPL species transport in the water and gas phases is coupled through the exchange term $E^G_{n/W}$.

### 6.1.2. NAPL-Phase Flow

Employing the chain rule of differentiation and rearranging, the NAPL-phase flow equation (4.8) becomes:

$$\varepsilon \frac{\partial S_N}{\partial t} + \boldsymbol{\nabla} \bullet \mathbf{q}^N = Q^N - \frac{\left(E^W_n + E^G_n\right)}{\rho^{Nr}} \tag{6.7}$$

where $\rho^N = \rho^{Nr}$ is a constant.

### 6.1.3. Gas-Phase Flow and Contaminant Transport

As with the water-phase, the gas-phase flow and transport equations (4.10 and 4.1 $[(\iota, \alpha) = (n, G)]$) are coupled through phase pressure and saturation variables, the composition-dependence of phase density and viscosity, and the mass exchange terms. Following an analogous series of steps as was used for the water-based equations, the equivalent form of the gas-phase flow equation (4.10) and the NAPL vapor transport equation (4.1 $[(\iota, \alpha) = (n, G)]$) are written as follows, respectively:

$$\begin{aligned} \varepsilon \frac{\partial S_G}{\partial t} + \boldsymbol{\nabla} \bullet \mathbf{q}^G &= Q^G + \frac{E^G_n + E^G_{n/W}}{\rho^{Nr}} \\ &+ r^G \left\{ \frac{\varepsilon S_G \kappa^G_n \rho^G_n}{\rho^{Gr}} - \frac{\boldsymbol{\nabla} \bullet \left[\varepsilon S_G \mathbf{D}^G \bullet \boldsymbol{\nabla} \rho^G_n\right]}{\rho^G} \right\} \end{aligned} \tag{6.8}$$

$$\begin{aligned} &\varepsilon S_G \frac{\partial \rho^G_n}{\partial t} + \mathbf{q}^G \bullet \boldsymbol{\nabla} \rho^G_n - \boldsymbol{\nabla} \bullet \left[\varepsilon S_G \mathbf{D}^G \bullet \boldsymbol{\nabla} \rho^G_n\right] \\ &\quad + \left(\frac{\rho^G}{\rho^{Gr}}\right) \varepsilon S_G \kappa^G_n \rho^G_n \\ &= \left(\widetilde{\rho}^G_n - \rho^G_n\right) Q^G \\ &\quad + \left(1 - \frac{\rho^G_n}{\rho^{Nr}}\right) \left[C^G_n \left(\overline{\rho}^G_n - \rho^G_n\right) + C^G_{n/W} \left(H \rho^W_n - \rho^G_n\right)\right] \end{aligned} \tag{6.9}$$

where $r^G = \left(1 - \rho^{Gr}/\rho^{Nr}\right)$, $\widetilde{\rho}_n^G$ is a known concentration when $Q^G$ represents a source ($Q^G$ positive), and $\widetilde{\rho}_n^G = \rho_n^G$ when $Q^G$ represents a sink ($Q^G$ negative), and $(\rho^{Gr}/\rho^G)$ is assumed to be approximately a constant. This form of the gas-based balance equations highlights the nonlinear relationship between the flow and transport parameters.

## 6.2. SEQUENTIAL, ITERATIVE SOLUTION

This section details the development of the time-discrete form of the balance equations, and the iteration method used to linearize the resulting equations.

The phase mass balance equations (6.4, 6.7 and 6.8) define the distribution of the phases given phase composition. The constituent balance equations (6.5 and 6.9) define the distribution of the NAPL species in the water- and gas-phases, given the phase distribution and velocity field. In an attempt to minimize the overall computational effort, an iterative scheme is adopted whereby the balance equations are solved by sequentially lagging certain dependent variables, such that the balance equations become uncoupled. This strategy minimizes the size of the matrix equation which is required to be solved at any one solution step.

The time scale, $t$, is discretized into a series of finite intervals, with each interval defining a time step, $\triangle\, t = (t^{k+1} - t^k)$, where $t^k$ is the current time at which the solution is known and $t^{k+1}$ is the advanced time at which the solution is sought. All time-dependent parameters are indexed with respect to where they are evaluated in time, where those terms dated at the current, known, time level are indexed by the superscript $(k)$ and those terms at the advanced, unknown time level are indexed by the superscript $(k+1)$. In addition, let us indicate those variables which are temporarily fixed in time by the superscript, $(k+1)^*$, indicating that the variable is dated at the last available solution step. The time-discrete system is summarized in the following subsections.

### 6.2.1. Time-Discrete/Linearized Form of the Flow Equations

The flow equations 6.4, 6.7 and 6.8 are solved using an algorithm based on the *total velocity formulation* of Spillette et al. (1973), which requires algebraic manipulation to generate an elliptic-like pressure equation and two parabolic-like saturation equations. The key computational feature in applying this method is that the total velocity is calculated after the solution of the pressure equation, and this velocity is then used in the saturation equations. This sequential solution

strategy has two major attributes (Peaceman, 1977):

- The total velocity obtained after the solution of the pressure equation will be the same regardless of whether the capillary pressures are evaluated explicitly or implicitly.
- The saturation equations, written in fractional flow form, are not susceptible to erroneous changes in a phase's saturation when that phase's mobility is zero.

The pressure equation is derived by adding the phase mass balance equations 6.4, 6.7 and 6.8 to eliminate the saturation time derivative, yielding:

$$\begin{aligned}\boldsymbol{\nabla} \bullet \left(\mathbf{q}^T\right)^{(k+1)} &= \left(Q^W + Q^N + Q^G\right)^{(k)} \\ &\quad - \frac{\left(E^S_{n/W}\right)^{(k+1)*}}{\rho^{Nr}} + \left(\Gamma^W_n\right)^{(k+1)*} + \left(\Gamma^G_n\right)^{(k+1)*}\end{aligned} \tag{6.10}$$

where $\mathbf{q}^T = \mathbf{q}^W + \mathbf{q}^N + \mathbf{q}^G$ is the total fluid flux, $\left(E^S_{n/W}\right)^{(k+1)*}$ defines adsorptive mass transfer (the time-discrete form of equation 4.37):

$$\left(E^S_{n/W}\right)^{(k+1)*} = \rho^b K_d \frac{\rho_n^{W(k+1)*} - \rho_n^{W(k)}}{\triangle t} + \rho^b \kappa_n^S \rho_n^{W(k+1)*} \tag{6.11}$$

and $\left(\Gamma^W_n\right)^{(k+1)*}$ and $\left(\Gamma^G_n\right)^{(k+1)*}$define respective changes in $\rho^{\,W}$ and $\rho^{\,G}$ due to the presence of NAPL species:

$$\left(\Gamma^W_n\right)^{(k+1)*} = r^W \left\{ \frac{\varepsilon S_W \kappa_n^W \rho_n^W}{\rho^{Wr}} - \frac{\boldsymbol{\nabla} \bullet \left[\varepsilon S_W \mathbf{D}^W \bullet \boldsymbol{\nabla} \rho_n^W\right]}{\rho^W} \right\}^{(k+1)*} \tag{6.12}$$

$$\left(\Gamma^G_n\right)^{(k+1)*} = r^G \left\{ \frac{\varepsilon S_G \kappa_n^G \rho_n^G}{\rho^{Gr}} - \frac{\boldsymbol{\nabla} \bullet \left[\varepsilon S_G \mathbf{D}^G \bullet \boldsymbol{\nabla} \rho_n^G\right]}{\rho^G} \right\}^{(k+1)*} \tag{6.13}$$

Choosing $P^W$ as the dependent variable, the phase fluxes used in equation 6.10 are defined from equations 4.23 as:

$$\mathbf{q}^W = -\lambda_W^{(k+1)*} \left(\boldsymbol{\nabla} P^{W(k+1)} - \gamma^{W(k+1)*} \boldsymbol{\nabla} z\right)$$

$$\begin{aligned}
\mathbf{q}^N &= -\lambda_N^{(k+1)*}\left(\boldsymbol{\nabla}\left[P^{W(k+1)} + P_{cNW}^{(k+1)*}\right] - \gamma^{N(k+1)*}\boldsymbol{\nabla} z\right) \\
\mathbf{q}^G &= -\lambda_G^{(k+1)*}\left(\boldsymbol{\nabla}\left[P^{W(k+1)} + P_{cNW}^{(k+1)*} + P_{cGN}^{(k+1)*}\right] - \gamma^{G(k+1)*}\boldsymbol{\nabla} z\right)
\end{aligned} \tag{6.14}$$

where $\lambda_\alpha = kk_{r\alpha}/\mu^\alpha$ ($\alpha$ = W, N, G), is the $\alpha-$phase *mobility* scalar.

Given its time-discrete form, the pressure equation 6.10 is a linear elliptic equation in terms of $P^W$, and thus it can be solved directly. Let us denote its solution by $P^{W(k+1)*}$. The total flux is now computed from equations 6.14 with $P^{W(k+1)}$ approximated by $P^{W(k+1)*}$. Let us denote this dated variable by $\mathbf{q}^{T(k+1)*}$.

The saturation equations are chosen to be the water phase balance equation (6.4) and the gas phase balance equation (6.8). Through algebraic manipulation of equations 6.14, $\mathbf{q}^W$ and $\mathbf{q}^G$can be rewritten in terms of $\mathbf{q}^T$ as follows:

$$\begin{aligned}
&\mathbf{q}^W = f^W \mathbf{q}^T \\
&+f^W\left\{\lambda_N\left[\boldsymbol{\nabla} P_{cNW} + \triangle\,\gamma_{WN}\boldsymbol{\nabla} z\right] + \lambda_G\left[\boldsymbol{\nabla}\left(P_{cNW} + P_{cGN}\right) + \triangle\,\gamma_{WG}\boldsymbol{\nabla} z\right]\right\}
\end{aligned} \tag{6.15}$$

$$\begin{aligned}
&\mathbf{q}^G = f^G \mathbf{q}^T \\
&-f^G\left\{\lambda_N\left[\boldsymbol{\nabla} P_{cGN} + \triangle\,\gamma_{NG}\boldsymbol{\nabla} z\right] + \lambda_W\left[\boldsymbol{\nabla}\left(P_{cNW} + P_{cGN}\right) + \triangle\,\gamma_{WG}\boldsymbol{\nabla} z\right]\right\}
\end{aligned} \tag{6.16}$$

where

$$f^\alpha = \lambda_\alpha / \left(\lambda_W + \lambda_N + \lambda_G\right), \qquad \alpha = W, G \tag{6.17}$$

is the $\alpha-$phase *fractional flow function*, and $\triangle\,\gamma_{\alpha\beta} = \gamma^\alpha - \gamma^\beta$.

With these definitions, consider the following time-discrete forms of the water- and gas-phase balance equations.

Water phase transport:

$$\begin{aligned}
&\varepsilon\frac{S_W^{(k+1)} - S_W^{(k)}}{\triangle\, t} + \boldsymbol{\nabla}\bullet\mathbf{q}^{W(k+1)} = Q^{W(k)} \\
&+\frac{\left(E_n^W - E_{n/W}^G - E_{n/W}^S\right)^{(k+1)*}}{\rho^{Nr}} + \left(\Gamma_n^W\right)^{(k+1)*}
\end{aligned} \tag{6.18}$$

where

$$\begin{aligned}
\mathbf{q}^{W(k+1)} &= f^{W(k+1)}\mathbf{q}^{T(k+1)*} \\
&\quad + \left(f^W\lambda_N\right)^{(k+1)}\left[\boldsymbol{\nabla}P_{cNW}^{(k+1)} + \triangle\,\gamma_{WN}^{(k+1)*}\boldsymbol{\nabla}z\right] \\
&\quad + \left(f^W\lambda_G\right)^{(k+1)}\left[\boldsymbol{\nabla}\left(P_{cNW}^{(k+1)} + P_{cGN}^{(k+1)}\right) + \triangle\,\gamma_{WG}^{(k+1)*}\boldsymbol{\nabla}z\right] \\
\left(E_n^W\right)^{(k+1)*} &= \left\{C_n^W\left(\overline{\rho}_n^W - \rho_n^W\right)\right\}^{(k+1)*} \\
\left(E_{n/W}^G\right)^{(k+1)*} &= \left\{C_{n/W}^G\left(H\rho_n^W - \rho_n^G\right)\right\}^{(k+1)*} \qquad (6.19)
\end{aligned}$$

and $\left(E_{n/W}^S\right)^{(k+1)*}$ and $\left(\Gamma_n^W\right)^{(k+1)*}$ are defined in equations 6.11 and 6.12, respectively.

Gas phase transport:

$$\begin{aligned}
-\varepsilon\frac{S_{Tw}^{(k+1)} - S_{Tw}^{(k)}}{\triangle\,t} + \boldsymbol{\nabla}\bullet\mathbf{q}^{G(k+1)} &= Q^{G(k)} \\
+\frac{\left(E_n^G + E_{n/W}^G\right)^{(k+1)*}}{\rho^{Nr}} + \left(\Gamma_n^G\right)^{(k+1)*} & \qquad (6.20)
\end{aligned}$$

where $S_{Tw} = (1 - S_G)$,

$$\begin{aligned}
\mathbf{q}^{G(k+1)} &= f^{G(k+1)}\mathbf{q}^{T(k+1)*} \\
&\quad - \left(f^G\lambda_N\right)^{(k+1)}\left[\boldsymbol{\nabla}P_{cGN}^{(k+1)} + \triangle\,\gamma_{NG}^{(k+1)*}\boldsymbol{\nabla}z\right] \\
&\quad - \left(f^G\lambda_W\right)^{(k+1)}\left[\boldsymbol{\nabla}\left(P_{cNW}^{(k+1)} + P_{cGN}^{(k+1)}\right) + \triangle\,\gamma_{WG}^{(k+1)*}\boldsymbol{\nabla}z\right] \\
\left(E_n^G\right)^{(k+1)*} &= \left\{C_n^G\left(\overline{\rho}_n^G - \rho_n^G\right)\right\}^{(k+1)*}
\end{aligned}$$

and $\left(E_{n/W}^G\right)^{(k+1)*}$ and $\left(\Gamma_n^G\right)^{(k+1)*}$ are defined in equations 6.19 and 6.13, respectively.

Equations 6.18 and 6.20 are nonlinear and coupled through phase saturation. To solve these equations the following *iterative sequential solution algorithm* is introduced:

- Equation 6.18 is solved for $S_W^{(k+1)}$ and equation 6.20 is solved for $S_{Tw}^{(k+1)}$.

- Each equation is linearized by a Picard-type iteration, wherein all functions of $S_W$ and $S_{Tw}$ in equations 6.18 and 6.20 are lagged an iteration.
- The uncoupled linearized equations are solved concurrently and in parallel if possible. That is, both equations are solved before the saturation-dependent terms are updated.
- Iteration continues until convergence is obtained.

This sequential solution strategy is chosen for the following reasons. First, it minimizes the computational effort required per solution step. Second, sequential solution requires that certain primary variables be temporarily lagged in order to de-couple the system as each balance equation is solved. In particular to our system, $S_{Tw}$ is lagged when the water balance is solved for $S_W$, and $S_W$ is lagged when the gas balance is solved for $S_{Tw}$. This is equivalent to saying that when solving either balance equation, a change in the dependent variable is due to a change in $S_N$. Since the NAPL has intermediate wettability between the water and gas, a symmetry is created in the form of the water and gas balance equations. This symmetry is shown in the phase velocity equations 6.15 and 6.16, where the last term in each equation is equivalent, and it represents water-gas interaction (recall that $P_{cGW} = P_{cNW} + P_{cGN}$). It is appropriate then, that this symmetry be preserved in the evaluation of the water and gas balance equations so that erroneous NAPL saturations are not created as the result of imperfect iterative convergence.

To denote iteration level the index '$m$' is used, and terms dated at time level $(k+1)$ are double indexed such that $(k+1, m)$ indicates evaluation at the last known iteration solution, and $(k+1, m+1)$ indicates the unknown quantity for which a solution is desired.

Using this notation, the linearized form of the water-phase transport equation (6.18) is:

$$\begin{aligned}
&\varepsilon \frac{S_W^{(k+1,m+1)} - S_W^{(k)}}{\triangle\, t} + \boldsymbol{\nabla} \bullet \left( f^{W(k+1,m)} \mathbf{q}^{T(k+1)*} \right) \\
&\quad + \boldsymbol{\nabla} \bullet \left\{ \left( f^W \lambda_N \right)^{(k+1,m)} \left[ \boldsymbol{\nabla} P_{cNW}^{(k+1,m+1)} + \triangle\, \gamma_{WN}^{(k+1)*} \boldsymbol{\nabla} z \right] \right\} \\
&\quad + \boldsymbol{\nabla} \bullet \left\{ \left( f^W \lambda_G \right)^{(k+1,m)} \left[ \boldsymbol{\nabla} \left( P_{cNW}^{(k+1,m+1)} + P_{cGN}^{(k+1,m+1)} \right) + \triangle\, \gamma_{WG}^{(k+1)*} \boldsymbol{\nabla} z \right] \right\} \\
&= Q^{W(k)} + \frac{\left( E_n^W - E_{n/W}^G - E_{n/W}^S \right)^{(k+1)*}}{\rho^{Nr}} + \left( \Gamma_n^W \right)^{(k+1)*}
\end{aligned} \tag{6.21}$$

Note that since $S_W$ is chosen as the dependent variable, $\bigtriangledown P_{cNW}^{(k+1,m+1)}$ must be expressed in terms of $S_W^{(k+1,m+1)}$. Consider the following strategy. First, approximate $\bigtriangledown P_{cNW}^{(k+1,m+1)}$ using a first order Taylor series expansion:

$$\boldsymbol{\nabla} P_{cNW}^{(k+1,m+1)} \approx \boldsymbol{\nabla} P_{cNW}^{(k+1,m)} + \boldsymbol{\nabla}\left[\left(\frac{dP_{cNW}}{dS_W}\right)^{(k+1,m)} \delta S_W^{(k+1,m+1)}\right] \tag{6.22}$$

where $\delta S_W^{(k+1,m+1)} = \left(S_W^{(k+1,m+1)} - S_W^{(k+1,m)}\right)$ is the *iterative increment*. Second, to minimize chaining requirements, simplify the second term on the right hand side of equation 6.22 as:

$$\boldsymbol{\nabla} P_{cNW}^{(k+1,m+1)} \approx \boldsymbol{\nabla} P_{cNW}^{(k+1,m)} + \left(\frac{dP_{cNW}}{dS_W}\right)^{(k+1,m)} \boldsymbol{\nabla}\delta S_W^{(k+1,m+1)} \tag{6.23}$$

Note that as the solution converges, the iterative increment goes to zero, and equation 6.23 becomes exact. Following a similar chaining procedure, the gas-water pressure derivative is written in terms of $S_W$ by using the capillary pressure scaling rule (4.14), i. e.:

$$\begin{aligned}
\boldsymbol{\nabla}\left(P_{cNW}^{(k+1,m+1)} + P_{cGN}^{(k+1,m+1)}\right) &= \boldsymbol{\nabla} P_{cGW}^{(k+1,m+1)} = \left(\tfrac{\sigma_{GW}}{\sigma_{NW}}\right)\boldsymbol{\nabla} P_{cNW}^{(k+1,m+1)} \\
&\approx \boldsymbol{\nabla}\left(P_{cNW}^{(k+1,m)} + P_{cGN}^{(k+1,m)}\right) \\
&\quad + \left(\tfrac{\sigma_{GW}}{\sigma_{NW}}\right)\left(\tfrac{dP_{cNW}}{dS_W}\right)^{(k+1,m)} \boldsymbol{\nabla}\delta S_W^{(k+1,m+1)}
\end{aligned} \tag{6.24}$$

This *mixed parameter iterative scheme* is used in lieu of more traditional procedures in order to correctly accommodate capillary pressure scaling with respect to heterogeneous fluid and soil distributions. Finally, substituting equations 6.23 and 6.24 into 6.21, and using $\delta S_W^{(k+1,m+1)}$ as the unknown quantity, one obtains the following linearized version of the water phase transport equation:

$$\begin{aligned}
&\varepsilon\frac{\delta S_W^{(k+1,m+1)} + S_W^{(k+1,m)} - S_W^{(k)}}{\triangle\, t} + \boldsymbol{\nabla}\bullet\left(f^{W(k+1,m)}\mathbf{q}^{T(k+1)*}\right) \\
&\quad + \boldsymbol{\nabla}\bullet\left\{\left(f^W\lambda_N\right)^{(k+1,m)}\left[\boldsymbol{\nabla} P_{cNW}^{(k+1,m)}\right.\right. \\
&\qquad \left.\left. + \left(\tfrac{dP_{cNW}}{dS_W}\right)^{(k+1,m)}\boldsymbol{\nabla}\delta S_W^{(k+1,m+1)} + \triangle\,\gamma_{WN}^{(k+1)*}\boldsymbol{\nabla} z\right]\right\}
\end{aligned}$$

$$
\begin{aligned}
&+\boldsymbol{\nabla}\bullet\left\{\left(f^{W}\lambda_{G}\right)^{(k+1,m)}\left[\boldsymbol{\nabla}\left(P_{cNW}^{(k+1,m)}+P_{cGN}^{(k+1,m)}\right)\right.\right.\\
&\quad\left.\left.+\left(\frac{\sigma_{GW}}{\sigma_{NW}}\right)\left(\frac{dP_{cNW}}{dS_{W}}\right)^{(k+1,m)}\boldsymbol{\nabla}\delta S_{W}^{(k+1,m+1)}+\triangle\,\gamma_{WG}^{(k+1)*}\boldsymbol{\nabla}z\right]\right\}\\
&=Q^{W(k)}+\frac{\left(E_{n}^{W}-E_{n/W}^{G}-E_{n/W}^{S}\right)^{(k+1)*}}{\rho^{Nr}}+\left(\Gamma_{n}^{W}\right)^{(k+1)*}
\end{aligned}
\tag{6.25}
$$

Following an analogous procedure, the linearized form of the gas-phase transport equation (6.20) is written in terms of the iterative increment $\delta S_{Tw}^{(k+1,m+1)}=\left(S_{Tw}^{(k+1,m+1)}-S_{Tw}^{(k+1,m)}\right)$:

$$
\begin{aligned}
&-\varepsilon\frac{\delta S_{Tw}^{(k+1,m+1)}+S_{Tw}^{(k+1,m)}-S_{Tw}^{(k)}}{\triangle\,t}+\boldsymbol{\nabla}\bullet\left(f^{G(k+1,m)}\mathbf{q}^{T(k+1)*}\right)\\
&\quad-\boldsymbol{\nabla}\bullet\left\{\left(f^{G}\lambda_{N}\right)^{(k+1,m)}\left[\boldsymbol{\nabla}P_{cGN}^{(k+1,m)}\right.\right.\\
&\qquad\left.\left.+\left(\frac{dP_{cGN}}{dS_{Tw}}\right)^{(k+1,m)}\boldsymbol{\nabla}\delta S_{Tw}^{(k+1,m+1)}+\triangle\,\gamma_{NG}^{(k+1)*}\boldsymbol{\nabla}z\right]\right\}\\
&\quad-\boldsymbol{\nabla}\bullet\left\{\left(f^{G}\lambda_{W}\right)^{(k+1,m)}\left[\boldsymbol{\nabla}\left(P_{cNW}^{(k+1,m)}+P_{cGN}^{(k+1,m)}\right)\right.\right.\\
&\qquad\left.\left.+\left(\frac{\sigma_{GW}}{\sigma_{GN}}\right)\left(\frac{dP_{cGN}}{dS_{Tw}}\right)^{(k+1,m)}\boldsymbol{\nabla}\delta S_{Tw}^{(k+1,m+1)}+\triangle\,\gamma_{WG}^{(k+1)*}\boldsymbol{\nabla}z\right]\right\}\\
&=Q^{G(k)}+\frac{\left(E_{n}^{G}+E_{n/W}^{G}\right)^{(k+1)*}}{\rho^{Nr}}+\left(\Gamma_{n}^{G}\right)^{(k+1)*}
\end{aligned}
\tag{6.26}
$$

After equations 6.25 and 6.26 are solved, the required variables are updated:

$$
\begin{aligned}
S_{W}^{(k+1,m+1)} &= S_{W}^{(k+1,m+1)}-\delta S_{W}^{(k+1,m)}\\
S_{Tw}^{(k+1,m+1)} &= S_{Tw}^{(k+1,m+1)}-\delta S_{Tw}^{(k+1,m)}
\end{aligned}
$$

Iterations continue until $\delta S_{W}^{(k+1,m+1)}$ and $\delta S_{Tw}^{(k+1,m+1)}$ are sufficiently small.

### 6.2.2. Time-Discrete/Linearized Form of the Transport Equations

In general, the fluid phase properties are only slightly affected by the contaminant species, thus the flow and contaminant transport equations are only weakly coupled. Therefore, the solution to the flow problem is used to define the flow

variables used in the transport equations (6.6 and 6.9). Indexing the most recent flow solution by the superscript $(k+1)*$, the following flow variables are defined: $S_W^{(k+1)*}$, $S_{Tw}^{(k+1)*}$, $\mathbf{q}^{W(k+1)*}$, $\mathbf{q}^{G(k+1)*}$, $\mathbf{D}^{W(k+1)*}$ and $\mathbf{D}^{G(k+1)*}$.

From equations 6.6 and 6.9 it is clear that the transport equations are coupled and nonlinear as the result of mass exchange processes. In order to solve the equations, consider the following *iterative sequential solution algorithm*:

- Equation 6.6 is solved for $\rho_n^{W(k+1)}$ and equation 6.9 is solved for $\rho_n^{G(k+1)}$.
- Each equation is linearized by a Picard-type iteration, where all functions of $\rho_n^{W(k+1)}$ and $\rho_n^{G(k+1)}$ are lagged an iteration.
- The uncoupled linearized equations are solved concurrently and in parallel if possible. That is, both equations are solved before the concentration-dependent terms are updated.
- Iteration continues until convergence is obtained.

Rewriting equations 6.6 and 6.9 in a linearized, time-discrete form consistent with iterative sequential solution, one obtains:

$$\begin{aligned}
&\left[\varepsilon S_W^{(k)} + \left(1 - \frac{\rho_n^{W(k+1,m)}}{\rho^{Nr}}\right)\rho^b K_d\right]\frac{\rho_n^{W(k+1,m+1)} - \rho_n^{W(k)}}{\triangle t} \\
&\quad + \left[\frac{\varepsilon S_W^{(k)}\rho^{W(k+1,m)}}{\rho^{Wr}} + \left(1 - \frac{\rho_n^{W(k+1,m)}}{\rho^{Nr}}\right)\rho^b K_d\right]\kappa_n^W \rho_n^{W(k+1,m+1)} \\
&\quad + \mathbf{q}^{W(k+1)*} \bullet \boldsymbol{\nabla}\rho_n^{W(k+1,m+1)} - \boldsymbol{\nabla} \bullet \left[\left(\varepsilon S_W \mathbf{D}^W\right)^{(k+1)*} \bullet \boldsymbol{\nabla}\rho_n^{W(k+1,m+1)}\right] \\
&= \left(\widetilde{\rho}_n^W - \rho_n^{W(k+1,m+1)}\right) Q^{W(k)} \\
&\quad + \left(1 - \frac{\rho_n^{W(k+1,m)}}{\rho^{Nr}}\right)\left[C_n^{W(k+1)*}\left(\overline{\rho}_n^W - \rho_n^{W(k+1,m+1)}\right)\right. \\
&\qquad \left. - C_{n/W}^{G(k+1)*}\left(H\rho_n^{W(k+1,m+1)} - \rho_n^{G(k+1,m)*}\right)\right] \qquad (6.27)
\end{aligned}$$

$$\begin{aligned}
&\left(\varepsilon S_G^{(k)}\right)\frac{\rho_n^{G(k+1,m+1)} - \rho_n^{G(k)}}{\triangle t} \\
&\quad + \mathbf{q}^{G(k+1)*} \bullet \boldsymbol{\nabla}\rho_n^{G(k+1,m+1)} - \boldsymbol{\nabla} \bullet \left[\left(\varepsilon S_G \mathbf{D}^G\right)^{(k+1)*} \bullet \boldsymbol{\nabla}\rho_n^{G(k+1,m+1)}\right]
\end{aligned}$$

$$
\begin{aligned}
&+\left(\frac{\varepsilon S_G^{(k)}\rho^{G(k+1,m)}\kappa_n^G}{\rho^{Gr}}\right)\rho_n^{G(k+1,m+1)}\\
&=\left(\widetilde{\rho}_n^G-\rho_n^{G(k+1,m+1)}\right)Q^{G(k)}\\
&\quad+\left(1-\frac{\rho_n^{G(k+1,m)}}{\rho^{Nr}}\right)\left[C_n^{G(k+1)*}\left(\overline{\rho}_n^G-\rho_n^{G(k+1,m+1)}\right)\right.\\
&\qquad\left.+C_{n/W}^{G(k+1)*}\left(H\rho_n^{W(k+1,m)*}-\rho_n^{G(k+1,m+1)}\right)\right] \qquad (6.28)
\end{aligned}
$$

where $\rho_n^{W(k+1,m)*}$ and $\rho_n^{G(k+1,m)*}$ represent a weighted average of the lagged variables, i. e.,

$$
\rho_n^{\alpha(k+1,m)*}=\theta\rho_n^{\alpha(k+1,m)}+(1-\theta)\,\rho_n^{\alpha(k+1,m-1)},\quad \alpha=W,G \qquad (6.29)
$$

and $\theta$ is a weighting parameter, $0\leq\theta\leq 2$.

## 6.3. SPATIAL APPROXIMATION

The three-dimensional domain is discretized into a finite number of brick-like elements (i. e., a regular rectangular mesh) with nodes located at element boundary intersections. *All spatially varying parameters are represented by a linear combination of basis functions where nodal values can be interpolated into adjacent elements in a continuous manner.* These parameters include the dependent variables and functions of the dependent variables, and soil properties and other physical constants which are allowed to vary spatially.

Consider first the dependent variables defining equations 6.10, 6.25, 6.26, 6.27 and 6.28: $P^W$, $S_W$, $S_{Tw}$, $\rho_n^W$ and $\rho_n^G$, respectively. Since these variables require continuous second-order derivatives, the $C^1$ continuous *Hermite cubic interpolation polynomials* are chosen. They are defined in Appendix B.

For three-dimensional discretizations, a general function, $u(\mathbf{x},t)$ is approximated over each grid block as:

$$
u(\mathbf{x},t)\approx\widehat{u}(\mathbf{x},t)=\sum_{i=1}^{8}\left\{U(t)\right\}_i^T\left\{\Phi(\mathbf{x})\right\}_i \qquad (6.30)
$$

where $\widehat{u}(\mathbf{x},t)$ is the spatially-discrete approximation to $u(\mathbf{x},t)$. At each of the eight $i$ nodes in a grid block is defined a vector of eight time-dependent undetermined

coefficients:

$$\{U(t)\}_i^T = \{U(t), U_{,x}(t), U_{,y}(t), U_{,z}(t), U_{,xy}(t), U_{,xz}(t), U_{,yz}(t), U_{,xyz}(t)\}_i$$

where the subscript $[\ ,(\bullet)]$ represents the partial derivative with respect to $(\bullet)$, and a vector of eight space-dependent Hermite interpolation functions, $\{\Phi(\mathbf{x})\}_i$, the form of which is detailed in Appendix B.

Each dependent variable is approximated spatially by an equation of the form 6.30, yielding for example, $\widehat{P^W}(\mathbf{x},t)$, $\widehat{S_W}(\mathbf{x},t)$, $\widehat{S_{Tw}}(\mathbf{x},t)$, $\widehat{\rho_n^W}(\mathbf{x},t)$ and $\widehat{\rho_n^G}(\mathbf{x},t)$. These approximations are then substituted into their respective balance equations yielding five equations in $5[8(I)]$ nodal unknowns (5 dependent variables, 8 undetermined coefficients per node, and I nodes).

The remaining parameters requiring spatial representation are either functions of a dependent variable (e.g. capillary pressure and fluid mobility) or spatially varying physical constants (e. g., soil properties $\varepsilon$ and $\mathbf{k}$). With respect to capillary pressures, because a *mixed parameter iterative scheme* (defined in equations 6.25 and 6.26) is employed where, as the iterative increment in saturation approaches zero, the space operator is defined by capillary pressure gradients, it is necessary to use a Hermite representation for $P_{cNW}(S_W)$ and $P_{cGN}(S_{Tw})$. The eight nodal coefficients are computed as functions of saturation, and, where applicable, the chain rule for differentiation is applied (see Appendix B for details). *The remaining coefficients are defined nodally using relevant data, and defined on each mesh block in terms of the tensor product ordering of the one-dimensional linear Lagrange polynomials.*

The combination of using piecewise continuous soil properties and Hermite interpolated pressure variables has the advantage of yielding a piecewise continuous velocity field for use in the transport equations.

The nodal unknowns generated from the Hermite discretization are determined by employing the *collocation method*, a method of weighted residuals where the weighting function is the displaced Dirac delta function (see Frind and Pinder [1979] for a detailed discussion). As a result, the residual errors incurred by using approximated dependent variables in the governing equations are driven to zero at specified points in the domain, called collocation points. If the Gauss quadrature points are chosen as the *collocation points*, the method is called *orthogonal collocation.*

Using the general function $\widehat{u}(\mathbf{x},t)$ as a surrogate for each approximated dependent variable, a system of linear algebraic equations is generated for each balance

equation by imposing the interpolation constraints:

$$\widehat{u}(\mathbf{x}_j, t) = u(\mathbf{x}_j, t), \quad j = 1, 2, ..., 8(NEL)$$

where $(\mathbf{x}_j)$ are the locations of the collocation points, and NEL is the number of elements. This results in a matrix equation of order $[8(NEL)]$ for each discretized balance equation. Note that equation generation requires no formal integrations, and therefore, collocation is computationally analogous to the finite difference method in that equations are written at points in the domain.

## 6.4. IMPOSED CONDITIONS

The problem posed in the previous sections is an initial, boundary value problem, and as such, requires initial and boundary conditions to mathematically close the system. In addition the method used to impose external flux conditions is detailed.

### 6.4.1. Initial Conditions

Initial conditions are specified such that saturation and composition are defined at $t = 0$. The following variables require initial data:

**Flow variables**

$$\begin{aligned} S_W(\mathbf{x}, 0) &= S_{W0}(\mathbf{x}) \\ S_{Tw}(\mathbf{x}, 0) &= S_{Tw0}(\mathbf{x}) \end{aligned}$$

where the specified values $S_{W0}(\mathbf{x})$ and $S_{Tw0}(\mathbf{x})$ define the initial $k - S - P$ functionals according the decision tree provided in Appendix C.

**Contaminant transport variables** In general the conditions are

$$\begin{aligned} \rho_n^W(\mathbf{x}, 0) &= \rho_{n0}^W(\mathbf{x}) \\ \rho_n^G(\mathbf{x}, 0) &= \rho_{n0}^G(\mathbf{x}) \end{aligned}$$

In addition, by default, at any node where the initial conditions for saturation indicate that NAPL is present, i. e., $(S_{Tw0} - S_{W0}) > 0$, the concentration variables are set to their respective solubility limits, i. e., $\rho_{n0}^W = \overline{\rho}_n^W$ and $\rho_{n0}^G = \overline{\rho}_n^G$.

### 6.4.2. Boundary Conditions

A sufficient number of boundary conditions must be specified to augment the collocation equations such that the number of equations equals the number of unknowns. This is accomplished by specifying as known a group of Hermite coefficients at each boundary node. The grouping is based on the particular *boundary condition-type* imposed and the *boundary node-type* at which the condition is applied:

1. *boundary condition-type*: three types of boundary conditions can be imposed at a given boundary node: Dirichlet (first-type), Neumann (second-type) or mixed (third-type)[1]. For Dirichlet data the function value is specified at the node. For Neuman data the derivative normal to a specific boundary plane associated with the node is specified. For mixed data, a linear combination of Dirichlet and Neumann data is specified at the node.

2. *boundary node-type*: typing is based on the orientation and number of plane(s) in which the node lies (x-y-plane, y-z plane, and x-z-plane). Along with the user-defined coefficients identified in (1), the simulator specifies, by default, those Hermite coefficients which are derivatives of the boundary data in the direction(s) tangential to the boundary plane(s) associated with the node, where the node-type is used to identify which coefficients apply.

For example, if Dirichlet data is to be applied to a node which is in an x-y boundary-plane, then the user specifies the Hermite coefficient $U$ (the Dirichlet data) and the simulator applies appropriate default conditions on the coefficients $U_{,x}$, $U_{,y}$ and $U_{,xy}$ (the tangential derivatives of $U$ in the x-y boundary-plane). The details of which degrees of freedom are associated with which boundary condition- and node-types are provided in Appendix B. Note that this discussion is specific to the three-dimensional case. An analogous procedure is applied for the two-dimensional case where the two-dimensional problem is equivalent to one plane of nodes in the three-dimensional problem.

This subsection provides a description of the specific boundary conditions used in the simulator. Imposition of point source and sink terms is discussed in the following subsection.

[1]The current version of the simulator only considers mixed boundary data for the NAPL species in the gas-phase transport equation.

**Flow Variables**

Two types of flow boundary conditions are considered in this simulator: Dirichlet and Neumann. A boundary which is considered closed to mass flux is modeled using a Neumann condition. A boundary which is considered open to mass flux is modeled using either a Dirichlet condition, or using the combination of a closed boundary Neumann condition and a point source or sink term representing the specified flux.

Consider a specification system which identifies a series of boundary-type cases defined on the basis of the three-phase flow condition. Each case is defined by the following criteria:

- for each of the phases, specify whether the boundary is open or closed to flow;
- a boundary which is considered open to flow of a given phase is defined by specifying either phase pressure, saturation or flux.

Table 6.1 provides a summary of the specification system used in the simulator for which five cases have been identified. This Table includes information on the flow status of the boundary, the Dirichlet variable(s) specified where applicable, and what kind of boundary condition results for each dependent variable. In addition, Table 6.1 provides information on whether the resulting boundary conditions are linear or nonlinear with respect to the flow variables. Note that any condition which involves gas- or NAPL-phase pressure related information is a nonlinear function of the solution. This is a direct result of the choice in primary variables, $P^W$, $S_W$ and $S_{Tw}$ (recall equations 4.16).

With respect to this simulator, all the boundary nodes are assumed to be no flow (Case 1) unless otherwise specified (i. e., *no flow is the default condition*). In addition, the nonlinear terms in each boundary condition equation are dated at the old time level (indexed by the superscript $k$). As a result, *boundary conditions are in general constant over a time step and time varying* (updated after each time step)

The specific boundary equations corresponding to each of the cases listed in Table 6.1 are presented below. Note that the superscript $(k+1)$ represents information dated at the advanced time level , and that the notation $(\bullet)_{,n}$ indicates the spatial derivative of the quantity $(\bullet)$ normal to the boundary.

| case | boundary open (o) closed(x) to flow of phase | | | variables specified | conditions for the primary variables, 1 = Dirichlet, 2 = Neuman (L = linear, NL = nonlinear) | | | comment |
|---|---|---|---|---|---|---|---|---|
| | W | N | G | | $P^W$ | $S_W$ | $S_{Tw}$ | |
| 1 | x | x | x | | 2(L) | 2(NL) | 2(NL) | the default condition |
| 2 | x | x | o | $P^G$ | 2(L) | 2(NL) | 2(NL) | replace with source term |
| 3 | x | o | x | $P^N$ | 2(L) | 2(NL) | 2(NL) | replace with source term |
| 4 | o | x | x | $P^W$ | 1(L) | 2(NL) | 2(NL) | |
| 5 | o | o | o | $P^W$ $S_W$ $S_{Tw}$ | 1(L) | 1(L) | 1(L) | |

Table 6.1: SUMMARY OF THE SYSTEM USED TO DEFINE BOUNDARY CONDITIONS FOR THE FLOW VARIABLES

**Case 1** The boundary is closed to water, NAPL and gas flow. *This is the default condition used in the simulator*, i. e., if no other flow condition is imposed at a given boundary node, then the simulator assumes it is a Case 1 boundary node. The boundary equations are derived by setting equations 6.14 equal to zero and solving for the respective variables, i. e.,

$$\begin{aligned} \left(P^W\right)_{,n}^{(k+1)} &= \rho^W g \cos\theta \\ \left(S_W\right)_{,n}^{(k+1)} &= \left[\frac{dS_W}{dP_{cNW}}\left(\rho^N - \rho^W\right)\right]^{(k)} g\cos\theta \\ \left(S_{Tw}\right)_{,n}^{(k+1)} &= \left[\frac{dS_{Tw}}{dP_{cGN}}\left(\rho^G - \rho^N\right)\right]^{(k)} g\cos\theta \end{aligned} \tag{6.31}$$

**Case 2** The boundary is made open to gas flow by specifying $P^G = P^{G0}$. Consider an algorithm which approximates the gas-phase pressure Dirichlet boundary condition by generating an appropriate source or sink term, the rate of which results in $P^G \approx P^{G0}$ at the boundary node. The algorithm takes advantage of the fact that a sequential total flow formulation is utilized. First equation 6.10 is solved with the following boundary data which satisfies the stated condition:

$$P^W = P^{G0} - P_{cNW}(S_W^{(k+1)*}) - P_{cGN}(S_{Tw}^{(k+1)*})$$

Second, $\mathbf{q}^{T(k+1)*}$ is computed from the solution. Before solving the saturation transport equations, the results from the total flow solution at Case 2 boundary nodes are interpreted as a combination of a no flow boundary with conditions defined in 6.31 and an active point source or sink with the rate defined as:

| | |
|---|---|
| for inflow conditions: | $Q^G = \mathbf{q}_n^{T(k+1)*}(area)$<br>$Q^W = Q^N = 0$ |
| for outflow conditions: | $Q^\alpha = f^{\alpha(k+1)*}\mathbf{q}_n^{T(k+1)*}(area)$, $\alpha = W, N, G$ |

where $\mathbf{q}_n^{T(k+1)*}$ is the normal component of the total flux vector at the boundary node, $(area) = 1/4$(element area about the node in the 2-D plane through which $\mathbf{q}_n^T$ is defined) is the area associated with the boundary node, and for outflow conditions the rate is allocated based on $\alpha$-phase fractional flow conditions, $f^{\alpha(k+1)*}$ (defined in equation 6.17). Note that if inflow conditions prevail at the node, then the boundary is open only to the gas-phase, but if outflow conditions are indicated, then the rate is allocated as indicated.

**Case 3** The boundary is made open to NAPL flow by specifying $P^N = P^{N0}$. Following the same logic as for Case 2, solve the total flow equation with the following boundary data which satisfies the stated condition:

$$P^W = P^{N0} - P_{cNW}(S_W^{(k+1)*})$$

Before solving the saturation transport equations the results from the total flow solution at Case 3 boundary nodes are interpreted as a combination of a no flow boundary with conditions defined in 6.31 and an active point source or sink with rate defined as:

| | |
|---|---|
| for inflow conditions: | $Q^N = \mathbf{q}_n^{T(k+1)*}(area)$<br>$Q^W = Q^G = 0$ |
| for outflow conditions: | $Q^\alpha = f^{\alpha(k+1)*}\mathbf{q}_n^{T(k+1)*}(area)$, $\alpha = W, N, G$ |

**Case 4** The boundary is made open to only the water-phase by specifying $P^W = P^{W0}$ (a linear Dirichlet condition) in combination with the no flow conditions for the NAPL- and gas-phases as defined in Case 1.

**Case 5** The boundary is made open to all three phases by specifying the following linear Dirichlet data:

$$\boxed{\begin{array}{l} P^W = P^{W0} \\ S_W = S_{W0} \\ S_{Tw} = S_{Tw0} \end{array}}$$

**Transport Variables**

**NAPL Species in the Water-Phase** The assumption is made herein that, with respect to water-phase contaminant transport, dispersion is small compared to advection, and therefore, the applicable conditions reduce to *Dirichlet* and *homogeneous Neumann*.

The *default conditions* used in the simulator are as follows:

if at a given boundary node, the boundary condition for flow is Case 5, and $S_N > 0$, then Dirichlet data are specified so that $\rho_n^W = \overline{\rho}_n^W$, otherwise a homogeneous Neumann condition is applied, i. e., $\frac{\partial \rho_n^W}{\partial n} = 0$.

Given the default conditions for $\rho_n^W$ at each boundary node, the user needs to specify only Dirichlet conditions, i. e., $\rho_n^W(\mathbf{x}, t) = \rho_{n0}^W$.

**NAPL Species in the Gas-Phase** Since diffusion in the gas-phase is a significant transport mechanism a mixed-type boundary condition is included to model gas-phase mass transport across a boundary which represents the ground surface. If the atmosphere is considered an infinite sink (i. e., $\rho_n^G\big|_{atm} = 0$) and the mass flux is defined by diffusion across a stagnant boundary layer of thickness $\delta$ then the mixed condition is written as:

$$\left(\rho_n^G \mathbf{q}^G - \varepsilon S_G \mathbf{D}^G \cdot \nabla \rho_n^G\right) \cdot \mathbf{n} = \frac{D_m^G}{\delta} \rho_n^G \tag{6.32}$$

where $\mathbf{n}$ is the inwardly directed unit vector normal to the boundary. Note that as $\delta$ goes to zero the condition becomes homogeneous Dirichlet, and that as $\delta$ gets large the condition becomes homogeneous Neumann.

The *default conditions* used in the simulator are as follows:

if at a given boundary node, the boundary condition for flow is Case 5, and $S_N > 0$, then Dirichlet data are specified so that $\rho_n^G = \overline{\rho}_n^G$, otherwise a homogeneous Neumann condition is applied, i. e., $\frac{\partial \rho_n^G}{\partial n} = 0$.

Given the default conditions for $\rho_n^G$ at each boundary node, the user has the choice of specifying either a Dirichlet condition by defining $\rho_n^G(\mathbf{x}, t) = \rho_{n0}^G$, or a mixed condition by defining the value of $\delta$.

### 6.4.3. External Flux Conditions

External flux conditions are point source or sink terms represented in equations 6.4, 6.7, 6.8, 6.3 and 6.28 as $Q^\alpha$ $[1/T]$. The user specifies $Q^\alpha$ at a node in units of $[L^3/T]$ and the simulator normalizes that flow rate by the volume associated with the node (1/8 of the volume of the elements surrounding the node). By convention positive $Q^\alpha$ represents a source and negative $Q^\alpha$ represents a sink. Numerically, $Q^\alpha$ is defined at a node and interpolated using linear Lagrange basis functions.

Source forcing terms are applied with known composition, and are thus incorporated directly into the mass balance equations. For sink forcing terms, however, fluid composition is not known, and the distribution of the phases must be determined in order to define the phase flow rates. The procedure used in the simulator to allocate flow rates to each of the phases as the solution evolves through time is based on fractional flow defined by phase mobilities. During any given time step, $(k)$ to $(k+1)$, the outflow phase fluxes will be allocated using information from the last time step (*explicit formulation*). Given that total flux is known at the current time level, $Q^T = Q^W + Q^N + Q^G = \left(Q^T\right)^{(k)}$, the phase fluxes are defined as:

$$\left(Q^\alpha\right)^{(k)} = \mathbf{f}^{\alpha(k)} \left(Q^T\right)^{(k)} \quad , \alpha = W, N, G \tag{6.33}$$

## 6.5. DIAGNOSTIC TOOLS

Solving for the temporal and spatial distribution of NAPL contaminants results in a problem with moving fronts. In addition, because the model considers the emplacement of residual NAPL in the vadose- and saturated-zones, it needs to consider problems which evolve to quasi-static flow conditions, with the distribution of phase saturations governed by system forcing, soil and fluid properties, and the nonlinear flow parameters. In a heterogeneous distribution of physical properties and forcing terms, the static solutions involve different length-scale boundary layers where phases appear and disappear. Therefore, any numerical model derived to solve this type of physical problem must be able to resolve a complex distribution of fluid saturations. As such, it is imperative that the spatial and temporal discretizations utilized be compatible with the flow parameters so

that discretization errors do not adversely affect the quality of the solution, and that the case of phase appearance and disappearance can be accommodated.

In light of this discussion a series of diagnostic numerical tools have been developed which are designed to ensure this compatibility. These tools can be separated into two categories: those which assess the spatial discretization and those which assess the temporal discretization. The spatial discretization is assessed through the use of a *Peclet constraint*. The temporal discretization is assessed through the use of a *Courant constraint* and a dynamic time-stepping scheme based on the number of iterations required for convergence on the nonlinearity.

Effectively, this section describes the diagnostic numerical tools designed to make the simulator more robust.

### 6.5.1. Peclet Constraint

It is well known that application finite element numerical methods to immiscible flow problems with sharp fronts will generate solutions which exhibit oscillations when the spatial truncation errors are unable to correctly propagate the short wave-length parts of the solution (Allen, 1983 and Mercer and Faust, 1976). Oscillations can lead to violation of the maximum principle, which results in non-physical values of the primary variables and potential instabilities in evaluating the nonlinear coefficients. In addition the combination of the inability of the approximation to propagate short wave-length oscillations with the sensitivity of the frontal velocity with respect to those short wave-length components, can result in convergence to the wrong solution (see Allen, 1983 for details).

Assuming that some physical capillarity exists for the problems under consideration herein, the relationship between the flow parameters which define the shape of the front and the grid spacing which defines the resolution scale, is quantified by the dimensionless group of parameters called the Peclet number, $Pe$, defined as:

$$Pe = \frac{(advection)(characteristic\ length\ scale)}{(diffusion)} \tag{6.34}$$

where in this case *the advection parameters are dominated by gravity forces*, *the diffusion parameters are dominated by capillary forces*, and *the characteristic length scale is related to the local grid spacing*. Large values of $Pe$ indicate a sharp front relative to the grid spacing, and small values indicate a diffused front relative to the grid spacing. Consider the definition of a critical working $Pe$, called here $Pe^{crit}$, for a particular finite element method. $Pe^{crit}$, determined from numerical experiment by successively refining the mesh for a given problem, is that

$Pe$ where the numerical solution exhibits oscillations at or below some tolerance. Therefore, given the flow parameter values, nonphysical numerical oscillations in the finite element solution can be minimized by using a spatial discretization for which $Pe \leq Pe^{crit}$.

However, because mesh refinement is computationally expensive, it is in general an impractical option. As a result, a second option is to alter the flow parameters given the grid spacing so that $Pe \leq Pe^{crit}$. Specifically one adds artificial diffusion sufficient to smooth the solution, and thus, eliminate the undesirable truncation errors.

Adding artificial diffusion alters the physical problem, resulting in a smooth but overly smeared front. Therefore, the term should maintain the following attributes:

1. be applied only where needed, and in minimum magnitude;
2. be a function of the local grid spacing, flow parameters, and solution evolution;
3. not be a function of coordinate rotation; and
4. provide a convergent solution as the grid is refined.

Upstream weighting is a common class of methods used to add diffusion by introducing a low-order spatial truncation error, the size of which is meaningful only near sharp fronts. Because the size of the non-physical error term introduced is in general dependent on the orientation of the front with respect to the grid, upstream weighting methods do not meet requirement (3.) for problems involving large mobility-ratio displacements (the viscosity of the invading fluid is much less than that of the displaced fluid, for example gas displacing NAPL).

The goal of this analysis is to define a physically-based diffusion term to be added to the governing equations which meets the three attributes identified above, and which is applicable for the general multiphase flow problem where a non-zero physical capillarity is inherent in the system..

The differential equations which describe phase transport can be classified as nonlinear parabolic advection-diffusion equations, with the advection term dominated by gravity forces and the diffusion term defined by capillary forces. The water- and gas-phase saturation equations can be written in advection-diffusion form by using the fractional flow formulation described in Section 6.2.1. For clarity in presentation and without loss in generality, consider the physically simplified

case of constant fluid density, isotropic porous medium, and no sources or sinks of mass. For this case the water and gas equations are written as:

$$\begin{aligned}
&\varepsilon\frac{\partial S_W}{\partial t} \\
&+\boldsymbol{\nabla}\bullet\left(f^W\mathbf{q}^T+\left[\left(f^W\lambda_N\right)\triangle\gamma_{WN}+\left(f^W\lambda_G\right)\triangle\gamma_{WG}\right]\boldsymbol{\nabla}z\right) \\
&+\boldsymbol{\nabla}\bullet\left[\Lambda_{WN}\left(f^W\lambda_N\right)\boldsymbol{\nabla}P_{cNW}+\Lambda_{WG}\left(f^W\lambda_G\right)\boldsymbol{\nabla}P_{cGW}\right] \\
&=0
\end{aligned} \tag{6.35}$$

$$\begin{aligned}
&-\varepsilon\frac{\partial S_{Tw}}{\partial t} \\
&+\boldsymbol{\nabla}\bullet\left(f^G\mathbf{q}^T-\left[\left(f^G\lambda_N\right)\triangle\gamma_{NG}+\left(f^G\lambda_W\right)\triangle\gamma_{WG}\right]\boldsymbol{\nabla}z\right) \\
&-\left[\Lambda_{NG}\left(f^G\lambda_N\right)\boldsymbol{\nabla}P_{cGN}+\Lambda_{WG}\left(f^G\lambda_W\right)\boldsymbol{\nabla}P_{cGW}\right] \\
&=0
\end{aligned} \tag{6.36}$$

On the left-hand-side of equations 6.35 and 6.36 *the second term represents the advective component of mass transport* which consists of two sub-components: advection due to total fluid velocity, and advection due to gravitational forces, and the third term represents *the diffusive component of mass transport* which arises from capillary forces where $P_{cGW} = P_{cNW} + P_{cGN}$, and the terms $\Lambda_{NW}$, $\Lambda_{NG}$ and $\Lambda_{GW}$ are new parameters which govern how much artificial physical diffusion is added to the system. Specifically, $\Lambda_{\alpha\beta} \geq 1$ ($\alpha\beta$ = WN, NG, WG), and the case when $\Lambda_{\alpha\beta} = 1$ represents no additional diffusion. The focus of this development is to derive an algorithm to calculate the terms $\Lambda_{NW}$, $\Lambda_{NG}$ and $\Lambda_{GW}$ based on an appropriate definition of grid Peclet number for two- and three-phase flow.

Section 6.2.1 provides the details of the sequential solution procedure, including the time-discrete nonlinear iteration algorithm. For the purposes of this discussion, note that the total flux vector ($\mathbf{q}^T$) is computed from the total flow equation and is then considered a known variable for the solution of the saturation equations. In addition, recall from Section 6.3 that all spatially-dependent parameters are defined nodally and interpolated into the elements using appropriate interpolation functions. Therefore, a Peclet number can be defined at each node $i$ in the domain, i. e.,

$$Pe_i = \frac{\max\left\{|advection|_s\triangle s\ ,\ s{=}x,y,z\right\}_i}{(diffusion)_i} \tag{6.37}$$

where $Pe_i$ is the Peclet number defined at node $i$. The numerator is a measure of the advective component of transport at node $i$, and it is defined by the largest component of the product of the advection vector and the grid spacing in each of the $s$-directions ($s = x, y, z$). The denominator is a measure of the scalar diffusion coefficient at node $i$.

To derive the expressions for grid Peclet number in the form of equation 6.37, equations 6.35 and 6.36 must be rewritten in terms of the dependent variables $S_W$ and $S_{Tw}$ by using the chain rule for differentiation. After performing the necessary chaining operations (see Appendix D for details) the Peclet equations for the water- and gas-phases are defined at each node $i$ in the domain as:

$$\begin{aligned} Pe_i^W &= \max\left\{ \left| \frac{\left(q_s^T (f^W)_{,W} + \left[ (f^W \lambda_N)_{,W} \triangle\gamma_{WN} + (f^W \lambda_G)_{,W} \triangle\gamma_{WG} \right] \cos\theta_s \right) \triangle s}{\left[ \left(f^W \lambda_N\right) + \left(\frac{\sigma_{GW}}{\sigma_{NW}}\right) \left(f^W \lambda_G\right) \right] (P_{cNW})_{,W}} \right|_i , \; s = x, y, z \right\} \\ Pe_i^G &= \max\left\{ \left| \frac{\left(q_s^T (f^G)_{,Tw} - \left[ (f^G \lambda_N)_{,Tw} \triangle\gamma_{NG} + (f^G \lambda_W)_{,Tw} \triangle\gamma_{WG} \right] \cos\theta_s \right) \triangle s}{Pe^{crit} \left[ \left(f^G \lambda_N\right) + \left(\frac{\sigma_{GW}}{\sigma_{GN}}\right) \left(f^G \lambda_W\right) \right] (P_{cGN})_{,Tw}} \right|_i , \; s = x, y, z \right\} \end{aligned} \tag{6.38}$$

where the notation $(\bullet)_{,W}$ and $(\bullet)_{,Tw}$ represents the partial derivative of the function $(\bullet)$ with respect to $S_W$ and $S_{Tw}$, respectively, and $\theta_s$ indicates the angle that the $s-$direction takes to the direction of gravity. In addition, when chaining the terms involving gas-water interactions, the following approximations based on capillary pressure scaling (equation 4.14) are used:

$$\begin{aligned} (P_{cGW})_{,W} &\cong \left(\frac{\sigma_{GW}}{\sigma_{NW}}\right) (P_{cNW})_{,W} \\ (P_{cGW})_{,Tw} &\cong \left(\frac{\sigma_{GW}}{\sigma_{GN}}\right) (P_{cGN})_{,Tw} \end{aligned}$$

Note that in equation 6.38 the Peclet number is defined by the largest spatial component. Finally, the derivatives with respect to saturation are in general computed numerically (see Appendix D for details).

Because the terms defining the discrete form of the balance equations used in the simulator are not the same as those which define equation 6.38, the Peclet numbers computed from equation 6.38 provide only an estimate of the actual discrete values. Realizing the approximate nature of the analysis, a second Peclet-like parameter is defined using a different set of discrete parameters in an effort

to provide an alternative measure (after El-Kadi and Ling, 1993):

$$\overline{Pe}_i^{\alpha} = \max\left\{\frac{(f^{\alpha})_{,s}\triangle s}{f^{\alpha}},\ s=x,y,z\right\}_i, \quad \alpha = W,N,G \tag{6.39}$$

where the subscript $(,s)$ represents the partial derivative in the $s-$dimension, and a $\overline{Pe}_i$ is defined for each phase. This expression represents a measure of the shape of the $\alpha-$phase saturation front relative to the mesh based on the fractional flow function. Equation 6.39 is made amenable to computation in the discrete model by chaining the numerator in terms of the saturation variables, i. e.:

$$\overline{Pe}_i^{\alpha} = \max\left\{\left|\frac{\left((f^{\alpha})_{,W}(S_W)_{,s}+(f^{\alpha})_{,Tw}(S_{Tw})_{,s}\right)\triangle s}{f^{\alpha}}\right|,\ s=x,y,z\right\}_i, \quad \alpha = W,N,G$$

where the three $\overline{Pe}^{\alpha}$ values are defined by the largest spatial component. Note that the derivatives $(S_W)_{,s}$ and $(S_{Tw})_{,s}$ are available from the nodal Hermite coefficient vector, and that the fractional flow derivatives are available from computing equation 6.38, therefore no additional computations are required to generate this information.

The parameters $\Lambda_{NW}$, $\Lambda_{NG}$ and $\Lambda_{GW}$ are computed at each node $i$ in the domain by requiring that $Pe^{crit}$ is not violated. The procedure is not so straight forward because the parameter $\Lambda_{GW}$ occurs in both balance equations, thus coupling the system. Therefore, consider the following algorithm which is based on numerical experiment and is designed to simplify the analysis:

$$\begin{aligned}
&\boxed{\begin{aligned}
&\Lambda_{WN_i} = \max\left\{1, Pe^W/Pe^{crit}, \overline{Pe}^W/Pe^{crit}\right\}_i \\
&\Lambda_{NG_i} = \max\left\{1, Pe^G/Pe^{crit}, \overline{Pe}^G/Pe^{crit}, \overline{Pe}^N/Pe^{crit}\right\}_i \\
&\Lambda_{WG_i} = \Lambda_{WN_i}
\end{aligned}} \quad \text{for } f_i^G > f_i^W \\
&\boxed{\begin{aligned}
&\Lambda_{WN_i} = \max\left\{1, Pe^W/Pe^{crit}, \overline{Pe}^W/Pe^{crit}, \overline{Pe}^N/Pe^{crit}\right\}_i \\
&\Lambda_{NG_i} = \max\left\{1, Pe^G/Pe^{crit}, \overline{Pe}^G/Pe^{crit}\right\}_i \\
&\Lambda_{WG_i} = \Lambda_{NG_i}
\end{aligned}} \quad \text{for } f_i^G \le f_i^W
\end{aligned} \tag{6.40}$$

where the particular combination is chosen based on the relative magnitudes of the gas- and water-phase fractional flow functions. Note that the equations in 6.40 reduce to the proper two-phase equations when applicable.

In summary, before each solution step for the saturation equations, equation 6.40 is computed at each node in the domain using the current nodal saturation data. This equation is based on two Peclet-like constraints and a user-defined critical value, $Pe^{crit}$. The result is that capillary diffusion is augmented where necessary, thereby ensuring that the flow variables are compatible with the spatial discretization. Finally, three important points should be highlighted:

1. based on numerical experiments conducted for a broad range of problem-types, $Pe^{crit} = 2$ appears to be the optimal value for the finite-element formulation chosen.

2. if $Pe^{crit}$ is made large enough, then no additional diffusion will be added to the system;

3. because diffusion is added in a point-wise manner and in a known magnitude, one can use this information in a diagnostic sense to either better qualify the solution or to design the mesh in a more appropriate manner.

### 6.5.2. Time Step Control

Stability, accuracy and computational efficiency considerations require that a dynamic time stepping control be included in the simulator. In general, the value of a given time step is based on one of three criteria:

1. a Courant constraint;

2. the number of iterations required to solve any one equation over a time step;

3. how much the soultion has changed over the last time step.

#### Based on a Courant constraint

One way to ensure that time truncation errors are not adversely affecting the flow solution as it evolves in time is to define a maximum time step size based on a Courant constraint. Advection-diffusion partial differential equations, such as those which describe phase mass transport, can be characterized by the dimensionless group of parameters called the Courant number, $Co$,

$$Co = \frac{(advection)(characteristic\ time\ scale)}{(characteristic\ space\ scale)} \tag{6.41}$$

As with the Peclet number, a discrete point-wise measure of the Courant number can be defined at a node $i$ as:

$$Co_i = \max\left\{|advection|_s \,/\, \triangle s \;,\; s = x, y, z\right\}_i \triangle t \tag{6.42}$$

where $\triangle t$ is the time step and the advective component of transport at node $i$ is defined by the largest component of the product of the advection vector and the grid spacing in each of the $s$-directions ($s = x, y, z$).

Given a constant spatial discretization and a user-defined upper limit for $Co$, called $Co^{crit}$, expression 6.42 can be used to provide a measure of the maximum time step as a function of flow variables and space step. Specifically, using an analogous derivation as was used for the Peclet constraint, given the current solution to the problem, the maximum time step allowed for the next solution interval is approximated as:

$$\triangle t_{\max} = \frac{Co^{crit}}{\max\left\{ \begin{array}{l} \left|\left(q_s^T(f^W)_{,W} + \left[(f^W\lambda_N)_{,W}\triangle\gamma_{WN} + (f^W\lambda_G)_{,W}\triangle\gamma_{WG}\right]\cos\theta_s\right)\right|/\triangle s, \\ \left|\left(q_s^T(f^G)_{,Tw} - \left[(f^G\lambda_N)_{,Tw}\triangle\gamma_{NG} + (f^G\lambda_W)_{,Tw}\triangle\gamma_{WG}\right]\cos\theta_s\right)\right|/\triangle s, \\ \qquad\qquad\qquad\qquad\qquad\qquad\qquad\qquad s = x, y, z \end{array} \right\}_{i=1,2,\ldots,I}} \tag{6.43}$$

where the denominator represents the maximum value of the quantity at all the $I$ nodes in the mesh.

Based on numerical experiments conducted for a broad range of problem-types, $Co^{crit} \leq 2$ appears to provide an effective constraint on time step for the finite-element formulation chosen. In general, $Co^{crit}$ should be smaller for three-phase flow problems ($Co^{crit} < 1$).

### Based on iterative convergence

While equation 6.43 provides a measure of the maximum time-step allowable over a time step, an adaptive time-stepping scheme is employed to determine an appropriate time-step size based on the number of iterations required for convergence of the nonlinear problem. This provides an effective tool which minimizes the cumulative number of iterations required over the course of the simulation.

$$\begin{aligned} \triangle t_{k+1} &= \epsilon_I \triangle t_k \text{ for } m \leq m_{\max},\ \epsilon_I > 1 \\ \triangle t_{k+1} &= \epsilon_R \triangle t_k \text{ for } m > m_{\max},\ 0 < \epsilon_R < 1 \end{aligned}$$

**Based on change in solution**

As discussed in subsection 5.4.3, when considering hysteresis, the denominator of equation 5.14 can become very small when scanning curves are generated. Therefore, small changes in saturation can yield large changes in effective saturation and capillary pressure which in turn can cause instabilities. As a result, a constraint is put on the maximum change in either $S_{eW}$ or $S_{eTw}$ over a time step, i. e., if during iterative convergence,

$$\left| S_e^{k+1,m+1} - S_e^k \right| > \delta S_e^{\max}$$

where $\delta S_e^{\max}$ is the maximum allowable change, then the time step is restarted with a new $\triangle t$ equal to the old $\triangle t$ times a factor $\epsilon < 1$. Based on numerical experiments, the following values provide useful limits: if considering hysteresis then $\delta S_e^{\max} \sim 1.0$, if not considering hysteresis then $\delta S_e^{\max} \sim 0.1$.

### 6.5.3. Phase Discontinuities

With respect to the solution of the phase flow equations, the appearance and disappearance of phases is accommodated by using the total flow formulation in conjunction with the requirement that the pressure variables are continuous in time and space. The result is that equations 6.10, 6.25 and 6.26 are representative of the system regardless of phase configuration.

With respect to the solution of the contaminant transport equations, note that equations 6.27 and 6.28 are undefined when $S_W = 0$ and $S_{Tw} = 0$, respectively. Therefore, a special algorithm is required to accommodate these conditions as the solution evolves through time. First assume that the variables $\rho_n^\alpha$ , $\alpha = W, G$, are continuous in time and space. Second, given the phase saturation distribution from the solution to the flow problem identify those nodes where $S_W^{(k+1)*} \leq \epsilon$ and $S_G^{(k+1)*} \leq \epsilon$, where $\epsilon$ is a small positive number of order 0.001. Third, a moving boundary condition problem is set up by specifying Dirichlet data for $\rho_n^{W(k+1)}$ at any node where $S_W^{(k+1)*} \leq \epsilon$, and for $\rho_n^{G(k+1)}$ at any node where $S_G^{(k+1)*} \leq \epsilon$. Therefore, the matrix equation for each of the NAPL species contains only those algebraic equations written at the collocation points associated with non-Dirichlet condition nodes.

## 6.6. SOLVING THE SYSTEM OF LINEAR EQUATIONS

The system matrix generated by the Hermite collocation finite-element method has the attributes of not being symmetric, positive definite, or diagonally dominant (Dyksen and Rice, 1986). In addition, the fact that the degrees of freedom and the collocation equations are defined at different locations in the domain (at the nodes and at the Gauss quadrature points, respectively), the collocation system matrix has a structure which depends strongly on the numbering scheme chosen. For regular meshes (as are used in this simulator) two desirable numbering schemes have been identified. First is termed *finite-element ordering* by Lai et al. (1994). In finite element ordering the collocation points are numbered consecutively within each element and each element is numbered in the shortest directions first, while the degrees of freedom are numbered consecutively by node and each node is numbered in the shortest directions first (see Frind and Pinder [1979] for an example in 2-D). This numbering scheme has the attribute of creating the most compact block-banded matrix possible, where the matrix bandwidth is given by:

$$2(4nel_{sm}(nel_{med}+1)+11)+1$$

where $nel_{sm}$ is the number of elements in the smallest dimension and $nel_{med}$ is the number of elements in the medium or next smallest dimension. It also has the attribute of creating a matrix with mostly zeros on the diagonal. As a result, the *finite-element ordering scheme is not generally amenable to iterative solution.* It is however amenable to direct solution, and this version of the simulator provides an option to use a banded LU decomposition with partial pivoting (LAPACK driver routine DGBSV, 1993).

The second numbering scheme termed *tensor-product ordering* by Lai et al. (1994), numbers degrees of freedom and equations in the following way (see Lai et al. [1994] for an example in 2-D):

1. associate each unknown with a nearest-neighbor collocation point.
2. sweep along lines in the mesh marching in the shortest directions first.
3. sweep along each line four times, each time numbering two unknowns and associated collocation points, where the pairing of unknowns is based on their association with Dirichlet and Neumann data (see Appendix C).

This numbering scheme creates a matrix with a block tri-diagonal structure, and non-zeros on the diagonal, which makes solution by an iterative method possible. This version of the simulator provides an option to use a preconditioned GMRES (generalized minimum residual) method (SLATEC driver routine DSLUGM, 1989 [incomplete LU GMRES]).

## 6.7. SUMMARY OF SEQUENTIAL ITERATION

The sequential solution iteration procedure can be summarized by the following series of computational steps:

1. Given $S_W$, $S_{Tw}$, $\rho_n^W$ and $\rho_n^G$ and boundary data at time-level $k$:

   compute $P^W$ using the total flow equation (6.10);

   compute $\mathbf{q}^T$, $\mathbf{q}^W$, $\mathbf{q}^G$ from equations 6.14;

   for boundary nodes with Dirichlet conditions 2, 3 or 4, convert the component of $\mathbf{q}^T$ normal to the boundary to the appropriate source/sink terms, $Q^W, Q^N, Q^G$, as described in Section 6.4.2.

2. Given $S_W$ and $S_{Tw}$, $\mathbf{q}^W$, $\mathbf{q}^G$, $Q^W$ and $Q^G$ from step 1:

   compute $\mathbf{D}^W$, $\mathbf{D}^G$;

   compute $\rho_n^W$ and $\rho_n^G$ via the *concurrent iteration algorithm* described in Section 6.2.2.

3. Given the current values of $\mathbf{q}^T$, $Q^W, Q^N$ and $Q^G$ from step 1, and the current values of $\rho_n^W$ and $\rho_n^G$ from step 2:

   compute $S_W$ and $S_{Tw}$ via the concurrent iteration algorithm described in Section 6.2.1.

4. Repeat steps 2 and 3 as required for convergence.

# 7. SIMULATOR DOCUMENTATION

The simulator has been written in standard FORTRAN 77 and does not require linkage to any external libraries. Input and output (I/O) files consist of a series of standard ASCII files. In general this section details I/O file content and format. The input files which provide the necessary data to run the simulator can be defined either manually or by using suitable pre-processing software designed to write to the necessary files in the required format. The output files can be read by appropriate post-processing software. This section is written so that the user can adapt appropriate pre- and post-processors in an efficient manner.

The documentation in this section consists of the following:

- *Data Input*: Detailed description of data input files, data requirements, and data format, including references to sections detailing important algorithmic aspects.
- *Input and output file description*: A listing of input and output files associated with the simulator and a brief explanation of file content and format.

Note, Chapter 8 provides a detailed description of several illustration problems intended to provide the user with examples of model capability and problem set-up and implementation strategies. Reference is made to the disk location of the appropriate input files used to set up and run each problem, and the output files used to analyze the results. As such, the description of simulator I/O contained in this Chapter can be augmented using the examples found in Chapter 8.

Finally, note that Appendix E contains a listing of the names of the source code FORTRAN files which are compiled and linked to create the executable application and a brief explanation of each file's contents and computational task.

## 7.1. DATA INPUT

With respect to data input, consider the following important notes:

| parameter | input file |
|---|---|
| permeability ($k$) | **perm.in** |
| porosity ($\varepsilon$) | **por.in** |
| soil dry bulk density ($\rho^b$) | **bulk.in** |
| fraction of organic carbon ($f_{oc}$) | **o_c.in** |
| residual saturations ($S_{Wr}, S_{Nnr}, S_{Nwr}, S_{Gr}$) | **residual.in** |
| $S-P$ model fitting parameters ($a_d, a_i, \eta$) | **shape.in** |
| soil used for $S-P$ model fit ($k^*, \varepsilon^*$) | **base.in** |

Table 7.1: TIME INDEPENDENT BUT SPATIALLY VARYING INPUT PARAMETERS AND THEIT ASSOCIATED INPUT FILES

1. All data must be input in self-consistent units.

2. The simulator employes un-formatted READ statements.

3. The simulator uses an INCLUDE statement referencing the file **include.f** (described in subsection 7.1.1) to account for all parameter and common block definition and array dimensioning.

4. As described subsection 7.1.2, the command file for simulator input is called **sm.in**. This file defines all parameter constants, and it also references a series of data files for nodally defined parameter data.

5. All spatially variable parameters are defined at the node and interpolated into the element using appropriate basis functions (either Hermite cubics or linear Lagrange).

6. The model parameters listed in Table 7.1 are considered constant in time and variable in space. Default global values are input in the main input driver file **sm.in.** Spatial variability of a specific parameter is incorporated by defining node-specific values in the appropriate file as listed (see discussion below and section 7.2.1 for details)..

7. There is a two-dimensional and a three-dimensional version of this simulator. The input files are the same for both. The two-dimensional simulator ignores all $z-$dimension data.

8. The problem domain and individual elements must have a rectangular shape.

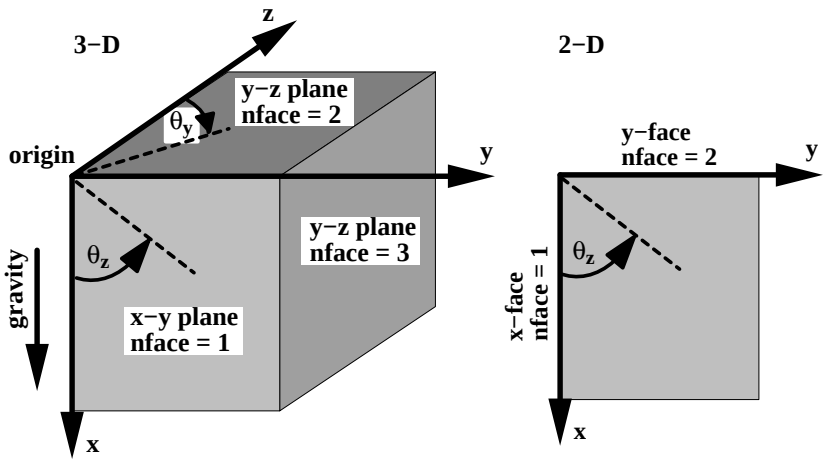


Figure 7.1: Default axis orientation for the 3-dimensional and the 2-dimensional versions of the simulator. Note that the x-axis is aligned with gravity in both versions. Also illustrated are the definitions of the grid rotation option and the input parameter $nface$ which is used in setting boundary conditions

9. The default axis orientation for both the three-dimensional and two-dimensional versions of the simulator is illustrated in Figure 7.1, where the $x-$direction is vertical and increasing downward, the $y-$direction is horizontal and increasing to the right, and the $z-$direction is horizontal and increasing into the plane of the paper. The two-dimensional version uses the same $(x, y)$ orientation and ignores the $z-$dimension. As described in more detail in subsection 7.1.2, an option for grid rotation is available where the user defines the angels to rotate the grid in the counter-clockwise direction about the $z-$ and $y-$axes ($\theta_z$ and $\theta_y$, respectively in Figure 7.1).

10. The rectangular mesh is defined by the union of rectangular elements where the total number of elements is defined by the product of the number of elements in the $x-$, $y-$, and $z-$directions ($nex$, $ney$, and $nez$, respectively). Note, the user must make sure that the dimension statements in the INCLUDE file, **include.f**, reflect these values (see subsection 7.1.1 for details).

11. The global node numbering scheme which is required for all input requiring a node number follows the rule: increment first in the $y-$direction, then in $x-$direction, and then in the $z-$direction, i. e.,

node 1: $x(1)$, $y(1)$, $z(1)$ [e.g. $(0, 0, 0)$]

node 2: $x(1)$, $y(2)$, $z(1)$

...

node $nny$: $x(1)$, $y(nny)$, $z(1)$

node $nny + 1$: $x(2)$, $y(1)$, $z(1)$

...

node $nny\ nnx$: $x(nnx)$, $y(nny)$, $z(1)$

...

node $nny\ nnx + 1$: $x(1)$, $y(1)$, $z(2)$

..., etc.

where $nnx = (nex + 1)$, $nny = (ney + 1)$ and $nnz = (nez + 1)$ are the number of nodes in the $x-$, $y-$, and $z-$directions respectively.

12. As discussed in subsection 6.4.2, the simulator assumes that all boundary nodes are no flow with respect to the phases and homogeneous Neumann with respect to the NAPL species, *unless otherwise specified*. When applying a Dirichlet or mixed condition at a boundary node it is necessary to provide the simulator with information qualifying the axis (in 2-D) or plane (in 3-D) that is normal to the applied condition. This is because the simulator uses Hermite cubic polynomials to interpolate the primary variables, and as discussed in subsection 6.4.2 and Appendix B, the group of Hermite coefficients which are associated with a given boundary condition is a function of the axis or plane which is normal to the direction from which the condition is applied. Using Figure 7.1 as a definition sketch, the simulator uses the following code to identify the axis or plane type, where for the 3-D simulator the code is: $nface = 1$ if the face is an $x - y$ plane, $nface = 2$ if the face is a $y - z$ plane, and $nface = 3$ if the face is an $x - z$ plane, and for the 2-D simulator the code is: $nface = 1$ if it is the $x - axis$ and $nface = 2$ if it is the $y - axis$. Finally, note that this information is technically only required at corner nodes in 2-D and edge and corner nodes in 3-D. For example, in 2-D, one can apply two different conditions at a corner node, such as a constant head condition on the horizontal side ($nface = 2$) and a no flow condition on the vertical side ($nface = 1$).

In the discussion which follows for reference purposes, all variable names written in *italic* font are those used in the FORTRAN source code, and all file names are written in **bold** font.

### 7.1.1. Set up for the include.f file

The **include.f** file defines the array dimensioning and common block definition, and for the 2-D version houses a flag which determines which linear algebraic equation solver to use.[1] There are three groups of PARAMETERS which must be set to reflect the particular problem one wishes to run.

1. Maximum mesh definition.

   For the two-dimensional version, set the PARAMETERS *mnnd_l*, the maximum number of nodes in the long dimension, and *mnnd_s*, the maximum number of nodes in the short dimension, where

   $$mnnd\_l \geq \max[(nex+1),(ney+1)]$$
   $$mnnd\_s \geq \min[(nex+1),(ney+1)]$$

   and *nex* and *ney* are the number of elements in each spatial dimension of the model mesh.

   For the three-dimensional version, set the PARAMETERS *mgnd_x*, *mgnd_y*, and *mgnd_z* such that

   $$mgnd\_x \geq (nex+1)$$
   $$mgnd\_y \geq (ney+1)$$
   $$mgnd\_z \geq (nez+1)$$

   *NOTE, setting these parameters to the minimum values minimizes run-time memory requirements.*

2. Flags to choose which linear algebraic solver to use. *For the 2-D version only.* Two options exist, use a direct solver (LU with partial pivoting), or use an iterative solver (GMRES with incomplete LU preconditioning). See subsection 6.6 for details on solver description. The flags are *itsol_t* and *itsol_f* where:

[1] The 2-D version allows one to choose between a direct solver and an iterative solver. The 3-D version employes only the iterative solver.

*itsol_t*: if = 1, then use the iterative solver for the transport-like equations (the equations for $S_W$, $S_{Tw}$, $\rho_n^W$ and $\rho_n^G$), if = 0, then use the direct solver.

*itsol_f*: if = 1, then use the iterative solver for the total flow equation (the equation for $P^W$), if = 0, then use the direct solver.

In general both these flags should be set equal to one. Note, the 3-D version employes only the GMRES solver.

3. For the GMRES iterative solver, the maximum number of search-direction vectors to be saved and orthogonalized against before restart is set:

$$nsave > 1$$

In general *nsave* should be as large as the maximum number of iterations allowed, however, this maximizes memory requirements. As *nsave* increases, the number of iterations required for convergence decreases, but the memory requirement increases. Results from numerical experimentation suggests $nsave = 10$ to 50. NOTE on the use of the GMRES solver. The combination of tensor-product ordering of the equations and unknowns (described in subsection 6.6) and the use of the GMRES solver, requires the following constraint-rules for problem setup: for the 3-D code, the first 2-D plane of nodes numbered (the smallest dimension boundary plane) must have at least one node with a Dirichlet condition, and for the 2-D code the first 1-D line of nodes numbered (the smallest dimension of x and y) must have at least one node with a Dirichlet condition applied for the method to work. This does not apply to the direct solver.

No other changes to the file **include.f** are required to be made.

### 7.1.2. Data Input Driver

The file **sm.in** is the 'driver' for data input. It either contains the required data which is read from the FORTRAN file **main.f**, or it defines the 'call' to other data input files. The other data input files define the mesh, the initial and boundary conditions, and all spatially varying parameters (Table 7.1). A description of these input files can be found in subsection 7.2.1.

The first 74 lines of **sm.in** are fixed, and each line requires a fixed set of one or more parameters as specified below. *All data must be input whether the data*

*is used or not* (e. g., if the problem is set up so that contaminant transport is switched off, then some 'dummy' numbers must be specified for all transport-specific parameters).

This section describes the input requirements for the file **sm.in** by line number. For each line number, the parameter list is specified in italics, where the names of these parameters are those which are used in the FORTRAN source code (provided for reference purposes). Following the parameter list is a brief description of the meaning of the parameter(s), where appropriate documentation subsections are referenced for additional detail.

1. *title*

   provide a character string (a maximum of 68 characters) for the title of the output to appear in file **echo.out** which echoes the data input (see section 7.2.5 for details on what **echo.out** contains).

2. *iphase*

   Determines which phases are to be modeled. The following code is used. Let water = 1, NAPL = 2, gas = 3, then you have three options:

   *iphase* = 12, water-NAPL flow problem (solve two flow equations and $S_G \equiv 0$)

   *iphase* = 13, water-gas flow problem (solve two flow equations and $S_N \equiv 0$)

   *iphase* = 123, water-NAPL-gas flow problem (solve three flow equations)

   Admissable values: 12, 13, or 123. If *iphase* does not equal one of these three values then an error message appears on the screen and the simulator stops. If one of the admissible values are input then a warning message is output to the screen to tell that you which phases are to be considered in the simulation.

3. *iscr*

   A switch to turn screen output on/off. If *iscr=1* then iteration, solution and time information is output to the screen during the simulation. If *iscr* is not equal to one then screen output is suppressed. Iteration and solution information is output to the screen in the order that the computations are performed. This output is diagnostic in nature and provides the user with run-time information on simulator performance. See subsection 7.2.4 for details on the contents of the screen output.

4. *iherm*

   Option to write Hermite data to file at print-intervals (see input line 8 for definition of print interval). If *iherm=1* then output the data, if *iherm* is not equal to one then do not. If enabled, then at each print interval in a separate file for each Hermite parameter, a time header is printed followed by a node list of the Hermite coefficients for that parameter. The files thus generated are: **pa.out** ($P^W$ data), **sw.out** ($S_W$ data), **st.out** ($S_{Tw}$ data), **oa.out** ($\rho_n^W$ data), **og.out** ($\rho_n^G$ data). The data for each print interval over the course of the simulation is concatenated. See subsection 7.2.5 for details on the contents of these files.

5. *mass*

   Option to perform and output mass balance information. If *mass=1* then compute and output the data, if *mass* is not equal to one then do not. If enabled, then after each time step a material mass balance is performed. The files thus generated are: **mass.out** (summary), **cmass.out** (cumulative mass balance as a function of time), **massw.out** (water mass balance over each time step), **massn.out** (NAPL mass balance over each time step), **massg.out** (gas mass balance over each time step), **masst.out** (total phase mass balance over each time step). Poor mass balance is an indication of incorrect time and/or space discretization, or incorrect specification of the problem forcing terms. See subsection 7.2.5 for details on the mass balance computations and output files.

6. *nex, ney, nez*

   The number of elements in the $x-$, $y-$ and $z-$dimensions (rectangular mesh). Note, make sure that the PARAMETER statements in the INCLUDE file **include.f** reflect these values, i. e., for the 2-D simulator:

$$mnnd\_l \geq \max[(nex+1),(ney+1)]$$
$$mnnd\_s \geq \min[(nex+1),(ney+1)]$$

   and for the 3-D simulator:

$$mgnd\_x \geq (nex+1)$$
$$mgnd\_y \geq (ney+1)$$
$$mgnd\_z \geq (nez+1)$$

7. *time*

   The time associated with the initial conditions (e. g., the reference time). For example, if one is restarting the simulator from a previous run, this input variable can be used to date the data associated with the restart files (see subsection 7.2.2 for details on restart file content and print frequency).

8. *t1pr, tmprnt, tmax*

   Define print interval and maximum simulation time, where:

   *t1pr* - first print when elapsed simulation time equals $time + t1pr$

   *tmprnt* - the time interval between prints after the first print.

   *tmax* - the maximum simulation time.

   Note, the time step is adjusted so that print times and *tmax* are honored. The following files are written to at each print interval and the data for each print interval, identified by its time, is concatenated:

   Hermite data (if output is enabled, see input line 4): **pa.out** ($P^W$ data), **sw.out** ($S_W$ data), **st.out** ($S_{Tw}$ data), **oa.out** ($\rho_n^W$ data), **og.out** ($\rho_n^G$ data)

   General solution: **sat.out** ($S_W$, $S_N$, $S_G$, $P_{cNW}$, $P_{cGN}$, $\rho_n^W$ and $\rho_n^G$)

   Mass balance (if output is enabled, see input line 5): **mass.out** (summary)

   Flux vector data: **velg.out** (gas), **veln.out** (NAPL), **velw.out** (water)

   Restart files: all files with the extension **rs** (data used for simulator restart, see input line 68)

   Reference subsection 7.2.5 for details on output file contents.

9. *itincs, itincc, tmult*

   Time step control based on the iterative solution of the nonlinear saturation and contaminant transport equations. In general larger time steps require more iterations to converge on the nonlinearity. After each solution interval, if the number of iterations required for convergence of each nonlinear equation is less than the values specified, where

   *itincs* - saturation iterations (suggestion: $3 < itincs < 15$)

*itincc* - contaminant transport iterations (suggestion: $3 < itincc < 15$)

then increase the time step for the next solution interval, i. e., $\triangle t_{new} = tmult \triangle t_{old}$, where

*tmult* - factor to increment ($tmult \geq 1.0$, and $tmult \approx 1.15$ is an appropriate value)

See subsection 6.5.2 for more detail on dynamic time-step control.

10. *itreds, itredc, tdiv*

    Time step control based on the iterative solution of the nonlinear saturation and contaminant transport equations. After each solution interval, if the number of iterations required for convergence of any one nonlinear equation is more than the value specified, where

    *itreds* - saturation iterations ($itreds > itincs$ and suggestion: $8 < itreds < 20$)

    *itredc* - contaminant transport iterations ($itredc > itincc$ and suggestion: $8 < itredc < 20$)

    then reduce the time step for the next solution interval, i. e., $\triangle t_{new} = \triangle t_{old}/tdiv$, where

    *tdiv* - factor to reduce ($tdiv \geq 1.0$, and $tdiv \approx 1.25$ is an appropriate value)

    See subsection 6.5.2 for more detail on dynamic time-step control.

11. *ithangs, ithangc, tdivh*

    Time step control based on the iterative solution of the nonlinear saturation and contaminant transport equations. If during a solution interval, the number of iterations required for convergence of any one nonlinear equation exceeds the specified value, where

    *ithangs* - saturation iterations ($ithangs > itreds$ and suggestion $10 < ithang < 25$)

    *ithangc* - contaminant transport iterations ($ithangc > itredc$ and suggestion $10 < ithanc < 25$)

then the current time step is restarted with a reduced time step, $\triangle t_{new} = \triangle t_{old}/tdivh$, where

*tdivh* - factor to reduce ($tdivh \geq 1.0$, and $tdivh \approx 1.5$ is an appropriate value)

This flag usually trips when the iterative scheme will not converge as the iteration solutions repeat with a period $\geq 2$ (a ringing phenomenon).

12. *itermx*

    When the GMRES solver is used, this parameter represents an upper limit on the number of iterations allowed to solve any one matrix equation. Typically, this variable applies to the elliptic pressure equation which is the most difficult to solve iteratively. This number may be based on the number of iterations required to solve the pressure equation for the first time step. After setting a reasonable value, if for a given time step, the pressure equation will not converge within this maximum number of iterations the simulator will stop without saving the current solution and an error message will be output to the screen. To restart after a 'crash' caused by a maximum iteration violation, one must go back to the time of the last output interval as specified by the print interval chosen (see input line 8). This type of 'crash' is indicative of an excessively coarse convergence criterion for the saturation equations. A number $\leq 200$ is appropriate.

13. *dslim*

    An upper limit for the change in $S_{eW}$ and $S_{eTw}$ over a time step. As discussed in subsection 5.4.3, when considering hysteresis, the denominator of the effective saturation (equation 5.14) can become very small as the $S-P$ curve is fit between the predefined constraint points. Therefore, small changes in saturation can yield large changes in effective saturation. If during iterative convergence this threshold is reached, then restart the time step with a new $\triangle t$ equal to the old $\triangle t$ divided by the factor *tdivh* (defined in input line 11). Suggested working values: if considering hysteresis then $dslim \sim 1.0$, if not considering hysteresis then $dslim \sim 0.1$. See also the discussion in subsection 6.5.2.

14. *co*

The critical Courant number, $Co^{crit}$ as defined in subsection 6.5.2. Used to define an upper limit on the time step size based on time truncation error. Appropriate values are case-specific, however, in general $co \leq 4$ and smaller values of *co* are appropriate for three-phase flow problems (e. g., $co \leq 1$). NOTE: make *co* a large number to avoid this upper limit time step constraint.

15. *dt0*

    The time step used to start the simulation. Typically the initial time step is relatively small so that the simulator can propagate boundary and forcing terms which are initially shock-like. Let the dynamic time stepping tools (defined by the parameters listed in input lines 9 through 14) bring the time step up to its 'optimal' value.

16. *tsmax, tsmin*

    The upper and lower limit for time step, respectively. Time steps which are too large or too small can lead to instabilities as numerical round-off errors dominate the solution. The value *tsmax* overrides all other time step incrementing computations. The maximum time step is problem specific and can be estimated or obviated by employing the Courant constraint. If the time step is cut to below *tsmin* due to lack of iterative convergence, then the simulation stops and the last solution is output as per a typical print interval. This type of 'crash' is an indication that the discrete problem and the physical problem are not compatible.

17. *grf_ on, grinc, ngrch, fgrch, gmax*

    Animated graphics output control. For the 2-D version of the simulator these files are formatted specifically for the Jacquard graphics software package[2]. For the 3-D version of the simulator these files are formatted specifically for the SciAn graphics software package[3] according to the STF format.

    The simulator generates files with the extension **stf** and **jin** to be read by the post-processing software for animated display of saturation (**sw.stf**, **st.stf**), concentration (**oa.stf**, **og.stf**) and velocity (**velw.stf**, **veln.stf** and

[2] An EPA sponsored pre- and post-processing graphics software package written specifically for Silicon Graphics computer hardware.

[3] SciAn is a public domain post processing software package. For information on obtaining SciAn, send email to: scian-info@scri.fsu.edu.

**velg.stf**). The **stf** files contain time-dated concatenated output where the output interval is defined as follows:

*grf_on* - if = 1 then enable graphics output, =0 then turn off.

*grinc* - the initial time increment to print

*ngrch* - the number of prints at current increment before changing the increment

*fgrch* - factor to change the current increment

*gmax* - maximum increment

18. *nloop*

    The number of sequential iteration loops between the pressure equation and the saturation equation(s) during sequential solution. Setting this value to zero results in sequential solution, values $> 0$ results in an iterative sequential solution. Use a value $> 0$ only for problems where separate phase velocities must be well defined. See section 6.2 for details on the sequential solution algorithm.

19. *erip*

    GMRES convergence criterion for the pressure equation. Experience suggests that values of order $1.0*10^{-6}$ provide accurate solutions with relatively low iteration requirements. Use mass balance as your ultimate guide.

20. *eris, eros*

    Convergence criteria for the saturation equations. The parameter *eris* is for the GMRES solver (inner iterations), and the parameter *eros* is for convergence on the nonlinearity (outer iteration). Experience suggests that $eris \approx eros \approx 1.0 * 10^{-3}$ provides accurate solutions with relatively low iteration requirements. Use mass balance as your ultimate guide.

21. *erit, erot*

    Convergence criteria for the contaminant transport equations. The parameter *erit* is for the GMRES solver (inner iterations), and the parameter *erot* is for convergence on the nonlinearity (outer iteration). Experience suggests that $erit \approx 1.0*10^{-5}$ and $erot \approx 1.0*10^{-3}$ provides accurate solutions with relatively low iteration requirements. Use mass balance as your ultimate guide.

22. *idxdy*

    Mesh definition flag. The main program now reads information from the file **space.in** and the flag *idxdy* defines what must be in the file. If $idxdy = 0$ then the simulator will generate a uniform mesh based on the number of elements specified in line 6 and the maximum dimensions listed in file **space.in**, i. e.,

    *xmax, ymax, zmax*

    If $idxdy = 1$ then the simulator will generate a mesh based on a catenated $x-$, $y-$ and $z-$dimension node spacing list in file **space.in**, i. e.,

    $x-$node spacing list, $x(i), i = 1, nex + 1$

    $y-$node spacing list, $y(i), i = 1, ney + 1$

    $z-$node spacing list, $z(i), i = 1, nez + 1$

23. *grav*

    The magnitude of the gravity vector $[L/T^2]$.

24. *th_ z, th_ y*

    Orient the grid at a specified angle to the horizontal, where *th_ z* is the angle to rotate the grid in the counter clockwise direction about the $z - axis$, and *th_ y* is the angle to rotate the grid in the counter clockwise direction about the $y - axis$. For example, $th\_z = 0$ and $th\_y = 0$ yields the default orientation with $+x =$ depth (see Figure 7.1), and $th\_z = 90$ and $th\_y = 0$ yields $-y =$ depth. Note, the two-dimensional version of the simulator only considers the angle *th_ z*.

25. *permb*

    The value of the intrinsic permeability scalar $[L^2]$ applied by default at every node in the domain. Spatial variability is defined in the next input line.

26. *ndev*

    The number of nod-specific deviations from the global value *permb*. If $ndev > 0$ then the simulator opens the file **perm.in** and reads *ndev* lines of information, where each line lists the node number and the value of permeability $(nod, perm)$

27. *porb*

    The value of the soil porosity scalar [*dimensionless*] applied by default at every node in the domain. Spatial variability is defined in the next input line.

28. *ndev*

    The number of node-specific deviations from the global value *porb*. If $ndev > 0$ then the simulator opens the file **por.in** and reads *ndev* lines of information, where each line lists the node number and the value of porosity $(nod, por)$.

29. *bulkb*

    The value of the dry bulk density $[M/L^3]$ applied by default at every node in the domain. This parameter is used to model adsorption mass transfer (see subsection 4.8.2). Spatial variability is defined in the next input line.

30. *ndev*

    The number of node-specific deviations from the global value *bulkb*. If $ndev > 0$ then the simulator opens the file **bulk.in** and reads *ndev* lines of information, where each line lists the node number and the value of the dry bulk density $(nod, bulk)$.

31. *vw_r, vn_r, vg_r*

    The viscosity (pure phase) $[M/(TL)]$ of the water-, NAPL- and gas-phases, respectively.

32. *rw_r, rn_r, rg_r*

    The density (pure phase) $[M/L^3]$ of the water-, NAPL- and gas-phases, respectively.

33. *siggw, signw, siggn*

    The fluid-fluid interfacial tension $[M/T^2]$ between the water and gas, the NAPL and water, and the gas and NAPL phases, respectively. These parameters are used to scale the capillary pressures for three-phase flow. Recall that the simulator assumes that the $S - P$ model parameters were fit to a two-phase displacement experiment (the type of which is defined in the next input line), and that it uses the interfacial surface tension data to scale

the $S-P$ model to represent the other fluid pairs. See sections 4.3, 5.1 and 5.5 for the details regarding the use of capillary pressure scaling in this simulator. Note, any set of self-consistent units can be used for these values since they are used to generate dimensionless ratios.

34. *n_phase*

This entry tells the simulator which phase pair was used to obtain the $S-P$ model fitting parameters. This information is used to define the capillary pressure scaling relationship. Given the following form of equation 4.14:

$$\beta_{GW} P_{cGW} = \beta_{GN} P_{cGN} = \beta_{NW} P_{cNW}$$

the $\beta$ parameters are defined as a function of the value of *n_phase*, i. e.,

| | |
|---|---|
| $n\_phase = 1$ | $\beta_{GW} = 1$<br>$\beta_{GN} = (\sigma_{GN} + \sigma_{NW}) / \sigma_{GN}$<br>$\beta_{NW} = (\sigma_{GN} + \sigma_{NW}) / \sigma_{NW}$ |
| $n\_phase = 2$ | $\beta_{GW} = (\sigma_{GW} - \sigma_{GN}) / \sigma_{GW}$<br>$\beta_{GN} = (\sigma_{GW} - \sigma_{GN}) / \sigma_{GN}$<br>$\beta_{NW} = 1$ |
| $n\_phase = 3$ | $\beta_{GW} = (\sigma_{GW} - \sigma_{NW}) / \sigma_{GW}$<br>$\beta_{GN} = 1$<br>$\beta_{NW} = (\sigma_{GW} - \sigma_{NW}) / \sigma_{NW}$ |

Admissable values: 1, 2, or 3. If *n_phase* does not equal one of these three values then an error message appears on the screen and the simulator stops. See sections 4.3, 5.1 and 5.5 for the details regarding the use of capillary pressure scaling in this simulator.

35. *swr, snnr, snwr, sgr*

Global definition of residual saturations applied by default at every node in the domain, where:

*swr* $\equiv$ residual water phase ($S_{Wr}$)

*snnr* $\equiv$ residual NAPL as a nonwetting phase ($S_{Nnr}$)

*snwr* $\equiv$ residual NAPL as a wetting phase ($S_{Nwr}$)

*sgr* $\equiv$ residual gas phase ($S_{Gr}$)

Spatial variability of these parameters is defined in the next input line.

36. *ndev*

    The number of node specific deviations from the global values *swr, snnr, snwr, sgr*. If $ndev > 0$ then the simulator opens the file **residual.in** and reads *ndev* lines of information, where each line lists the node number and the four residual values *swr, snnr, snwr, sgr*. Use this option if the domain contains different soil types which warrant the specification of unique $S-P$ model fitting parameters. This file is usually set up in concert with the files **shape.in** (input line 38) and **base.in** (input line 40).

37. *asd, asi, eta*

    The $S-P$ model curve shape parameters (equation 5.13) applied by default at every node in the domain, where:

    $asd \equiv$ the pressure scale for drainage ($a_d$) $[1/L]$

    $asi \equiv$ the pressure scale for imbibition ($a_d$) $[1/L]$

    $asi \equiv$ the pore connectivity parameter ($\eta$)

    Spatial variability of these parameters is defined in the next input line.

38. *ndev*

    The number of node specific deviations from the global values *asd, asi, eta*. If $ndev > 0$ then the simulator opens the file **shape.in** and reads *ndev* lines of information, where each line lists the node number and the three fitting parameters *asd, asi, eta*. Use this option if the domain contains different soil types which warrant the specification of unique $S-P$ model fitting parameters. This file is usually set up in concert with the files **residual.in** (input line 36) and **base.in** (input line 40).

39. *perm_b, por_b*

    The soil-type parameters upon which the residual saturations (input line 35) and the curve shape parameters (input line 37) are based. Applied by default at every node in the domain, where:

    $perm\_b \equiv$ intrinsic permeability scalar $[L^2]$

    $por\_b \equiv$ porosity

These parameters are equivalent to $k^*$ and $\varepsilon^*$ defined in section 5.5, equation 5.41. Note that the soil parameters *permb* and *porb* defined in input lines 24 and 26 are equivalent to $k$ and $\varepsilon$ in equation 5.41. The combination of these soil property definitions defines capillary pressure scaling relationship with respect to soil properties.

40. *ndev*

    The number of node specific deviations from the global values *perm_b* and *por_b*. If $ndev > 0$ then the simulator opens the file **base.in** and reads *ndev* lines of information, where each line lists the node number and the two parameters $k^*$ and $\varepsilon^*$. Use this option if the domain contains different soil types which warrant the specification of unique $S - P$ model fitting parameters. This file is usually set up in concert with the files **residual.in** (input line 36) and **shape.in** (input line 38).

41. *alfw, nsew1, nsew2*

    These parameters define the $k_{rW}(S_W)$ functional (equation 5.19), where,

    *alfw* is the connectivity parameter $\zeta$

    *nsew1* is a flag which determines the definition of ${}^aS_{eW}$, i.e.,

| | |
|---|---|
| $nsew1 = 1$ | ${}^aS_{eW} = (S_W - S_{Wt}) \,/\, (1 - S_{Wt} - S_{Nt} - S_{Gt})$ |
| $nsew1 = 2$ | ${}^aS_{eW} = (S_W - S_{Wt}) \,/\, (1 - S_{Wt})$ |

    *nsew2* - a flag which determines the definition of ${}^bS_{eW}$, i.e.,

| | |
|---|---|
| $nsew2 = 1$ | ${}^bS_{eW} = (S_W - S_{Wt}) \,/\, (1 - S_{Wt} - S_{Nt} - S_{Gt})$ |
| $nsew2 = 2$ | ${}^bS_{eW} = (S_W - S_{Wt}) \,/\, (1 - S_{Wt})$ |

    If these flags do not equal one of the numbers indicated then an error message is printed and the simulator stops.

42. *alfn, nsen1, nsen2, nsen3*

    These parameters define the $k_{rN}(S_W, S_G)$ functional (equation 5.38), where,

    *alfn* is the connectivity parameter $\xi$

*nsen1* is a flag which determines the definition of $S_{eN}$, i.e.,

| | |
|---|---|
| $nsen1 = 1$ | $S_{eN} = (S_N - S_{Nt}) \,/\, (1 - S_{Wt} - S_{Nt} - S_{Gt})$ |
| $nsen1 = 2$ | $S_{eN} = (S_N - S_{Nt}) \,/\, (1 - S_{Nt})$ |

*nsen2* - a flag which determines the definition of $S_{eTn}$, i.e.,

| | |
|---|---|
| $nsen2 = 1$ | $S_{eTn} = \frac{S_N + S_G - S_{Nt} - S_{Gt}}{(1 - S_{Wt} - S_{Nt} - S_{Gt})}$ |
| $nsen2 = 2$ | $S_{eTn} = \frac{S_N + S_G - S_{Nt} - S_{Gt}}{(1 - S_{Nt} - S_{Gt})}$ |
| $nsen2 = 3$ | $S_{eTn} = \frac{S_N + S_G - S_{Nt}}{(1 - S_{Nt})}$ |

*nsen3* - a flag which determines the definition of $S_{eTw}$, i.e.,

| | |
|---|---|
| $nsen3 = 1$ | $S_{eTw} = \frac{S_N + S_W - S_{Nt} - S_{Wt}}{(1 - S_{Wt} - S_{Nt} - S_{Gt})}$ |
| $nsen3 = 2$ | $S_{eTw} = \frac{S_N + S_W - S_{Nt} - S_{Wt}}{(1 - S_{Nt} - S_{Wt})}$ |
| $nsen3 = 3$ | $S_{eTw} = \frac{S_N + S_W - S_{Nt}}{(1 - S_{Nt})}$ |

If these flags do not equal one of the numbers indicated then an error message is printed and the simulator stops.

43. *alfg, nseg1, nseg2*

These parameters define the $k_{rG}(S_G)$ functional (equation 5.23), where,

*alfg* is the connectivity parameter $\zeta$

*nseg1* is a flag which determines the definition of ${}^{a}S_{eG}$, i.e.,

| | |
|---|---|
| $nseg1 = 1$ | ${}^{a}S_{eG} = (S_G - S_{Gt}) \,/\, (1 - S_{Wt} - S_{Nt} - S_{Gt})$ |
| $nseg1 = 2$ | ${}^{a}S_{eG} = (S_G - S_{Gt}) \,/\, (1 - S_{Gt})$ |

*nseg2* - a flag which determines the definition of ${}^{b}S_{eG}$, i.e.,

| | |
|---|---|
| $nseg2 = 1$ | ${}^{b}S_{eG} = (S_G - S_{Gt}) \,/\, (1 - S_{Wt} - S_{Nt} - S_{Gt})$ |
| $nseg2 = 2$ | ${}^{b}S_{eG} = (S_G - S_{Gt}) \,/\, (1 - S_{Gt})$ |

If these flags do not equal one of the numbers indicated then an error message is printed and the simulator stops.

44. *se_ sl, se_ rl*

    Linearly extrapolate the $S-P$ functionals at effective saturations near one and zero to make them amenable to numerical model implementation as discussed in subsection 5.4.3, Part 1, where the meaning of these parameters is as follows:

    if $S_e > (1 - se\_sl)$ then linearize the $S-P$ functional ($se\_sl \equiv S^c_{es}$ in equation 5.39)

    if $S_e < se\_rl$ then linearize the $S-P$ functional ($se\_rl \equiv S^c_{er}$ in equation 5.39)

    Numerical experiments suggest that values between 0.001 and 0.01 have no noticeable effect on the solution.

45. *sfact_ kr*

    Force $k_{r\alpha}(S_e) = 0$ for $S_e \leq sfact\_kr$. This parameter eliminates the effect that small oscillations in the saturation and concentration solutions have on residual saturations. Numerical experiments suggest that $sfact\_kr \approx 0.01$ has no noticeable effect on the solution.

46. *nhyst*

    Switch to turn on/off the hysteresis option. If $nhyst = 1$, then use the hysteretic $k-S-P$ model definition as defined in Chapter 5, equations 5.13 and 5.14. If $nhyst = 0$, then use the model for monotonic displacement, equations 5.10 and 5.11 with $S_s = 1$ and $S_r = S_{Wr}$.

47. *e_ r*

    Phase entrapment/release definition - the blending parameter ($e$) defined in equation 5.7 which governs how fast the phase becomes entrapped during drainage flow conditions or released from entrapment during imbibition flow conditions (see also subsection 5.4.1). $e\_r = 1$ yields a linear entrapment/release model.

48. *b_ a*

    Blend the $S-P$ model scale parameter ($a_{(f)}$ in equation 5.13) between reversal points. This is the blending parameter $\beta$ as used in Table 5.2 which defines how fast the van Genuchten scale parameter ($a_{(f)}$) changes after a

reversal occurs. In general $b\_a \gtrsim 0.2$. See subsection 5.4.2 for additional detail.

49. *sp_ min, sr_ min*

    Restriction parameters for $S - P$ curve generation and update, where:

    *sp_ min* is the minimum span (the denominator defining effective saturation), for which a new set of scaling parameters will be calculated. See subsection 5.4.3, Part 2, where $sp\_\min \equiv span$. Numerical experiments suggest a range: $0.025 > sp\_\min > 0.1$

    *sr_ min* is a minimum tolerance away from the $S-P$ curve end points above which a scanning curve will be generated after a flow reversal, i. e., if $sr\_\min < S_e < (1 - sr\_\min)$ then a scanning curve will be generated after a flow reversal otherwise the computation will be suppressed. See subsection 5.4.3 Part 3, where $sr\_\min \equiv \epsilon$. Numerical experiments suggest a range: $0.025 > sr\_\min > 0.1$ and $sr\_\min > sp\_\min$.

50. *factd, facti*

    The tolerance in saturation change to indicate a reversal from drainage to imbibition (*factd*) or from imbibition to drainage (*facti*). See subsection 5.4.3 Part 4, where $factd \equiv r_d$ and $facti \equiv r_i$. In general $factd = facti \gtrsim 0.001$.

51. *pe_ w, pe_ g*

    The critical Peclet numbers for the water and gas phases, respectively. The parameter $Pe^{crit}$ in equation 6.40, where *pe_ w* is used for the water equation and *pe_ g* is used for the gas equation. In general $pe\_w = pe\_g \gtrsim 2$. See section 6.5.1 for details.

52. *pg_ ref*

    The reference gas phase pressure $[M/(LT^2)]$. Usually set to atmospheric pressure (e. g., $1 * 10^6 dynes/cm^2$).

53. *ntr_ ow, ntr_ og*

    Switches to turn on/off constituent mass transport and mass transfer computations, where:

*ntr_ow* - if =1 then model dissolved NAPL contaminant transport (solve for $\rho_n^W$); if =0, then bypass

*ntr_og* - if =1 then model NAPL vapor contaminant transport (solve for $\rho_n^G$); if =0, then bypass

As indicated below, when either or both of the contaminant transport computation switches is (are) turned off, then the input parameters required for contaminant transport are set internally by the simulator to appropriate values, thereby overriding user defined input. If either *ntr_ow = 0* or *ntr_og = 0* then a warning message is output to the screen to tell that you have turned off appropriate transport mechanisms.

54. *theta*

The projection parameter used to model the coupling between the water- and gas-phase contaminant transport equations due to mass transfer of the NAPL species between phases. The parameter $\theta$ in equation 6.29. This parameter is used only if *ntr_ow* = *ntr_og* = 1.

55. *along, atran, diffw, diffg*

Dispersion tensor definition (see subsection 4.6), where:

*along* - longitudinal dispersivity - the parameter $a_L$ [L] in equation 4.25 where $a_L$ is the same for both phases.

*atran* - transverse dispersivity - the parameter $a_T$ [L] in equation 4.25 where $a_T$ is the same for both phases.

*diffw* - molecular diffusion in water - the parameter $D_m^W$ $[L^2/T]$ in equation 4.25

*diffg* - molecular diffusion in gas - the parameter $D_m^G$ $[L^2/T]$ in equation 4.25

These parameters are used only if mass transport is switched on.

56. *p_oc, focb*

Soil adsorption/desorption coefficient definition (as detailed in subsection 4.8.2, equation 4.36), where:

*p_oc* is the organic carbon partition coefficient, the parameter $K_{oc}$

*focb* is the fraction of organic carbon in the soil, the parameter $f_{oc}$, applied by default to every node in the domain.

Note, these parameters are used only if *ntr_ow = 1.*

57. *ndev*

The number of node specific deviations from the global value *focb*. If $ndev > 0$ then the simulator opens the file **o_c.in** and reads *ndev* lines of information, where each line lists the node number and the value of the fraction of organic carbon in the soil $(nod, foc)$. Note, if *ntr_ow = 0* then *ndev* is set to zero internally.

58. *d_layer*

The thickness of the boundary layer which separates the boundary between the domain and the atmosphere. Used for the mixed boundary condition on the $\rho_n^G$ transport equation, where *d_layer* defines a constant parameter $\delta$ (equation 6.32). See subsection 6.4.2 for more detail. Note, this parameter is used only if *ntr_og = 1* and a third-type boundary condition is specified.

59. *bow_1, bow_2, bow_3*

Definition for the first-order mass transfer kinetic for the NAPL-phase dissolving into the water-phase (see subsection 4.8.1), where

*bow_1*: the rate coefficient $\beta_1^{WN}$ $[1/T]$ in equation 4.29

*bow_2*: the coefficient $\beta_2$ in equation 4.29

*bow_3*: the coefficient $\beta_3$ in equation 4.29

Note, if *ntr_ow = 0* then *bow*_1 is set to zero internally.

60. *parow*

The equilibrium concentration of the NAPL species in the water phase (solubility limit), the parameter $\overline{\rho}_n^W$ $[M/L^3]$ in equation 4.28. Note, if *ntr_ow = 0* then *parow* is set to zero internally.

61. *bog_1, bog_2*

Definition for the first-order mass transfer kinetic for the NAPL-phase vaporizing into the gas-phase (see subsection 4.8.1), where

*bog_ 1*: the rate coefficient $\beta_1^{GN}$ $[1/T]$ in equation 4.31

*bog_ 2*: the coefficient $\beta_2$ in equation 4.31

Note, if *ntr_ og = 0* then *bog*_1 is set to zero internally.

62. *parog*

The equilibrium concentration of the NAPL species in the gas-phase (solubility limit), the parameter $\overline{\rho}_n^G$ $[M/L^3]$ in equation 4.30. Note, if *ntr_ og = 0* then *parog* is set to zero internally.

63. *bowg_ 1, bowg_ 2*

Definition for the first-order mass transfer kinetic for the dissolved NAPL species ($\rho_n^W$) vaporizing into the gas-phase (see subsection 4.8.1), where

*bowg_ 1*: the rate coefficient $\beta_1^{GW}$ $[1/T]$ in equation 4.34

*bowg_ 2*: the coefficient $\beta_2$ in equation 4.34

Note, if either *ntr_ ow = 0* or *ntr_ og = 0* then *bowg*_1 is set to zero internally.

64. *e_ henry*

The dimensionless Henry's law constant. The parameter $H$ in equation 4.33. Note, used only if both *ntr_ ow = 1* and *ntr_ og = 1.*

65. *t_ half*

The effective half-life of the NAPL species in the water and gas phases [T] (the parameter $t_{1/2}$ in equation 4.26). By default the decay coefficients, $\kappa_n^W$ and $\kappa_n^G$, are set to zero if the input parameter $t\_half \leq 0$. If $t\_half > 0$ then equation 4.26 is used to define the decay coefficients.

66. *swinit*

The global initial condition for water saturation (the parameter $S_{W0}$ in subsection 6.4.1).

67. *stinit*

The global initial condition for total wetting phase saturation ($S_{Tw0} = S_{W0} + S_{N0}$). Note, an error message will appear on the screen and the simulator will stop if any of the following input combinations occur:

$iphase = 12$ (see input line 2) and $stinit \neq 1$

$iphase = 13$ (see input line 2) and $stinit \neq swinit$

$swinit > stinit$

See Appendix C for the decision tree which defines initial $k - S - P$ model given initial saturations.

68. *roainit*

The global initial condition for dissolved contaminant concentration (the parameter $\rho_{n0}^{W}$ in subsection 6.4.1). Note, that if $ntr\_ow = 0$ then *roainit* is set to zero internally, and if $ntr\_ow = 1$, $(stinit - swinit) > 0$, and $swinit > 0$, then *roainit* is set to the solubility limit, *parow*, internally. These operations override the user-defined input.

69. *roginit*

The global initial condition for vapor contaminant concentration ($\rho_{n0}^{G}$). Note, that if $ntr\_og = 0$ then *roginit* is set to zero internally, and if $ntr\_og = 1$, $(stinit - swinit) > 0$ and $(1 - stinit) > 0$, then *roginit* is set to the solubility limit, *parog*, internally. These operations override the user-defined input.

70. *ncont*

Restart option switch. If $ncont = 1$ (yes) $= 0$ (no). If yes, then the default initial values defined in lines (64 through 67) are overwritten and the initial conditions are read in from the set of files with the **rs** extension (for restart). These files are in binary format, and they contain output from the last output interval of the previous simulation. See input line 8 for output interval definition and subsection 7.2.2 for description of restart files.

71. *ndev_ s*

Number of deviations from initial global saturation definition. If $ndev\_s > 0$ then the simulator opens the file **sat.in** and reads *ndev* lines of information, where each line lists the node number and the values of $S_W$ and $S_{Tw}$ $(nod, sw, st)$. This data over-writes all previous data. Note an error message will appear on the screen and the simulator will stop if any of the following input combinations occur:

$iphase = 12$ (see input line 2) and $st \neq 1$

$iphase = 13$ (see input line 2) and $st \neq sw$

$sw > st$

Also note, at all nodes where $(st - sw) > 0$, if $ntr\_ow = 1$ and $sw > 0$, $\rho_{n0}^{W}$ is set internally to the solubility limit, $parow$, and if $ntr\_og = 1$ and $1 - st > 0$, $\rho_{n0}^{G}$ is set internally to the solubility limit, $parog$. Finally, see Appendix C for the decision tree which defines initial $k - S - P$ model given initial saturations.

72. *ndev_ roa*

Number of deviations from initial global definition. If $ntr\_ow = 0$ and you input $ndev\_roa > 0$ then the code prints a WARNING to the file **echo.out** alerting you that transport is off before setting *ndev_roa* to zero internally. Otherwise, if $ndev\_roa > 0$ then the simulator opens the file **roa.in** and reads *ndev_roa* lines of information, where each line lists the node number and the value of $\rho_{n0}^{W}$ $(nod, roa)$. This data overwrites all previous data.

73. *ndev_ rog*

Number of deviations from initial global definition. If $ntr\_og = 0$ and you input $ndev\_rog > 0$ then the code prints a WARNING to the file **echo.out** alerting you that transport is off before setting *ndev_rog* to zero internally. Otherwise if $ndev\_rog > 0$ then the simulator opens the file **rog.in** and reads *ndev_rog* lines of information, where each line lists the node number and the value of $\rho_{n0}^{G}$ $(nod, rog)$. This data overwrites all previous data.

74. *nbcroa*

The number of Dirichlet boundary conditions for the parameter $\rho_{n}^{W}$ (recall from subsection 6.4.2 that since homogeneous Neumann conditions are applied as the default at all boundary nodes, the user needs to specify only Dirichlet conditions). If $ntr\_ow = 0$ and you input $nbcroa > 0$ then the code prints a WARNING to the file **echo.out** alerting you that transport is off before setting *nbcroa* to zero internally. Otherwise, if $nbcroa > 0$ then the simulator opens the file **bc_ roa.in** and reads *nbcroa* lines of information, where each line lists the following:

*nface*, *nod*, *roa*

where,

*nface* is the mesh face which is normal to the direction from which the condition is applied. See figure 7.1 for the definition of $nface$ for the 2- and 3-D simulators.

*nod* is the node number for specified boundary condition

*roa* is the value of the known concentration $[M/L^3]$

75. *nbcrog*

The number of Dirichlet boundary conditions for the parameter $\rho_n^G$ (recall from subsection 6.4.2 that since homogeneous Neumann conditions are applied as the default at all boundary nodes, the user needs to specify only Dirichlet and mixed conditions)[4]. If $ntr\_og = 0$ and you input $nbcrog > 0$ then the code prints a WARNING to the file **echo.out** alerting you that transport is off before setting *nbcrog* to zero internally. Otherwise, if $nbcrog > 0$ then the simulator opens the file **bc_rog.in** and reads *nbcrog* lines of information, where each line lists the following:

*nface*, *nod*, *rog*

where,

*nface* is the mesh face which is normal to the direction from which the condition is applied. See figure 7.1 for the definition of $nface$ for the 2- and 3-D simulators.

*nod* is the node number for specified boundary condition

*rog* represents one of two things. If $rog \geq 0$, then *rog* is the value of the known concentration $[M/L^3]$ at the node. If $rog < 0$, then the 2-D simulator assumes that the condition is of the mixed type and applies equation 6.32 at the node. The 3-D simulator will not accept $rog < 0$ as a valid entry, and it will print an error and then stop.

76. *ncondf*

The number of flow-variable boundary conditions different from the default no flow condition. If $ncondf > 0$ then the simulator opens the file **bc_flow.in** and reads the data for *ncondf* boundary nodes, where each node requires the following:

[4]The 2-D version allows both Dirichlet and mixed conditions. The 3-D version allows only Dirichlet conditions.

*nface*, *nod*, *ncode*

where

*nface* is the mesh face which is normal to the direction from which the condition is applied. See Figure 7.1 for the definition of $nface$ for the 2- and 3-D simulators, and the for the significance of this parameter refer to the discussion in Section 7.1, Item 12. Note, while this information is only important at corner and edge boundary nodes, a value must be specified even at internal boundary nodes. If at any boundary node there is a discrepancy between the user-defined value of $nface$ and the admissible values, then an error message will appear on the screen and the simulator will stop.

*nod* is the node number for the specified boundary condition.

*ncode* defines the condition-type, where the code follows from the numbering scheme used in Table 6.1. In summary:

if $ncode = 2$ then prescribe gas-phase head ($h^G = P^G/\gamma^G$)

if $ncode = 3$ then prescribe the NAPL-phase head ($h^N = P^N/\gamma^N$)

if $ncode = 4$ then prescribe the water-phase head ($h^W = P^W/\gamma^W$)

if $ncode = 5$ then prescribe $h^W$, $S_W$ and $S_G$

Refer to subsection 6.4.2 for additional details on admissable boundary conditions. Note if *ncode* does not equal one of these values, then an error message will appear on the screen and the simulator will stop.

Depending on the value of *ncode* the simulator expects the following information on the following input line:

If $ncode = 2$, list the gas head value [L], $h\_g$

If $ncode = 3$ list the NAPL head value [L], $h\_n$

If $ncode = 4$ list the water head value [L], $h\_w$

If $ncode = 5$ list the parameter $n\_opt$, and then the values for water head [L], water saturation and gas saturation values,$h\_w, s\_w, s\_g$, where

$n\_opt$ tells the simulator whether to use the Dirichlet data listed ($n\_opt = 0$), or to define the Dirichlet data using the initial conditions from a previous run or stress period ($n\_opt = 1$). Note, by setting $n\_opt = 1$ the code assumes that the current solution at the node is the Dirichlet data, therefore, $n\_opt = 1$ can only

be used in conjunction with either *ncont = 1* (see input line 68) or after a stress period change (see input line 68). If neither form of initial data is available then an error message will be printed to the screen and the simulator will stop. Also note that if any of the following input parameter combinations are used an error message will be printed to the screen and the code will stop:
$ncode = 2$ and $iphase = 12$
$ncode = 3$ and $iphase = 13$

77. *nwella*

Specification of point sources and sinks (wells), where *nwella* is the number of nodes at which a point source or sink condition is to be applied. If $nwella > 0$ then the simulator opens the file **well.in** and reads *nwella* lines of information, where each line lists the following:

*nod*, *q_tot*, *ff_w*, *ff_g*, *roa*, *rog*

where

*nod* is the node number where the well is idealized

*q_tot* is the total well flow rate $[L^3/T]$ ($Q^T$ in subsection 6.4.3), where injection is positive (+), extraction is negative (-).

*ff_w* is the fractional flow of water of the injected fluid, where the simulator internally computes the water flow rate as[5]: $Q^W = ff\_w\ q\_tot$.

*ff_g* is the fractional flow of gas of the injected fluid, where the simulator internally computes the gas flow rate as[2] : $Q^G = ff\_g\ q\_tot$.[6]

*roa* is the concentration of the NAPL species in the water-phase in the injected fluid when *ntr_ow = 1*, and no NAPL is present.[2] If NAPL is present and *ntr_ow = 1*, then *roa* is set internally to the solubility limit *parow*. If *ntr_ow = 0* then *roa* is set to zero internally.

*rog* is the concentration of the NAPL species in the gas-phase in the injected fluid when *ntr_og = 1*, and no NAPL is present.[2] If NAPL is present

[5] Note that this only applies for injection wells (i. e., $q\_tot > 0$) where the makeup of the source fluid is known. At extraction wells (i. e., $q\_tot < 0$) the the makeup of the sink fluid is a function of the solution. See equation 6.33.

[6] At injection wells, given $q\_tot$, $ff\_w$ and $ff\_g$, the NAPL flow rate is known since $Q^N = q\_tot - Q^W - Q^G$.

and *ntr_og = 1*, then *rog* is set internally to the solubility limit *parog*. If *ntr_og = 0* then *rog* is set to zero internally.

78. *timec, iph_new, dtnew, co_new, dtmax*

    Define a new stress period: change the boundary and external flux conditions at specified times during the simulation without stopping, where

    *timec* - time for new stress period.

    *iph_new* - define number and types of phases modelled (redefines the parameter *iphase* initially defined on input line 2)

    *dtnew* - new initial time step.

    *co_new* - new Courant constraint (redefines the parameter *co* initially defined on input line 14)

    *dtmax* - new maximum time step (redefines the parameter *tsmax* initially defined on input line 16).

    If the simulation time is greater than or equal to *timec* then what follows is a re-specification of boundary conditions starting at (72.). Therefore, repeat input lines 72 through 76 for each stress period change.

This concludes the description on data input. Examples of the actual input files can be found in Chapter 8.

## 7.2. INPUT- AND OUTPUT-FILE DESCRIPTION

### 7.2.1. Input Files

All the files are written in standard ASCII format. Reference to specific input lines refers to those described in subsection 7.1.2. Input files are listed by category.

1. Main data driver

   **sm.in** - defines all data input for the simulator. Defines calls to other data input files.

2. Grid spacing

**space.in** - grid spacing information, list first nodal x-coordinates ($nnx$ entries) and then nodal y-coordinates ($nny$ entries)

3. Initial conditions

**roa.in** - list of nodal exceptions to global specification of $\rho_n^W$ as defined in input line 70 of file **sm.in**. Lists the node number and the specified value.

**rog.in** - list of nodal exceptions to global specification of $\rho_n^G$ as defined in input line 71 of file **sm.in**. Lists the node number and the specified value.

**sat.in** - list of nodal exceptions to global specification of $S_W$ and $S_{Tw}$ as defined in input line 69 of file **sm.in**. Lists the node number and the specified $S_W$ and $S_{Tw}$ values.

4. Spatially-varying physical constants (Table 7.1)

**bulk.in** - list of nodal exceptions to global specification of the soil dry bulk density as defined in input line 30 of file **sm.in**. Lists the node number and the value of the soil bulk density.

**o_c.in** - list of nodal exceptions to global specification of the fraction of organic carbon in the soil as defined in input line 55 of file **sm.in**. Lists the node number and the value of organic carbon content.

**perm.in** - list of nodal exceptions to global specification of permeability scalar as defined in input line 26 of file **sm.in**. Lists the node and the permeability value.

**por.in** - list of nodal exceptions to global specification of porosity as defined in input line 28 of file **sm.in**. Lists the node and the porosity value.

**shape.in** - list of nodal exceptions to global specification of $S - P$ curve fitting parameters $a_d$, $a_i$ and $\eta$ as defined in input line 38 of file **sm.in**. Lists the node number and the values of $a_d$, $a_i$ and $\eta$.

5. Boundary and external forcing conditions

**bc_flow.in** - list of nodal Dirichlet data for flow for each stress period. Data for each stress period is concatenated.

**bc_roa.in** - list of nodal Dirichlet data for dissolved NAPL concentration. Data for each stress period is concatenated.

**bc_rog.in** - list of nodal Dirichlet or mixed data for NAPL vapor concentration. Data for each stress period is concatenated.

**well.in** - list of nodal point source and sink data for each stress period. Data for each stress period is concatenated.

### 7.2.2. Restart Files

Restart files contain un-formatted double precision output written at the last specified output interval (as determined by the print command), and they constitute all the necessary nodal information required to restart the simulator from the time of the last specified output interval. Used for either a planned continuation, or after an unexpected program stoppage. The files contain nodal solution data, and they are categorized into two groups:

1. those files associated with the hysteretic $k - S - P$ model:

   **a.rs** -the scaling parameters $a_{(f)}$ used in equation 5.13 and defined in Table 5.2.

   **nhc.rs** - the integer curve-type indicator $f$.

   **s_max.rs** - the highest $\alpha$-phase saturation that has occurred since it was last at immobile residual conditions, $S_\alpha^{\max}$ (equation 5.7).

   **sb.rs** - the saturation at which curve $f$ was spawned, $S_{0(f)}$ used in Tables 5.2, 5.3 and 5.4.

   **sr.rs** - the minimum wetting phase saturation for curve-type $f$, $S_{r(f)}$ used in equation 5.13 and defined in Table 5.3 $S_{r(f)}$.

   **ss.rs** - the maximum wetting phase saturation for curve-type $f$, $S_{s(f)}$ used in equation 5.13 and defined in Table 5.4.

   **trap_c.rs** - the current trapped quantity, $S_{\alpha t}$, defined in equation 5.7.

   **trap_mn.rs** - the lower limit of entrapped $\alpha$-phase $S_{\alpha t}^{\min}$ used in equation 5.7 and defined in equation 5.8.

   **trap_mx.rs** - the magnitude of the residual $\alpha$-phase at the terminus of an $\alpha$-phase drainage process, $S_{\alpha r}^*$, used in equation 5.7 and defined in equation 5.9.

2. those files associated with the solution variables:

   **oa.rs** - the nodal Hermite $\rho_n^W$ data
   **og.rs** - the nodal Hermite $\rho_n^G$ data
   **pa.rs** - the nodal Hermite $P^W$ data
   **sw.rs** - the nodal Hermite $S_W$ data
   **st.rs** - the nodal Hermite $S_{Tw}$ data

### 7.2.3. Compilation Files

The simulator uses the FORTRAN 77 INCLUDE statement. The file **include.f** is used to set the dimensions for the arrays used in the simulator. See subsection 7.1.1 for proper dimensioning requirements.

After changing the **include.f** file one needs to compile the code. A file called **makefile** contains the UNIX system commands which create and link the object files to yield the executable file **napl**.

### 7.2.4. Screen output

If the output flag *iscr = 1* (set in line 3 of file **sm.in** ) then iteration and solution information is output to the screen in the order that the computations are performed (see subsection 6.7 for a summary of the computational steps). This output is diagnostic in nature and provides the user with run-time information on simulator performance.

- *P - GMRES (number of iterations)* or *P - DIRECT*. The total flow equation was just solved for $P^W$. Note, this equation is linear, therefore iteration is necessary only when the GMRES iterative solver is employed.
- *FLUX CONVERSION FOR BCs 2, 3 and 4*. At each boundary node where a Case 2, 3 or 4 flow boundary condition is applied, the boundary fluxes were just converted into point source/sink conditions. The output lists the phase flux data for each node:

  $$\text{node number} \quad Q^W \quad Q^N \quad Q^G$$

  where $Q^\alpha$ $[L^3/T]$ is the equivalent volumetric flux of the $\alpha-$phase at the node.

- *Rog - GMRES (number of iterations)* or *Rog - DIRECT.* .
  *Roa - GMRES (number of iterations)* or *Roa - DIRECT.*
  The contaminant transport equations were just solved for $\rho_n^G$ and $\rho_n^W$, respectively. Note, this information is displayed only if contaminant transport is turned on (i. e., *ntr_ow = 1* and/or *ntr_og = 1* in input line 48 of file **sm.in**), otherwise it is suppressed. Also, if contaminant transport is on, then since the concentration equations are nonlinear, the iteration information for nonlinear convergence is displayed in the next line, where the respective entries from left to right are:

  Equation-type : NL_C,
  iteration number,
  node where the largest change occurred,
  the values of $\rho_n^W$ and $\rho_n^G$ at that node,
  the $L2$ norm of the iterative increment,
  the infinity norm of the iterative increment.

- *STw - GMRES (number of iterations)* or *STw - DIRECT.*
  *Sw - GMRES (number of iterations)* or *Sw - DIRECT.*
  The saturation equations were just solved for $S_{Tw}$ and $S_W$, respectively. Note, if *iphase = 12*, then only $S_W$ is solved, and if *iphase = 13*, then only $S_{Tw}$ is solved (see input line 2 in file **sm.in**). Also, since the saturation equations are nonlinear, the iteration information for nonlinear convergence is displayed in the next line, where the respective entries from left to right are:

  Equation-type : NL_S,
  iteration number,
  node where the largest change occurred,
  the values of $S_W$, $S_N$ and $S_G$ at that node,
  in parentheses, the maximum change in $S_{eW}$ or $S_{eTw}$ over the time step,
  the L2 norm of the iterative increment,
  the infinity norm of the iterative increment.

After a convergent solution is computed for the time step, the time information is printed, including from left to right,

the elapsed time (in the units specified) since the beginning of the simulation,

the time step value for the last time step,

the number of times the time step had to be restarted because of lack of iterative convergence (see input line 12),

the number of time steps taken since beginning of the simulation.

### 7.2.5. Output files

Output files are grouped according to the information they provide. We identify three groups:

1. Output files to be used by post-processing graphics software. These files are generated only if the graphics output is enabled (see input line 17 in file **sm.in**):

   solution vectors (see input line 16 for output interval definition)

   **sw.stf** and **st.stf** (saturations $S_W$ and $S_{Tw}$)
   **oa.stf** and **og.stf**(concentrations, $\rho_n^W$ and $\rho_n^G$ )
   **velw.stf**, **veln.stf** and **velg.stf** (fluid velocities $\mathbf{v}^W$ , $\mathbf{v}^N$ and $\mathbf{v}^G$ )

   soil properties

   **soil.stf** - column 1 is nodal values of permeability, column 2 is nodal values of porosity.

   mesh information

   **mfile.jin** - contains a list of nodal coordinates and element-to-node connectivity

2. Output files containing mass balance and simulation performance information. this information is output only if the mass balance computations are turned on. There are six files that contain mass balance information.

   **cmass.out** - cumulative mass balance calculation after each time step. Mass balance for each phase at time $T > 0$ is defined as:

   (the cumulative phase mass that has crossed the boundary from $t = 0$ to $T$)

/ (the total phase mass in the domain at time $T$ ).

The file lists the following nine entries for each time step:

elapsed time,
water phase mass error,
NAPL phase mass error,
gas phase mass error,
$\triangle\ t$,
number of $P^W$ iterations,
number of $S_W$ iterations,
number of $S_G$ iterations,
number of iteration hang-up/restarts.

**mass.out** - for each specified solution output (as defined by the print interval), summarizes mass, time step, and iteration performance.

**massg.out** - gas mass balance error per time step. Mass balance over the time step is defined as:

(the change in the amount of phase mass in the computational domain over $\triangle t$)
/ (the phase mass that has crossed the boundary over $\triangle t$)

Perfect mass balance is indicated by a ratio of one. The following six entries are listed for each time step:

elapsed time
gas mass in over boundary over $\triangle t$
gas mass out over boundary over $\triangle t$
change in gas mass over the boundary over $\triangle t$
change in gas mass in the domain over $\triangle t$
mass balance ratio defined above.

**masso.out** - same as **massg.out** except for NAPL phase.

**massw.out** - same as **massg.out** except for water phase.

**masst.out** - total fluid mass balance error per time step. For each time step, lists the elapsed time and the ratio:

(the change in the amount of total phase mass in the computational domain over $\triangle t$)

/ (the total phase mass that has crossed the boundary over $\triangle t$)

3. Output files containing information on the solution. The frequency of the output is defined by the print interval (see input line 8 in file **sm.in**), and the output is concatenated.

   If Hermite data output is enabled (see input line 4 in file **sm.in**), then the following Hermite coefficient information at each node in the domain is provided:

   **sw.out**, **st.out** (saturations $S_W$ and $S_{Tw}$)

   **pa.out** (water pressure)

   **oa.out** and **og.out** (concentrations $\rho_n^W$ and $\rho_n^G$)

   Referenced by time information, each print interval lists the solution data for each node:

   node number, values of the 4 (8) degrees of freedom.[7]

   **echo.out** - echoes parameter input, and lists WARNING messages.

   **sat.out** - Solution summary. Referenced by time information, each print interval lists the following solution data for each node:

   $S_W$, $S_N$, $S_G$, $P_{cNW}$, $P_{cGN}$, $\rho_n^W$ and $\rho_n^G$

   **velg.out** - the computed gas flux components at each node.

   **veln.out** - the computed NAPL flux components at each node.

   **velw.out** - the computed water flux components at each node.

[7] Four degrees of freedom for the 2-D simulator and eight degrees of freedom for the 3-D simulator.

# 8. MODEL TESTING AND EXAMPLE PROBLEMS

The focus of this Section is on testing the model for self-consistency and its ability to simulate experimental procedures and results. Self-consistency is established by investigating spatial and temporal convergence attributes and mass balance performance. A series of pseudo-one-dimensional example problems are presented in order to evaluate convergence and mass balance, and to give the user an indication of appropriate discretization for a given set of input data. In addition to addressing self-consistency, four example problems were designed to simulate specific physical experiments:

1. a three-phase LNAPL spill and redistribution experiment (Van Geel and Sykes, 1995);
2. a three-phase DNAPL spill and redistribution experiment conducted at the EPA's Subsurface Protection and Remediation Division of the National Risk Management Research Laboratory in Ada, OK;
3. an experimental investigation of the dissolution of residual DNAPL in a saturated sand (Imhoff et al, 1992);
4. an experimental investigation of DNAPL vapor transport in an unsaturated sand (Lenhard et al., 1995).

As discussed in subsection 8.3, the data sets for these problems 1, 2, and 4 are included with the software in the appropriate dedicated directory.

## 8.1. CONVERGENCE AND MASS BALANCE

### 8.1.1. Compatibility of the grid and the flow model

Because we are modeling the emplacement and dissolution of NAPL in the vadose zone, we need to consider problems which evolve to quasi-static flow conditions.

As a result, it is imperative that the spatial discretization be compatible with the flow parameters, especially those defining the $S-P$ model, so that oscillations in the saturation solutions are minimized. This point is illustrated in Figure 8.1 which compares the capillary rise for two different soils.

The problem is to simulate water drainage in a one-dimensional soil column, 1.2 meters long and initially saturated with water. The relevant soil properties, $S-P$ model parameters, and resulting van Genuchten $PDC$ are shown in Figures 8.1a [for a relatively fine sand] and 8.1c [for a relatively coarse sand]. The boundary conditions are: at the top, open to the atmosphere, and at the bottom, specified water head (fine sand = 10 cm, coarse sand = 60 cm). The columns are then allowed to drain under the influence of gravity until quasi-static conditions prevail. Figure 8.1b shows that for the fine sand, an appropriate grid spacing is approximately 10 cm, and Figure 8.1d shows that for the coarse sand an appropriate grid spacing is approximately 2 cm. It must be noted here that the simulator includes no implicit mechanism to add artificial diffusion, or capillarity, to the system (for example, an upstream weighting algorithm is not employed). Artificial capillarity must be included explicitly either by altering the $S-P$ curve fitting parameters or by utilizing the Peclet criterion (see Section 6.5.1 for details).

With respect to time step, we note the following. Because the Dirichlet pressure data is a nonlinear function of saturation, and because no saturation Dirichlet data has been specified, the time step represents the only explicit mechanism to damp oscillations in the pressure solution as the system approaches steady-state. The appropriate size of the time step is problem-dependent, and in general, the more nonlinear the $S-P$ functional the smaller the quasi-steady-state time step must be. For example, the quasi-steady-state $\triangle t$ for the problem in Figure 8.1b is of order 1000 seconds, while that for the problem in Figure 8.1d is of order 25 seconds. It is suggested that as the system approaches steady state, the gas pressure boundary condition be changed to Dirichlet conditions on $P^W$, $S_W$ and $S_G$ (a case 5 boundary condition, see Section 6.4.2).

### 8.1.2. Analysis of the three-phase hysteretic k-S-P model

Here we consider convergence and mass balance attributes of the simulator when the three-phase hysteretic $k-S-P$ model is employed. Consider the model problem presented in Figure 8.1d, and the result therein to be the initial conditions for a DNAPL spill simulation. Relevant model parameters are presented in Table 8.1. These parameters mimic those to be used in an artificial aquifer experiment

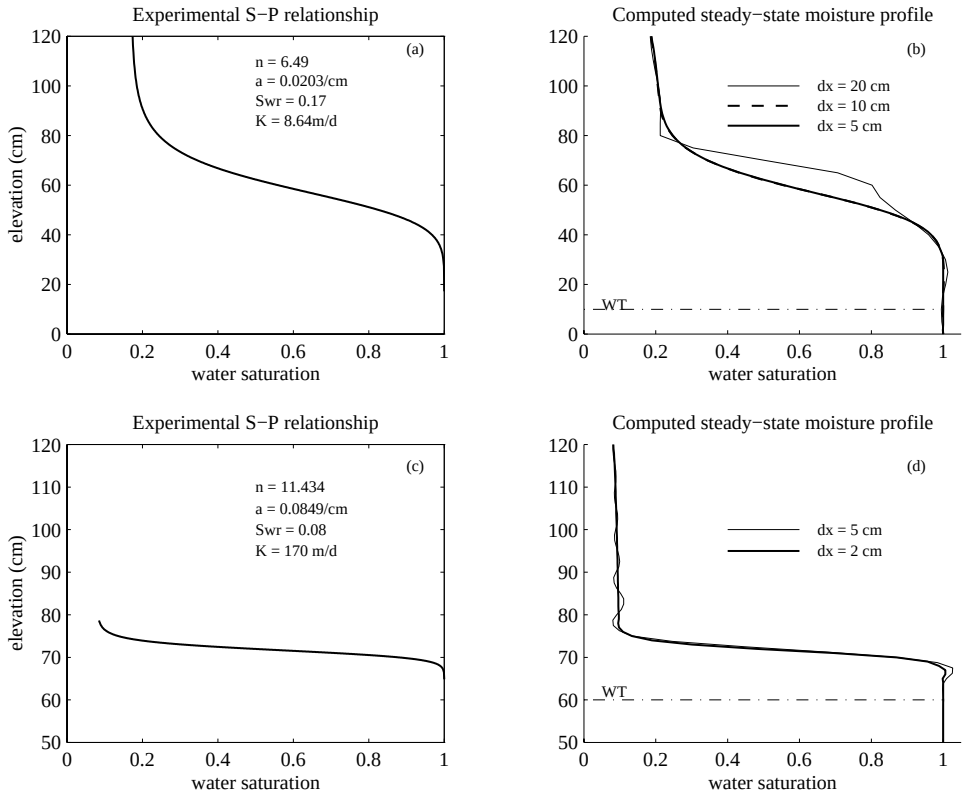


Figure 8.1: Analysis of appropriate grid spacing to compute capillary rise for different soil-types. Parts (a) and (b) are for a relatively fine sand, and parts (c) and (d) are for a relatively coarse sand.

| **Fluid properties** | | |
|---|---|---|
| $\rho^W = 0.9982\ g/cm^3$<br>$\mu^W = 0.01\ poise$<br>**S-P model definition** | $\rho^N = 1.626\ g/cm^3$<br>$\mu^N = 0.0093\ poise$ | $\rho^G = 0.00129\ g/cm^3$<br>$\mu^G = 0.0002\ poise$ |
| $a_d = 0.0849/cm$ | $a_i = 0.12/cm$ | $\eta = 11.434$ |
| $S_{Wr} = 0.08$ | $S_{Gr} = 0.16$ | $S_{Nnr} = 16$, $S_{Nwr} = 0.08$ |
| $\sigma_{GW} = 72.75\ dynes/cm$ | $\sigma_{NW} = 39.5\ dynes/cm$ | $\sigma_{GN} = 31.74\ dynes/cm$ |
| **k-S model definition** | | |
| ${}^aS_{eW}$ from eq 5.25 | ${}^bS_{eW}$ from eq 5.25 | |
| ${}^aS_{eG}$ from eq 5.26 | ${}^bS_{eG}$ from eq 5.26 | |
| $S_{eN}$ from eq 5.30 | $S_{eTw}$ from eq 5.32 | $S_{eTn}$ from eq 5.35 |
| $\zeta = \varphi = \xi = 0.5$ | | |
| **Field properties** | | |
| $\varepsilon = 0.3115$ | $k = 170\ m/d$ | |

Table 8.1: PARAMETERS USED TO MODEL THREE-PHASE PCE MIGRATION IN OTTAWA SAND

being conducted at RSKERL involving a controlled release of a DNAPL. The boundary conditions for the current problem are given as: $h^W = 60\ cm$ at the bottom boundary for all time, and, at the top boundary, the following time-varying conditions are applied:

1. For time = 0 to 100 s, DNAPL is injected at a constant volume rate of 0.03 $cm^3/s$.

2. For time = 100 s to the end of the simulation, $P^G$ = atmospheric.

This problem is considered a severe test of the numerical model for two reasons:

1. The $S - P$ functionals are extremely nonlinear.

2. The incompressible gas-phase assumption (while not appropriate for this simulation) leads to a result in which, as the DNAPL is injected, the water table is depressed. Then, after the source is removed and the top re-opened to the atmosphere, the water table rebounds, forcing the gas-phase to percolate up through the descending DNAPL.

Simulation results for two different discretizations are presented in Figure 8.2. A time step of order 2 seconds was required to obtain a solution for this problem, as larger time steps caused convergence problems. Figure 8.2a shows the total liquid saturation solution at initial conditions (T = 0) and at T = 200 s (100 s after the DNAPL source was removed). One can see that while both discretizations capture the sharp DNAPL front, the x = 2.5 cm solution exhibits oscillations behind the front. Figure 8.2b presents saturation results at time = 5000 s, after the DNAPL has migrated to near static, residual state. It is apparent that for these model parameters, a grid spacing of approximately 1 cm is required. Figures 8.2c and 8.2d present mass balance results for this simulation. The definition of the mass balance ratio used in the figure is:

(the change in the amount of total phase mass in the computational domain over $\triangle$t)

/(the total phase mass that has crossed the boundary over $\triangle$t)

Perfect mass balance over a time step is indicated by a ratio of one. One can see that in general the model performs well with respect to mass balance except when boundary forcing is changed, and several time steps are needed to accommodate the discontinuity imposed.

### 8.1.3. Analysis of the mass transfer model

Here we investigate the convergence attributes of the kinetic mass transfer model. Consider the following one-dimensional water flow and contaminant transport problem where the domain is the same as that defined in Figure 8.1c, and the model parameters are those given in Table 8.1. The initial conditions are set such that the domain is saturated, and there is a zone of residual DNAPL, $S_N = 0.15$, uniformly distributed from $x = 25\ cm$ to the bottom. The boundary conditions are set such that there is a constant influx of clean water at the top at a rate of 0.008 $cm/s$, and an equivalent efflux of contaminated water at the bottom. Relevant mass transfer and transport parameters are: $\beta_2 = 0.5$ and $\beta_3 = 1.0$, $a_L^W = 1$ $cm$, and $\overline{\rho}_n^W = 0.001\ gm/cm^3$. The results for different values of the exchange rate coefficient, $\beta_1^{WN}$, are presented in Figures 8.3a and 8.3b. As shown in the Figure, a distinct dissolution front is created, the shape of which is a function of the size of $\beta_1^{WN}$. High values effectively approximate the equilibrium partitioning approximation and produce a sharp front, while low values produce a broad front. From a numerics standpoint, the dissolution front should be resolved over several elements to minimize oscillations in the solution which can cause erroneous NAPL saturations upstream of the source area.

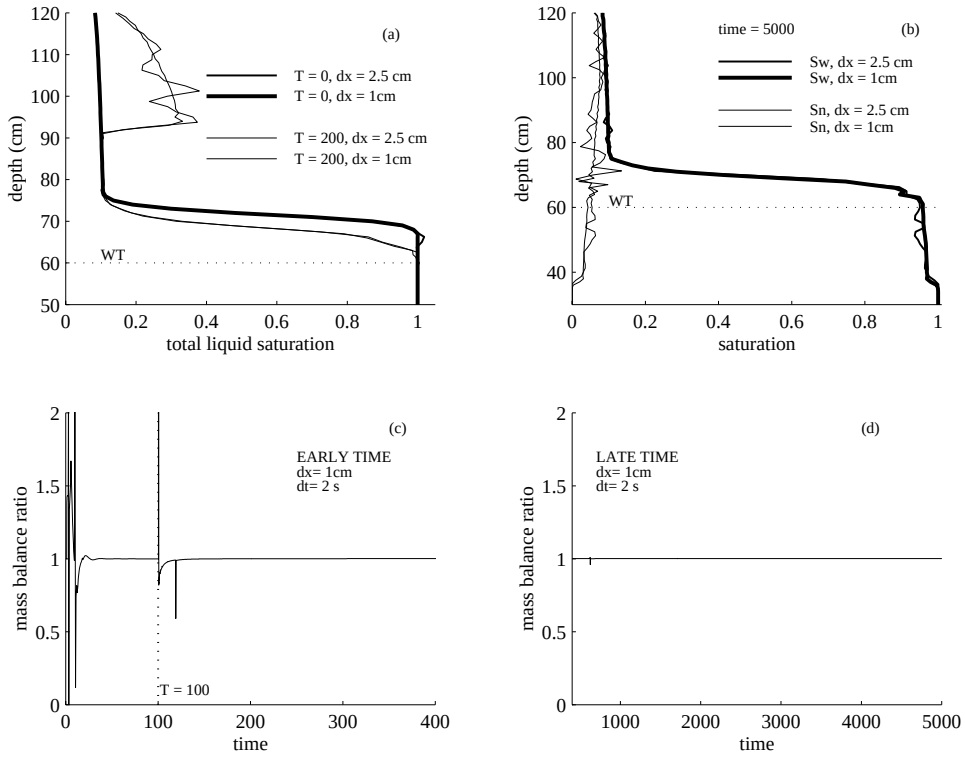


Figure 8.2: Results of a one-dimensional, three-phase, DNAPL injection and redistribution simulation, highlighting spatial convergence and mass balance.

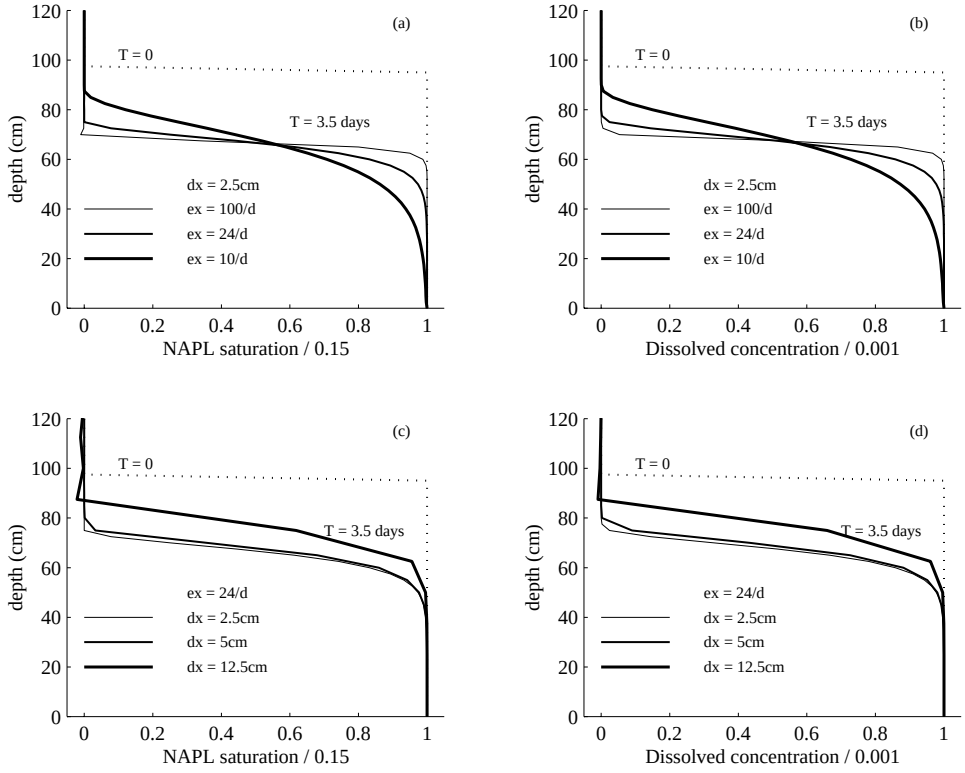


Figure 8.3: Computational analysis of the dissolution model. Parts (a) and (b) illustrate the effect that the rate constant (ex in the figure, expressed in units of 1/day) has on the solution. As the dissolution front sharpens, oscillations appear indicating that a finer grid spacing is required. Parts (c) and (d) illustrate spatial convergence for ex = 24/d. For the parameters chosen a grid spacing of approximately 5 cm is appropriate.

| **Fluid properties** | | |
|---|---|---|
| $\rho^W = 0.9982\ g/cm^3$<br>$\mu^W = 0.01\ poise$<br>**S-P model definition** | $\rho^N = 0.6858\ g/cm^3$<br>$\mu^N = 0.00409\ poise$ | $\rho^G = 0.00129\ g/cm^3$<br>$\mu^G = 0.0002\ poise$ |
| $a_d = 0.0203/cm$ | $a_i = 0.0271/cm$ | $\eta = 6.49$ |
| $S_{Wr} = 0.17$ | $S_{Gr} = 0.20$ | $S_{Nnr} = S_{Nwr} = 0.18$ |
| $\beta_{GW} = 1$ | $\beta_{NW} = 0.5128$ | $\beta_{GN} = 0.27397$ |
| **k-S model definition** | | |
| $^aS_{eW}$ from eq 5.25 | $^bS_{eW}$ from eq 5.25 | |
| $^aS_{eG}$ from eq 5.26 | $^bS_{eG}$ from eq 5.26 | |
| $S_{eN}$ from eq 5.30 | $S_{eTw}$ from eq 5.34 | $S_{eTn}$ from eq 5.37 |
| $\zeta = \varphi = \xi = 0.5$ | | |
| **Field properties** | | |
| $\varepsilon = 0.374$ | $k = 1.02x10^{-7}\ cm^2$ | |

Table 8.2: PARAMETERS USED IN THE LNAPL SPILL PROBLEM

Spatial convergence is illustrated in Figures 8.3c and 8.3d. For a constant rate coefficient, $\beta_1^{WN} = 24/d$, the model exhibits convergence as the mesh is refined. As with the previous example, oscillations in the saturation solution appear behind the front when the grid scale is too large. As with diffusion in contaminant transport, the size of the exchange coefficient is limited by the spatial discretization.

## 8.2. COMPARISONS TO EXPERIMENTAL RESULTS

### 8.2.1. LNAPL Spill

Here we compare current model results to the experimental and simulation results of Van Geel and Sykes (1995 a and b). The model parameters are presented in Table 8.2 (note, these are the same parameters as those used in the problem defined in Figures 8.1a and 8.1b). A plot of the $S - P$ model primary and main curves for the simulation is shown in Figure 8.4. The two-dimensional problem domain and boundary conditions are defined in Figure 8.5.

With reference to Figure 8.5, the forcing conditions for the problem can be separated into three stress periods:

1. From time = 0 to 63000 s (part a), the initially saturated sand is allowed to

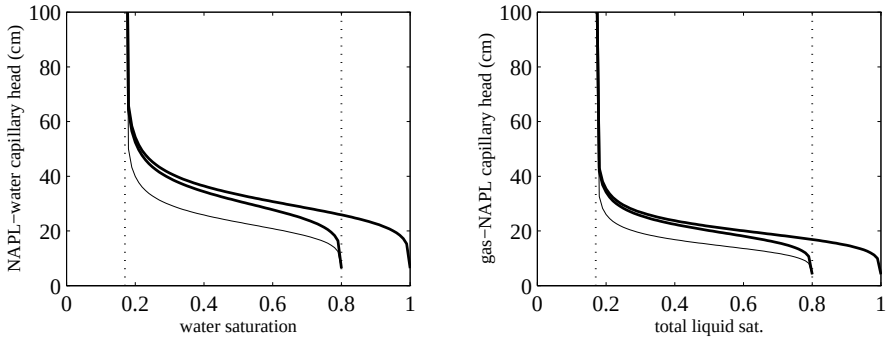


Figure 8.4: Plot of the primary and main S-P functionals defined by the current model for the LNAPL spill simulation, where the drainage curves are represented by the thick lines and the imbibition curves are represented by the thin lines. Here the fitting parameters, assumed to be valid for a water-gas system, have been scaled to represent the water-NAPL and NAPL-gas systems.

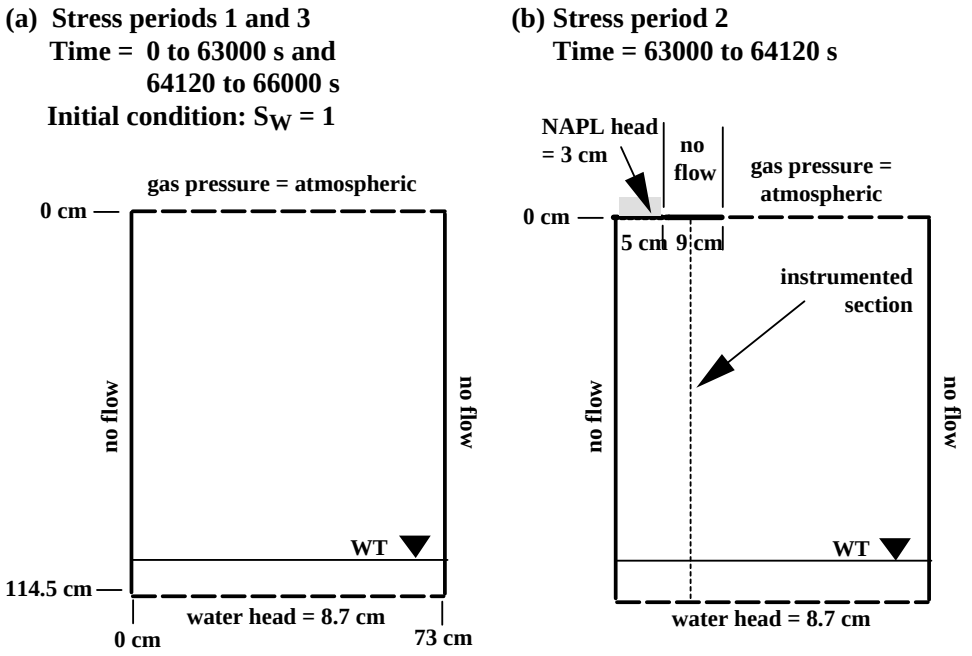


Figure 8.5: Definition sketch for the LNAPL spill simulation, showing spatial scale and boundary conditions.

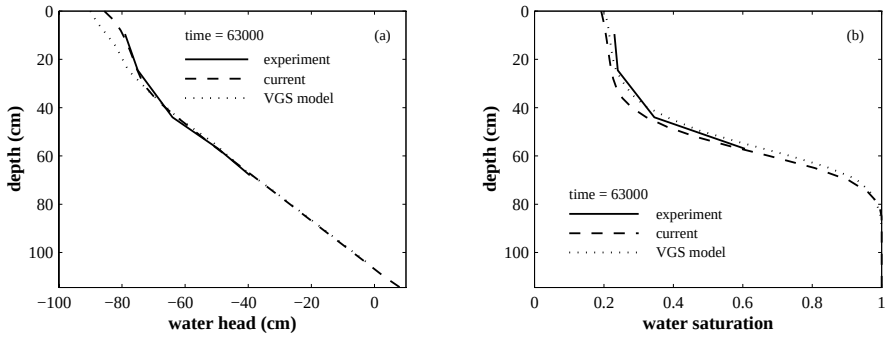


Figure 8.6: Comparison of results from the physical experiment, the current model, and the model used by Van Geel and Sykes (VGS). Part (a) shows the vertical distribution of water pressure head and Part (b) shows the vertical distribution of water saturation.

drain, thereby creating a quasi-steady-state moisture profile.

2. From time = 63000 to 64120 s (part b), an LNAPL source is applied to the top left corner. Specifically, a constant LNAPL head of 3 cm is applied for 1120 s to yield a cumulative infiltrated volume of 2 L.

3. From time = 64120 to 66000 s (part a), the LNAPL source is removed, and the resulting infiltrated volume is allowed to redistribute.

The results of this comparison study are presented in Figures 8.6 and 8.7. Figures 8.6a and 8.6b show the water pressure head and saturation solutions, respectively, at the end of the initial water drainage regime. The current model results match the experimental data.

Figures 8.7 illustrate the results during and after the LNAPL spill, where the times are given in elapsed time after the LNAPL was first applied (i. e., $T = 0$ at the start of stress period two). The plots on the left show the LNAPL distribution computed from the current model, and the plots on the right compare the three simulation results along the instrumented section shown in Figure 8.5. The current model captures the experimental data quite well.

The following additional details of this study are provided to highlight specific aspects of the current model:

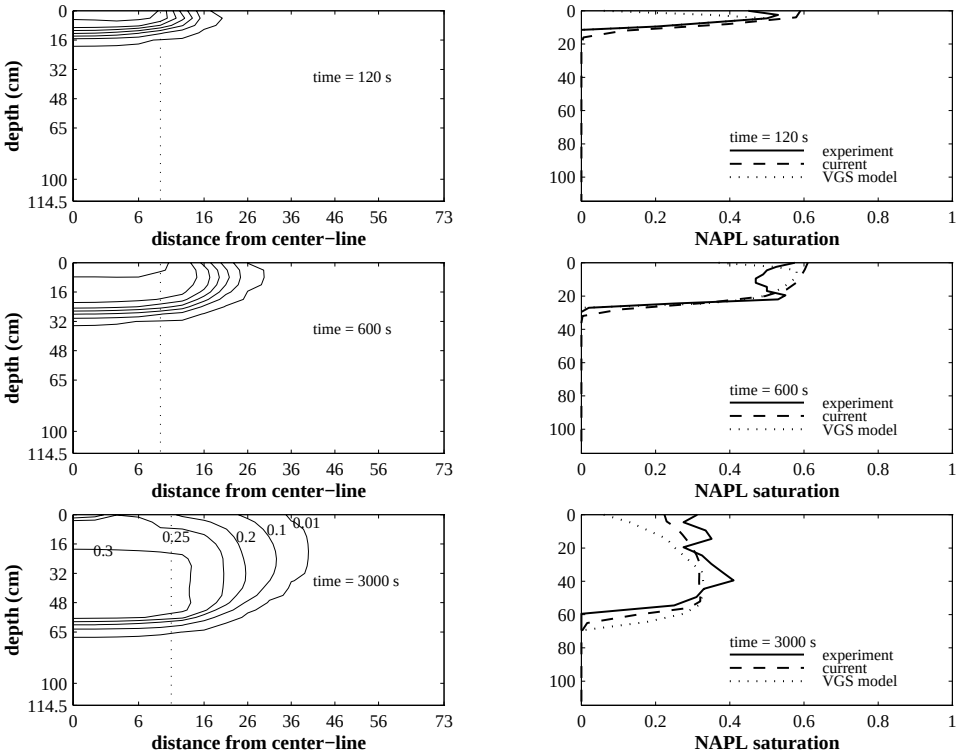


Figure 8.7: Comparison of results for the LNAPL spill problem. The plots on the left show the NAPL saturation contours as computed by the current model at the times indicated from the initiation of the LNAPL spill. The plots on the right compare results taken along the instrumented vertical section (the vertical dotted line in the plots on the left).

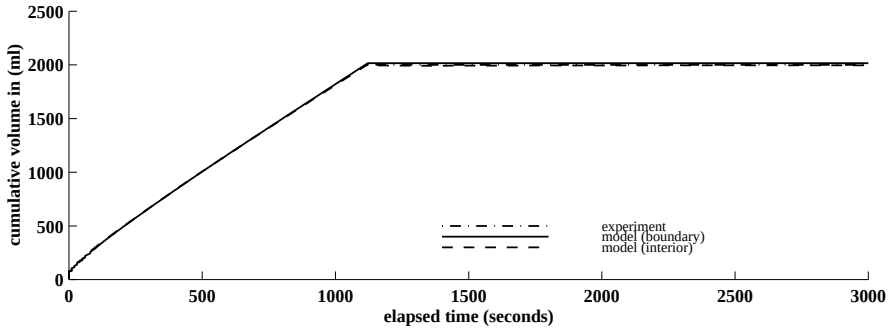


Figure 8.8: A comparisson of the cumulative LNAPL mass which has entered the domain as a function of time. At time = 1120 s the LNAPL source was removed. The solid line is the computed cumulative mass which has crossed the boundary. The dashed line is the change in mass in the domain. The dash-dot line is the experimental data.

1. Mesh definition (number of elements [spacing]): *horizontal* - 3 (2 cm), 2 (2.5 cm), 11 (5 cm), and 1 (7 cm); *vertical*- 15 (4 cm), 10 (5 cm), and 1 (4.5 cm), *into page* - 1 (6 cm).

2. Memory requirements (using the GMRES solver): 16 Mb RAM.

3. Time stepping information: stress period (1) - $\triangle\, t_{\max} = 2000$s, stress period (2) - $\triangle\, t_{\max} = 10$ s, , stress period (3) - $\triangle\, t_{\max} = 100$ s

4. The LNAPL mass balance computation is illustrated in Figure 8.8 which plots the cumulative LNAPL mass entering the domain as a function of time. The solid line is the computed cumulative mass which has crossed the boundary, while the dashed line is the computed change in mass in the domain. A zero mass balance error is indicated when the lines are coincident. The dash-dot line represents the experimental data for which the LNAPL mass equals 2000 ml at time $\geq 1120$ seconds.

5. The close match with the experimental data effectively verifies the algorithm used to impose gas and NAPL pressure boundary conditions.

6. The Van Geel and Sykes model (VGS model) utilizes the hysteretic $k-S-P$ model of Parker and Lenhard (1987) and Lenhard and Parker (1987). This

| **Fluid properties** | | |
|---|---|---|
| $\rho^W = 0.9982 g/cm^3$<br>$\mu^W = 0.01$ *poise*<br>**S-P model definition** | $\rho^N = 1.6 g/cm^3$<br>$\mu^N = 0.009$ *poise* | $\rho^G = 0.00129 g/cm^3$<br>$\mu^G = 0.0002$ *poise* |
| $a_d = 0.04/cm$ | $a_i = 0.06/cm$ | $\eta = 10$ |
| $S_{Wr} = 0.12$ | $S_{Gr} = 0.02$ | $S_{Nnr} = S_{Nwr} = 0.16$ |
| $\sigma_{GW} = 72.75$ *dynes/cm* | $\sigma_{NW} = 31.74$ *dynes/cm* | $\sigma_{GN} = 47.5$ *dynes/cm* |
| **k-S model definition** | | |
| $^a S_{eW}$ from eq 5.25 | $^b S_{eW}$ from eq 5.25 | |
| $^a S_{eG}$ from eq 5.26 | $^b S_{eG}$ from eq 5.26 | |
| $S_{eN}$ from eq 5.30 | $S_{eTw}$ from eq 5.32 | $S_{eTn}$ from eq 5.35 |
| $\zeta = \varphi = \xi = 0.5$ | | |
| **Field properties** | | |
| $\varepsilon = 0.37$ | $k = 3.5x10^{-7} cm^2$ | |

Table 8.3: PARAMETERS USED IN THE DNAPL SPILL PROBLEM

particular $k - S - P$ model does not account for NAPL entrapment as it is being displaced by the gas-phase (a wetting phase cannot be trapped by a nonwetting phase). This explains the under-prediction of the NAPL-phase saturation behind the front. The comparison results support the empirical hysteretic $k - S - P$ model described herein.

7. Some of the $k - S - P$ model parameters are different for the two empirical models. Specifically, the definition of residual saturation and the capillary scaling term $\beta_{GW}$.

### 8.2.2. DNAPL Spill

An artificial aquifer experiment was conducted by Mikhail Fishman at the EPA's Subsurface Protection and Remediation Division of the National Risk Management Research Laboratory in Ada, OK. The model parameters are presented in Table 8.3, and the details of the experimental setup can be found in Appendix F.

The purpose of the experiment was to gather *quantitative* and *qualitative* data on DNAPL migration through a variably saturated homogeneous sand. The DNAPL used in the experiment is called tetrachloroethylene (PCE, a common chlorinated hydrocarbon used in the dry cleaning industry). As is detailed in

Appendix F, the data from the experiment consists of several types:

- soil and fluid properties;
- moisture retention data for the sand used in the experiment;
- experimental initial and boundary conditions;
- DNAPL influx data;
- video images of the box at various points in time showing the areal extent of the DANPL which is dyed to maximize contrast.

There are three main types of physical experimental results which are available for model validation:

1. The steady-state moisture profile (Table F.1). A comparison plot of the experimental and model moisture profile data is provided in Figure 8.9. This data represents the initial condition for the DNAPL flood.
2. The volume of PCE infiltrated as a function of time (Table F.2). The DNAPL source was applied until 200 $cm^3$ infiltrated into the aquifer. Figure 8.10 provides a comparison plot of the cumulative volume of PCE infiltrated as a function of time. In addition, with respect to the model results, we provide a volume balance check by superimposing the plots for the cumulative PCE volume which has crossed the boundary and the change in PCE volume in the domain as a function of time (for a perfect volume balance the curves would be coincident).
3. A series of video frames at specific times (e. g., Figures F.7, F.8, F.9 and F.10). Figures 8.11, 8.12, 8.13 and 8.14 provide a comparison between the experimental and model results for the times indicated. It appears that the model had the most difficulty in simulating the behavior in the vicinity of the capillary fringe where all three phases have a meaningful mobility. This indicates that the three-phase relative permeability model is missing some important information.

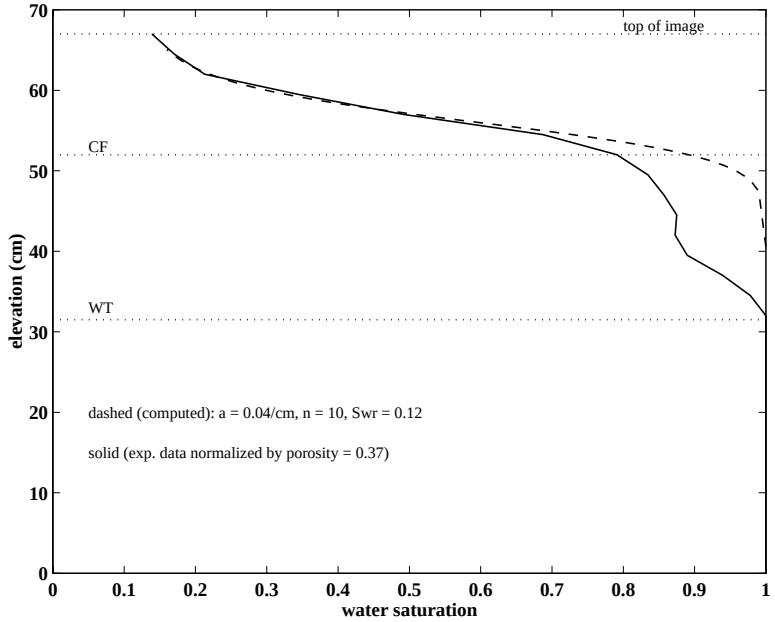


Figure 8.9: A comparison plot of the experimental and model moisture profile used as the initial condition for the DNAPL flood.

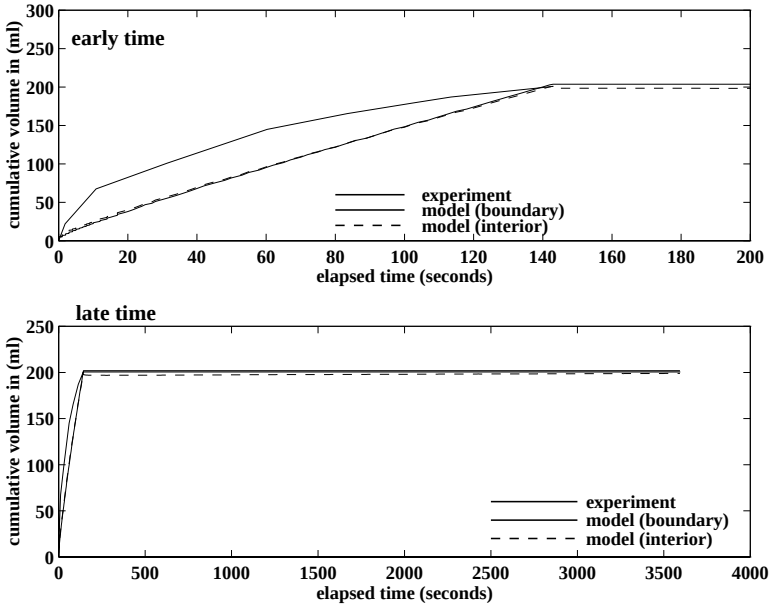


Figure 8.10: A comparison plot of the experimental and model data quantifying the cumulative volume of PCE infiltrated as a function of time. Specific to the experiment, it took 143 seconds for 200 $cm^3$ of PCE to infiltrate.

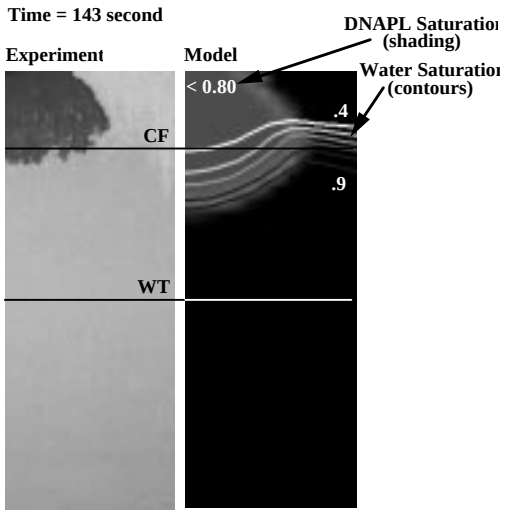


Figure 8.11: Comparison between experiment and model results at time = 143 seconds (the time when the DNAPL source was removed).

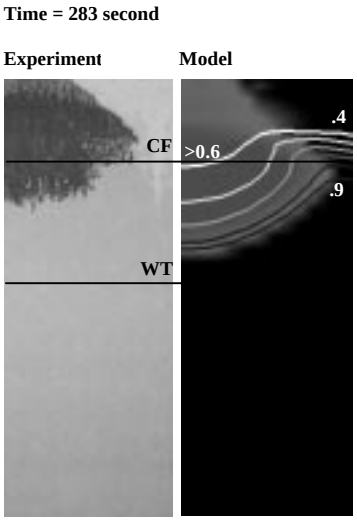


Figure 8.12: Comparison between experiment and model results at time = 283 seconds after the DNAPL source was first applied.

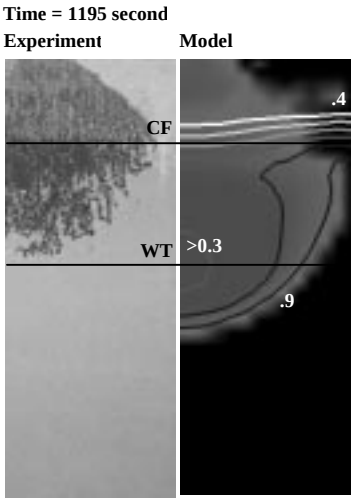


Figure 8.13: Comparison between experiment and model results at time = 1195 seconds after the DNAPL source was first applied.

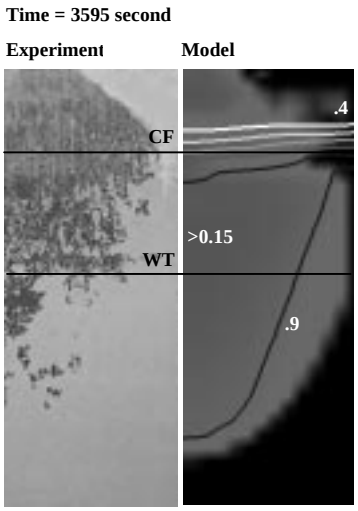


Figure 8.14: Comparison between experiment and model results at time = 3595 seconds after the DNAPL source was first applied.

### 8.2.3. DNAPL Dissolution

The mass exchange/transport portion of the simulator was verified by numerically simulating a laboratory experiment which was designed to study dissolution kinetics of residual trichloroethylene (TCE) in a uniform sand column by flushing the system with clean water and tracking the dissolution front as a function of time. Problem definition and model results can be found in Guarnaccia et al. (1992).

### 8.2.4. DNAPL Vapor Transport

Here we consider the simulation of a two-phase, water-gas, flow and contaminant transport experiment conducted by Lenhard et al. (1995). The experiment is described as follows. A one meter deep by 2 meter long by 7.5 cm wide experimental box is filled with a relatively coarse, homogeneous, sand. A water table is maintained near the bottom of the sand column with a small head differential imposed such that water flows from right to left. The experiment is set up such that the water saturation profile is initially in static equilibrium. A zone near the top center of the column is excavated, and a container filled with sand and residual TCE is placed in the void to act as the contaminant vapor source. The spatial and temporal distribution of TCE vapor concentration is measured using a regularly spaced assemblage of sampling points. Please refer to Lenhard et al. (1995) for additional detail.

The idealization of the experimental setup for simulation purposes, including the model domain dimensions and initial and boundary conditions is presented in Figure 8.15. Table 8.4 provides the relevant physical parameter data. With respect to Table 8.4, note that several simulation parameters (identified by an asterisk) had to be estimated either because the data was not reported or because the model problem setup required an augmented data set. For example, the porosity was estimated from the reported value of the soil bulk density ($\rho^b = 1.4$ $g/cm^3$), i.e., $\varepsilon \approx 1 - \rho^b/\rho^s = 1 - 1.4/2.65 = 0.47$.

With respect to the DNAPL vapor source, the authors state that the vapor concentration as a function of time is known (i.e., measured experimental data), but they did not report these data. As a result, we mimic the DNAPL vapor source by placing a volume of residual NAPL saturation in the vicinity of the experimental source (see Figure 8.15). Volatilization and dissolution of this residual saturation occurs as the result of kinetic mass transfer processes. The rate coefficients are defined in Table 8.4.

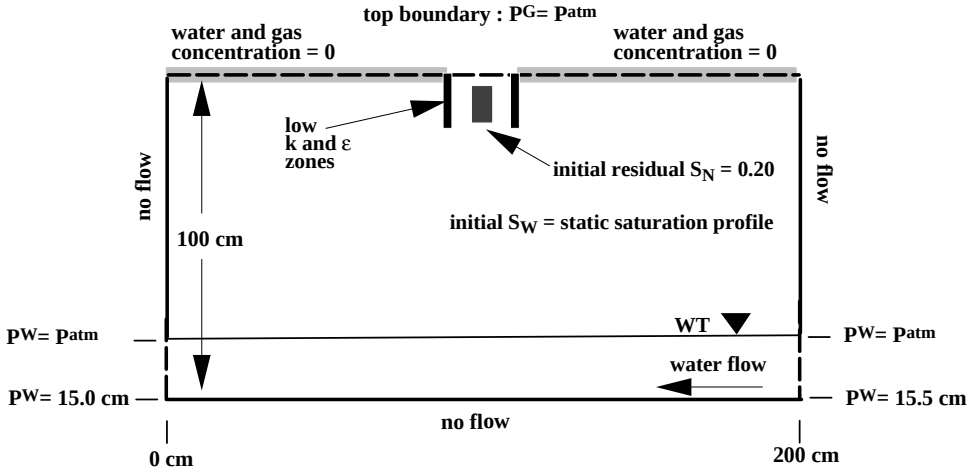


Figure 8.15: An illustration of the DNAPL vapor transport model problem domain including initial and boundary conditions.

We mimic the presence of a container with the sides impermeable and the top and bottom permeable by placing low permeability and porosity zones on either side of the source as shown in Figure 8.15.

Figure 8.16 provides a comparison plot of the experimental and model gas-phase concentration distribution after 12 hours of source loading. Because the source forcing conditions for the two simulation experiments are different, it is not surprising that only the relatively low concentration values could be matched.

## 8.3. SOFTWARE

This section describes the material available on disk. The material can be categorized into four file-types:

1. README files (documentation-like files)
2. FORTRAN source code files
3. Executable files
4. Data input files

| **Fluid properties** | | |
|---|---|---|
| $\rho^W = 0.9982\ g/cm^3$<br>$\mu^W = 0.01\ poise$<br>**S-P model definition** | $\rho^N = 0.00553\ g/cm^3$<br>$\mu^N = 0.0002\ poise$ | $\rho^G = 0.00117\ g/cm^3$<br>$\mu^G = 0.0002\ poise$ |
| $a_d = 0.156/cm$ | $a_i = 0.156/cm$ | $\eta = 4.26$ |
| $S_{Wr} = 0$ | $S_{Gr} = 0$ | $S_{Nnr} = S_{Nwr} = 0.20$ |
| $\sigma_{GW} = 72.75\ dynes/cm$ | $\sigma_{NW} = 31.74\ dynes/cm$ | $\sigma_{GN} = 47.5\ dynes/cm$ |
| **k-S model definition** | | |
| ${}^aS_{eW}$ from eq 5.25 | ${}^bS_{eW}$ from eq 5.25 | |
| ${}^aS_{eG}$ from eq 5.26 | ${}^bS_{eG}$ from eq 5.26 | |
| $\zeta = \varphi = \xi = 0.5$ | | |
| **Transport parameters** | | |
| $D_m^W = 0.00001cm^2/s$ * | $D_m^G = 0.009cm^2/s$ | |
| $\beta_1^{GN} = 1/day$ * | $\beta_1^{GW} = 1/day$ * | $\beta_1^{NW} = 0$ |
| $H = 0.236$ * | $\overline{\rho}_n^G = 0.00052\ g/cm^3$ | $\overline{\rho}_n^W = 0.0011\ g/cm^3$ |
| **Field properties** | | |
| $\varepsilon = 0.41$ * | $k = 2.1x10^{-6}cm^2$ | |

Table 8.4: PARAMETERS USED IN THE DNAPL VAPOR TRANSPORT EXPERIMENT (note, parameters with an asterisk are estimated)

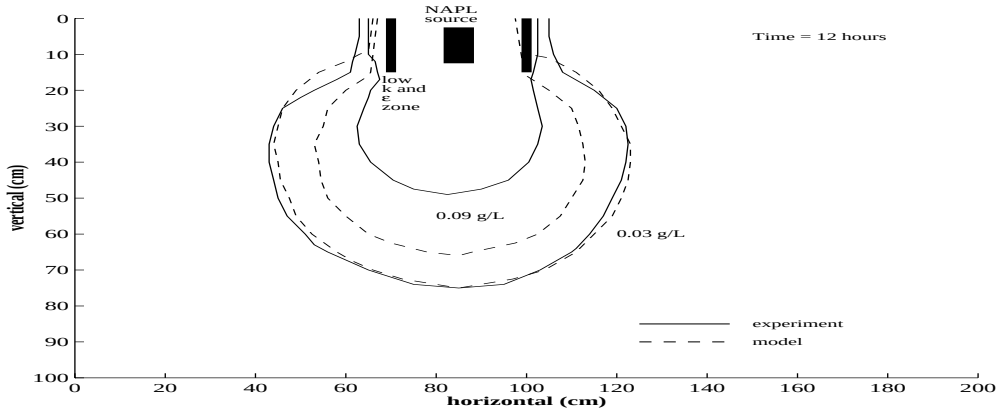


Figure 8.16: A comparison plot of the experimental (solid line) and model (dashed line) results at time = 12 hours.

The main directory (the highest level) houses an information README file and two sub-directories:

**2D** - the two-dimensional version of the simulator

**3D -** the three-dimensional version of the simulator

Each of these sub-directories house a relevant set of FORTRAN, executable, and data input files. Specifically, sub-directories **2D** and **3D** each house five sub-directories:

**For** - the FORTRAN source code files and makefile:

- **For/UNIX** - the UNIX version
- **For/Dos** - the DOS version (the makefile is set up to use the Lahey F77 compiler)

**Exe** - the executable application:

- **Exe/UNIX** - the UNIX version (compiled on the Silicon Graphics platform)
- **Exe/Dos** - the DOS version (Lahey F77 compiler)

**Ex_1** - the complete set of data input files required to run the problem described in sub-section 8.2.1.

**Ex_2** - the complete set of data input files required to run the problem described in sub-section 8.2.2:

- **Ex_2/IC** - generate the static moisture profile to be used as an initial condition for the DNAPL flood experiment.
- **Ex_2/Flood** - simulate the DNAPL flood and redistribution experiment.

**Ex_3** - the complete set of data input files required to run the problem described in sub-section 8.2.4:

- **Ex_3/IC** - generate the static moisture profile to be used as an initial condition for the DNAPL vapor transport experiment.
- **Ex_3/Force** - simulate the DNAPL vapor transport experiment.

# Bibliography


[1] Abriola, L. M., Multiphase migration of organic compounds in a porous medium, Lecture notes in engineering, number 8, Springer-Verlag, New York, 1984.

[2] Allen, M. B., Collocation simulation of multiphase porous-medium flow, SPEJ of AIME, pages 135-142, February 1983.

[3] Armstrong, J. E., E. O. Frind, and R. D. McClellan, Non-equilibrium mass transfer between the vapor, aqueous, and solid phases in unsaturated soils during vapor extraction, Water Resour. Res., 30(2), 355-368, 1994.

[4] Bear, J., Dynamics of Fluids in Porous Media, Dover Publications, Inc., New York, 764 pages, 1972.

[5] Bradford, S. A., and F. J. Leij, Fractional wettability effects on two- and three-fluid capillary pressure-saturation relations, J. Contaminant Hydrology, 20, 89-109, 1995.

[6] Bradford, S. A., and F. J. Leij, Predicting two- and three-fluid capillary pressure-saturation relationships of porous media with fractional wettability, Water Resour. Res., 32(2), 251-259, 1996.

[7] Brusseau, M. L., Transport of organic chemicals by gas advection in structured or heterogeneous porous media: Development of a model and application to column experiments, Water Resour. Res., 27(12), 3189-3199, 1991.

[8] Brusseau, M. L., Rate-limited mass transfer and transport of organic solutes in porous media that contain immobile immiscible organic liquid, Water Resour. Res., 28(1), 33-45, 1992.

[9] Demond, A. H., and P. V. Roberts, Effect of interfacial forces on two-phase capillary pressure-saturation relationships, Water Resour. Res., 27(3), 423-437, 1991.

[10] Delshad, M., G. A. Pope, and K. Sepehrnoori, A compositional simulator for modeling surfactant enhanced aquifer remediation, J. Contaminant Hydrology, accepted for publication, 1995.

[11] Dyksen, W. R., and J. R. Rice, The importance of scaling for the Hermite bicubic collocation equations, SIAM J. Sci. Stat. Comput., 7(3), 707-719, 1986.

[12] Eckberg, D. K., and D. K. Sunada, Nonsteady three-phase immiscible fluid distribution in porous media, Water Resour. Res., 20(12), 1891-1897, 1984.

[13] El-Kadi, A. I. and G. Ling, The Courant and Peclet number criteria for the numerical solution of the Richards equation, Water Resour. Res., 29(10), 3485-3494, 1993.

[14] Essaid, H. I., W. N. Herkelrath, and K. M. Hess, Simulation of fluid distributions observed at a crude oil site incorporating hysteresis, oil entrapment, and spatial variability of hydraulic properties, Water Resour. Res., 29(6), 1753-1770, 1993.

[15] Falta, R. W., I. Javandel, K. Pruess, and P. A. Witherspoon, Density-driven flow of gas in the unsaturated zone due to the evaporation of volatile organic compounds, Water Resour. Res., 25(10), 2159-2169, 1989.

[16] Falta, R. W., K. Pruess, I. Javandel, and P. A. Witherspoon, Numerical modeling of steam injection for the removal of nonaqueous phase liquids from the subsurface: 1. Numerical formulation, Water Resour. Res., 28(2), 433-449, 1992a.

[17] Falta, R. W., K. Pruess, I. Javandel, and P. A. Witherspoon, Numerical modeling of steam injection for the removal of nonaqueous phase liquids from the subsurface: 2. Code validation and application, Water Resour. Res., 28(2), 451-465, 1992b.

[18] Faust, C. F., Transport of immiscible fluids within and below the unsaturated zone: A numerical model, Water Resour. Res., 21(4), 587-596, 1985.

[19] Faust, C. F., J. H. Guswa, and J. W. Mercer, Simulation of three-dimensional flow of immiscible fluids within and below the unsaturated zone, Water Resour Res., 25(12), 2449-2464, 1989.

[20] Fayers, F. J. and J. D. Matthews, Evaluation of Normalized Stone's methods for estimating three-phase relative permeabilities, SPEJ, pages 224-232, April 1984.

[21] Ferrand, L. A., P. C. D. Milly, G. F. Pinder, and R. P. Turrin, A comparison of capillary pressure-saturation relations for drainage in two- and three-fluid porous media, Adv. Water Res., 13(2), 54-62, 1990.

[22] Forsyth, P. A., and B. Y. Shao, Numerical simulation of gas venting for NAPL site remediation, Adv. Water Res., 14, 354-367, 1991.

[23] Frind, E.O., and G.F. Pinder, A collocation finite element method for potential problems in irregular domains, Int. J. Num. Meth. Engrg., 11, 681-701, 1979.

[24] Guarnaccia, J. F., P. T. Imhoff, B. C. Missildine, M. Oostrom, M. A. Celia, J. H. Dane, and G. F. Pinder, Multiphase chemical transport in porous media, EPA Environmental Research Brief, EPA/600/S-92/002, 19 pages, 1992.

[25] Guarnaccia, J. F., G. F. Pinder, and M. Fishman, NAPL, Simulator Documentation, Final Report, EPA Cooperative Agreement No. CR-820499, 1997.

[26] Huyakorn, P. S., S. Panday, and Y. S. Wu, A three-dimensional multiphase flow model for assessing NAPL contamination in porous and fractured media, 1. Formulation, J. Contaminant Hydrology, 16, 109-130, 1994.

[27] Imhoff, P. T., P. R. Jaffe, and G. F. Pinder, An experimental study of the dissolution of trichloroethylene in saturated porous media, Princeton University Water Resources Program Report: WR-92-1, 1992.

[28] Janes, D. B., Comparison of soil-water hysteresis models, J. Hydrol., 75, 287-299, 1984.

[29] Kool, J. B., and J. C. Parker, Development and evaluation of closed form expressions for hysteretic soil hydraulic properties, Water Resour. Res., 23 (1), 105-114, 1987.

[30] Kueper, B. H., and E. O. Frind, Two-phase flow in heterogeneous porous media: 1. Model development,Water Resour. Res., 27 (6), 1049-1057, 1991.

[31] Kaluarachchi, J. J., and J. C. Parker , An efficient finite element method for modeling multiphase flow, Water Resour. Res., 25(1), 43-54, 1989.

[32] Kuppusamy, T., J. Sheng, J. C. Parker, and R. J. Lenhard, Finite-element analysis of multiphase immiscible flow through soils, Water Resour. Res., 23(4), 625-631, 1987.

[33] Lai, Y., A. Hadjidimos, E. N. Houstis, and J. R. Rice, General interior collocation methods for second-order elliptic partial differential equations, Applied Numerical Mathematics, 16, 83-200, 1994.

[34] LAPACK driver routine DGBSV, version 1.1, Univ. of Tennessee, March 1993.

[35] Land, C. S., Calculation of imbibition relative permeability for two- and three-phase flow from rock properties, Trans. Am. Inst. Min. Metall. Pet. Eng., 243, 149-156, 1968.

[36] Lenhard, R. J., and J. C. Parker, A model for hysteretic constitutive relations governing multiphase flow: 2 Permeability-saturation relations, Water Resour. Res., 23(12), 2197-2206, 1987.

[37] Lenhard, R. J., and J. C. Parker, Experimental validation of the theory of extending two-phase saturation-pressure relations to three-fluid phase systems for monotonic drainage paths, Water Resour. Res., 24(3), 373-380, 1988.

[38] Lenhard, R. J., J. H. Dane, J. C. Parker, and J. J. Kaluarachchi, Measurement and simulation of one-dimensional transient three-phase flow for monotonic liquid drainage, Water Resour. Res., 24(6), 853-863, 1988.

[39] Lenhard, R. J., J. C. Parker, and J. J. Kaluarachchi, A model for Hysteretic constitutive relations governing multiphase flow: 3. Refinements and numerical simulations, Water Resour. Res., 25(7), 1727-1736, 1989.

[40] Lenhard, R. J., J. C. Parker, and J. J. Kaluarachchi, Comparing simulated and experimental hysteretic two-phase transient fluid flow phenomena, Water Resour. Res., 27(8), 2113-2124, 1991.

[41] Lenhard, R. J., Measurement and modeling of three-phase saturation-pressure hysteresis, J. Contaminant Hydrology, 9, 243-269, 1992.

[42] Lenhard, R. J., M. Oostrom, C. S. Simmons, and M. D. White, Investigation of density-dependent gas advection of trichloroethylene: Experiment and a model validation exercise, J. Contaminant Hydrology, 19, 47-67, 1995.

[43] Leverett, M. C., Capillary behavior in porous solids, Trans. AIME, 142, 152-169, 1941.

[44] Luckner, L., M. T. van Genuchten, and D. R. Nielsen, A consistent set of parametric models for the two-phase flow of immiscible fluids in the subsurface, Water Resour. Res., 25 (10), 2187-2193, 1989.

[45] McBride, J. F., C. S. Simmons, and J. W. Cary, Interfacial spreading effects on one-dimensional organic liquid imbibition in water-wetted porous media, J. Contaminant Hydrology, 11, 1-25, 1992.

[46] Mendoza, C. A., and E. O. Frind, Advective-dispersive transport of dense organic vapors in the unsaturated zone: 1. Model development, Water Resour. Res., 26(3), 379-387, 1990.

[47] Mercer, J. W., and C. R. Faust, The application of finite-element techniques to immiscible flow in porous media, Proc., Intl, Conf. in Water Resources, Penteuch Press, London, pages 1.21-1.57, 1976.

[48] Miller, C. T., M. M. Poirier-McNeill, and A. S. Mayer, Dissolution of trapped nonaqueous phase liquids: mass transfer characteristics, Water Resour. Res., 26(11), 2783-2796, 1990.

[49] Mualem, Y., A new model for predicting the hydraulic conductivity of unsaturated porous media, Water Resources Res., 14(2), 325-334, 1978.

[50] Nielsen, D. R. and L. Luckner, Theoretical aspects to estimate reasonable initial parameters and range limits in identification procedures for soil hydraulic properties, in *Indirect Methods for Estimating the Hydraulic Properties of Unsaturated Soils*, edited by van Genuchten et al., published by the University of California, Riverside, 147-160, 1992.

[51] Parker, J. C., R. J. Lenhard, and T. Kuppusamy, A parametric model for constitutive properties governing multiphase flow in porous media, Water Resour. Res., 23(4), 618-624, 1987.

[52] Parker, J. C. and R. J. Lenhard, A model for hysteretic constitutive relations governing multiphase flow: 1 Saturation-pressure relations, Water Resour. Res., 23(12), 2187-2196, 1987.

[53] Peaceman, D. W., Fundamentals of Numerical Reservoir Simulation, Developments in Petroleum Science, 6, Elsevier, New York, 176 pages, 1977.

[54] Pinder, G. F., and L. M. Abriola, On the simulation of nonaqueous phase organic compounds in the subsurface, Water Resour. Res., 22 (9), 109s-119s, 1986.

[55] Powers, S. E., C. O. Loureiro, L. M. Abriola, and W. J. Weber, Theoretical study of the significance of nonequilibrium dissolution of nonaqueous phase liquids in subsurface systems, Water Resour. Res., 27(4), 463-477, 1991.

[56] Powers, S. E., C. O. L. M. Abriola, and W. J. Weber, An experimental investigation of NAPL dissolution in saturated subsurface systems: Steady-state mass transfer rates, Water Resour. Res., 28, 2691-2706, 1992.

[57] Rabideau, A. J., and C. T. Miller, Two-dimensional modelling of aquifer remediation influenced by sorption nonequilibrium and hydraulic conductivity heterogeneity, Water Resour. Res., 30(5), 1457-1470, 1994.

[58] SLATEC driver routine DSLUGM, Lawrence Livermore National Laboratory, Livermore, Ca., 1989.

[59] Scott, P. S., G. J. Farquhar, and N. Kouwen, Hysteretic effects on net infiltration, in Advances in Infiltration, American Society of Agricultural Engineers, 163-170, 1983. Sleep, B. E. and J. F. Sykes, Modeling the transport of volatile organics in variably saturated media, Water Resour. Res., 25(1), 81-92, 1989.

[60] Sleep, B. E., and J. F. Sykes, Modeling the transport of volatile organics in variably saturated media, Water Resour. Res., 25(1), 81-92, 1989.

[61] Sleep, B. E., and J. F. Sykes, Compositional simulation of groundwater contamination by organic compounds: 1. Model development and verification, Water Resour. Res., 29(6), 1697-1708, 1993a.

[62] Sleep, B. E. and J. F. Sykes, Compositional simulation of groundwater contamination by organic compounds: 2. Model applications, Water Resour. Res., 29(6), 1709-1718, 1993b.

[63] Sleep, B. E., A method of characteristics model for equation of state compositional simulation of organic compounds in groundwater, J. Contaminant Hydrology, 17, 189-212, 1995.

[64] Spillette, A. G., J. G. Hillestad, and H. L. Stone, A high-stability sequential solution approach to reservoir simulation, Soc. Pet. Eng. 48th Annual Meeting, Las Vegas, Nev., S.P.E. Paper No. 4542, 14 pages, 1973.

[65] van Genuchten, M. Th., A closed form equation for predicting the hydraulic conductivity of unsaturated soils, Soil Sci. Soc. of Am. J., 44, 892-898, 1980.

[66] Van Geel, P. J., and J. F. Sykes, Laboratory and model simulations of a LNAPL spill in a variably-saturated sand medium: 1. Laboratory experiment and image analysis techniques, Journal of Contaminant Hydrology, 17(1), 1-26, 1995a.

[67] Van Geel, P. J., and J. F. Sykes, Laboratory and model simulations of a LNAPL spill in a variably-saturated sand medium: 2. Comparison of laboratory and model results, Journal of Contaminant Hydrology, 17(1), 27-53, 1995b.

[68] Wilson, J. L., S. H. Conrad, W. R. Mason, W. Peplinski, and E. Hagan, Laboratory investigation of residual liquid organics from spills, leaks, and the disposal of hazardous wastes in groundwater, EPA/600/6-90/004, April 1990.

# A. PARAMETER LIST

$a_{(f)}$ - the curve shape fitting parameter for curve-type $f$

$a_d$ - the curve shape fitting parameter for water drainage curves

$a_i$ - the curve shape fitting parameter for water imbibition curves

$C_n^G$ - the NAPL-water mass transfer rate coefficient $[1/T]$

$C_n^W$ - the NAPL-water mass transfer rate coefficient $[1/T]$

$C_{n/W}^G$ - the NAPL species water-gas mass transfer rate coefficient $[1/T]$

$\mathbf{D}^G$ - the gas-phase dispersion tensor, $[L^2/T]$ (equation 4.25)

$\mathbf{D}^W$ - the water-phase dispersion tensor, $[L^2/T]$ (equation 4.25)

$e$ - the blending parameter which governs how fast the phase becomes entrapped during drainage flow conditions or released from entrapment during imbibition flow conditions ($e > 0$) [see equation 5.7]

$E_n^W$ represents *dissolution mass transfer* of the NAPL species from the NAPL phase to the water phase;

$E_{n/W}^G$ represents *volatilization mass transfer* of the NAPL species from the water phase to the gas phase;

$E_n^G$ represents *volatilization mass transfer* of the NAPL species from the NAPL phase to the gas phase;

$E_{n/W}^S$ represents *adsorption mass transfer* of the NAPL species from the water phase to the soil.

$f$ - the curve-type index, takes on a value from 1 to 6 (see Table 5.1)

$F$ - the maximum number of curve-types considered (= 6, see Table 5.1)

$f_{oc}$ - the mass fraction of organic carbon [dimensionless]

$f^{\alpha}$ - $\alpha-$phase fractional flow function (equation 6.17)

$g$ - gravity $[L/T^2]$

$H$ - Henry's law coefficient

$h_c$ - the capillary pressure head: $h_c = P_c/(\rho^W g)$

$k$ the intrinsic permeability scalar $[L^2]$

$k$ (as a superscript) - indicates the time level of parameter evaluation.

$k^*$ - the intrinsic permeability magnitude $[L^2]$ of the soil used to measure the S-P model curve fit (see equation 5.41)

$K_d$ - the distribution coefficient $[L^3/M]$ (equation 4.36)

$K_{oc}$ - the organic carbon partition coefficient [dimensionless] (equation 4.36)

$k_{r\alpha}$ - the relative permeability of the $\alpha-$phase, $\alpha$ = W, N, G [dimensionless]

$k_{rG}$ - the relative permeability of the gas-phase [dimensionless]

$k_{rN}$ - the relative permeability of the NAPL-phase [dimensionless]

$k_{rW}$ - the relative permeability of the water-phase [dimensionless]

$m = 1 - 1/\eta$ - a fitting parameter used in the $k - S - P$ model

$m$ (as a superscript) - indicates the iteration level of parameter evaluation.

$MDC$ - the main drainage curve

$MIC$ - the main imbibition curve

$PDC$ - the primary drainage curve

$PIC$ - the primary imbibition curve

$P^{\alpha}$ - pressure of the $\alpha-$phase, $\alpha$ = W, N, G $[F/L^2]$

$P_{cNW}$ - capillary pressure for the NAPL-water system $[F/L^2]$

$P_{cGN}$ capillary pressure for the gas-NAPL system $[F/L^2]$

$Q^{\alpha}$ - point sources (+) or sinks (-) of the $\alpha-$phase, $\alpha =$ W, N, G $[1/T]$

$R_{\alpha} = \left(S_{\alpha r} - S_{\alpha t}^{\min}\right)^{-1} - \left(1 - S_{\alpha t}^{\min}\right)^{-1}$

$S_e$ - the *effective wetting-phase saturation* for a given $S-P$ curve (equation 5.10)

$S_{e(f)}$ - the *effective water saturation* for a specific $S-P$ curve type $f$ (equation 5.13)

$\overline{S}_e$ - the effective saturation as computed from equation 5.13 given $h_c$ and $a_{(f)}$ (used during parameter update)

$S_{eG}$ - the *effective gas saturation* used to define the $k_{rG}$ functional (equations 5.26 and 5.28

${}^{a}S_{eG}$ - the *effective gas saturation* used to define the connectivity term of the $k_{rG}$ functional (see equation 5.23)

${}^{b}S_{eG}$ - the *effective gas saturation* used to define the integral of the $k_{rG}$ functional (see equation 5.23)

$S_{eN}$ - the *effective NAPL saturation* used to define the $k_{rN}$ functional (equations 5.30 and 5.31)

$S_{eTw}$ - the *effective total wetting-phase saturation* used to define the $k_{rN}$ functional (equations 5.32, 5.33 and 5.34)

$S_{eTn}$ - the *effective total nonwetting-phase saturation* used to define the $k_{rN}$ functional (equations 5.35, 5.36 and 5.37)

$S_{eW}$ - the *effective water saturation* used to define the $k_{rW}$ functional (equations 5.25 and 5.27)

${}^{a}S_{eW}$ - the *effective water saturation* used to define the connectivity term of the $k_{rW}$ functional (see equation 5.19)

${}^{b}S_{eW}$ - the *effective water saturation* used to define the integral of the $k_{rW}$ functional (see equation 5.19)

$S_r$ - the minimum saturation for a given $S - P$ curve

$S_{r(f)}$ - the minimum saturation for a specific $S - P$ curve type $f$

$S_s$ - the maximum for a given $S - P$ curve

$S_{s(f)}$ - the maximum saturation for a specific $S - P$ curve type $f$

$S_{Gr}$ - a fitting parameter representing the maximum residual gas-phase saturation

$S_{Nr}$ - the residual NAPL-phase saturation computed from equation 5.24

$S_{Nnr}$, a fitting parameter representing the maximum residual NAPL-phase saturation in a two-phase NAPL-water system (NAPL as a nonwetting phase)

$S_{Nwr}$, a fitting parameter representing the maximum residual NAPL-phase saturation in a two-phase NAPL-gas system (NAPL as a wetting phase)

$S_{Wr}$ - a fitting parameter representing the maximum residual water-phase saturation

$S_\alpha$ - the $\alpha-$phase saturation, $\alpha =$ W, N, G

$S_{\alpha f}$ - the $\alpha-$phase saturation which is free to flow

$S_{\alpha t}$ - the $\alpha-$phase saturation which is trapped and unable to flow

$S_{\alpha t}^{\min}$ - the lower limit of entrapped $\alpha$-phase (equation 5.8)

$S_{\alpha r}^*$ - the magnitude of the residual $\alpha$-phase, $0 \leq S_{\alpha r}^* \leq S_{\alpha r}$, at the terminus of an $\alpha$-phase drainage process (equation 5.9)

$S_\alpha^{\max}$ - the highest $\alpha$-phase saturation that has occurred since it was last at immobile residual conditions, i. e., the maximum imbibed $\alpha$-phase saturation which is available for displacement

$S_{\alpha r(j)}$ - the magnitude of the residual at the origin of a *main curve*

$S_{Gr}$ - the maximum $S_{Gt}$ value for the system

$S_{Tw}$ - total wetting phase saturation $= S_W + S_N$

$\mathbf{v}^\alpha$ - mass average $\alpha-$phase velocity vector $[L/T]$, $\alpha =$ W, N, G (equation 4.21)

$\mathbf{v}^T = \mathbf{v}^W + \mathbf{v}^N + \mathbf{v}^G$ - the total velocity

$\delta S_W = S_W^{n+1} - S_W^n$

$\beta_2$ - dimensionless fitting parameter for mass transfer

$\beta_3$ - dimensionless fitting parameter for mass transfer

$\beta_1^{WN}$ - the rate coefficient for NAPL-water mass transfer, $[1/T]$

$\beta_1^{GN}$ - the rate coefficient for NAPL-gas mass transfer, $[1/T]$

$\beta_1^{GW}$ - the rate coefficient for gas-water mass transfer, $[1/T]$

$\varsigma$ - the pore connectivity parameter for the $k_{rW}$ functional [equation 5.19]

$\varphi$ - the pore connectivity parameter for the $k_{rG}$ functional [equation 5.23]

$\xi$ - the pore connectivity parameter for the $k_{rN}$ functional [equation 5.38]

$\eta$ - a curve fitting parameter for the $S-P$ model [see equations 5.10 and 5.13]

$\varepsilon$ - porosity of the porous medium [dimensionless]

$\varepsilon^*$ - the porosity of the soil used to measure the S-P model curve fit (see equation 5.41)

$\gamma^\alpha = \rho^\alpha g$ is the specific weight of the phase $[M/T^2]$, $\alpha$ = W, N, G

$\Gamma_n^W$ - defines the change in $\rho^W$ due to the presence of NAPL species (equation 6.12)

$\Gamma_n^G$ - defines the change in $\rho^G$ due to the presence of NAPL species (equation 6.13)

$\lambda_\alpha = kk_{r\alpha}/\mu^\alpha$ ($\alpha$ = W, N, G), is the $\alpha-$phase *mobility* scalar $[L^4/FT]$

$\mu^\alpha$ -the phase viscosity $[FT/L^2]$

$\omega_n^S$ is the *mass fraction* of the adsorbed NAPL on the solid [dimensionless]

$\rho^\alpha$ - $\alpha-$phase mass density $[M/L^3]$ $\alpha$ = W, N, G

$\rho^s$ - the density of the soil $[M/L^3]$

$\rho_n^W$ - the mass concentration of NAPL in the water-phase, $[M/L^3]$

$\rho_n^G$ - the mass concentration of NAPL in the gas-phase, $[M/L^3]$

$\rho_\iota^\alpha$ - the mass concentration of a species $\iota$ in the $\alpha-$phase, $[M/L^3]$

$\overline{\rho}_n^W$ $[M/L^3]$ - the equilibrium concentration of the NAPL species in the water phase (solubility limit)

$\overline{\rho}_n^G$ $[M/L^3]$ - the constant equilibrium vapor concentration of the NAPL species in the gas-phase (vapor solubility limit)

$\widehat{\rho}_\iota^\alpha$ - the source or sink of mass for a species $\iota$ in the $\alpha$-phase $[M/L^3T]$ due to *interphase mass exchange* (i. e., dissolution, volatilization and adsorption).

$\triangle\ \gamma_{\alpha\beta} = \gamma^\alpha - \gamma^\beta$

$\sigma_{GW}$ - the interfacial tension between the gas and water phases

$\sigma_{GN}$ - the interfacial tension between the gas and the NAPL phases

$\sigma_{NW}$ - the interfacial tension between the NAPL and water phases

# B. PARTICULARS OF HERMITE COLLOCATION

This appendix contains details regarding the three-dimensional, Hermite collocation formulation.

## B.1. Nodal Degrees of Freedom

Each node has eight degrees of freedom (DF), and the vector representing the values, **U**, is numbered as:

$$\begin{array}{cccccccc} 1 & 2 & 3 & 4 & 5 & 6 & 7 & 8 \\ U & U_{,x} & U_{,y} & U_{,z} & U_{,xy} & U_{,xz} & U_{,yz} & U_{,xyz} \end{array} \tag{B.1}$$

where the subscript $[\ ,(\bullet)]$ represents the partial derivative with respect to $(\bullet)$.

## B.2. Basis Function Definition

The $C^1$ continuous Hermite cubic interpolation polynomials are defined on a general one-dimensional interval $(\xi_0, \xi_1)$ as:

$$\begin{array}{|l|} \hline \phi^0(\xi) = \begin{cases} \left(1 - \frac{\xi-\xi_0}{\xi_1-\xi_0}\right)^2 \left(1 + 2\frac{\xi-\xi_0}{\xi_1-\xi_0}\right) & \text{defined at } \xi = \xi_0 \\ \left(1 + \frac{\xi-\xi_1}{\xi_1-\xi_0}\right)^2 \left(1 - 2\frac{\xi-\xi_1}{\xi_1-\xi_0}\right) & \text{defined at } \xi = \xi_1 \end{cases} \\ \hline \phi^1(\xi) = \begin{cases} \phi_2^1(\xi) = \left(1 - \frac{\xi-\xi_0}{\xi_1-\xi_0}\right)^2 (\xi - \xi_0) & \text{defined at } \xi = \xi_0 \\ \phi_4^1(\xi) = \left(1 + \frac{\xi-\xi_1}{\xi_1-\xi_0}\right)^2 (\xi - \xi_1) & \text{defined at } \xi = \xi_1 \end{cases} \\ \hline \end{array} \tag{B.2}$$

where there are four functions defined on each one-dimensional interval (element).

The three dimensional version of the Hermite cubic can be derived from the tensor product ordering of the one-dimensional Hermite basis functions. At each of the $i$ nodes in a three-dimensional grid block, $i = 1, 2, ...8$, the following eight Hermite polynomials are defined:

$$\{\Phi(\mathbf{x})\}_i = \begin{bmatrix} \phi_i^0(x)\phi_i^0(y)\phi_i^0(z) \\ \phi_i^1(x)\phi_i^0(y)\phi_i^0(z) \\ \phi_i^0(x)\phi_i^1(y)\phi_i^0(z) \\ \phi_i^0(x)\phi_i^0(y)\phi^1(z) \\ \phi_i^1(x)\phi_i^1(y)\phi_i^0(z) \\ \phi_i^1(x)\phi_i^0(y)\phi_i^1(z) \\ \phi_i^0(x)\phi_i^1(y)\phi_i^1(z) \\ \phi_i^1(x)\phi_i^1(y)\phi_i^1(z) \end{bmatrix}$$

where the ordering is consistent with the degree of freedom ordering in B.1.

## B.3. Hermite Interpolation of Capillary Pressure

Given capillary pressure as a function of saturation, and saturation interpolated by Hermite cubics, then the Hermite cubic interpolation coefficients of $P_c(S)$ are generated using the chain rule, i. e.,

$$\begin{array}{cccccccc} 1 & 2 & 3 & 4 & 5 & 6 & 7 & 8 \\ P_c(S) & P_c^{'}S_{,x} & P_c^{'}S_{,y} & P_c^{'}S_{,z} & P_c^{'}S_{,xy} & P_c^{'}S_{,xz} & P_c^{'}S_{,yz} & P_c^{'}S_{,xyz} \end{array}$$

where $P_c^{'} = dP_c/dS$, and terms 5 through 8 have been simplified by assuming the chained terms which include the derivatives $d^2P_c/dS^2$ and $d^3P_c/dS^3$ are small compared to the other terms and can thus be neglected.

## B.4. Boundary Condition Specification

The set of DF's which are specified at a boundary node is defined as a function of: node-type and boundary condition-type. There are three boundary-node-types to be considered:

| node-type | number of DF specified | number of DF free |
|---|---|---|
| midside (on a plane) | 4 | 4 |
| edge (intersection of two planes = line) | 6 | 2 |
| corner (intersection of three planes = point) | 7 | 1 |

The following lists the DF's (referenced by the nodal degree of freedom numbering system shown in B.1) that are specified for each node-type and boundary condition-type (Dirichlet or Neumann).

Midside Nodes (lie in a plane) - The DF's specified depend on the plane and the boundary condition imposed:

| | x-y plane | y-z plane | x-z plane |
|---|---|---|---|
| Dirichlet | 1, 2, 3, 5 | 1, 3, 4, 7 | 1, 2, 4, 6 |
| Neumann | 4, 6, 7, 8 | 2, 5, 6, 8 | 3, 5, 7, 8 |

Edge Nodes (lie along a line) - The DF's specified depend on what boundary condition is imposed on each intersecting plane:

- When the edge is parallel to the x-axis (intersection of the x-y and x-z planes):

| | Dirichlet on x-y side | Neumann on x-y side |
|---|---|---|
| Dirichlet on x-z side | 1, 2, 3, 4, 5, 6 | 1, 2, 4, 6, 7, 8 |
| Neumann on x-z side | 1, 2, 3, 5, 7, 8 | 3, 4, 5, 6, 7, 8 |

- When the edge is parallel to the y-axis (intersection of the x-y and y-z planes):

| | Dirichlet on x-y side | Neumann on x-y side |
|---|---|---|
| Dirichlet on y-z side | 1, 2, 3, 4, 5, 7 | 1, 3, 4, 6, 7, 8 |
| Neumann on y-z side | 1, 2, 3, 5, 6, 8 | 2, 4, 5, 6, 7, 8 |

- When the edge is parallel to the z-axis (intersection of the x-z and y-z planes):

| | Dirichlet on x-z side | Neumann on x-z side |
|---|---|---|
| Dirichlet on y-z side | 1, 2, 3, 4, 6, 7 | 1, 3, 4, 5, 7, 8 |
| Neumann on y-z side | 1, 2, 4, 5, 6, 8 | 2, 3, 5, 6, 7, 8 |

Corner Nodes - The DF's specified depend on what boundary condition is imposed on each intersecting plane. There are 8 combinations:

Dirichlet on x-y, Dirichlet on x-z, Dirichlet on y-z: 1, 2, 3, 4, 5, 6, 7

Neumann on x-y, Dirichlet on x-z, Dirichlet on y-z: 1, 2, 3, 4, 6, 7, 8

Dirichlet on x-y, Neumann on x-z, Dirichlet on y-z: 1, 2, 3, 4, 5, 7, 8

Dirichlet on x-y, Dirichlet on x-z, Neumann on y-z: 1, 2, 3, 4, 5, 6, 8

Neumann on x-y, Neumann on x-z, Dirichlet on y-z: 1, 3, 4, 5, 6, 7, 8

Neumann on x-y, Dirichlet on x-z, Neumann on y-z: 1, 2, 4, 5, 6, 7, 8

Neumann on x-y, Dirichlet on x-z, Neumann on y-z: 1, 2, 3, 5, 6, 7, 8

Neumann on x-y, Neumann on x-z, Neumann on y-z: 2, 3, 4, 5, 6, 7, 8

# C. INITIALIZE TRAPPING PARAMETERS

Given the initial phase saturation distribution, $S_{W0}, S_{N0}$ and $S_{G0}$, this is the decision tree which determines the initial phase trapping parameters.

- if $S_{N0} = 0$

$S_{Nt} = 0$

if $(S_{G0} \leq S_{Gr})$ (gas is at residual)

$S_{Gt} = S_{G0}$, $S_{Wt} = 0$, and $f = 1$ for both $S - P$ functionals

else if $(S_{W0} \leq S_{Wr})$ (water is at residual)

$S_{Wt} = S_{W0}$, $S_{Gt} = 0$, and $f = 2$ for both $S - P$ functionals

else (both phases are mobile)

$S_{Wt}$ from equation 5.7, $S_{Gt} = 0$, and $f = 1$ for both $S - P$ functionals

endif

- else if $S_{G0} = 0$

$S_{Gt} = 0$, and $f = 1$ for $S_{Tw}(P_{cGN})$ functional

if $(S_{N0} \leq S_{Nnr})$ (NAPL is at residual)

$S_{Nt} = S_{N0}$, $S_{Wt} = 0$, and $f = 1$ for $S_W(P_{cNW})$ functional

else if $(S_{W0} \leq S_{Wr})$ (water is at residual)

$S_{Wt} = S_{W0}$, $S_{Nt} = 0$, and $f = 2$ for $S_W(P_{cNW})$ functional

else (both phases are mobile)

$S_{Wt}$ from equation 5.7, $S_{Nt} = 0$, and $f = 1$ for $S_W(P_{cNW})$ functional

endif

- else if $S_{N0} > 0$ and $S_{G0} > 0$

if $(S_{G0} \leq S_{Gr})$ (gas is at residual)

$S_{Gt} = S_{G0}$, and $f = 1$ for $S_{Tw}(P_{cGN})$ functional
if $(S_{N0} \leq S_{Nnr})$ (NAPL is at residual)
$S_{Nt} = S_{N0}$, $S_{Wt} = 0$, and $f = 1$ for $S_W(P_{cNW})$ functional
else if $(S_{W0} \leq S_{Wr})$ (water is at residual)
$S_{Wt} = S_{W0}$, $S_{Nt} = 0$, and $f = 2$ for $S_W(P_{cNW})$ functional
else (both water and NAPL phases are mobile)
$S_{Wt}$ from equation 5.7, $S_{Nt} = 0$, and $f = 1$ for $S_W(P_{cNW})$ functional
endif

else if $(S_{W0} \leq S_{Wr})$ (water is at residual)

$S_{Wt} = S_{W0}$ and $f = 2$ for $S_W(P_{cNW})$ functional
if $(S_{N0} \leq S_{Nwr})$ (NAPL is at residual)
$S_{Nt} = S_{N0}$, $S_{Gt} = 0$, and $f = 2$ for $S_{Tw}(P_{cGN})$ functional
else (both gas and NAPL phases are mobile)
$S_{Gt}$ from equation 5.7, $S_{Nt} = 0$, and $f = 2$ for $S_{Tw}(P_{cGN})$ functional
endif

else (mobile water and gas after full drainage and imbibition cycles)

$S_{Wt} = S_{Wr}$ and $S_{Gt} = S_{Gr}$
if $(S_{N0} \leq S_{Nnr} + S_{Nwr})$ (NAPL is at residual)
$S_{Nt}$ from equation 5.24

else (NAPL is mobile)

$S_{Nt} = 0$

endif

endif

- endif

# D. PECLET CONSTRAINT

To derive the expressions for grid Peclet number, equations 6.35 and 6.36 must be written in terms of the dependent variables $S_W$ and $S_{Tw}$ by using the chain rule for differentiation:

$$
\begin{aligned}
&\varepsilon\frac{\partial S_W}{\partial t} \\
&+\left(\mathbf{q}^T(f^W)_{,W}+\left[(f^W\lambda_N)_{,W}\ \triangle\ \gamma_{WN}+(f^W\lambda_G)_{,W}\ \triangle\ \gamma_{WG}\right]\nabla z\right)\bullet\nabla S_W \\
&+\left(\mathbf{q}^T(f^W)_{,Tw}+\left[(f^W\lambda_N)_{,Tw}\ \triangle\ \gamma_{WN}+(f^W\lambda_G)_{,Tw}\ \triangle\ \gamma_{WG}\right]\nabla z\right)\bullet\nabla S_{Tw} \\
&+\nabla\bullet\left\{\left[\Lambda_{WN}\left(f^W\lambda_N\right)(P_{cNW})_{,W}+\Lambda_{WG}\left(f^W\lambda_G\right)(P_{cGW})_{,W}\right]\nabla S_W\right\} \\
&+\nabla\bullet\left\{\left[\Lambda_{WG}\left(f^W\lambda_G\right)(P_{cGW})_{,Tw}\right]\nabla S_{Tw}\right\} \\
&=-f^W\nabla\bullet\mathbf{q}^T
\end{aligned}
\tag{D.1}
$$

$$
\begin{aligned}
&-\varepsilon\frac{\partial S_{Tw}}{\partial t} \\
&+\left(\mathbf{q}^T(f^G)_{,W}+\left[(f^G\lambda_N)_{,W}\ \triangle\ \gamma_{NG}+(f^G\lambda_W)_{,W}\ \triangle\ \gamma_{WG}\right]\nabla z\right)\bullet\nabla S_W \\
&+\left(\mathbf{q}^T(f^G)_{,Tw}+\left[(f^G\lambda_N)_{,Tw}\ \triangle\ \gamma_{NG}+(f^G\lambda_W)_{,Tw}\ \triangle\ \gamma_{WG}\right]\nabla z\right)\bullet\nabla S_{Tw} \\
&+\nabla\bullet\left\{\left[\Lambda_{WG}\left(f^G\lambda_W\right)(P_{cGW})_{,W}\right]\nabla S_W\right\} \\
&+\nabla\bullet\left\{\left[\Lambda_{NG}\left(f^G\lambda_N\right)(P_{cGN})_{,Tw}+\Lambda_{WG}\left(f^G\lambda_W\right)(P_{cGW})_{,Tw}\right]\nabla S_{Tw}\right\} \\
&=-f^G\nabla\bullet\mathbf{q}^T
\end{aligned}
\tag{D.2}
$$

where the subscripts $(,W)$ and $(,Tw)$ represent the partial derivative of the function with respect to $S_W$ and $S_{Tw}$, respectively, and the fractional flow derivatives are defined as:

$$
\begin{aligned}
(f^W)_{,W}&=\tfrac{(\lambda_W)_{,W}-f^W(\lambda_T)_{,W}}{\lambda_T} & (f^W)_{,Tw}&=-\tfrac{f^W(\lambda_T)_{,Tw}}{\lambda_T} \\
(f^N)_{,W}&=\tfrac{(\lambda_N)_{,W}-f^N(\lambda_T)_{,W}}{\lambda_T} & (f^N)_{,Tw}&=\tfrac{(\lambda_N)_{,Tw}-f^N(\lambda_T)_{,Tw}}{\lambda_T} \\
(f^G)_{,W}&=-\tfrac{f^G(\lambda_T)_{,W}}{\lambda_T} & (f^G)_{,Tw}&=\tfrac{(\lambda_G)_{,Tw}-f^G(\lambda_T)_{,Tw}}{\lambda_T}
\end{aligned}
\tag{D.3}
$$

and

$$
\begin{aligned}
&(f^W\lambda_N)_{,W} = f^W(\lambda_N)_{,W} + f^N(\lambda_W)_{,W} - f^W f^N(\lambda_T)_{,W}\\
&(f^W\lambda_N)_{,Tw} = f^W(\lambda_N)_{,Tw} - f^W f^N(\lambda_T)_{,Tw}\\
&(f^G\lambda_N)_{,W} = f^G(\lambda_N)_{,W} - f^G f^N(\lambda_T)_{,W}\\
&(f^G\lambda_N)_{,Tw} = f^G(\lambda_N)_{,Tw} + f^N(\lambda_G)_{,Tw} - f^G f^N(\lambda_T)_{,Tw}\\
&(f^W\lambda_G)_{,W} = (f^G\lambda_W)_{,W} = f^G(\lambda_W)_{,W} - f^G f^W(\lambda_T)_{,W}\\
&(f^W\lambda_G)_{,Tw} = (f^G\lambda_W)_{,Tw} = f^W(\lambda_G)_{,Tw} - f^G f^W(\lambda_T)_{,Tw}\\
&(\lambda_T)_{,W} = (\lambda_W)_{,W} + (\lambda_N)_{,W}\\
&(\lambda_T)_{,W} = (\lambda_G)_{,Tw} + (\lambda_N)_{,Tw}
\end{aligned}
$$

The derivative definitions (D.3) are chosen such that:

$$(f^W)_{,\alpha} + (f^N)_{,\alpha} + (f^W)_{,\alpha} = 0 \ , \quad \alpha = W, Tw$$

which is necessary in order that equations D.1 and D.2 sum to the NAPL balance equation. In addition the derivatives are evaluated using numerical differentiation, e. g.,

$$(f^\alpha)_{,\beta} \approx \frac{f^\alpha(S_\beta) - f^\alpha(S_\beta + \epsilon)}{\epsilon}$$

where $\epsilon$ is a small positive number of order $10^{-6}$.

Finally, the terms $(P_{cGW})_{,W}$ and $(P_{cGW})_{,Tw}$ are computed from equation 4.14 as:

$$
\begin{aligned}
(P_{cGW})_{,W} &\cong \left(\frac{\sigma_{GW}}{\sigma_{NW}}\right)(P_{cNW})_{,W}\\
(P_{cGW})_{,Tw} &\cong \left(\frac{\sigma_{GW}}{\sigma_{GN}}\right)(P_{cGN})_{,Tw}
\end{aligned}
$$

# E. SOURCE FILE DESCRIPTION

The following provides a list of the FORTRAN program routines which make up the simulator and a brief description of what each routine does. Programs are listed in alphabetical order

BASIS.F: Set up arrays for Hermite and Lagrange basis functions evaluated at local orthogonal collocation points.

Subroutine BASIS_3D: 3-D Hermite and Lagrange basis functions.

Subroutine BASIS_2D: 2-D Hermite and Lagrange basis functions.

BCSET.F - Set up boundary conditions.

Subroutine BCSET: Set up default Neumann conditions for all dependent variables.

Subroutine BC_FLOW: Set up Dirichlet conditions for phase flow equations.

Subroutine BC_OA: Set up Dirichlet conditions for dissolved NAPL species contaminant transport equations.

Subroutine BC_OG: Set up Dirichlet conditions for NAPL vapor species contaminant transport equations.

Subroutine BC_UP: Update nonlinear boundary conditions after each time step.

Subroutine PR_BC: Set flux terms for gas and NAPL pressure conditions after total flow solution.

Subroutine PR_SAVE: for flow boundary conditions 2 and 3 save the $P^G$ and $P^N$ values at the beginning of each time step.

Subroutine NO_FLOW: For no flow boundary nodes, set the $S - P$ curve slope to a high value to mimic a linear no flow condition.

DIRECT_SOLVE.F The LAPACK library routine dgbsv.f (LU with partial pivoting)

DSLUGM.F The SLATEC library routine of the same name (incomplete LU preconditioned GMRES)

EQ_NUMBER.F Number the non-boundary data degrees of freedom for each dependent variable (column of the system matrix)

- Subroutine DF_NUM_P: Degree of freedom numbering for $P^W$
- Subroutine DF_NUM_S: Degree of freedom numbering for $S_W$ and $S_{Tw}$
- Subroutine DF_NUM_T: Degree of freedom numbering for the NAPL species.
- Subroutine NUMBER: Set the number for the degrees of freedom.

EXCHANGE.F Compute the mass exchange terms for the water and gas phases.

- Subroutine EXCH_W: exchange terms for the water-phase
- Subroutine EXCH_G: exchange terms for the gas-phase

FUNCTIONS.F Set nodal values of all functions of the dependent variables

- Subroutine FLOW_FUN Set nodal values of all functions of saturation
- Subroutine WATER_PROP Compute water-phase properties based on composition.
- Subroutine GAS_PROP Compute gas-phase properties based on composition.
- Subroutine FUN_AT_N Set nodal values of all functions dated at the current time level.
- Subroutine VEL_W Compute the nodal values of water velocity for the transport equation
- Subroutine VEL_G Compute the nodal values of water velocity for the transport equation
- Subroutine VEL_N Compute the nodal values of NAPL velocity for mass balance and output

Subroutine V_TOT Compute the nodal values of total velocity for the saturation equations

Subroutine DISP_W Compute the dispersion tensor for the water transport equation

Subroutine DISP_G Compute the dispersion tensor for the gas transport equation

Subroutine DFDS3 Compute the terms which make up the Peclet and Courant constraints.

HYST.F Set nodal values of all the hysteresis variables

Subroutine HYST_IC Initialize hysteresis variables

Subroutine TRAP_UP Update nodal values of trapping variables

Subroutine SW_PC Update nodal values defining $S_W(P_{cNW})$ functionals

Subroutine ST_PC Update nodal values defining $S_{Tw}(P_{cGN})$ functionals

ICSET.F: Set up initial conditions for the simulation.

Subroutine ICSET Set the global initial conditions for all the variables.

Subroutine IC_SAT Set the node-specific initial conditions for the saturation variables.

Subroutine IC_ROA Set the node-specific initial conditions for the dissolved NAPL species variables.

Subroutine IC_ROG Set the node-specific initial conditions for the NAPL vapor species variables.

INCLUDE.F: Account for all parameter definition, array dimensioning, and common block definition.

MAIN.F: Driver program taking care of I/O for the simulator.

MBAL.F: Mass balance computations.

Subroutine MBAL Determine mass in the system based on Gauss quadrature integration of the solution.

Subroutine MBALB Determine the mass in and out of the system along the boundaries of the domain.

Subroutine PORE_VOL Compute the pore-volume of the domain.

PE_CO.F Compute the Peclet and Courant constraints.

Subroutine MP_DIFF Compute the Peclet and Courant constraints.

Subroutine DT_CNTRL Time step control.

POINT_SOURCE.F: Definition of source and sink terms.

Subroutine PT_SRCE: Read from input file and set initial nodal point source/sink data

Subroutine QOUT: For outflow wells, distribute the rate between phases based on the saturation solution at the node where the well is idealized.

Subroutine QOUT_ADJ: For outflow wells defined from case 2 and 3 flow boundary conditions. Distribute the rate between phases based on the saturation solution at the node where the well is idealized.

Subroutine WELL_MASS: Compute contribution to mass balance from point source/sink data

POINTER.F Generates pointer vectors to map between default numbering and shortest-direction- first numbering

Subroutine POINT Set the pointer arrays

Subroutine RELEM Generate element index list

PW_SOL.F: Driver for the total flow equation solution algorithm.

RESTART.F: Setup to restart the time step because of non-convergence

SAT_SOL.F: Driver for the saturation equation solution algorithm.

Subroutine SAT_SOL: Takes care of I/O for saturation solution and computes convergence

Subroutine SW_SOL: Driver for the $S_W$ equation solution algorithm

Subroutine ST_SOL: Driver for the $S_{Tw}$ equation solution algorithm

SATPAR.F: Compute the functions of saturation: capillary pressure and relative permeability

Subroutine PC_GN: Compute the $S_W(P_{cNW})$ functional.

Subroutine PC_NW: Compute the $S_{Tw}(P_{cGN})$ functional.

Subroutine SFUNKW: Compute the $k_{rW}(S_W)$ functional

Subroutine SFUNKN: Compute the $k_{rN}(S_W, S_G)$ functional

Subroutine SFUNKG: Compute the $k_{rG}(S_G)$ functional

Subroutine LEV_SW_P: Interfacial tension scaling.

Subroutine LEV_ST_P: Interfacial tension scaling.

SYS_OA.F Set up and solve system of equations for the dissolved NAPL species contaminant transport equation.

Subroutine SYS_OA_I: Version for iterative solver.

Subroutine SYS_OA_D: Version for direct solver.

SYS_OG.F Set up and solve system of equations for the NAPL vapor species contaminant transport equation.

Subroutine SYS_OG_I: Version for the iterative solver.

Subroutine SYS_OG_D: Version for the direct solver.

SYSTEM_G.F Set up and solve the system of equations for the linearized $S_{Tw}$ equation.

Subroutine SYSTEM_GI: Version for the iterative solver.

Subroutine SYSTEM_GD: Version for the direct solver.

SYSTEM_P.F Set up and solve the system of equations for the total flow equation.

Subroutine SYSTEM_PI: Version for the iterative solver.

Subroutine SYSTEM_PD: Version for the direct solver.

SYSTEM_W.F Set up and solve the system of equations for the linearized $S_W$ equation.

Subroutine SYSTEM_WI: Version for the iterative solver.

Subroutine SYSTEM_WD: Version for the direct solver.

TRAN_SOL.F: Driver for the contaminant transport equation solution algorithm.

Subroutine TRAN_SOL: Takes care of I/O for the transport solution and computes convergence

Subroutine ROA_SOL: Driver for the $\rho_n^W$ equation solution algorithm

Subroutine ROG_SOL: Driver for the $\rho_n^G$ equation solution algorithm

WRITE_OUT.F Takes care of most file I/O

Subroutine READ_RS: Read restart files

Subroutine WRITE_RS: Write restart files

Subroutine PRINT: Write to files *.out

Subroutine GRAPH: Write to files for animated graphical display

Subroutine JAQ_SET: Write grid and soil definition for animated graphical display

Subroutine ECHO: Echo data input to file echo.out

# F. NAPL PROJECT

## F.1. Purpose

The purpose of this project is to:

1. build and calibrate a simulation model which approximates the transient behavior of a two-dimensional, three-phase DNAPL flood experiment;
2. obtain a sense of how certain physical parameters affect the solution;
3. obtain a sense of how discretization errors affect the solution.

In addition, the analysis thus conducted can be used to verify whether the mathematical representation of three-phase flow through porous media that is used in the simulator represents reality. In other words, is the simulator a surrogate for reality or are there aspects of the mathematical interpretation of the physics which are either erroneous or simply incomplete?

## F.2. Scope

An artificial aquifer experiment was conducted by Mikhail Fishman at the EPA's Subsurface Protection and Remediation Division of the National Risk Management Research Laboratory in Ada, OK (formerly RSKERL) to gather *quantitative* and *qualitative* data on DNAPL migration through a variably saturated homogeneous sand. The DNAPL used in the experiment is called tetrachloroethylene (PCE, a common chlorinated hydrocarbon used in the dry cleaning industry). As will be detailed in subsection F.3, the data from the experiment consists of several types:

- soil and fluid properties;
- moisture retention data for the sand used in the experiment;

- experimental initial and boundary conditions;
- DNAPL influx data;
- video images of the box at various points in time showing the areal extent of the DANPL which is dyed to maximize contrast.

At this point it may be clear that this information represents only a subset of that required to model the experiment. Thus, part of this project is to identify the data requirements for the model, to generate a cause and effect relationship between specific parameters and simulation results, and to quantify the physical limits of specific parameters.

The overall project has been separated into a series of Tasks, with each subsequent Task using information generated from the previous one. Each Task highlights an important aspect of model development, and leads the user in a sequential manner to developing the full three-phase model. The Tasks are summarized as follows:

**Task 1** Define the $S-P$ model fitting parameters $a_d, \eta$ and $S_{Wi}$.

**Task 2** Define appropriate model discretizations (i. e., node spacing and time step). Identify and quantify those input parameters which are used to ensure compatibility between the physical and the discrete problems.

**Task 3** Set up the two-dimensional model for the DNAPL flood. Define appropriate boundary conditions. Identify a subset of input parameters which can be used to fit the model to the experimental data. Estimate a physical range of acceptable values for these data, and qualify how the solution should respond to a change in a particular parameter or set of parameters. Identify how the experimental data can be used to calibrate the model.

**Task 4** Model the experiment and calibrate the model.

## F.3. Experimental Setup and Data Base

A photograph of the actual experimental apparatus is provided in Figure F.1, and an idealization showing dimensions is provided in Figure F.2. The inside dimensions of the box (defining the volume of the sand) are 67 cm deep, 49 cm wide, and 2 cm thick. The top boundary is open to the atmosphere and the bottom

boundary is impermeable. The vertical sides are constructed such that water can flow across the boundary but not air. A constant phreatic surface is defined by specifying appropriate water source/sink ports along the vertical sides. The box is filled with a uniform medium-grained sand in a manner which is assumed to result in a homogeneous, isotropic porous medium. The soil properties are reported to be:

| | |
|---|---|
| permeability | $3.5x10^{-7}cm^2$ |
| porosity | 0.37 |

The sand-filled box is imbibed with water to the top and allowed to equilibrate to create an initial condition where the system is in static equilibrium and $S_W = 1$ throughout. The following fluid properties are provided:

| | water | NAPL | gas |
|---|---|---|---|
| density $(g/cm^3)$ | 1.0 | 1.626 | 0.00129 |
| viscosity $(p)$ | 0.01 | 0.0093 | 0.0002 |

| | | | |
|---|---|---|---|
| interfacial tension $(dynes/cm)$ | $\sigma_{NW} = 39.5$ | $\sigma_{GN} = 31.74$ | $\sigma_{GW} = 72.75$ |

From this initial condition, three sequential displacement experiments are run:

1. The phreatic surface is lowered to elevation 35.5 cm from the top of the box and, the system is allowed to return to equilibrium conditions. The data reported which defines the moisture content as a function of depth is given in Table F.1.

2. Given the initial condition from Part 1, the PCE source is applied as shown in Figure F.2. That is, a 0.5 cm head of PCE is applied uniformly over a 10 $cm^2$ surface at the center/top of the box until 200 $cm^3$ enters the domain. Note that for the experiment this took 143 seconds. For this forcing condition, Table F.2 provides the data which relates the cumulative volume of PCE entering the domain to the elapsed time. Other information qualifying this phase of the experiment is a series of video images of the front face of the box similar to the one shown in Figure F.1. Video images are available for the following times (elapsed time in seconds since the DNAPL was applied: 5, 14, 62, 143.

3. Given the initial condition from Part 2, that is, the data at time = 143s, the PCE source is removed and the system is allowed to return to equilibrium for a period of 3452 seconds (total elapsed time since the DNAPL was applied is

| **depth from top (cm)** | **moisture content** |
|---|---|
| 0 | .0514 |
| 2.5 | .063 |
| 5 | .0788 |
| 7.5 | .1273 |
| 10 | .1822 |
| 12.5 | .2543 |
| 15 | .2927 |
| 17.5 | .3088 |
| 20 | .3171 |
| 22.5 | .3237 |
| 25 | .3229 |
| 27.5 | .3292 |
| 30 | .3476 |
| 32.5 | .3619 |
| 35 | .37 |
| 67 | .37 |

Table F.1: EXPERIMENTAL DATA - MOISTURE CONTENT AS A FUNCTION OF DEPTH

| **ELAPSED TIME (s)** | **CUMULATIVE VOLUME IN ($cm^3$)** |
|---|---|
| 0 | 0 |
| 1.88 | 22.0 |
| 10.84 | 67.5 |
| 23.12 | 87.5 |
| 31.41 | 101.0 |
| 60.29 | 145.0 |
| 83.47 | 165.5 |
| 102.72 | 179.5 |
| 113.41 | 187.0 |
| 143.0 | 200.0 |
| $> 143.0$ | 200.0 |

Table F.2: EXPERIMENTAL DATA - PCE VOLUME ENTERING THE DOMAIN AS A FUNCTION OF TIME

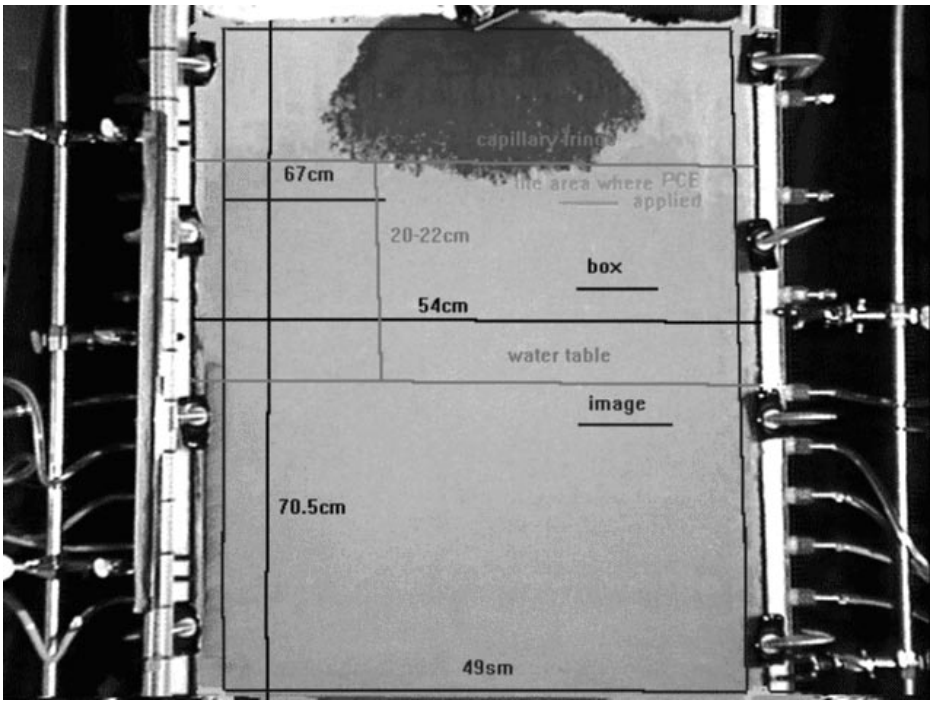


Figure F.1: Photo of the experimental apparatus just after the PCE was removed, showing dimensions and vertical constant head boundaries. The PCE (dark grey) has been dyed red to maximize contrast.

3595 seconds) . Information qualifying this phase of the experiment consists of a series of video images for the following times (elapsed time in seconds since the DNAPL was applied: 285, 185, 1195, 1795, 3595.

## F.4. TASK 1

### F.4.1. Purpose

Given the initial static moisture profile as defined in Table F.1, determine the appropriate $S-P$ model parameters: $a_d, \eta, S_{Wi}$. That is, fit the van Genuchten $S-P$ model (equation 5.10) to the experimental data.

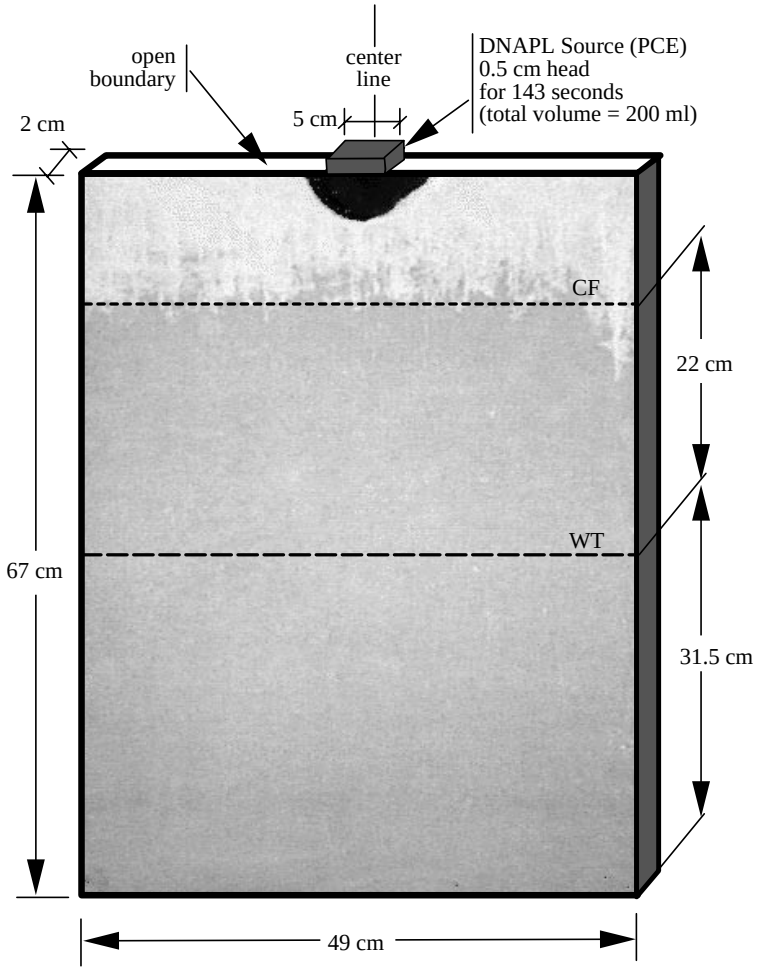


Figure F.2: Idealization of the experimental setup superimposed on a video image of the box (5 seconds after the PCE source was applied).

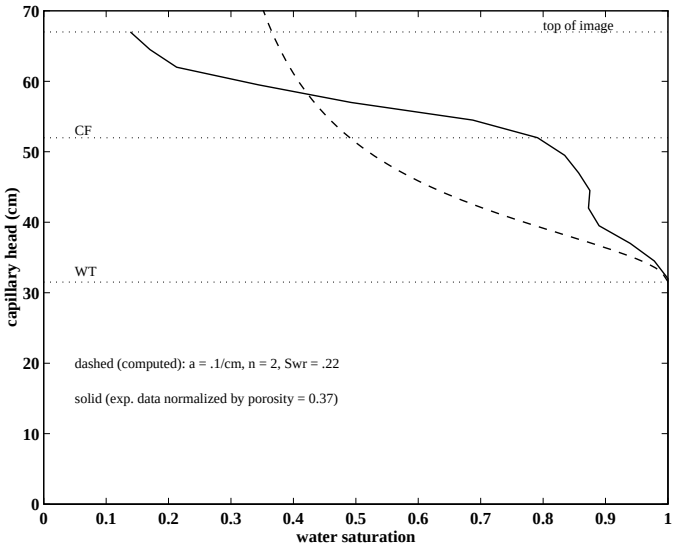


Figure F.3: Plot of the initial static saturation profile. The computed curve is fit to the experimental data by altering the S-P model curve fitting parameters.

### F.4.2. Procedure

Use a trial-and-error sequential approach wherein you systematically vary the parameters $a_d, \eta$, and $S_{Wi}$ until a qualitatively "good" fit is obtained. Equation 5.10 is used because the experiment represents a uni-directional displacement process.

For each parameter set chosen, superimpose the plots of equation 5.10 and the data from Table F.1. An example of such a plot is provided in Figure F.3.

This is a heuristic analysis, that is, you should try to fit the model to the data by iteratively choosing different parameter sets and "eye-balling" the fit. Given some knowledge of how the model is affected by the three parameters, your analysis should converge quickly. In addition, please note that there is no 'correct' answer, and that this data represents only a piece of the calibration puzzle. Therefore, it behooves you to generate a suite of parameter sets which give a good fit so that you can make more meaningful decisions when trying to fit the model to the three-phase flow problem.

### F.4.3. Results

In addition to providing a plot of the fitted data, please answer the following questions:

1. What type of $S - P$ curve is defined by this data?
2. From a qualitative perspective, how is the $S - P$ curve affected by the parameters $a_d$ and $\eta$?
3. What are the ranges of the values of $a_d$, $\eta$ and $S_{Wi}$ which provide a qualitatively good fit?
4. What data points are worth fitting and why?
5. What can you say about the grain- and pore-size distribution of the sand?

## F.5. TASK 2

### F.5.1. Purpose

From Task 1 you have generated the parameters which define the primary drainage curve for the soil. This curve can be used to define the resolution length-scale that must be used to simulate the experiment. Specifically, this moisture retention curve represents the characteristic shape of the interface between two fluids in static equilibrium, and it is the result of the balance between gravity and capillary forces. The node spacing must be chosen such that the front can be resolved by the interpolation functions.

In addition to defining an appropriate spatial discretization, an appropriate dynamic time stepping scheme must be designed which balances efficiency (the fewest number of total iterations) and accuracy (minimize time truncation error and solution instabilities).

### F.5.2. Procedure

Use the simulator to model the first displacement experiment as described in subsection F.3. Since this is effectively (and theoretically) a one-dimensional two-phase displacement experiment, you can get the most information bang for the computational buck by running the model in one-dimensional mode. That is, set the model up with one element in the horizontal direction and define an

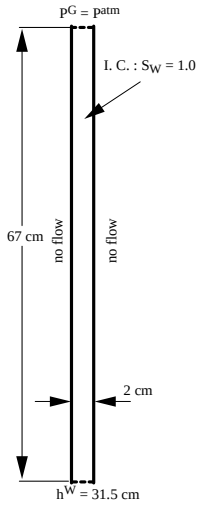


Figure F.4: Illustration of the one-dimensional water-gas displacement experiment showing boundary and initial conditions and dimensions. The mesh has one 2 cm element in the horizontal direction, and the vertical direction is discretized in an appropritate manner.

appropriate discretization to resolve the vertical direction. An illustration of the computational domain including initial and boundary conditions is provided in Figure F.4. Run the simulation for 5000 seconds (this should be near steady state).

Focus your attention on the following aspects of model input:

1. GRID DEFINITION - The grid must be able to resolve not only the steady-state moisture profile, but also the transient gas-phase front as the water drains from the soil. A general rule of thumb is that the front should be resolved in by about four elements (an increase in resolution will have little effect on the solution, and a decrease in resolution will result in oscillations). Associated with grid definition is the Peclet number (file **sm.in** input line 51). By using a small enough value of $Pe^{crit}$ (e. g., $Pe^{crit} \leq 2$), one alters the problem by increasing the amount of the capillary force, thereby fitting the physical problem to the fixed grid.

2. TIME STEP CONTROL - The size of the time step is defined in file **sm.in**, input lines 8 through 15. Time step definition is based on:

the initial time step - must be relatively small in order to resolve the upper boundary condition which is a shock to the system.

the number of iterations required for convergence over any given time step - there is a direct relationship between the time step size and the number of iterations it takes to converge on the nonlinear problem.

the Courant constraint - a check on the time truncation error.

the change in effective saturation over the time step - the effective saturation is a normalized saturation, and for 'tight' scanning curves small changes in saturation can lead to large changes in effective saturation.

the maximum and minimum specified values - the time step cannot be too large or too small because at these extremes round-off errors can dominate the solution and cause instabilities.

3. K-S-P CURVE DEFINITION - You already have the parameters $a_d$, $\eta$, and $S_{Wi}$ from Task 1. The remaining parameters which constitute the $k-S-P$ model are defined in file **sm.in**, input lines 33 through 50.

### F.5.3. Results

Please respond to the following:

1. From the screen output, note the initial and final total flux across the horizontal boundaries.

2. Run the model with different uniform grids using no additional diffusion (i.e., set $Pe^{crit} > 100$), use $\triangle z = 10cm$, $\triangle z = 5cm$ and $\triangle z = 2.5cm$. Note how the model resolves the moisture profile (if it does). Is the solution converging to something? How do these profiles compare the one defined in Task 1?

3. Try running the model with added diffusion, $Pe^{crit} = 2$, and $\triangle z = 5cm$. See how the solution is altered.

4. Write Darcy's law for the water and gas phases for the case of static equilibrium.

5. What role does the relative permeability play in defining the static moisture profile?

6. What role do the following parameters play in this experiment: $S_{Nnr}, S_{Nwr}, S_{Gr}$ and $a_i$?

7. From the screen output, watch the fluxes crossing the boundary as the solution approaches 5000s. Note that the physical problem involves monotonic displacement, so the fluxes should monotonically approach zero as the system approaches steady-state. Is there a critical time step above which the solution begins to oscillate? What is the Courant number associated with this time step? Why can't the time step increase unbounded as the solution approaches steady-state?

## F.6. TASK 3

### F.6.1. Purpose

With the results obtained from Tasks 1 and 2 you should now have a quantitative sense of the following physical parameters:

1. the ranges of the values of $a_d$, $\eta$ and $S_{Wi}$ (also known as $S_{Wr}$) which provide a qualitatively good fit to the experimental data.

2. the appropriate discretizations required for this physical data. Specifically, along with the boundary conditions chosen, the following parameters effectively define the appropriate space- and time-step scales:

   $k$, $a_d$, $\eta$ and $S_{Wi}$

For the purpose of this exercise let us set the following hysteretic $k-S-P$ model '*curve fixing*' parameters (i. e., parameters designed to ensure that the empirical model is amenable for use in the numerical model) to the following constant values (see file **sm.in**, input lines 44, 45, 47 through 50.):

- $S-P$ model curve restriction parameters $e = 1$, $\beta = 0.2$, $sp\_\min = 0.05$, $sr\_\min = 0.05$, $factd = facti = 0.001$, $S^c_{es} = 0.01$, $S^c_{er} = 0.001$
- $k-S$ model curve restriction parameter $\epsilon = 0.01$

The purpose of this Task is three fold:

1. set up the two-dimensional model for the DNAPL flood experiment. Specifically, you need to define the following modeling parameters:

   - appropriate boundary conditions,
   - discretization in the horizontal dimension,
   - the remaining parameters which define the hysteretic $k-S-P$ model[1], i. e.,

     $a_i$, $S_{Nnr}$, $S_{Nwr}$, $S_{Gr}$, $\varsigma$, $\xi$, and $\varphi$

2. identify which experimental data can be used to calibrate the model and how it can be used; and

3. identify a subset of physical parameters for which the solution is most sensitive and with which you can calibrate the model.

### F.6.2. Procedure

As introduced in Section F.3, think of the DNAPL experiment model as a series of three sequential sub-models, i. e.,

1. Starting with the initial condition of full water phase saturation, drop the water table to match the experimental condition, and allow the system to approach steady-state conditions. This is the 2-D version of the model you set up for Task 2.

2. Given the initial conditions from sub-model 1, apply the DNAPL source for the specified time period (i. e., 143 seconds).

3. Given the initial conditions from sub-model 2, remove the DNAPL source and allow the system to re-equilibrate for 3452 seconds.

Let us itemize the procedure into three steps: (1) define the horizontal discretization, (2) set up the appropriate boundary conditions for the three sub-experiments, and (3) get the feel of the physics.

[1] One should estimate a physical range of acceptable values for these data, and qualify how the solution should respond to a change in a particular parameter or set of parameters.

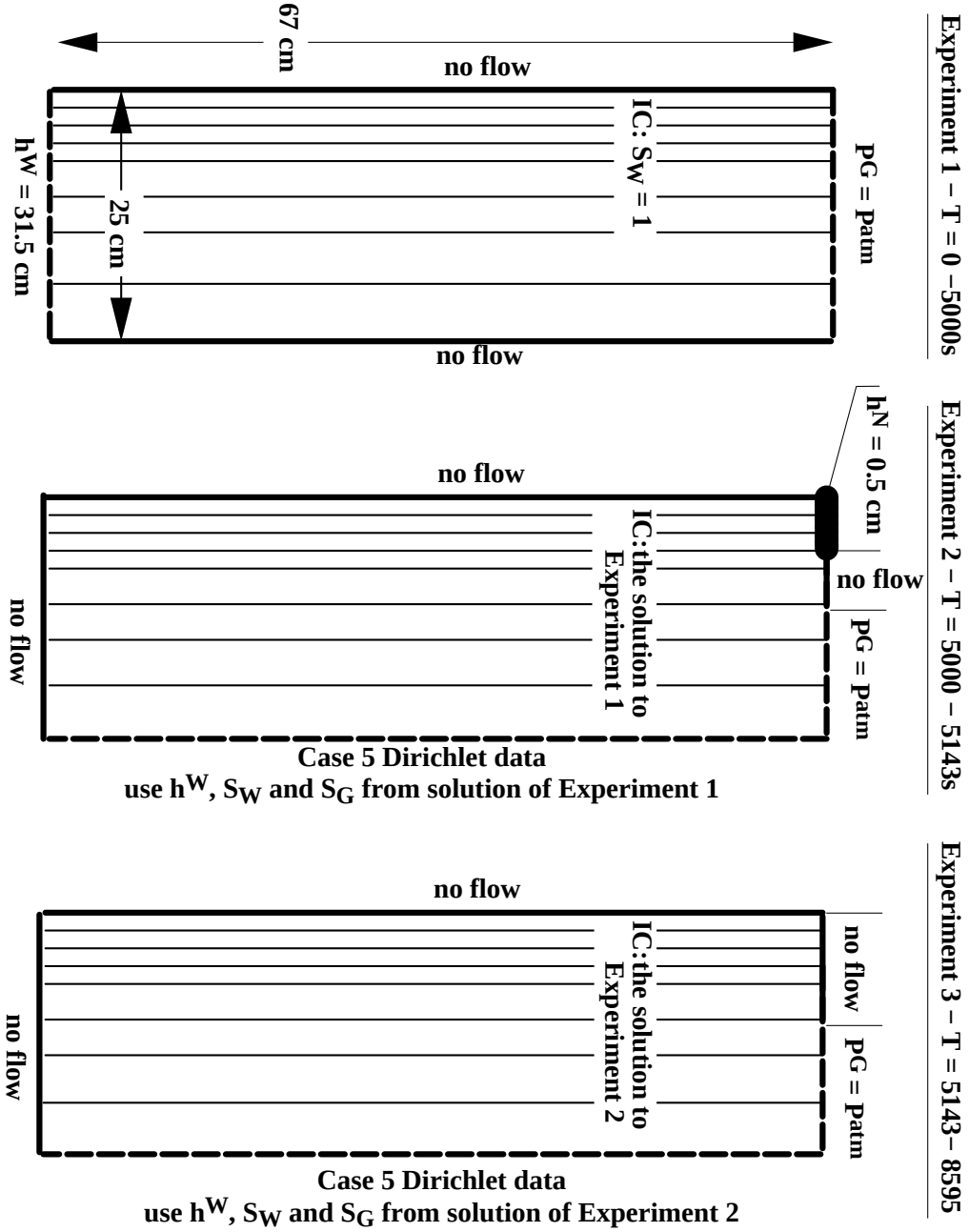


Figure F.5: Illustration of the 2-D model setup for the three sequential simulations, showing boundary and initial conditions and the time frame for each experiment.

### Horizontal Discretization

There are two important issues to consider with respect to spatial discretization: computational efficiency and numerical accuracy. As the number of grid nodes increases linearly, the computational effort increases exponentially. Therefore, when designing the mesh consider the following:

1. The experimental setup is symmetrical about the center line, and you should take advantage of this fact from a computational efficiency point of view.

2. The mesh should be refined in the vicinity of the NAPL source so that the model can accurately represent it. The mesh can coarsen away from the source.

3. In general the mesh scale in the horizontal dimension can be coarser than that in the vertical dimension because gravitational forces are absent and capillary forces dominate (i. e., the saturation front is more diffused in the horizontal that in the vertical because of gravitational effects).

Figure F.5 provides a diagrammatic representation of the first two considerations, where the three experiments shown refer to the three sequential sub-models referenced above.

The only physical constraint with respect to defining the horizontal discretization, aside from defining the appropriate width of the domain, is that relating to the definition of the NAPL source area. If we realize that the 2-D model has unit length in the omitted dimension, then the area of the surface associated with a node normal to the direction from which the condition is applied is equal to 1/2 the length of the elements surrounding the node times unit length in the omitted dimension. To mimic the experimental conditions then, the grid spacing at the source must be set such that the NAPL is applied over an area equal to $2.5cm^2$. An example of an appropriate horizontal mesh is provided in Figure F.6.

### Boundary Conditions

The model boundary conditions should be set up to mimic the experimental boundary conditions to the extent possible. This task may not be so straightforward especially when the physical boundary conditions do not match the simulator capabilities.

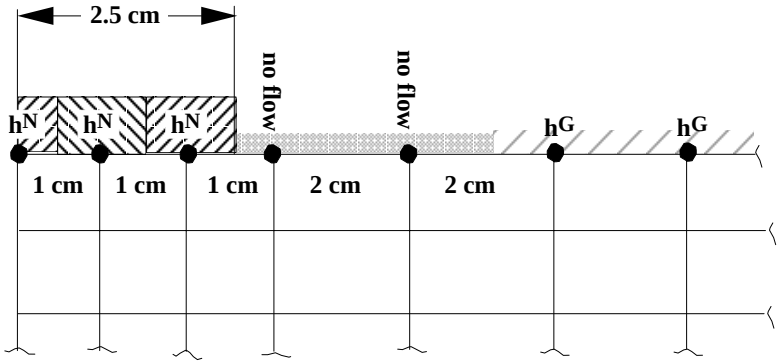


Figure F.6: Illustration of the uniform distribution of forcing conditions about a node. For this example, NAPL is ponded with head $h^N$ over an area equal to 2.5 $cm^2$.

For the sequence of experimental conditions described above, consider the example of boundary condition specification shown in Figure F.5. Let us look at each experiment in turn. In Experiment 1 the vertical sides are set as **no flow** boundaries[2], and for the conditions specified on the top and bottom sides, the problem becomes essentially 1-D (in fact, the same one you solved in Task 2).

With regard to the setup for Experiment 2, in order to make the model conditions mimic the experimental conditions, first the bottom side is set as a **no flow** boundary. Second, the right-vertical side is opened to flow by assuming that the data for the dependent variables $(P^W, S_W, S_G)$ from Experiment 1 at each of these boundary nodes will not change over the course of the second simulation. That is, the data from Experiment 1 at each of these boundary nodes becomes **Dirichlet data**. Note, by specifying Dirichlet data at a node for a given variable we are effectively solving for the gradient normal to the boundary of that variable. Using Darcy's law to compute flow, the boundary is therefore open to flow of the phase if the phase is mobile (i. e., the relative permeability is nonzero). By making this side a Dirichlet boundary, we are assuming that it is far enough away from the action so that changes in $S_W, S_G$ and $S_N$ remain effectively zero and that changes in vertical gradients are negligible..

Finally, with respect to Experiment 2, let us consider the top boundary. As

[2]The fact that symmetry in the solution is utilized here requires, by definition, that the left-vertical boundary be set as no flow.

introduced in the discussion on the horizontal discretization, in order to mimic the NAPL source condition[3], we need to apply a 0.5 cm NAPL head uniformly over 2.5 $cm^2$. Figure F.6 provides an example of an appropriate boundary condition. Note, that there are several nodes between the two different head conditions which are set to **no flow**. This separation is employed because the NAPL- and gas-phase head conditions are nonlinear[4], and numerical experiments suggest that, for the updating algorithm used in the simulator, putting a no flow buffer between them is more computationally robust.

Given the setup for Experiment 2, the setup for Experiment 3 is straight forward. As shown in Figure F.6, the NAPL head conditions are replaced by no flow conditions.

It must be emphasized that the boundary condition setup used in Figure F.6 is only one of several admissable strategies.

### Get to know the physics

Everything you need to know regarding the cause-and-effect relationship between the model parameters and the model solution can be found in the simulator documentation. So by all means, read relevant sections.

### F.6.3. Results

Please respond to the following:

1. Define an appropriate horizontal discretization and set up and run Experiment 1 in Figure F.5. This result is your initial condition for the next simulation. The files with the extension **rs** contain all the data necessary for the code to restart the simulation (see see file **sm.in**, input line 70). Since these files are over-written at each print interval, copy them into another directory so that, if you have to, you can go back to this simulation time (e. g., 5000s).

2. What role do the interfacial tension parameters play in modeling the three-phase flow problem? How can you use them as calibration parameters?

[3]The experimental source area is 5 cm by 2 cm. The model is assuming symmetry, and the 2-D domain has unit length in the omitted dimension. Therefore, the model source area is 2.5 cm by 1 cm.

[4]Actually the code converts the conditions to $P^W$, i. e., $P^W = P_{cNW}(S_W) + P_{cGN}(S_{Tw}) + P^G$ for the gas condition, and $P^W = P_{cNW}(S_W) + P^N$ for the NAPL condition.

3. Assuming that your discretization is defined such that numerical errors are not significantly affecting the solution, focus your attention on the following 'short list' of calibration parameters:

   - permeability, $k$
   - residual saturations:$S_{Wr}$, $S_{Nnr}$, $S_{Nwr}$, $S_{Gr}$
   - $S-P$ model fitting parameters: $a_d, a_i, \eta$
   - $k-S$ model fitting parameters: $\varsigma$, $\xi$, and $\varphi$
   - interfacial tension data: $\sigma_{GW}, \sigma_{GN}, \sigma_{NW}$

   Provide a brief description of how the three-phase solution might be affected by each of these parameters.

4. An example of an appropriate set of boundary conditions fro this experimental setup was provided. Provide a second option for the conditions applied on the bottom and right-vertical sides. Note, these conditions do not necessarily have to represent the physical experimental boundary conditions, they just need to be set such that for all intents and purposes the model feels the same system forcings as the experiment. Do you anticipate that the model solution should be sensitive to the choice of boundary conditions for this experiment?

5. With respect to physical experimental results available for model calibration we have three main types:

   **i** steady-state moisture profile (Table F.1)

   **ii** volume of PCE infiltrated as a function of time (Table F.2)

   **iii** video frames at specific times (as in Figure F.1)

   Provide a brief description of how the three data-types might be useful for model calibration.

## F.7. TASK 4

### F.7.1. Purpose

The purpose of this Task is to simulate the two-dimensional DNAPL spill experiment using the numerical model, and after comparing results, to consider alternative data sets which may provide a qualitatively better match to the available experimental data.

### F.7.2. Procedure

From Task 3, you should be set up to run the DNAPL spill experiment. Choose an appropriate parameter set for the three-phase flow problem. Run the model as a series of sub-models, as described in Task 3 and as illustrated in Figure F.5, where you use the simulator's restart facility to set the initial conditions as the solution of the previous problem. It is suggested that after each successful model experiment you save a copy of the restart files in another directory so that you can restart from that point if necessary.. For example, much of your calibration efforts will be focused on Experiments 2 and 3 in Figure F.5, therefore, being able to use the restart data from Experiment 1 several times is appropriate.

Given an appropriate set of boundary conditions, consider the following procedural summary for calibrating the model:

1. Choose an appropriate set of values for the following '*short-list*' parameters:

   - permeability, $k$
   - residual saturations:$S_{Wr}$, $S_{Nnr}$, $S_{Nwr}$, $S_{Gr}$
   - $S - P$ model fitting parameters: $a_d, a_i, \eta$
   - $k - S$ model fitting parameters: $\varsigma$, $\xi$, and $\varphi$
   - interfacial tension data: $\sigma_{GW}, \sigma_{GN}, \sigma_{NW}$

2. Generate a solution for Experiment 1. Save the restart files.

3. Using the solution to Experiment 1 as initial conditions, generate a solution for Experiment 2. You will need to start with a very small time step ($\approx 0.02s$), because the initial PCE infiltration rate is very high (observe the screen output of the boundary fluxes). Let the simulator increase the time step based on iteration count. Set the Courant number to $\approx 0.5$. Visually

compare the computed solution with the experimental result (i. e., Figure F.7). Compare the volumetric rate of PCE infiltration predicted by the model with the experimental results (i. e., Table F.2).

4. If the match is not qualitatively good, especially with respect to the infiltrated PCE volume, then adjust one or more of the '*short-list*' parameters and re-run step 3 until you think the solution is acceptable. Note, depending on which parameters you change you may have to re-run Experiment 1 to generate appropriate initial conditions.

5. After capturing the PCE infiltration phase of the experiment (Experiment 2), run the PCE re-distribution phase of the experiment (Experiment 3) using as initial conditions the solution to Experiment 2. Visually compare the computed solution with the experimental results (i. e., Figures F.8, F.9 and F.10).

6. If the match is not qualitatively good, especially with respect to the vertical distribution of PCE, then adjust one or more of the '*short-list*' parameters and re-run step 5 until you think the solution is acceptable. Note, depending on which parameters you change you may have to re-run Experiments 1 and 2 to generate appropriate initial conditions for Experiment 3.

### F.7.3. Results

Please respond to the following:

1. What are the values of the '*short-list*' parameters which gave the best results?

2. Plot the model solutions for the following times (where $T = 0$ is assumed to represent the initial conditions for Experiment 2: 143, 283, 683, 1195, 1795 and 3595 seconds.

3. For which '*short-list*' parameters is the model most sensitive with regard to the cumulative volume of PCE infiltrated? Briefly discuss why.

4. For which '*short-list*' parameters is the model most sensitive with regard to the areal distribution of the PCE over time? Briefly discuss why.

5. After the DNAPL penetrates the capillary fringe, the rate of vertical migration of the model solution should equal that of the experimental results. For example, even if the model DNAPL front is ahead of the experimental front in the liquid saturated zone, the difference should not increase remarkably as time progresses. What parameters define the DNAPL front speed in the liquid saturated zone?

6. When trying to calibrate the model to Experiment 2, which '*short-list*' parameters can you change without necessarily having to re-run Experiment 1.

7. Given your understanding of the mathematical model (i. e., the physical problem is translated into a series of interrelated mass balance equations and constitutive relationships), and the results from the model calibration exercise, does it seem to you that the model is '*missing*' some of the physics? For example, no matter how you adjust it, the model can not capture the shape of the PCE front as it moves through the capillary fringe, therefore, something must be missing. Recall that, when building the mathematical model, a series of major simplifying assumptions were incorporated either to make the physical problem tractable from a computational point of view, or to effectively 'fill in the blanks' with respect to data which can not currently be measured (e. g., three-phase relative permeability). Briefly discuss which major simplifying assumptions may contribute to the to the fact that the model is physically flawed?

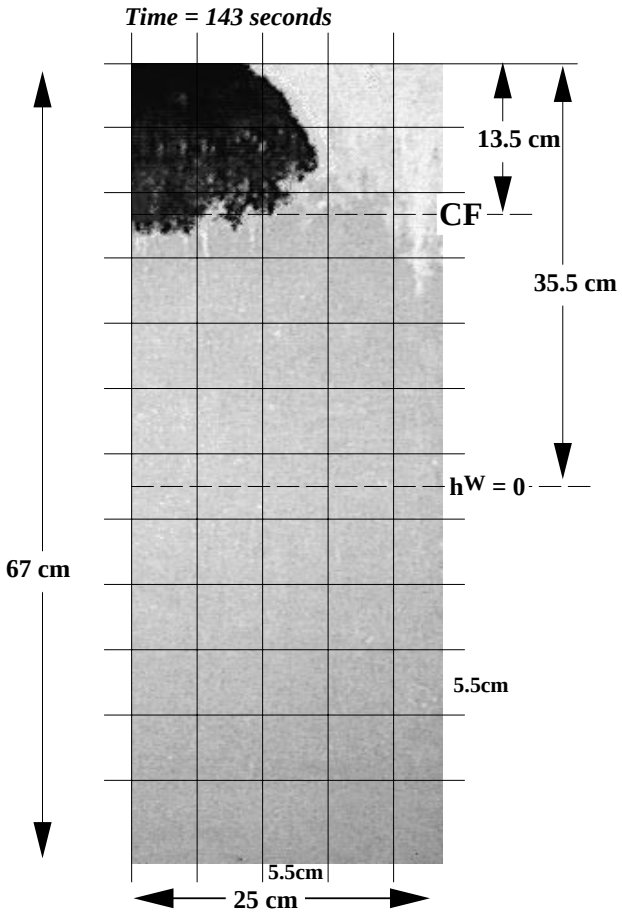


Figure F.7: Video image at time = 143 seconds just after the DNAPL source was removed (i. e., at the end of Experiment 2), showing dimensions, where the superimposed grid is for reference purposes (elements are 5.5cm by 5.5 cm)

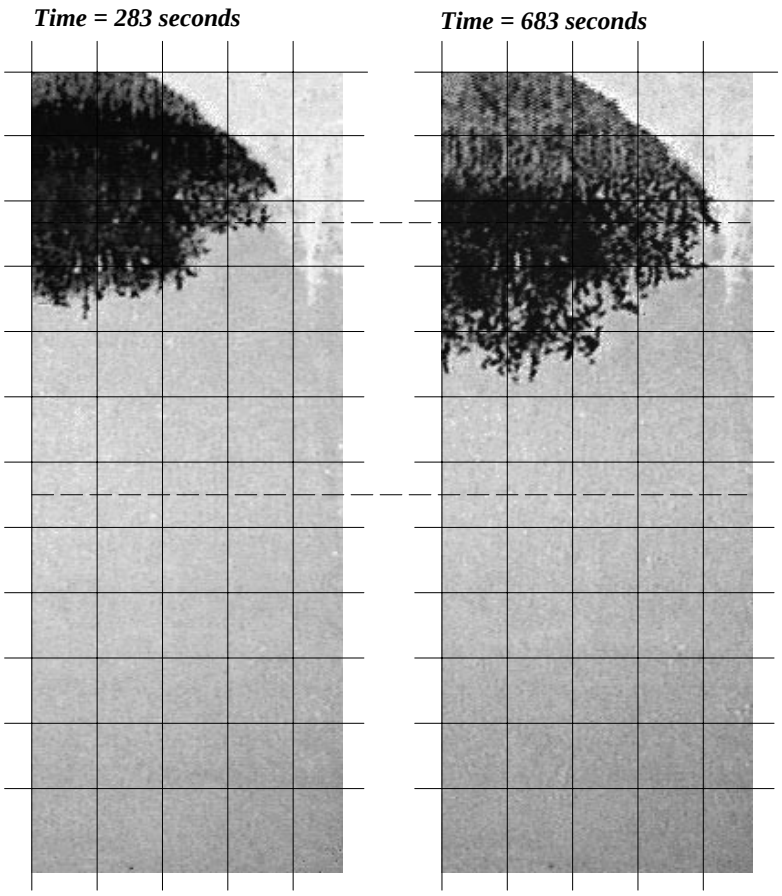


Figure F.8: Video images at time = 283 and 683 seconds after the DNAPL spill began (i. e., take Time = 0 as the initial condition for Experiment 2).

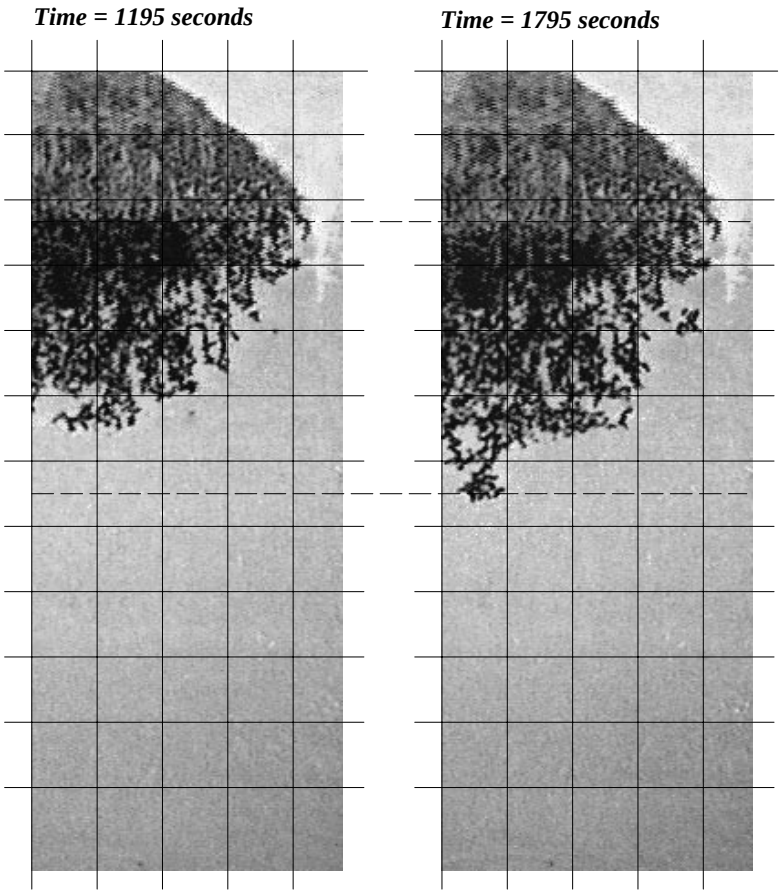


Figure F.9: Video images at Time = 1195 and 1795 seconds after the DNAPL spill began.

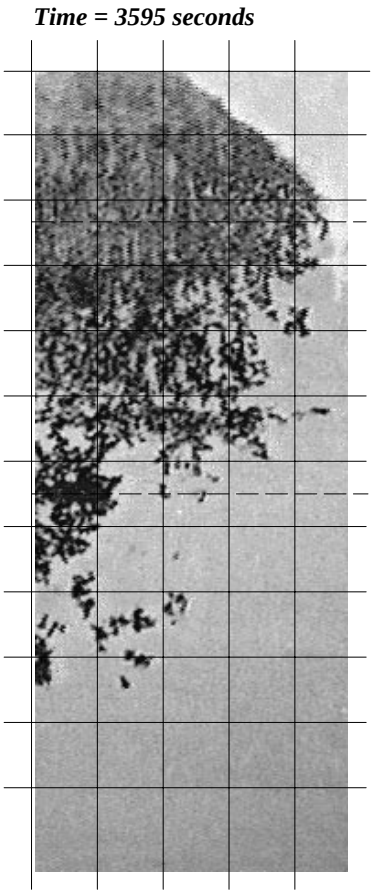


Figure F.10: Video image at Time = 3595 seconds after the DNAPL spill began.